TESIS DE LA UNIVERSIDAD DE ZARAGOZA

2025 116

Miguel González Martín

Experimental and Kinetic Study of bimetallic Pd-based catalysts for Selective Reduction of Nitrates in Aqueous Phase

Director/es
Latorre Sierra, María Nieves
Monzón Bescós, Antonio

ISSN 2254-7606

Prensas de la Universidad Universidad Zaragoza

Universidad de Zaragoza
Servicio de Publicaciones

ISSN 2254-7606

Universidad Zaragoza
1542

Tesis Doctoral

EXPERIMENTAL AND KINETIC STUDY OF BIMETALLIC PD-BASED CATALYSTS FOR SELECTIVE REDUCTION OF NITRATES IN AQUEOUS PHASE

Autor

Miguel González Martín

Director/es

Latorre Sierra, María Nieves
Monzón Bescós, Antonio

UNIVERSIDAD DE ZARAGOZA
Escuela de Doctorado

2025

Universidad Zaragoza
1542

Tesis Doctoral

Experimental and Kinetic Study of bimetallic Pd-based catalysts for Selective Reduction of Nitrates in Aqueous Phase

Autor

Miguel González Martín

Director/es

Antonio Monzón Bescós
María Nieves Latorre Sierra

Programa de Doctorado en Ingeniería Química y del Medio Ambiente
2024

AGRADECIMIENTOS

En este apartado quiero expresar mi agradecimiento a todas aquellas personas e instituciones con las que he tenido la suerte de encontrarme y que me han ayudado a completar este trabajo. Gracias de corazón.

En primer lugar, me gustaría agradecer al Ministerio de Ciencia, Innovación y Universidades por la concesión de mi beca FPI (PRE2018-086557) gracias al cual he podido realizar este trabajo de investigación. Y a los proyectos "Aprovechamiento de biomasa y producción sostenible de energía mediante (foto)catalizadores y reactores estructurados basados en materiales carbonosos" (ENE2017-82451-C3-1-R) y "Catalizadores Basados en Carbón Derivado de Biomasa para la Producción y Uso de Hidrógeno Verde" (PID2020-113809RB-C31).

Quiero agradecer a mis directores de Tesis, Dr. Antonio Monzón Bescós y Dra. María Nieves Latorre Sierra. Primeramente, me gustaría dar las gracias a Antonio Monzón por la gran cantidad de conocimientos que ha compartido conmigo y por su ayuda con las mayores dudas de mi tesis. También le agradezco sobre todo el haber sembrado en mí la semilla de la curiosidad por los modelos cinéticos. A Nieves Latorre, le agradezco por todas sus enseñanzas, apoyo, comprensión y, sobre todo, paciencia durante estos años de arduo trabajo.

Quiero dar las gracias al Instituto de Nanociencia y Materiales de Aragón, así como a la Escuela Politécnica Superior de Huesca por los equipos que han puesto a mi disposición y el maravilloso equipo de profesionales del personal técnico por su ayuda. Especialmente me gustaría dar las gracias a José Antonio Manso, a Inmaculada, Begoña y a Ester por todas las veces que me han ayudado cuando yo no veía una posible solución.

También quiero agradecer a la gente del grupo de investigación del GPT, a Pilar Tarifa por los análisis de caracterización de TPD-MS, y sobre todo por ayudarme a interpretarlos, así como por mostrarse siempre tan animada. A Fernando Cazaña, por la infinidad de análisis de caracterización realizados, los métodos de preparación de catalizadores que me ha enseñado y la infinidad de dudas sobre problemas en el

laboratorio que me ha resuelto, eres un gran referente en la ciencia. A David Martín por esa gran compañía en los congresos. A Eva, por toda la ayuda prestada. Y, a David Chaos, que me ha hecho compañía en los últimos años, que ahora se ha quedado a cargo del laboratorio donde tanto tiempo he pasado.

Quiero agradecer al Prof. Juan José Delgado Jaén de la Universidad de Cádiz por las maravillosas imágenes HAADF-STEM que me han permitido visualizar mi trabajo.

Quiero hacer especial mención a las personas de la Universidad de Oporto del LSRE-LCM, al Dr. M. Fernando R. Pereira y a la Dra. O. Salomé. G. Pinto Soares por su acogida y enseñanzas en un periodo tan corto de tiempo. También quiero dar las gracias a todos los compañeros que tuve allí y me prestaron toda su ayuda, José, Sofía, Patricia y Liliana.

I would also like to show my gratitude to my flat mates during this stay in Portugal for making it an unforgettable experience, Jana, Bianca, Gertruda, Maya, Ondra and Anastasia.

Por supuesto no pueden faltar mis compañeros de laboratorio Christian (porcellino) los largos días en el laboratorio, por todas las experiencias vividas juntos y las que quedan por vivir. A Dario, por sus innovadoras ideas y su alegría en el laboratorio, a Dani, por su compañía y simplemente ser como es.

A los compañeros de los laboratorios de los sótanos del grupo de Bioflora, Miguel, Fer, Alba, Samira y Yana. Hay que hacer una especial mención a Mai, con quien he compartido muchos ratos y muchas penurias, y con quien seguiré pasando mucho más tiempo. También quiero dar las gracias al resto de compañeros laboratorio Andoni, Marta, Silvia, Miriam, Matias y Alvaro. Gracias a Daniel Valero y el proyecto de OpenHuerto por dar esa desconexión.

En especial debo agradecer a mi familia por todo su apoyo, a mis padres, Miguel y Juani, y a mis hermanas, Rocío, Cristina y María por ser referentes en mi vida. Gracias a mis sobrinos, Luna, Nerea y Nico, por ser la alegría de la huerta y animarme.

Gracias al resto de familiares que me han apoyado y me han dado unas palabras de ánimo.

Gracias a todos mis amigos por su apoyo y en especial a mis amigos de toda la vida, el Club de la Trucha, Héctor, Jorge, Diego, Rebeca, Inés, Gloria, Raúl, Kibu y Marina por animarme a seguir adelante y aguantarme de forma incondicional. A mis amigos y compañeros de la universidad que me han acompañado en gran parte de este trayecto y nos hemos enfrentado a las mismas dificultades y apoyándonos entre nosotros, gracias a Sara, Isma, Alberto, Fran, Ester, Puri y Adri.

También tengo que agradecer a mi primera compañera de piso y primer contacto de Huesca Marta, así como a mi segundo compañero de piso y de aventuras Jimmy por ser un soporte en los días más complicados.

Debo y quiero hacer un especial agradecimiento a Julia, a quien he conocido gracias a iniciar esta aventura y quién me ha sufrido mis peores momentos dándome su apoyo constante en este largo viaje.

Y, por último, pero no menos importante, quiero darle las gracias a mis gatos, Pelusa y Melocotón por acompañarme durante las noches en vela y mantener mi cordura durante el confinamiento. Y a mi perra Freyja por recibirme siempre con la máxima de las alegrías transmitiéndome esa felicidad y obligarme a salir de casa y despejarme, al menos 3 veces al día.

“The most important step a man can take.
It's not the first one, is it?
It's the next one.
Always the next step, Dalinar.”

Brandon Sanderson,
Oathbringer

Index

1. INTRODUCTION

1.1. Water contamination by nitrates

1.1.1. Origin of the nitrate contamination problem

The population is constantly growing, which also produces an increase in the demand for food. According to United Nations data, in 1950, there were 2.6 billion people in the world; In 1987, there were already 5,000 million; In 2011, they reached 7,000, and by 2050 the world population is expected to be approximately 9.7 billion. This growth presents an enormous challenge: supplying food to the population with guarantees and without destroying the planet.

Nutrients such as nitrogen and phosphorus are essential elements for the growth of plants. In agriculture they are usually introduced in the form of fertilizers to guarantee greater production and quality. However, the increasing demand for food has led to an increase in production and use of fertilizers associated with inefficiency considerable, which has caused pollution of water, air and soil and has affected, therefore, to human health and the environment. The excess of nitrogen introduced with the fertilizers and not used by the plants, degraded, or stored in soil, is transported to the groundwater, usually in the form of nitrates (NO_3^-) [1,2], which damage the environment and, potentially, the human health [3]. This contamination of ground waters by nitrates is a worldwide problem where humans contribute with reactive nitrogen to terrestrial ecosystems about three times more than natural sources [4].

Despite the legislation efforts to control these spills, over 18% of the area of groundwater bodies in Europe were affected by nitrates between 2012 and 2015 [5]. Figure 1.1 shows the zones according to the concentration of nitrates in the groundwater of Europe for the period 2016-2019 [3]. Besides, according to these data published by the European Commission, Spain is one of the countries in Europe most affected by water pollution by nitrates. In 2022, 197 Spanish municipalities exceeded the legal limit of nitrates in drinking water, affecting approximately 2% of the population of Spain [6]. The nitrate pollution also affects the surface waters, at EU level, 36% of rivers, 32% of lakes, 31% of coastal,32% of transitional water and 81% of marine waters were reported as eutrophic, due to the nitrate contamination [6].

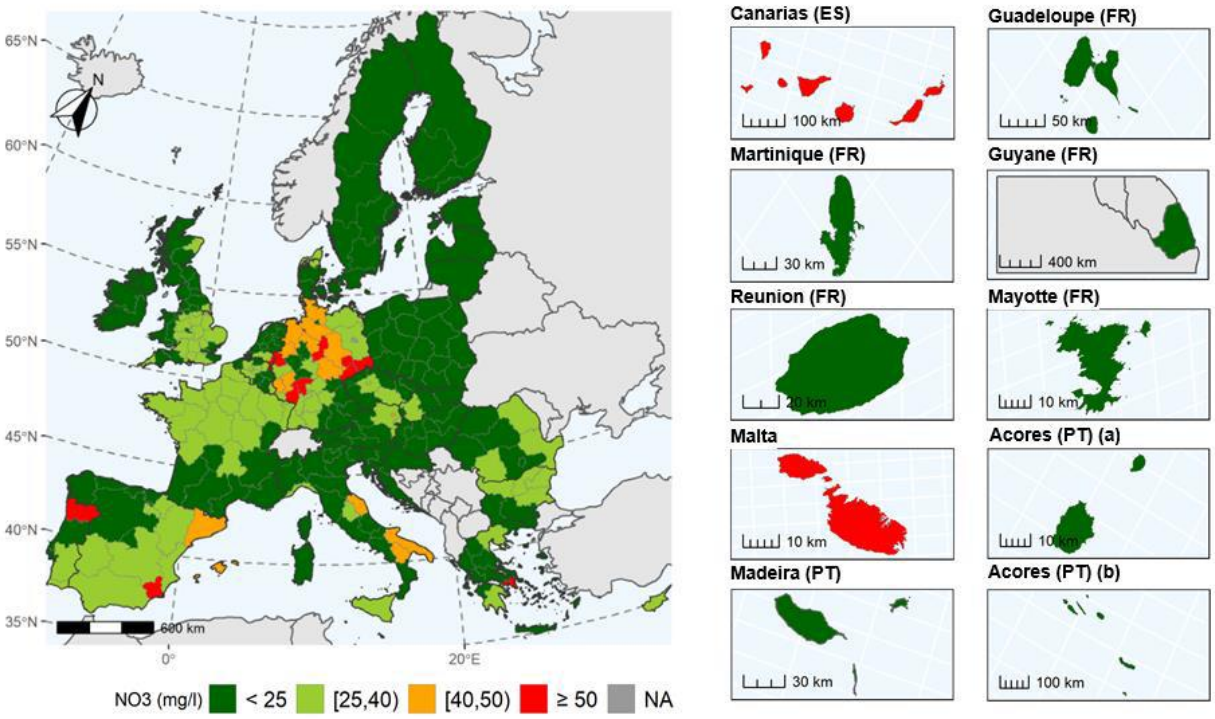

Figure 1.1 *Annual average nitrate concentrations in groundwater at the autonomous communities and cities level for the reporting period 2016-2019 [3].*

1.1.2. Sources of nitrate contamination

The formation of nitrate is an integral part of the nitrogen cycle in our environment. Globally, about 260 million tons of atmospheric nitrogen are fixed annually. Biological fixation accounts for 193 million tons per year, which is 67.25% of the total. The remaining 32.75% is fixed through non-biological processes such as atmospheric lightning and industrial discharges. Nitrates are also formed due to the decomposition of fertilizers by microorganisms, decaying plants, manures, or other organic residues, which further increase the nitrate content in the soil. Plants use this nitrate from the soil to fulfill their nutrient requirements and may accumulate nitrate in their leaves and stems [7].

The natural sources of formation and addition of nitrates to the soil normally mean that the background nitrate content of the soil is 10mg/L. Concentrations higher than this are considered contamination and are of anthropogenic origin. The anthropogenic sources of nitrate contamination in groundwater are grouped in 2 main categories: point sources of pollution such as improper disposal of industrial waste, poor construction of septic tanks and leaching pits; and diffuse sources, as heavy fertilizer application or deforestation, which are primarily responsible for high nitrate values infiltrating the groundwater regime (Figure 1.2) [7,8].

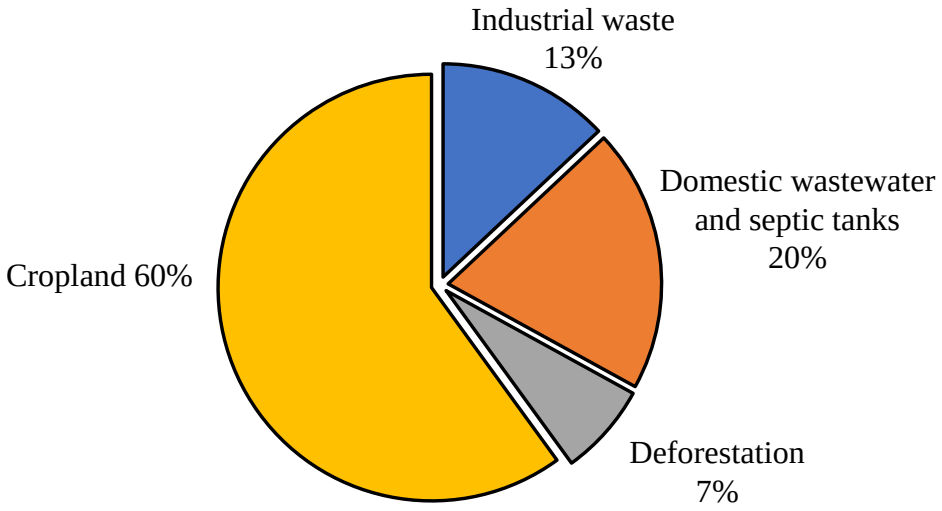

Figure 1.2 *Anthropogenic sources of nitrate contamination in groundwater [7].*

Among these activities, fertilizer application and subsequent leaching are considered the main reasons for nitrate contamination of shallow aquifers. This is supported, among other arguments, by the relationship between the increase in nitrate content in water and the expansion of agricultural land, the rise in fertilizer consumption, and the emergence of intensive livestock farming. Another variable to consider is the chemical form of the nitrogen compound in the fertilizer. Fertilizers containing nitrates, which are highly mobile molecules, are easily carried away by infiltration water, whereas ammoniacal fertilizers take longer as these molecules have lower mobility. However, the conversion of urea and ammoniacal compounds to nitrates occurs rapidly under suitable temperature and humidity conditions, increasing the risk of contamination.

Additionally, there are organic fertilizers in which nitrogen is present in an organic form (not directly assimilable by plants but converted to a mineral form by soil microorganisms) and in a mineral form. The organic fertilizers have traditionally been

applied as manure in cultivation areas, but their use has significantly declined with the advent of synthetic fertilizers and the specialization of agricultural activities. Another important factor related to nitrate contamination is manure production. In Spain, the manure generated by animals in stables amounts to 76 million tons annually, of which 30 million tons are solid manure and 46 million tons are liquid or semi-solid. The large volume of liquid manure, particularly from pigs, generated in areas of intensive livestock farming is causing significant nitrate contamination problems in groundwater, either due to inadequate utilization in agriculture or improper treatment and purification [8].

Is also important to remark the importance of the rain and water as the vehicle of dispersion of this soluble pollutant. In this context, the deforestation and the loss of vegetation cover that acted as a "tampon" to assimilate these nitrates is also a contributing factor to the increase in nitrates on the groundwaters.

1.1.3. Environmental and health effects of nitrates

Water with excess nitrates may not be harmful for irrigation, but it is harmful for human consumption. Nitrates are harmful to human beings due to the ease with which they are transformed, within the body, into nitrites and nitrosamines, with toxic and carcinogenic effects [9–13]. However, one of the main consequences of nitrate ingestion is methemoglobinemia or blue baby syndrome, a potentially fatal disease in children under six months. In an intermediate step, nitrates are reduced to nitrites producing the oxidation of the ferrous iron in the blood to ferric iron. In this way, hemoglobin becomes methemoglobin, unable to transport oxygen in the blood [9,14,15].The main symptoms of blue baby syndrome are headache, fatigue, respiratory failure, lack of energy, diarrhea, vomiting, possible shock, seizures and in severe cases, death. An excess of nitrates in the body especially affects pregnant women, since it is common for methemoglobin levels to rise from the normal level (0.5% to 2.5%) up to 10% in the 30th week of pregnancy. Therefore, pregnant women are particularly susceptible to methemoglobinemia [9].

The greatest environmental drawback derived from an excess of nitrogenous compounds in surface waters (rivers, lakes and reservoirs) is eutrophication caused by excessive enrichment of C, N and P in the waters, favoring the massive growth of plants

and organisms. This excessive growth degenerates into the proliferation of algae and an alarming decrease in dissolved oxygen levels in the aquatic system. These anaerobic conditions cause the death of marine species due to asphyxiation. The collateral damage to the eutrophication process is the increase in operating expenses of public water supply systems due to taste and odor problems, difficulty in navigation and alterations of fish species [16].

1.1.4. Legislation on nitrates

Council Directive 91/676/EEC, of December 12, on the protection of waters against pollution caused by nitrates of agricultural origin [17], establishes maximum admissible values for nitrogen compounds in drinking water at 50, 0.1 and 0.5 mg/L for NO_3^-, NO_2^- and NH_4^+, respectively. This directive forces member states to define a Code of Good Agricultural Practice (CBPA) in order to protect Community waters against nitrates of agricultural origin, as they are the main cause of water pollution. The Nitrates Directive requires Member States to:

- Identify waters affected and at risk of being affected by nitrates pollution as well as designate as Nitrates Vulnerable Zones (NVZ) the areas draining into these waters where agriculture contributes significantly to this pollution.
- Develop action schedules with measures to reduce and prevent nitrates pollution, apply such measures to NVZ or to the whole territory, and to reinforce these measures as soon as it appears that they are not sufficient to achieve the objectives of the Directive.

Directive 2000/60 EC of October 23, known as the Water Framework Directive (WFD) introduces a new legislative approach to water management and protection based on natural geographic and hydrological formations (river basins) and not on national and political boundaries. It also requires the coordination of different EU policies [18]. On the basis of this directive, Directive 2006/118/EC, of December 12, on the protection of groundwater against chemical pollution and deterioration, as it is the main source of public drinking water supply, was enacted [19]. The objective is to reduce the level of purification treatment required to produce drinking water. Reference is made to the establishment of quality standards for nitrates to ensure consistency with Directive 91/676/EEC.

Continuing the same line of thought, Directive 2020/2184 regulates new parameters and limits for the quality of the water for human consumption, and designates concentration limits at 50, 0.5 and 0.5 mg/L for NO_3^-, NO_2^- and NH_4^+, respectively. It also includes that the Member States shall ensure that the concentration of nitrates divided by 50 plus the concentration of nitrites divided by 3 is less than 1ppm [20].

Finally, Royal Decree 3/2023, of January 10, establishes the technical and sanitary criteria for drinking water quality, its control, and supply, being the partial inclusion of Directive 2020/2184 into Spanish legislation and establishing same limit values for drinking water and its supply and distribution [21].

Similarly, Directive 2008/105/EC of 16 December 2008 [22] on environmental quality standards in the field of water policy refer to the protection of water against various pollutants, including nitrates, nitrites, and ammonium. These laws include concentration limits for assessing quality depending on the type of water being assessed. These directives have been transposed into Spanish law through Royal Decree 817/2015, of 11 September [23], which establishes the criteria for monitoring and assessing the status of surface waters and environmental quality standards, and Royal Decree 1514/2009, of 2 October[24], which regulates the protection of groundwater against pollution and deterioration.

The most specific and recent legal instrument is Royal Decree 47/2022 of 18 January [25] on the protection of water against diffuse pollution caused by nitrates from agricultural sources. This law is the most recent transposition of the Council Directive 91/676/EEC and consider waters affected by nitrates:

- Superficial water bodies with nitrate concentration higher than 25mg/L.
- Underground water bodies with nitrate concentration higher than 37.56mg/L.
- Superficial water bodies which suffer from eutrophication or may be affected by it in a close future.

1.2. Nitrate removal methods in aqueous streams

Nitrate is a stable anion highly soluble in water, hard to remove with conventional techniques, like co-precipitation or adsorption [26–28]. However, there are some physic-chemical, biological and catalytic treatments that are able to obtain a clean stream without nitrates. There are mainly two kinds of techniques: separation techniques and reduction techniques.

The separation techniques use physical means to separate the stream to be treated into two effluents, one clean of the pollutant, in this case nitrates, and another concentrated flow. On the other hand, reduction techniques employ biological or catalytic methods to reduce nitrates to a more stable and harmless compound as N_2.

1.2.1. Separation techniques

1.2.1.1. Reverse osmosis

Reverse osmosis is a method that uses a semipermeable membrane to remove ions, molecules, and larger particles. The main advantage of this technique is the opportunity to treat multiple pollutants at the same time, as well as a nitrate removal efficiency of 59% to 95%. The drawbacks associated with the implementation of this technique are mainly related to the necessary pressure used and the deterioration of the membranes themselves (fouling, compaction, and deterioration with use) due to contact with soluble matter, organic matter, as well as colloidal or suspended particles. Additionally, they are also affected by variations in water pH and by exposure to chlorine. Another drawback of this technique is the necessary subsequent removal of the concentrated waste stream [29].

1.2.1.2. Electrodialysis

The process of nitrate removal from water using electrodialysis is quite similar to reverse osmosis; however, in electrodialysis, ions are transferred through an ion-exchange semipermeable membrane from a higher concentration solution to a lower concentration solution by applying a direct electric current. This technique has higher recovery than reverse osmosis, but it still produces a high nitrate concentrated waste that must be treated later. While this method has successfully achieved substantial

reductions in nitrate concentrations, significant challenges exist due to its lack of selectivity towards nitrate anion. Furthermore, the ion-exchange membrane, which is selective for either cations or anions, limits the versatility of this technique and is an expensive technique [27,29].

1.2.1.3. Ion exchange

Conventional ion exchange, the most common method for nitrate removal, utilizes a strong base anion exchange resin. The process involves pre-treating the raw water to remove suspended solids and other constituents that could saturate the resin column. The nitrate-laden treatment stream then enters the ion exchange column, where nitrate displaces the mobile ion of the membrane from the resin surface sites, thus removing nitrate from the water. The exhausted resin is regenerated, which is the reverse process, and its purpose is to return the ion exchange resin to its initial exchange capacity. This is done by passing solutions containing the original mobile ion, which deposits on the resin and dislodges the ions captured during depletion.

The ion exchange process removes not only nitrate but also sulfate from the water. Reports from 1965 already showed it efficiency in as solution to remove various pollutants from water in batch or continuous reactor [30]. However, ion exchange faces two major limitations: the lack of resin with high selectivity for nitrates commonly present in groundwater, and the need for adequate resin regeneration to prevent disposal issues. To address these problems, ion exchange can be combined with other techniques to optimize nitrate removal efficiency [29].

Finally, a resume of separation techniques is shown on Table 1.1 where the principal advantages and disadvantages are shown.

Table 1.1 *Comparation of separation techniques for nitrate removal*

	Ion exchange	**Reverse osmosis**	**Electrodialysis**
Pre-treatment	Pre-filter, harness control	Pre-filter,	Pre-filter
Post-treatment	Adjustment of pH, remineralization	Adjustment of pH, remineralization	Adjustment of pH, remineralization
Residue	Brine	Brine	Brine
Start-up time	Minutes	Minutes	Minutes
Efficiency	85-98%	59-95%	71-100%
Advantages	Elimination of various pollutants	Elimination of various pollutants	Elimination of various pollutants
Disadvantages	Membrane obstruction, high pressure, brine recycling	Membrane obstruction, brine recycling	Membrane obstruction, brine recycling

1.2.2. Elimination techniques

1.2.2.1. Biological denitrification

Biological denitrification is a widely utilized and highly effective method in both urban and industrial wastewater treatment. However, this technique is slowly being adapted for drinking water treatment due to several critical factors: long operational times, bacterial contamination of treated water, presence of organic residues, and potential need for increased chlorine dosages.

Biological denitrification takes place under anoxic conditions, where nitrate is reduced to nitrogen gas through a series of intermediate stages producing nitrite, nitric oxide, and nitrous oxide [29]. This process can be carried out using either heterotrophic or autotrophic bacteria. Heterotrophic bacteria mainly utilize organic substrates such as methanol, ethanol, and acetic acid, though methods using gases like carbon monoxide and methane as substrates have also been developed. In autotrophic denitrification, hydrogen or reduced sulfur compounds act as substrates, and carbon dioxide or bicarbonate is used as a carbon source for cellular growth. Heterotrophic biological denitrification processes are more commonly applied on an industrial scale due to their faster reaction rates [27].

1.2.2.2. Electrochemical reduction

Electrochemical reduction technology consists of carrying out the reduction of the nitrate ion directly on an electrode that acts as a cathode of an electrolytic cell and using electrical energy to achieve a low-cost reduction of nitrate. The selectivity of the process to nitrogen gas depends on many factors, such as the design of the electrolytic cell, the working mode or the specific composition of the water to be treated, but the most important variable is the cathode material that will act as electrocatalyst. Varying the catalyst and experimental parameters allows efficient and controlled reduction of nitrate to nitrogen or other high value products including ammonia and hydroxylamine [31]. This technique reduces the nitrates, which have the nitrogen in it most oxidizing state (+V), to N_2, the most stable zero oxidation state of nitrogen on the cathode of an electrocatalytic reactor. However, this technique faces the challenge of avoiding an over reduction to ammonia NH_4^+ the highest reduced state of nitrogen (-III) [32]. The ammonium is an undesired product of the reaction due to its higher health threaten and far below the legal concentration levels than nitrates.

1.2.2.3. Catalytic selective nitrate reduction (CSNR)

Another potential method is the removal of both nitrates and nitrites using a reducing agent such as hydrogen or formic acid along with a catalyst. This process, also known as catalytic denitrification, follows a reaction pathway similar to biological denitrification and electrocatalysis, culminating in the formation of nitrogen gas. However, an undesirable byproduct, ammonium, can also be produced. Therefore, the catalytic system is a critical factor in developing this process to achieve maximum selectivity towards nitrogen gas. This is the technique on which the thesis will focus, and which will be explained in depth. It is a very attractive technique as it can reduce nitrates in a very short period of time and very compact, transforming them into an inert product such as N_2.

In the 1990s, noble metal-based catalysts were employed, but they only demonstrated suitable characteristics for the hydrogenation of nitrites. The development of bimetallic catalysts was necessary to eliminate nitrates and achieve high selectivity towards the non-toxic final product, nitrogen gas. The preparation method significantly influences the catalyst's activity and selectivity, making the choice of support material crucial. Alumina has been the most studied support, although silica, titanium oxide, zirconium

oxide, and activated carbon have also been used. While the results are promising, there are currently no industrial plants implementing this treatment. However, if the trend in legislation towards lowering nitrate levels continues, this technique would be a strong candidate for achieving that goal [13,27].

Finally, a resume of elimination techniques is shown on Table 1.2 where the principal advantages and disadvantages are shown.

Table 1.2 *Comparation of elimination techniques for nitrate removal*

	Biological denitrification	**Electrocatalysis**	**Catalytic reduction**
Pre-treatment	Adjustment of pH, addition of nutrients and carbon source, anaerobic condition	Adjustment of pH, preparation of the electrolyte.	Adjustment of pH
Post-treatment	Filtration, biological disinfection.	Adjustment of pH, ammonium control	Adjustment of pH, ammonium control
Residue	Sludge	None	None
Start-up time	Weeks or even a month	Minutes	Minutes
Efficiency	~100%	90%	~100%
Advantages	No brine,NO_3^- reduction	No brine, NO_3^- reduction	No brine,NO_3^- reduction
Disadvantages	Long operational time, biological contamination, sensibility to ambiental conditions, continuous monitoring, sludge recycling	Ammonium production	Ammonium production

1.3. State of the art of the CSNR

The CSNR is a triphasic process where nitrates are catalytically reduced to nitrogen using hydrogen as the reducing agent and a solid catalyst. The reaction is carried out under atmospheric pressure and ambient temperature conditions.

The hydrogenation process occurs in two consecutive stages. In the first stage, the nitrate ion is reduced to nitrite ion as an intermediate reaction product. Subsequently, in

the second stage, the nitrite is transformed into nitrogen gas and/or ammonium. The objective is to achieve high conversion rates of nitrates and nitrites while maximizing the formation of nitrogen gas (the desired product), as it competes with the formation of ammonium (the undesired product). Therefore, it is essential to use a catalyst that is active, stable, and selective towards nitrogen formation [33].

1.3.1. Catalytic active phase

Previous studies demonstrated that the reaction needs the use of two active catalytic phases: a noble metal and a promoter [34,35]. The reduction of nitrates to nitrites is carried out by the bimetallic pair composed by the promoter metal (Cu, Sn, Ag, In, Ni, Fe, etc.) and a noble metal, usually Pd or Pt. Recent studies proved the possibility of the reduction of these nitrates over non noble metals like Ni or Fe. However, these catalysts show high selectivity towards ammonium formation.

One of the pioneering studies on catalytic nitrate reduction was realized by Vorlop and Tacke [36] in 1989. They demonstrated that monometallic catalysts of Pd or Pt supported on silica or alumina were inactive in the reduction of nitrates to nitrites; however, they could reduce nitrite, with Pd/alumina showing the best results. Years later, Horold et al. [34] presented studies with bimetallic catalysts, achieving high activity in nitrate elimination. The best results were obtained with the Pd-Cu catalyst, which had a nitrate elimination activity of 3.13 mgNO_3^-/min·g cat, representing an activity 30 times higher than that achieved with biological denitrification. However, the bimetallic catalyst was much more selective towards ammonium compared to the monometallic catalyst used for nitrite reduction.

Prussen et al. [37] opened a new field of research by studying novel bimetallic catalysts such as Pd-Sn and Pd-In. Although these catalysts were less active than Pd-Cu, they demonstrated better selectivity for nitrogen. Since then, various bimetallic combinations have been investigated, including Pd(Pt)In [37], Pd(Pt)-Ag, and Pd(Pt)-Au [38]. Nonetheless, the best results have been obtained with Pd-Cu [35,39–42] and Pd-Sn catalysts [43].

Regarding Pd-Cu catalysts supported on alumina, several studies focused on finding the optimal Cu/Pd ratio. Some authors [38,44] have claimed that the optimal ratio is 0.5 wt. for nitrate reduction. Other subsequent investigations established the optimal atomic

ratio for this bimetallic pair to be 1-1.7, depending on the support and the noble metal weight percentage [33,45]. Soares et al. [46] determined that the optimal noble metal/Cu atomic ratio for catalysts supported on activated carbon is approximately 1. In the same year, Wang et al. [47] optimized the PdCu/activated carbon catalyst with a molar ratio of 0.66 for 3.6% Cu by weight, achieving high conversion, stability, and nitrogen selectivity (98%). Epron et al. [48] found an optimal Pt/Cu weight ratio of 1 for a $PtCu/Al_2O_3$ catalyst with 1% Pt by weight.

Until 2002, all research focused on finding the optimal bimetallic pair. Since then, new supports based on reducible oxides were explored, allowing the addition of a single active catalytic phase of Pd or Pt [49,50], with the support assuming the role of the non-noble metal. Epron et al. [49] found that Pd catalysts supported on reducible oxides exhibited high activity in nitrate reduction, directly related to the redox properties of these materials. Subsequently, other researchers studied materials such as SnO_2 [50–52] or TiO_2 [53] corroborating these hypothesis [49]. The common characteristic of all these supports is that they change oxidation state during the reaction, acting as both support and active catalytic phase.

Soares et al. studied mixtures of various mono (Rh, Pd, Pt and Cu over activated carbon) and bimetallic catalysts (RhCu, PdCu and PtCu over activated carbon) [54], achieving the highest nitrogen selectivity with the PdCu catalyst with a weight ratio Pd/Cu of one. Besides, the mix of Pt-Cu catalysts with Pd catalysts produced a synergistic effect, increasing nitrogen selectivity. Tests with mixtures of monometallic catalyst of Pd and monometallic catalyst of Cu, and as well with Pt and Rh noble metal catalysts were realized. This combination of monometallic catalysts proved to be active in the nitrate reduction and obtained low selectivity towards NH_4^+, similar to the bimetallic catalyst, demonstrating that for nitrate reduction, the presence of bimetallic sites in the initial catalyst is unnecessary, as long as they are in contact during the reaction.

In recent years, research on monometallic Fe catalysts supported on various activated carbons has gained importance, as described by Shukla et al. [55] or by using Fe directly or in combination with other non-noble metals [56–63]. These catalysts are characterized by the ease of exchanging oxidation states between Fe^{2+} and Fe^{3+}, low toxicity and low cost. Mikami et al. [64] also performed a research of a noble metal free catalyst employing Ni, which proved to be active in the conversion of nitrates. They

performed various studies combining various metals with Ni in order to boost their activity, stability and selectivity [64–66]. Ni modified with Zr reached full conversion of nitrates without showing nitrite at the exit of the reactor and neither deactivation. Based on these studies, Kobune et al. [67] developed a Ni/Al_2O_3 catalyst which was much more active than the unsupported Ni. On the other hand, Soares et al. performed an extensive test on monometallic catalysts with an activated carbon support and a variety of metals Pt, Pd, Cu, Sn, Ru, Rh, Ni, Ir, Fe and Zn. All of these catalysts were inactive for the nitrate reduction, and the monometallic catalysts based on non-noble metals were also inactive in the conversion of nitrites [68]. Neither way, all these catalysts tested based on non- noble metal show high selectivity towards NH_4^+, in most cases near 100%.

Garron et al. [69] used trimetallic catalysts, adding a third metal (Au) to PdSn catalysts supported on alumina or silica, achieving a nitrogen selectivity of 97.5% for the $Pd5Sn1.5Au3/SiO_2$ catalyst. The authors demonstrated that the support influences the morphology of the trimetallic catalyst, with competition between the deposition of Au and Sn on Pd during preparation, with Au preferentially depositing on the free Pd surface. This is a good result for the activity and selectivity of the catalysts but increase the price of this catalysts due to their high content in noble metals.

Analyzing the existing literature in this field, it can be concluded that in general Pd is the active phase most active and selective to nitrogen. It is also important a good contact between the noble and the promoter metal without avoiding the alloying of both. The most commonly promoter metals employed are Sn and Cu but due to the important role of the support there is no agreement in which is a better option. Because of this, a really important parameters to consider in the synthesis stages, aside of choice of active phases, is to select an adequate catalytic support, which can greatly influence the activity and selectivity of the catalyst.

1.3.2. Supports

As stated before, the choice of catalyst support is crucial in heterogeneous catalysis. A stable support in the reaction environment with a high specific surface area is essential to ensure that the catalytic active phases are well-dispersed, thereby increasing the catalyst's activity.

For monometallic catalysts, supports with redox properties are required to play also the role of the promoter metal. The most commonly used supports are TiO_2 [53, 54, 75], SnO_2 [52], and CeO_2 [49].

The most commonly used material with good results as a support for bimetallic catalysts is γ-alumina [34,36,38,67,69–75]. Studies comparing alumina and silica supports [75] concluded that silica-supported catalysts are less active because supports with a lower point of zero charge (PZC) reduce nitrate ion adsorption on their surface [76]. Other supports studied include SiO_2 [69,75,77], TiO_2 [78], activated carbon [54,68,79–81], zeolites [82], hydrotalcites [83], exchange resins [84–87] and carbon nanotubes [78,81,88–91].

Palomares et al. [83] used mixed oxides based on hydrotalcites for nitrate reduction, employing a Pd-Cu catalyst supported on a Mg/Zn hydrotalcite. These double-layer structures form mixed oxides when calcined, which act as catalyst supports with interesting properties for nitrate reduction. One notable property is the "memory effect", the ability to reconstruct the hydrotalcite structure after calcination, regaining its laminar structure upon contact with an aqueous solution. Nitrates are reduced to nitrites between the positive charges of the hydrotalcite. In the same position, nitrites are reduced to nitrogen and, to a lesser extent, ammonia. The formed ammonia, due to its inappropriate charge, is rapidly released into the solution, reducing diffusion limitation problems that significantly affect reaction selectivity. Additionally, Barrabés et al. [92] demonstrated that varying the HT composition, specifically the Mg/Zn ratio, modifies the acid-base properties of the support, thereby influencing selectivity to final products, as these are strongly affected by pH.

For the treatment of natural waters containing other ions, Palomares et al. [93] compared various supports and found that the best catalysts are those supported on materials with a BET area of 100-300 m^2/g, acidic characteristics, and low electrical conductivity, such as alumina.

Aside from the metal oxides, carbon materials are a promising support due to their stability under reaction conditions, their inertness and physical properties, as high surface area and porosity, in addition to their large potential for functionalization and activation. These treatments enlarge the possibilities of this kind of supports allowing a detailed modification of porosity, specific surface area, as well as chemical properties like acidity and hydrophilicity. It also allows an easy way to recover the noble metal

impregnated in them just by burning the carbon support. For example, carbon nanotubes are a widely used support due to their mesoporous structure and the ease of being able to modify their properties. Santos et al. proved that the use as support of ball milling of CNT increased the surface area and the nitrate reduction activity, reducing also the ammonium selectivity of the PdCu catalysts [94]. Other authors like Gonzalez et al. tested a variety of carbon supports like graphite carbon nanofibers, and active carbons concluding that depending on the support employed it can be controlled the mass transfer, which control the selectivity towards ammonium [95].

1.4. Objectives

The main objective of this work is the study and development of active, selective and stable Pd-based catalysts in the reaction of selective nitrate reduction. In order to achieve this main objective, the following points have been developed:

- Selection of promotors (Cu, Sn) and supports and of the operating conditions of the catalyst preparation method.
- Physicochemical characterization (N_2 adsorption isotherm, TGA-Air, XRD, XPS, Raman spectroscopy, TPD-MS, atomic absorption, SEM and TEM) of the catalysts before and after reaction.
- Study of the influence of the operating conditions on the activity, selectivity, and stability of PdCu and PdSn catalysts supported on Al_2O_3.
- Study of the global performance of the simultaneous reaction with PdCu/Al_2O_3 catalysts, and ammonia adsorption with cation exchange resins on the elimination ammonia production.
- Study of the influence of thermal treatment and of the modifications with urea or nitric acid, of the graphitic support during the preparation of PdCu catalysts supported on graphite.
- Development of a rigorous kinetic model based on the mechanism of the reaction that accounts for the evolution of the main relevant species involved in the reaction.

The content of the rest of the chapters of the Thesis is briefly described below. Thus, Chapter 2 describes the experimental methodology developed for the synthesis of the

catalysts and for the performance of the catalytic tests. This chapter also describes the physicochemical characterisation techniques used.

Chapter 3 shows the mechanism of reaction proposed for the catalytic selective nitrate reduction reaction as well as the development of a kinetic model for the reaction that allows the adjustment, interpretation and quantification of the studies carried out. The chapter also includes the ammonium adsorption model and the effect of the resin on the overall selectivity of the process.

In chapter 4, Pd-based catalysts supported on alumina are developed and the influence of the synthesis variables and operating reaction conditions on the activity and selectivity of the catalysts are studied. The chapter is divided in two parts, based on the development of PdCu and PdSn catalysts. The synthesis variables studied are: weight ratio of Pd, weight ratio of Sn, order of impregnation and influence of the reduction temperature. The reaction operating conditions studied are: initial nitrate concentration, rate agitation, catalyst loading, influence of other ions in the solution and influence of H_2/CO_2 ratio fed. This chapter is completed with the study of a combined treatment reaction-adsorption. The CSNR reaction is combined in this case with the introduction of a cation exchange resin for the adsorption of the ammonium produced. In this case, the influence of the type of resin and its concentration has been studied. In addition, all the experimental results have been fitted with the kinetic model developed in the previous chapter, studying the adequacy of the model and allowing to explain and quantify the effects observed experimentally.

The activity and selectivity results of PdCu catalysts supported on a commercial graphite supplied for Asbury® are presented in Chapter 5. For the development of these catalysts, the results obtained in the previous chapter on the optimum composition of the PdCu catalysts and the influence of the operating conditions in the reaction have been taken into account. From these considerations, in this chapter, the influence of the thermal decomposition atmosphere used in the catalyst synthesis process is studied, as well as the modification of the characteristics of the support by the addition of urea or by its treatment with nitric acid. The influence of these variables on the physicochemical characteristics of the catalysts obtained (studied by characterizing all the materials prepared) and their catalytic behaviour in the nitrate removal reaction, is analysed. In addition, all the results are completed by adjusting all the experimental results with the kinetic model developed in Chapter 3.

Finally, Chapter 6 contains the summary and the most relevant conclusions of the Thesis.

1.5. References

[1] M. Sebilo, B. Mayer, B. Nicolardot, G. Pinay, A. Mariotti, Long-term fate of nitrate fertilizer in agricultural soils, Proc Natl Acad Sci U S A 110 (2013) 18185–18189. https://doi.org/10.1073/pnas.1305372110.

[2] H. Gurevich, S. Baram, T. Harter, Measuring nitrate leaching across the critical zone at the field to farm scale, Vadose Zone Journal 20 (2021). https://doi.org/10.1002/vzj2.20094.

[3] E.C. Directorate-General for Environment, REPORT FROM THE COMMISSION TO THE COUNCIL AND THE EUROPEAN PARLIAMENT on the implementation of Council Directive 91/676/EEC concerning the protection of waters against pollution caused by nitrates from agricultural sources based on Member State reports for the period 2016–2019, 2021.

[4] F. Ortmeyer, B. Hansen, A. Banning, Groundwater nitrate problem and countermeasures in strongly affected EU countries—a comparison between Germany, Denmark and Ireland, Grundwasser 28 (2023) 3–22. https://doi.org/10.1007/s00767-022-00530-5.

[5] G.B. (NTUA) Peter Kristensen, Caroline Whalley, Fernanda Néry Nihat Zal, Trine Christiansen, Ursula Schmedtje (Umweltbundesamt), Anne Lyche Solheim (Norwegian Institute for Water Research, NIVA), Kari Austnes (NIVA), Eleftheria Kampa (Ecologic), Josselin Rouillard (E, EEA 2018: European Waters Assessment of Status and Pressures. EEA Report No 7/2018, 2018.

[6] K. Hernández, K. García, S.M. Barajas, J. Martínez, Estudio del contenido en nitratos de las aguas de consumo humano, 2022. https://ecologistasenaccion.org/216302.

[7] S. Shukla, A. Saxena, Current Science Association Sources and leaching of nitrate contamination in groundwater, 118 (2020) 883–891. https://doi.org/10.2307/27226382.

[8] L. Fernández Ruiz, The Nitrates And The Groundwaters In Spain, Enseñanza de Las Ciencias de La Tierra, 15 (2007) 257–265.

[9] M.H. Ward, R.R. Jones, J.D. Brender, T.M. de Kok, P.J. Weyer, B.T. Nolan, C.M. Villanueva, S.G. van Breda, Drinking water nitrate and human health: An updated review, Int J Environ Res Public Health 15 (2018) 1–31. https://doi.org/10.3390/ijerph15071557.

[10] M.H. Ward, R.R. Jones, J.D. Brender, T.M. de Kok, P.J. Weyer, B.T. Nolan, C.M. Villanueva, S.G. van Breda, Drinking water nitrate and human health: An updated review, Int J Environ Res Public Health 15 (2018). https://doi.org/10.3390/ijerph15071557.

[11] S.-T. Du, Y.-S. Zhang, L. Xian-Yong, Accumulation of Nitrate in Vegetables and Its Possible Implications to Human Health, (2007). www.sciencedirect.com.

[12] N.S. Bryan, D.D. Alexander, J.R. Coughlin, A.L. Milkowski, P. Boffetta, Ingested nitrate and nitrite and stomach cancer risk: An updated review, Food and Chemical Toxicology 50 (2012) 3646–3665. https://doi.org/10.1016/j.fct.2012.07.062.

[13] Archna, S.K. Sharma, R.C. Sobti, Nitrate removal from ground water: A review, E-Journal of Chemistry 9 (2012) 1667–1675. https://doi.org/10.1155/2012/154616.

[14] N.S. Bryan, H. van Grinsven, The Role of Nitrate in Human Health, in: Advances in Agronomy, Academic Press Inc., 2013: pp. 153–182. https://doi.org/10.1016/B978-0-12-407247-3.00003-2.

[15] A. Cockburn, G. Brambilla, M.L. Fernández-Cruz, D. Arcella, L.R. Bordajandi, B. Cottrill, C. van Peteghem, J. Lou Dorne, Nitrite in feed: From animal health to human health, Toxicol Appl Pharmacol 270 (2013) 209–217. https://doi.org/10.1016/j.taap.2010.11.008.

[16] T.G. Huntington, Evidence for intensification of the global water cycle: Review and synthesis, J Hydrol (Amst) 319 (2006) 83–95. https://doi.org/10.1016/j.jhydrol.2005.07.003.

[17] European Parliament, Council of the European Union, Directive 91/676/EEC of the European Parliament and of the Council of 12 December 1991 concerning the

protection of waters against pollution caused by nitrates from agricultural sources., L375, 1991.

[18] European Parliament, Council of the European Union, Directive 2000/60/EC of the European Parliament and of the Council of 23 October 2000 establishing a framework for Community action in the field of water policy., L327, 2000.

[19] European Parliament, Council of the European Union, Directive 2006/118/EC of the European Parliament and of the Council of 12 December 2006 on the protection of groundwater against pollution and deterioration., L372 , 2006.

[20] European Parliament, Council of the European Union, Directive (EU) 2020/2184 of the European Parliament and of the Council of 16 December 2020 on the quality of water intended for human consumption, 435, 2020.

[21] R. with P. and D.M. Ministry of the Presidency, Royal Decree 3/2023 of 10 January establishing the technical-sanitary criteria for the quality of drinking water, its control and supply., 9, Spain, 2023.

[22] European Parliament, Council of the European Union, Directive 2008/105/EC of the European Parliament and of the Council of 16 December 2008 on environmental quality standards in the field of water policy, amending and subsequently repealing Council Directives 82/176/EEC, 83/513/EEC, 84/156/EEC, 84/491/EEC, 86/280/EEC and amending Directive 2000/60/EC of the European Parliament and of the Council, 348, 2008.

[23] F. and E. Ministry of Agriculture, Royal Decree 817/2015, of 11 September, establishing the criteria for monitoring and evaluation of the status of surface waters and environmental quality standards., 219, Spain, 2015.

[24] Ministry of the Environment and Rural and Marine Affairs, Royal Decree 1514/2009 of 2 October 2009 regulating the protection of groundwater against pollution and deterioration., 255, 2009.

[25] R. with P. and D.Memory. Ministry of the Presidency, Royal Decree 47/2022 of 18 January on the protection of water against diffuse pollution caused by nitrates from agricultural sources., 17, Spain, 2022.

[26] V.B. Jensen, J.L. Darby, C. Seidel, C. Gorman, Nitrate in potable water supplies: Alternative management strategies, Crit Rev Environ Sci Technol 44 (2014) 2203–2286. https://doi.org/10.1080/10643389.2013.828272.

[27] C. Franch Martí, Continuous Catalytic Nitrate Removal in Natural Waters, Mixed University Institute of Chemical Technology (UPV-CSIC), 2011.

[28] F. Ruiz-Beviá, M.J. Fernández-Torres, Effective catalytic removal of nitrates from drinking water: An unresolved problem?, J Clean Prod 217 (2019) 398–408. https://doi.org/10.1016/j.jclepro.2019.01.261.

[29] F. Rezvani, M.H. Sarrafzadeh, S. Ebrahimi, H.M. Oh, Nitrate removal from drinking water with a focus on biological methods: a review, Environmental Science and Pollution Research 26 (2019) 1124–1141. https://doi.org/10.1007/s11356-017-9185-0.

[30] R. Eliassen, B.M. Wyckoff, C.D. Tonkin, Ion Exchange for Reclamation of Reusable Supplies, Journal AWWA 57 (1965) 1113–1122. https://doi.org/10.1002/j.1551-8833.1965.tb01500.x.

[31] J. Zhou, S. Gao, G. Hu, Recent Progress and Perspectives on Transition Metal-Based Electrocatalysts for Efficient Nitrate Reduction, Energy and Fuels 38 (2024) 6701–6722. https://doi.org/10.1021/acs.energyfuels.4c00415.

[32] S. Meng, Y. Ling, M. Yang, X. Zhao, A.I. Osman, A.H. Al-Muhtaseb, D.W. Rooney, P.S. Yap, Recent research progress of electrocatalytic reduction technology for nitrate wastewater: A review, J Environ Chem Eng 11 (2023). https://doi.org/10.1016/j.jece.2023.109418.

[33] N. Barrabés, J. Sá, Catalytic nitrate removal from water, past, present and future perspectives, Appl Catal B 104 (2011) 1–5. https://doi.org/10.1016/j.apcatb.2011.03.011.

[34] S. Hôrold, T. Tacke, K.D. Vorlop, Catalytical removal of nitrate and nitrite from drinking water: 1. screening for hydrogenation catalysts and influence of reaction conditions on activity and selectivity, Environmental Technology (United Kingdom) 14 (1993) 931–939. https://doi.org/10.1080/09593339309385367.

[35] U. Prüsse, K.D. Vorlop, Supported bimetallic palladium catalysts for water-phase nitrate reduction, J Mol Catal A Chem 173 (2001) 313–328. https://doi.org/10.1016/S1381-1169(01)00156-X.

[36] K.D. Vorlop, T. Tacke, First steps towards noble-metal catalyzed removal of nitrate and nitrite from drinking water, Chemieingenieurtechnik 61 (1989) 836–837. https://doi.org/10.1002/cite.330611023.

[37] U. Prüsse, M. Hähnlein, J. Daum, K.D. Vorlop, Improving the catalytic nitrate reduction, Catal Today 55 (2000) 79–90. https://doi.org/10.1016/S0920-5861(99)00228-X.

[38] F. Gauthard, F. Epron, J. Barbier, Palladium and platinum-based catalysts in the catalytic reduction of nitrate in water: Effect of copper, silver, or gold addition, J Catal 220 (2003) 182–191. https://doi.org/10.1016/S0021-9517(03)00252-5.

[39] A. Pintar, J. Batista, J. Levec, T. Kajiuchi, Kinetics of the catalytic liquid-phase hydrogenation of aqueous nitrate solutions, Appl Catal B 11 (1996) 81–98. https://doi.org/10.1016/S0926-3373(96)00036-7.

[40] A. Pintar, J. Batista, J. Levec, Catalytic denitrification: direct and indirect removal of nitrates from potable water, 2001.

[41] I. Mikami, Y. Sakamoto, Y. Yoshinaga, T. Okuhara, Kinetic and adsorption studies on the hydrogenation of nitrate and nitrite in water using Pd-Cu on active carbon support, Appl Catal B 44 (2003) 79–86. https://doi.org/10.1016/S0926-3373(03)00021-3.

[42] Y. Sakamoto, Y. Kamiya, T. Okuhara, Selective hydrogenation of nitrate to nitrite in water over Cu-Pd bimetallic clusters supported on active carbon, J Mol Catal A Chem 250 (2006) 80–86. https://doi.org/10.1016/j.molcata.2006.01.041.

[43] C. Franch, E. Rodríguez-Castellón, Á. Reyes-Carmona, A.E. Palomares, Characterization of (Sn and Cu)/Pd catalysts for the nitrate reduction in natural water, Appl Catal A Gen 425–426 (2012) 145–152. https://doi.org/10.1016/j.apcata.2012.03.015.

[44] S. Hörold, K.D. Vorlop, T. Tacke, M. Sell, Development of catalysts for a selective nitrate and nitrite removal from drinking water, Catal Today 17 (1993) 21–30. https://doi.org/10.1016/0920-5861(93)80004-K.

[45] N. Barrabés, J. Just, A. Dafinov, F. Medina, J.L.G. Fierro, J.E. Sueiras, P. Salagre, Y. Cesteros, Catalytic reduction of nitrate on Pt-Cu and Pd-Cu on active carbon using continuous reactor: The effect of copper nanoparticles, Appl Catal B 62 (2006) 77–85. https://doi.org/10.1016/j.apcatb.2005.06.015.

[46] O.S.G.P. Soares, J.J.M. Órfão, M.F.R. Pereira, Bimetallic catalysts supported on activated carbon for the nitrate reduction in water: Optimization of catalysts composition, Appl Catal B 91 (2009) 441–448. https://doi.org/10.1016/j.apcatb.2009.06.013.

[47] Y. Wang, Y. Sakamoto, Y. Kamiya, Remediation of actual groundwater polluted with nitrate by the catalytic reduction over copper-palladium supported on active carbon, Appl Catal A Gen 361 (2009) 123–129. https://doi.org/10.1016/j.apcata.2009.04.006.

[48] F. Epron, F. Gauthard, C. Pinéda, J. Barbier, Catalytic Reduction of Nitrate and Nitrite on Pt-Cu/Al2O3 Catalysts in Aqueous Solution: Role of the Interaction between Copper and Platinum in the Reaction, J Catal 198 (2001) 309–318. https://doi.org/10.1006/jcat.2000.3138.

[49] F. Epron, F. Gauthard, J. Barbier, Catalytic reduction of nitrate in water on a monometallic Pd/CeO2 catalyst, J Catal 206 (2002) 363–367. https://doi.org/10.1006/jcat.2001.3498.

[50] R. Gavagnin, L. Biasetto, F. Pinna, G. Strukul, Nitrate removal in drinking waters: The effect of tin oxides in the catalytic hydrogenation of nitrate by Pd/SnO2 catalysts, Appl Catal B 38 (2002) 91–99. https://doi.org/10.1016/S0926-3373(02)00032-2.

[51] M. D'Arino, F. Pinna, G. Strukul, Nitrate and nitrite hydrogenation with Pd and Pt/SnO2 catalysts: The effect of the support porosity and the role of carbon dioxide in the control of selectivity, Appl Catal B 53 (2004) 161–168. https://doi.org/10.1016/j.apcatb.2004.05.015.

[52] J. Sá, J. Montero, E. Duncan, J.A. Anderson, Bi modified Pd/SnO2 catalysts for water denitration, Appl Catal B 73 (2007) 98–105. https://doi.org/10.1016/j.apcatb.2006.06.012.

[53] W. Gao, N. Guan, J. Chen, X. Guan, R. Jin, H. Zeng, Z. Liu, F. Zhang, Titania supported Pd-Cu bimetallic catalyst for the reduction of nitrate in drinking water, Appl Catal B 46 (2003) 341–351. https://doi.org/10.1016/S0926-3373(03)00226-1.

[54] O.S.G.P. Soares, J.J.M. Órfão, M.F.R. Pereira, Nitrate reduction with hydrogen in the presence of physical mixtures with mono and bimetallic catalysts and ions in solution, Appl Catal B 102 (2011) 424–432. https://doi.org/10.1016/j.apcatb.2010.12.017.

[55] A. Shukla, J. V. Pande, A. Bansiwal, P. Osiceanu, R.B. Biniwale, Catalytic Hydrogenation of Aqueous Phase Nitrate over Fe/C Catalysts, Catal Letters 131 (2009) 451–457. https://doi.org/10.1007/s10562-009-9899-9.

[56] G.C.C. Yang, H.L. Lee, Chemical reduction of nitrate by nanosized iron: Kinetics and pathways, Water Res 39 (2005) 884–894. https://doi.org/10.1016/j.watres.2004.11.030.

[57] T. Suzuki, M. Moribe, Y. Oyama, M. Niinae, Mechanism of nitrate reduction by zero-valent iron: Equilibrium and kinetics studies, Chemical Engineering Journal 183 (2012) 271–277. https://doi.org/10.1016/j.cej.2011.12.074.

[58] Z. Zhang, Z. Hao, Y. Yang, J. Zhang, Q. Wang, X. Xu, Reductive denitrification kinetics of nitrite by zero-valent iron, Desalination 257 (2010) 158–162. https://doi.org/10.1016/j.desal.2010.02.031.

[59] Y.H. Liou, C.J. Lin, S.C. Weng, H.H. Ou, S.L. Lo, Selective decomposition of aqueous nitrate into nitrogen using iron deposited bimetals, Environ Sci Technol 43 (2009) 2482–2488. https://doi.org/10.1021/es802498k.

[60] S. Hamid, S. Bae, W. Lee, M.T. Amin, A.A. Alazba, Catalytic Nitrate Removal in Continuous Bimetallic Cu-Pd/Nanoscale Zerovalent Iron System, Ind Eng Chem Res 54 (2015) 6247–6257. https://doi.org/10.1021/acs.iecr.5b01127.

[61] J.M. Rodríguez-Maroto, F. García-Herruzo, A. García-Rubio, C. Gómez-Lahoz, C. Vereda-Alonso, Kinetics of the chemical reduction of nitrate by zero-valent iron, Chemosphere 74 (2009) 804–809. https://doi.org/10.1016/j.chemosphere.2008.10.020.

[62] H.Y. Hu, N. Goto, K. Fujie, Effect of ph on the reduction of nitrite in water by metallic iron, Water Res 35 (2001) 2789–2793. https://doi.org/10.1016/S0043-1354(00)00570-4.

[63] G. Vilardi, L. Di Palma, Kinetic Study of Nitrate Removal from Aqueous Solutions Using Copper-Coated Iron Nanoparticles, Bull Environ Contam Toxicol 98 (2017) 359–365. https://doi.org/10.1007/s00128-016-1865-9.

[64] I. Mikami, T. Okuhara, Removal of Nitrate in Water by Hydrogenation with a Noble Metal-Free Ni-Base Catalyst, Chem Lett 31 (2002) 923–933.

[65] I. Mikami, R. Kitayama, T. Okuhara, Hydrogenations of nitrate and nitrite in water over Pt-promoted Ni catalysts, Appl Catal A Gen 297 (2006) 24–30. https://doi.org/10.1016/j.apcata.2005.08.038.

[66] I. Mikami, Y. Yoshinaga, T. Okuhara, Rapid removal of nitrate in water by hydrogenation to ammonia with Zr-modified porous Ni catalysts, Appl Catal B 49 (2004) 173–179. https://doi.org/10.1016/j.apcatb.2003.12.009.

[67] M. Kobune, D. Takizawa, J. Nojima, R. Otomo, Y. Kamiya, Catalytic reduction of nitrate in water over alumina-supported nickel catalyst toward purification of polluted groundwater, Catal Today 352 (2020) 204–211. https://doi.org/10.1016/j.cattod.2020.01.037.

[68] O.S.G.P. Soares, J.J.M. Órfão, M.F.R. Pereira, Activated carbon supported metal catalysts for nitrate and nitrite reduction in water, Catal Letters 126 (2008) 253–260. https://doi.org/10.1007/s10562-008-9612-4.

[69] A. Garron, K. Lázár, F. Epron, Characterization by Mössbauer spectroscopy of trimetallic Pd-Sn-Au/Al2O3 and Pd-Sn-Au/SiO2 catalysts for denitration of drinking water, Appl Catal B 65 (2006) 240–248. https://doi.org/10.1016/j.apcatb.2006.02.010.

[70] A. Garron, K. Lázár, F. Epron, Effect of the support on tin distribution in Pd-Sn/Al2O 3 and Pd-Sn/SiO2 catalysts for application in water denitration, Appl Catal B 59 (2005) 57–69. https://doi.org/10.1016/j.apcatb.2005.01.002.

[71] T. Tacke, K.-D. Vorlop, Kinetische Charakterisierung von Katalysatoren zur selektiven Entfernung von Nitrat und Nitrit aus Wasser, Chemie Ingenieur Technik 65 (1993) 1500–1502. https://doi.org/10.1002/cite.330651216.

[72] T. Salmi, J. Warna, T. Maunulas, I. Turunen, Kinetics of nitrate reduction reactor, Chem Eng Sci 49 (1994) 5763–5773. https://doi.org/https://doi.org/10.1016/0009-2509(94)00331-9.

[73] P. Xu, S. Agarwal, L. Lefferts, Mechanism of nitrite hydrogenation over Pd/γ-Al2O3 according a rigorous kinetic study, J Catal 383 (2020) 124–134. https://doi.org/10.1016/j.jcat.2020.01.003.

[74] M.A. Jaworski, V. Vetere, H.P. Bideberripe, G.J. Siri, M.L. Casella, Structural aspects of PtSn/γ-Al2O3 catalysts prepared through surface-controlled reactions: Behavior in the water denitrification reaction, Appl Catal A Gen 453 (2013) 227–234. https://doi.org/10.1016/j.apcata.2012.12.034.

[75] F.A. Marchesini, S. Irusta, C. Querini, E. Miró, Spectroscopic and catalytic characterization of Pd-In and Pt-In supported on Al2O3 and SiO2, active catalysts for nitrate hydrogenation, Appl Catal A Gen 348 (2008) 60–70. https://doi.org/10.1016/j.apcata.2008.06.026.

[76] Y. Tsuchiya, Y. Yamaya, Y. Amano, M. Machida, Effect of two types of adsorption sites of activated carbon fibers on nitrate ion adsorption, J Environ Manage 289 (2021). https://doi.org/10.1016/j.jenvman.2021.112484.

[77] W. Sun, W. Yang, S. Gao, Z. Xu, Q. Du, L. Chen, Q. Li, Elevated N2 selectivity in catalytic denitrification by amino group-assisted in-situ buffering effect of NH2-SiO2 supported PdCu bimetallic nanocatalyst, Chemical Engineering Journal 390 (2020). https://doi.org/10.1016/j.cej.2020.124617.

[78] A.S.G.G. Santos, J. Restivo, C.A. Orge, M.F.R. Pereira, O.S.G.P. Soares, Nitrate Catalytic Reduction over Bimetallic Catalysts: Catalyst Optimization, C (Basel) 6 (2020) 78. https://doi.org/10.3390/c6040078.

[79] K. Ota, Y. Amano, M. Aikawa, M. Machida, Removal of nitrate ions from water by activated carbons (ACs) - Influence of surface chemistry of ACs and coexisting chloride and sulfate ions, Appl Surf Sci 276 (2013) 838–842. https://doi.org/10.1016/j.apsusc.2013.03.053.

[80] L. Lemaignen, C. Tong, V. Begon, R. Burch, D. Chadwick, Catalytic denitrification of water with palladium-based catalysts supported on activated carbons, Catal Today 75 (2002) 43–48. https://doi.org/10.1016/S0920-5861(02)00042-1.

[81] O.S.G.P. Soares, J.J.M. Órfão, M.F.R. Pereira, Nitrate reduction in water catalysed by Pd-Cu on different supports, Desalination 279 (2011) 367–374. https://doi.org/10.1016/j.desal.2011.06.037.

[82] R. Rodríguez, C. Pfaff, L. Melo, P. Betancourt, Characterization and catalytic performance of a bimetallic Pt-Sn/HZSM-5 catalyst used in denitratation of drinking water, Catal Today 107–108 (2005) 100–105. https://doi.org/10.1016/j.cattod.2005.07.070.

[83] A.E. Palomares, J.G. Prato, F. Rey, A. Corma, Using the "memory effect" of hydrotalcites for improving the catalytic reduction of nitrates in water, J Catal 221 (2004) 62–66. https://doi.org/10.1016/j.jcat.2003.07.013.

[84] C. Neyertz, F.A. Marchesini, A. Boix, E. Miró, C.A. Querini, Catalytic reduction of nitrate in water: Promoted palladium catalysts supported in resin, Appl Catal A Gen 372 (2010) 40–47. https://doi.org/10.1016/j.apcata.2009.10.001.

[85] J. Shi, Y. Ma, Z. Shen, D. Liu, C. Long, X. Zhang, J. Shi, C. Wang, Fe-Pd bimetallic composites supported by resins for nitrate reduction: Role of surface functional groups in controlling rate and selectivity, Environ Eng Sci 36 (2019) 295–304. https://doi.org/10.1089/ees.2018.0204.

[86] D. Gašparovičová, M. Králik, M. Hronec, Z. Vallušová, H. Vinek, B. Corain, Supported Pd-Cu catalysts in the water phase reduction of nitrates: Functional resin versus alumina, J Mol Catal A Chem 264 (2007) 93–102. https://doi.org/10.1016/j.molcata.2006.08.081.

[87] C. Bradu, C. Căpăţ, F. Papa, L. Frunza, E.A. Olaru, G. Crini, N. Morin-Crini, É. Euvrard, I. Balint, I. Zgura, C. Munteanu, Pd-Cu catalysts supported on anion exchange resin for the simultaneous catalytic reduction of nitrate ions and reductive dehalogenation of organochlorinated pollutants from water, Appl Catal A Gen 570 (2019) 120–129. https://doi.org/10.1016/j.apcata.2018.11.002.

[88] C. Dagan-Jaldety, N. Fridman-Bishop, Y. Gendel, Nitrate hydrogenation by microtubular CNT-made catalytic membrane contactor, Chemical Engineering Journal 401 (2020) 126142. https://doi.org/10.1016/j.cej.2020.126142.

[89] O.S.G.P. Soares, X. Fan, J.J.M. Órfão, A.A. Lapkin, M.F.R. Pereira, Kinetic modeling of nitrate reduction catalyzed by Pd-Cu supported on carbon nanotubes, Ind Eng Chem Res 51 (2012) 4854–4860. https://doi.org/10.1021/ie202957v.

[90] O.S.G.P. Soares, J.J.M. Órfão, M.F.R. Pereira, Pd-Cu and Pt-Cu catalysts supported on carbon nanotubes for nitrate reduction in water, Ind Eng Chem Res 49 (2010) 7183–7192. https://doi.org/10.1021/ie1001907.

[91] O.S.G.P. Soares, J.J.M. Órfão, M.F.R. Pereira, Nitrate reduction catalyzed by Pd-Cu and Pt-Cu supported on different carbon materials, Catal Letters 139 (2010) 97–104. https://doi.org/10.1007/s10562-010-0424-y.

[92] N. Barrabés, M.A. Garrido, A. Frare, A. Monzón, D. Tichit, Pt-MgZnCuAl hydrotalcite-derived catalysts in the reduction of nitrates using continuous and batch reactors, Catal Today 175 (2011) 328–337. https://doi.org/10.1016/j.cattod.2011.03.063.

[93] A.E. Palomares, C. Franch, A. Corma, A study of different supports for the catalytic reduction of nitrates from natural water with a continuous reactor, in: Catal Today, 2011: pp. 90–94. https://doi.org/10.1016/j.cattod.2011.05.015.

[94] A.S.G.G. Santos, J. Restivo, C.A. Orge, M.F.R. Pereira, O.S.G.P. Soares, Nitrate Catalytic Reduction over Bimetallic Catalysts: Catalyst Optimization, C (Basel) 6 (2020) 78. https://doi.org/10.3390/c6040078.

[95] D.T. González, A. Marí, J.A. Baeza, L. Calvo, M.A. Gilarranz, Enhancement of activity and selectivity to nitrogen in catalytic nitrate reduction by use of conductive carbon catalytic supports and control of hydrogen mass transfer regime, J Environ Chem Eng 9 (2021). https://doi.org/10.1016/j.jece.2021.106419.

2. METHODOLOGY

This work has been carried out in the Laboratory of the Department of Chemical Engineering and Environmental Technologies (IQTMA) of the Technological College (Agri-food and Environment) of Huesca (University of Zaragoza). This section describes the methodology that has been carried out for its development, as well as the materials, experimental plants and procedures used to synthesize and test the catalysts in the catalytic selective reduction of nitrates reaction. Finally, a description of the characterization techniques used is made.

2.1. Materials and reactants

The materials and reagents used for the development of this thesis are listed below.
Gases:

- Hydrogen (H_2), 99.999% pure, Linde.
- Nitrogen (N_2),99.999% pure, Linde.
- Carbon dioxide (CO_2), 99.995% pure, Linde.

Liquids:

- Hydrochloric acid (HCl, 35 %), Labkem.
- Nitric acid 65% (HNO_3), PanReac.

Solids:

- Urea crystalline for analysis ($CO(NH_2)_2$), PanReac.
- Palladium nitrate 99.8% ($Pd(NO_3)_2 \cdot xH_2O$), AlfaAesar.
- Copper nitrate (98%, $Cu(NO_3)_2 \cdot 2.5H_2O$), AlfaAesar.
- Tin chloride dihydrate ($ClSn_2 \cdot 2H_2O$), AlfaAesar
- γ-alumina (Spheralite 505), Procatalyse.
- Sodium nitrate (99%, $NaNO_3$), PanReac.
- Graphite 4124, Asbury Carbons.
- Amberlite IR120 H^+, Sigma Aldrich.

2.2. Catalyst synthesis

This section describes the experimental techniques used for the synthesis of the catalysts used during the realization of this doctoral thesis as well as the equipment employed.

2.2.1. Catalyst supported on Al_2O_3

The catalyst series of $PdCu/Al_2O_3$ and $PdSn/Al_2O_3$ were synthesised via successive incipient wetness impregnation of the overnight dried γ-alumina. In this method, the volume of the solution employed is the same than the pore volume of the support impregnated, avoiding any excess of the solution and ensuring that all the promoter metal dissolved ends in the surface of the support. This method produces a good dispersion of the metal on the support, in most cases, the only drawback is that it can only be employed when the metal load is low. First, an aqueous solution of the promoter metallic precursor, $Cu(NO_3)_2$ or $ClSn_4$, was prepared at an appropriate concentration to attain the desired weight composition (wt. %) in the catalyst. Cu concentration in the $PdCu/Al_2O_3$ catalyst was fixed at 0.4% wt. for all the series, while in the $PdSn/Al_2O_3$ series, Sn varied from 0.2 to 2.5% wt. After this step, the impregnated support was dried at 100°C for 12 h and calcined in an open-air oven at 350°C for 12 h at a heating rate of 5°C/min. Subsequently, the solid was impregnated with a solution of the noble metallic precursor $Pd(NO_3)_2$ to achieve the selected weight composition of Pd, which ranged from 0.25% to 1% wt. for the $PdCu/Al_2O_3$ catalyst series and from 0.6% to 4% wt. for the $PdSn/Al_2O_3$ series. Following Pd impregnation, the solid was dried and calcined at 500°C for 12 h at a heating rate of 5°C/min.

Finally, the solid was milled and sieved to obtain a particle-size distribution of 80–200 μm. This particle size selection ensured that the data presented were not influenced by internal mass transport limitations. These catalysts were named as Pd(wt. %)$Cu0.4/Al_2O_3$ or Pd(wt. %)Sn(wt. %)/Al_2O_3 (Table 2.1).

Table 2.1 *Resume of the catalysts synthetized over Al_2O_3.*

Name	Noble metal (wt. %)	Promoter metal (wt. %)	Thermal treatment
0.25Pd0.4Cu/Al_2O_3	0.25	0.4	1st Impregnation (Sn or Cu): 350ºC;12h; β=5ºC/min in air 2nd Impregnation (Pd): 500ºC; 12h; β=5ºC/min in air
0.5Pd0.4Cu/Al_2O_3	0.5		
0.75Pd0.4Cu0.4/Al_2O_3	0.75		
1Pd0.4Cu/Al_2O_3	1		
1Pd0.2Sn/Al_2O_3	1	0.2	
1Pd0.4Sn/Al_2O_3		0.4	
1Pd1Sn/Al_2O_3		1	
1Pd1.2Sn/Al_2O_3		1.2	
1Pd2Sn/Al_2O_3		2	
1Pd2.5Sn/Al_2O_3		2.5	
0.6Pd1.2Sn/Al_2O_3	0.6	1.2	
1Pd1.2Sn/Al_2O_3	1		
2Pd1.2Sn/Al_2O_3	2		
4Pd1.2Sn/Al_2O_3	4		
0.4Sn1Pd/Al_2O_3	1	0.4	1st Impregnation Pd: 350ºC; 12 h; β=5ºC/min in air 2nd Impregnation Sn: 500ºC; 12h; β=5ºC/min in air

2.2.2. Catalysts supported on Asbury® graphite 4124

A series of catalysts based on Asbury® graphite (GA) as support was synthesised. Graphite Asbury® is a graphite with high specific surface area, between 325 and 375 m^2/g with mostly microporous structures, this porous are formed due to the aggregation of the flakes.

The initial step of this preparation involved overnight drying of graphite, followed by impregnation using incipient wetness impregnation method, as well as in the previous section. For the incipient wetness impregnation the graphite was impregnated with an aqueous solution containing both metallic precursor salts ($Pd(NO_3)_2$ and $Cu(NO_3)_2$) at an appropriate concentration to achieve a loading of 1% wt. of Pd and 0.4% wt. for Cu for all catalysts. For catalysts incorporating urea (named as -U catalysts), 1 g of urea per gram of graphite was introduced during the incipient wetness impregnation step, in combination with the metal precursors.

Nitric acid treatment was employed to induce chemical modifications in the support material. Before metal impregnation, the graphite was mixed with HNO_3 6M at a weight ratio of 1:6 (10 g of GA and 60 g of HNO_3 6M). This mixture was stirred for 1 h and subsequently washed with distilled water until neutral pH was achieved. Finally, the samples were dried overnight at 100°C. These catalysts were denoted as -HNO_3.

The last stage of catalyst synthesis treatment was the heat treatment, which was realized using two different methods:

a) Reducing atmosphere treatment (referred to as -r catalysts): The catalysts were subjected to a thermic treatment at 500 °C using a heating rate of 3ºC/min and with a total flow of 300 NmL/min (H_2/N_2:1/1). The synthesis temperature was maintained for 180 min. The catalysts were then cooled in the same flow till room temperature and, afterwards, passivated overnight with 100 NmL/min N_2. The experimental system used is explained in detail in section 2.3.1.

b) Oxidising atmosphere treatment (referred to as -a catalysts): The catalysts were exposed to a thermic treatment at 500 °C using a heating rate of 3ºC/min 500 °C for 3 min, using an open-air oven.

A summary of the synthetized catalysts is provided in Table 2.2.

Table 2.2 *Resume of the catalysts synthetized over GA.*

Name	Noble metal (wt. %)	Promoter metal (wt. %)	Chemical treatment	Thermal treatment
PdCu/GA-r	1	0.4	-	Co-Impregnation: 500ºC, 3h, β=3ºC/min, total flow of 300 NmL/min (H_2/N_2: 1/1)
PdCu/GA-U-r			Urea treatment	
PdCu/GA-HNO_3-r			HNO_3 treatment	
PdCu/GA-a			-	Co-Impregnation: 500ºC; β=3ºC/min,3 min in air
PdCu/GA-U-a			Urea treatment	
PdCu/GA-HNO_3-a			HNO_3 treatment	

2.3. Experimental systems

2.3.1. Description of the experimental setup

Thermal treatment for synthesis under oxidising atmosphere was realized in an open-air oven of Carbolite, model CWF 1200, with a maximum use temperature of 1200ºC and with a temperature controller Eurotherm 3216. On the other hand, the system for the shyntesis in reducing is composed by: i) horizontal quartz reactor ii) horizontal oven, iii) temperature measurement and control system and iv) system for measurement and control of inlet gas flows. A picture of this system for catalyst preparations under reducing atmosphere can be observed in Figure 2.1, as well as a scheme in Figure 2.1.

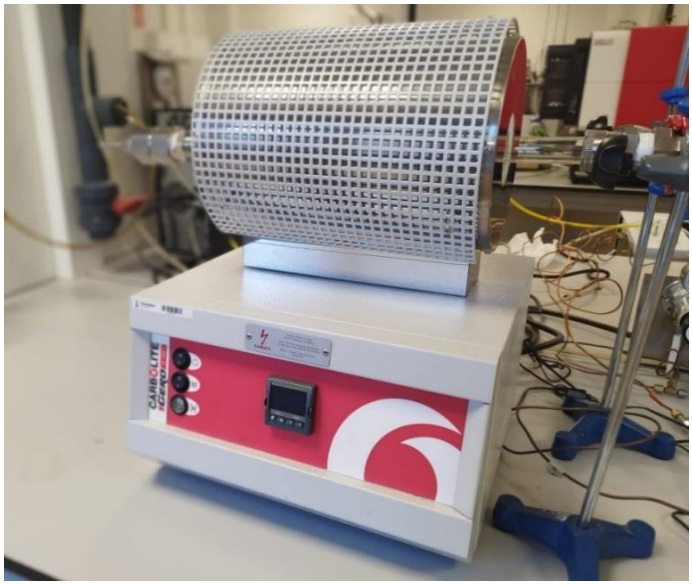

Figure 2.1 *Picture of the experimental plant for heat treatment in reducing atmosphere.*

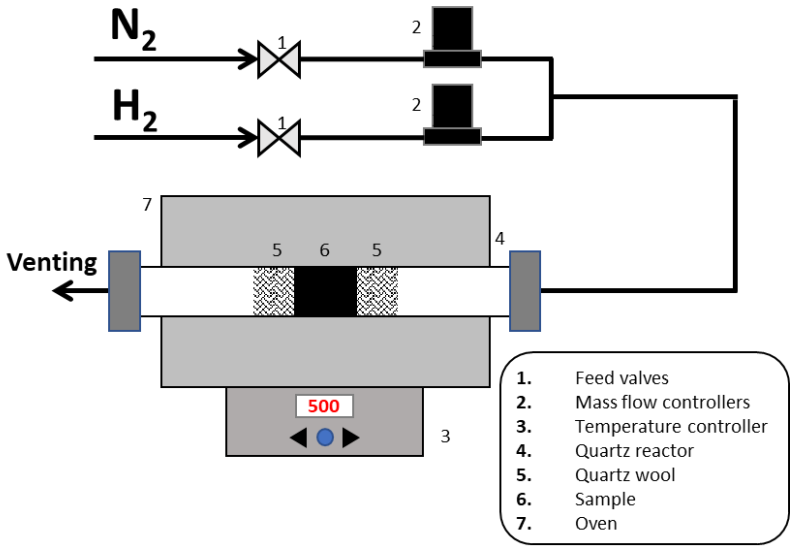

Figure 2.2 *Scheme of the experimental plant used for heat treatment in reducing atmosphere.*

The dimensions of quartz reactors used are 2.5 cm external diameter, 2.2 internal diameter and 46 cm length. They are introduced in the Carbolite cylindrical oven (model MTF 12-38-250), 300 mm long and 40 mm internal diameter, designed to work at a maximum temperature of 1200 ºC. The temperature is measured by a type K thermocouple, housed inside the oven. The temperature control is carried out by means of a Eurotherm controller, model 3216. The inlet flow of the gases introduced is measured and controlled by two mass flow controllers from the brand Allicat, which reach a maximum flow of 500 mL/min.

2.3.2. Operational description

In case of treatments carried out in an oxidizing atmosphere, the impregnated support (Al_2O_3 or GA) was placed in a crucible without cover and introduced in the open-air oven, selecting the heating rate, temperature and holding time treatment. The conditions selected for each catalyst are specified in Table 2.1 and 2.2.

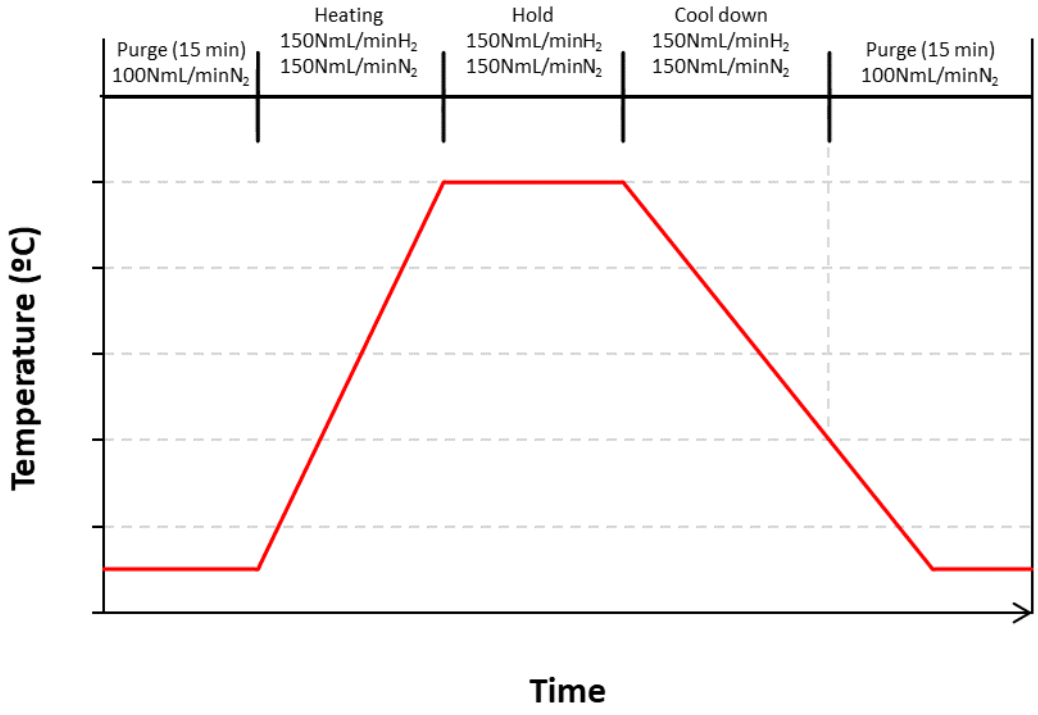

Figure 2.3 *Stages of the thermal treatment in reducing.*

For the preparations in reducing atmosphere, 5 g of GA previously impregnated were introduced in the reactor between two quartz wool beds to avoid the loss of the sample. A schematic diagram of the placement inside the reactor is shown in Figure 2.2. During thermal decomposition, unwanted liquid products such as bio-oil are formed. To decompose them, it introduced after the bed of impregnated graphite a commercial Ni/SiO_2-Al_2O_3 catalyst (AlfaAesar) with 66% wt. of Ni. After the introduction of the quartz reactor in the horizontal oven and plugged the connections, a flow of 100 NmL/min N_2 was set to purge the air for 15 min. After this, a total flow of 300 NmL/min (H_2/N_2:1/1) was set, heated at a rate of 3ºC/min until 500 °C and held at that temperature for 2h. Once the treatment was completed and the reactor was at a temperature lower than 100ºC, the flows was changed to 100 NmL/min of N_2 for 12h to passivate the catalyst (Figure 2.3). With this process, a stable catalyst is obtained once

extracted and exposed to the environment, which can be preserved without modifying its characteristics.

2.4. Catalyst reduction

2.4.1. Description of the experimental setup

Because of the different methods of catalyst synthesis used, different oxidation states of the metal phase of the catalysts can be found. To ensure that the metal phase of all catalysts was in its active form, they were subjected to reduction before their use. To prevent the oxidation with air during transfer from the reduction reactor to the reactor used for catalytic selective reduction of nitrates reaction, a passivation step was performed after reduction.

The scheme of the equipment used for this purpose is shown in Figure 2.4. It consists of the following fundamental parts: i) vertical quartz reactor of 1 cm diameter and 42 cm length, ii) vertical oven, iii) temperature measurement and control system (RKC REX-P90). A thermocouple type K protected by a quartz sheath was placed inside the reactor and, iv) system for measurement and control of inlet gas flows. Two gas flowmeters (Brooks Instruments B. V.) were used for the introduction of N_2 and H_2.

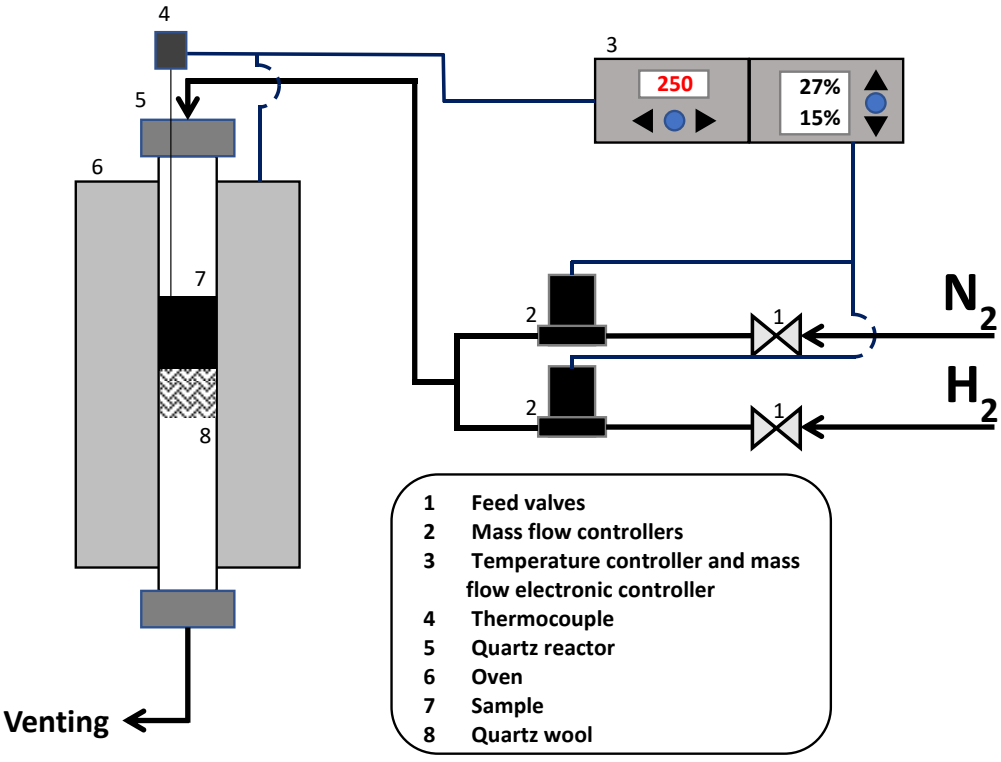

Figure 2.4 *Scheme of the experimental plant used for reduction of the catalysts.*

2.4.2. Operational description

The reduction-passivation step was performed as follows. First, a bed of quartz wool was placed at the centre of the reactor, after which the catalyst was weighed (700 mg) and placed on top of the wool. The thermocouple was then introduced into the reactor and its tip was placed on the top of the catalyst bed. The reactor was connected to pipes and a flow of 100 NmL/min N_2 was set to purge the air reactor. After 15 min, the flow was changed to 100 NmL/min of H_2, heated at a rate of 5ºC/min till the designed reduction temperature, and held at that temperature for 2h, excepts in some cases that can be observed in Table 2.5. Once the treatment was completed and the reactor was at a temperature lower than 100ºC, the flows was changed to 100 NmL/min for 12h to passivate the catalyst (Figure 2.5). In this way, the small amounts of oxygen in the N_2 gas produce mild oxidation of the external layers of the metal nanoparticles and avoid strong oxidation during the time in contact with air.

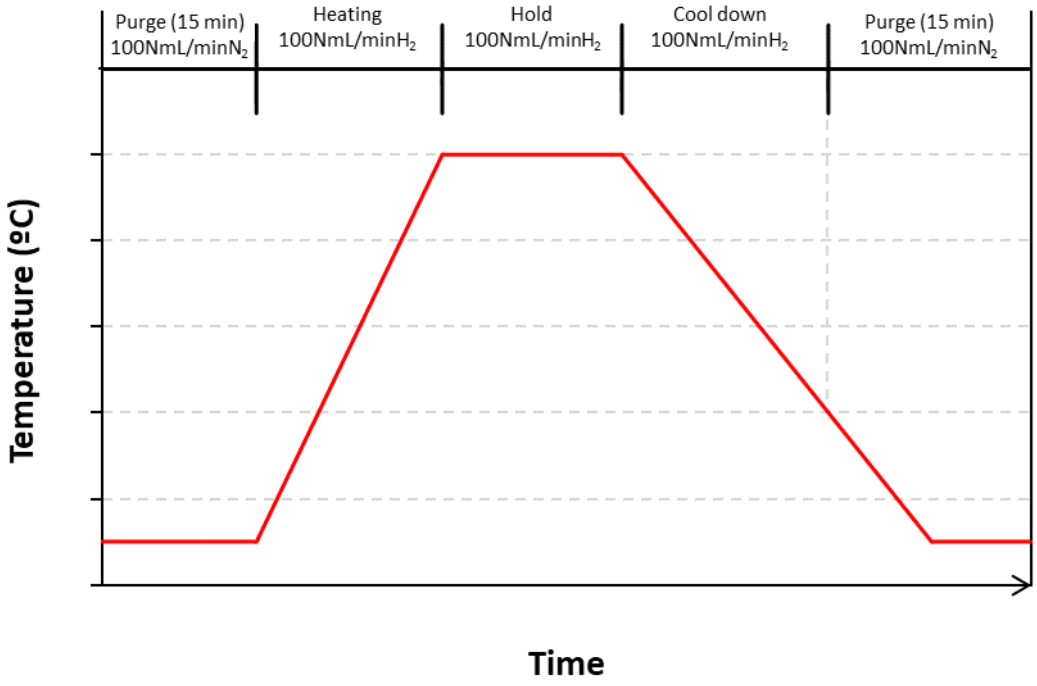

Figure 2.5 *Stages of the thermal reductions process before the CSNR.*

2.5. Experimental system for the Catalytic Selective Reduction of Nitrates (CSRN)

2.5.1. Description of the experimental setup

Figure 2.6 shows a scheme of the equipment used for the catalytic selective reduction of nitrates (CSRN). The experimental setup is formed for:

i) a 1-L semi-batch quartz reactor, which runs in semi-continuous mode at atmospheric temperature and pressure,

ii) a selective electrode (Mettler Toledo), which is employed to measure the pH of the reaction,

iii) Inlet gas flow measurement and control system. Three gas flowmeters (Alicat) are used for the introduction of H_2, N_2 and CO_2 gases, used respectively to purge the reactor of air, as reductant agent and as pH regulator,

iv) solution agitation control system with a magnetic stirrer (2.5 cm length and 0.7 cm diameter), which allows to select the agitation between 0 and 1500 r.p.m,

v) syringe sample extraction system.

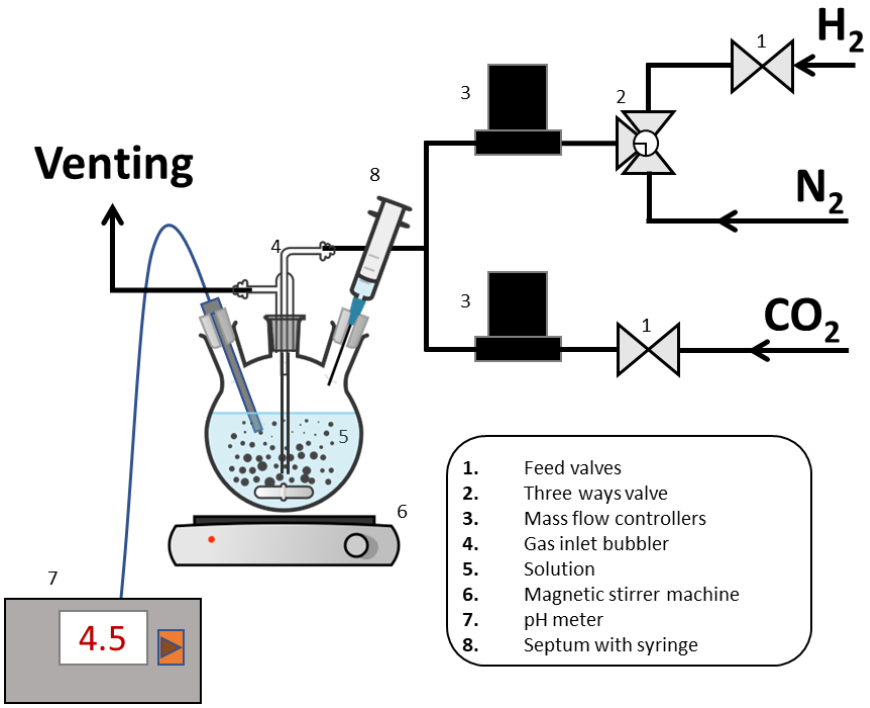

Figure 2.6 *Scheme of the Catalytic Selective Nitrate Reduction (CSNR) equipment.*

As can be seen in the Figure 2.6, the reactor has four inlets, two of which were threaded and 2 ground glass. The threaded sockets have a size of 29/32' (internal

diameter/external diameter). One of this is used for the selective electrode, which is introduced using a PVC-threaded plug, suitable for introducing the electrode, with a silicone gasket. The other one is used to introduce the catalyst into the reactor. On the other hand, one of the ground glass sockets was closed with a silicone septum of 14/23', that was used to introduce the solution with the initial concentration of nitrates and to collect the sample at different times with a syringe and a 15 cm long needle.

The last ground glass socket has a diameter of 29/32' and was located on the top of the round flask, which was used to introduce and extract the gases through a bubbler. The inlet and outlet pipes were 1/4" of nylon, which allowed the introduction of N_2 to purge the reactor of air, H_2 as reductant agent, and CO_2 as pH regulator.

2.5.2. Operational description

The steps involved in carrying out a nitrate reduction reaction test are described below. First, 600 mL of distilled water was introduced into the reactor, the desired stirring rate was set, and pipes were connected to the reactor by closing the entrances with plugs and inserting a pH meter. Subsequently, the reactor was purged with a flow of 100 NmL/min N_2 bubbling for 15 min to eliminate air. The pre-reduced catalyst was introduced into the CSRN reactor. Subsequently, the reactor was purged again to eliminate traces of air due to the introduction of the catalyst. Then, a flow of 100 NmL/min H_2 was bubbling for 1h to eliminate the oxide layer produced during the passivation step and ensure complete reduction of the catalysts. Finally, a flow of CO_2 was used to maintain an adequate pH and H_2 as the reducing agent; the flow is shown in each study. Then, a solution of 2500 ppm of NO_3^- made from $NaNO_3$ was introduced to obtain 625 mL of the solution and the desired initial concentration of NO_3^-. The exact operational conditions for the different catalysts are shown in Table 2.3, 2.4 and 2.5. This moment was set as time zero for reaction (t_0). Samples were extracted at fixed times with a syringe, filtered with a nylon filter of 25 mm diameter and 0.45 µm pore size, and saved in vials. At the end of the reaction, a flow of 100 NmL/min N_2 was fed for 30 min to eliminate H_2 present in the flask before opening it. Subsequently, the solution was filtered through a filtration flask with filter paper (5 µm) and a Buchner funnel. The solid was then dried at 100ºC for 12h and saved; the filtered liquid was saved.

Table 2.4 *Experimental conditions for the PdCu/Al_2O_3 catalysts*

Catalyst	**Nitrates (ppm)**	**Mod.**	**Red.Tº (ºC)**	**T. flow (NmL/min)**	**H_2/CO_2**	**r.p.m**	**Cat. load (g/L)**
1Pd0.4Cu/ Al_2O_3	100	-	250	500	1/1	520	1
						750	
						800	
						900	
						1200	
						1500	
1Pd0.4Cu/ Al_2O_3	100	-	250	500	1/1	750	1
0.75Pd0.4Cu/ Al_2O_3							
0.5Pd0.4Cu/ Al_2O_3							
0.25Pd0.4Cu/ Al_2O_3							
1Pd0.4Cu/ Al_2O_3	100	-	250	500	1/1	750	0.25
							0.5
							1
							2
1Pd0.4Cu/ Al_2O_3	100	-	250	900	No CO_2	750	2
					1/1		
					1/2		
					1/3		
1Pd0.4Cu/ Al_2O_3	100	Distilled water	250	500	1/1	750	1
		Mineral water					
		Tap water					
1Pd0.4Cu/ Al_2O_3	100	Cationic resin 0g	250	500	1/1	750	1
		Cationic resin 2g					
		Cationic resin 4g					
		Cationic resin 5g					
		Cationic resin 6g					

Table 2.5 *Experimental conditions for the PdSn/Al_2O_3 catalysts*

Catalyst	Nitrates (ppm)	Mod.	Red. Tº (Cº)	T. flow (NmL/min)	H_2/CO_2	r.p.m	Cat. Load (g/L)
1Pd0.4Sn/ Al_2O_3	100	-	250	300	1/2	750	1
0.4Sn1Pd/ Al_2O_3							
1Pd0.2Sn/ Al_2O_3	100	-	250	300	1/1	750	1
1Pd0.4Sn/ Al_2O_3							
1Pd0.8Sn/ Al_2O_3							
1Pd1.2Sn/ Al_2O_3							
1Pd2Sn/ Al_2O_3							
1Pd2.5Sn/ Al_2O_3							
4Pd1.2Sn/ Al_2O_3	100	-	250	300	1/1	750	1
2Pd1.2Sn/ Al_2O_3							
1Pd1.2Sn/ Al_2O_3							
0.6Pd1.2Sn/ Al_2O_3							
1Pd1.2Sn/ Al_2O_3	100	-	250	200	No Co2	750	1
				300	1/2		
				500	1/4		
1Pd1.2Sn/ Al_2O_3	100	-	250	300	1/2	750	1
			300				
			350				
			450				
			550				
1Pd1.2Sn/ Al_2O_3	100	Distilled water	250	300	1/1	750	1
		Tap water					

Table 2.6 *Experimental conditions for the PdCu/GA catalysts*

Catalysts	Nitrates (ppm)	Red. Tº (Cº)	T. flow (NmL/min)	H_2/CO_2	r.p.m	Cat. load (g/L)
1Pd0.4Cu/GA-r	100	250	500	1/1	1250	1
1Pd0.4Cu/GA-a						
1Pd0.4Cu/GA-U-r						
1Pd0.4Cu/GA-U-a						
1Pd0.4Cu/GA-HNO_3-r						
1Pd0.4Cu/GA-HNO_3-r						

2.5.3. Operational mode with cationic exchange resins

In some of the experiments, a cationic exchange resin (Amberlite IR120 H^+) was added simultaneously to the CSNR process to adsorb the NH_4^+ formed during the reaction. This resin was employed as a postoperative technique in combination with CSNR.

The adsorption isotherm of the resin and the nitrate solution used in the reactions was developed before carrying out the combined process. For this purpose, 10 ppm solution of NH_4Cl was prepared with a total volume of 625mL in the reactor employed for the CSNR. In addition, a quantity of resin Amberlite IR120 H^+ (0.05-6 g) was introduced in a vegetable fibre filter bag. This bag was closed manually with cotton threads and suspended in solution, as shown in Figure 2.7. The solution was agitated at a constant rate of 1200 r.p.m. and the starting time for the test (t_0) was the moment when the bag containing the resin was introduced into the solution. Through the septum, 2 mL samples were collected at fixed times until equilibrium was reached. NH_4^+ concentration was measured using a photometer as explained in section 2.5.4. The adsorption time was enough for the solution to reach the equilibrium. Afterwards, the adsorption isotherms were calculated by plotting the NH_4^+ concentration per gram of resin (ppm/g_{resin}) versus the cationic resin concentration (g_{resin}/L). The kinetic model of the adsorption of the NH_{4+} is explained in detail in section 3.2.3.1.

Tests with a combination of CSNR and NH_4^+ adsorption on the resin were performed according to the protocol described in section 2.4.2. Cationic exchange resin was introduced before the addition of 100 ppm NO_3^- to the solution.

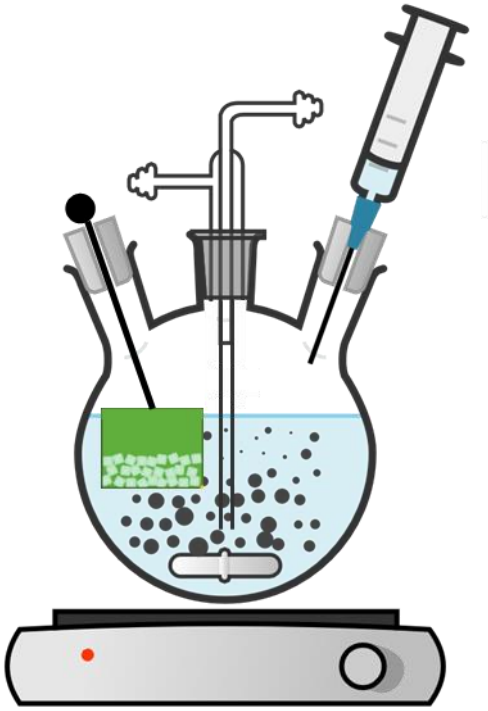

Figure 2.7 *Modification of the experimental setup for the CSNR when adding cationic resin.*

2.5.4. Sample analysis

The concentrations of NO_3^-, NO_2^-, and NH_4^+ of the samples obtained during the reaction were measured using a multiparameter photometer (COD HI83399, HANNA Instruments). The specific absorption of the light beam emitted by the different species at different wavelengths allows their quantification based on Beer–Lambert law, which relates the absorption of light to the properties of the sample using the following equation:

$$A = \varepsilon_\lambda \cdot l \cdot c \qquad (2.1)$$

Where A is the absorbance, ε_λ is the molar extinction coefficient at a wavelength (L/g.cm), l is the optical path through the substance (cm) and c is the molar concentration (g/L).

For the measures, the commercial 16 mm vials kits from HANNA were used. First, the ion to be analysed must be selected on the method selection screen of the photometer. Afterwards, a determinate amount of the sample is introduced in the vial, which depends on the ion and its estimated concentration. After carefully cleaning the surface of the vial, it was introduced into the holder of the photometer. “Zero” is then pressed to create a baseline value of absorption in case the sample itself absorbs part of the beam.

After this step, the reagent included in the kits is introduced in the vial, which is agitated and after the stipulated time and cleaning of the surface, it is introduced again in the photometer to obtain the concentration of the ion in ppm.

The methods employed for each kit were obtained from the instruction manual of the HANNA equipment employed and are as follows:

- Nitrates (NO_3^-): chromotropic acid method. Light beam wavelength: 420 nm.
- Nitrites (NO_2^-): adaptation of the Standard Method for the Examination of Water and Wastewater, 23rd Edition, 4500 B Diazotization Method, Nitrogen Nitrite. Light beam wavelength: 525 nm.
- Ammonium (NH_4^+): adaptation of the ASTM Manual of Water and Environmental Technology, D1426 Nessler method. Light beam wavelength: 420 nm.

After converting the data obtained to molar concentrations, nitrate conversion and nitrite and ammonium selectivities were calculated using Equations (2.2) and (2.3), respectively.

$$X_{NO_3^-} = 1 - \frac{[NO_3^-]_t}{[NO_3^-]_0} \tag{2.2}$$

$$S_i = \frac{[i]_t}{[i]_0 \cdot X_{NO_3^-}}; i = NO_2^-; NH_4^+ \tag{2.3}$$

In these equations, $X_{NO_3^-}$ is the nitrate conversion while $[NO_3^-]_t$ and $[NO_3^-]_0$ are the concentration of nitrates at the studied time the initial nitrate concentration respectively. S_i is the selectivity of a determined specie, calculated from the concentration of this specie at the study time $[i]_t$, the initial concentration of that specie $[i]_0$ and the nitrate conversion. There is an agreement that there are mainly four reaction products on this reaction: nitrites, nitrogen monoxide, diatomic nitrogen and ammonium. Because we only could measure nitrite and ammonium during the hydrogenation of nitrates [1–7], selectivity towards nitrogen and nitrogen monoxide were calculated based on the difference in selectivities (equation 2.4):

$$S_{(NO+N_2)} = 1 - S_{NO_2^-} - S_{NH_4^+} \tag{2.4}$$

Finally, the product yields (Y_i) were calculated using Equation 2.5.

$$Y_i = \frac{[i]_t}{\left[NO_3^-\right]_0}; i = NO_2^-; NH_4^+ \quad (2.5)$$

Where $[i]_t$, the concentration of this specie at the study time and $[NO_3]_0$ is the initial nitrate concentration.

2.6. Characterization techniques

It is important to know the composition, morphology, and structure of a catalyst because its activity depends on these properties. The chemical reactions carried out during this work depend mostly on the surface and textural properties. Therefore, it is essential to use different characterization techniques to thoroughly understand all the properties that influence catalytic activity.

In this work, two significantly different types of supports have been used, alumina and graphite.

Next, the different characterization techniques used in this doctoral thesis are detailed and described. These techniques have provided information about the entire sample, from the surface of the solid to its interior at an atomic level. The techniques used are X-ray diffraction, Transmission Electron Microscopy, Nitrogen adsorption analysis, Temperature Programmed Reduction, Atomic Absorption Spectroscopy, Temperature Programmed Desorption coupled with Mass Spectrometry and Raman spectroscopy.

2.6.1. X-ray diffraction (XRD)

XRD is an analytical technique that allows the identification of the crystal structure of a solid sample using a monochromatic X-ray beam with a variable incidence angle. Diffraction appears because the wavelength of the X-ray beam is of the same magnitude as the interplanar spacing in the crystal lattice. The incidence angle is related to the interplanar distance of the crystal lattice following Bragg's law (Equation 2.6):

$$2d \cdot sen\theta = n\lambda \quad (2.6)$$

where d is the interplanar distance of the crystal lattice, θ is the diffraction angle between the incident ray and diffraction plane, n is a whole number called the reflection order, and λ is the wavelength [8].

Each substance emits a different diffraction pattern, allowing the distinction of allotropes because diffraction depends not only on the composition of the substance but also on the distribution of the crystal lattice. This fact allows the identification of a particular substance in a mixture of compounds or crystal phases. To do this, a qualitative analysis is necessary to compare the position and intensity of the peaks in the diffraction pattern of the sample with a database that records the diffraction patterns of different substances. *The International Centre for Diffraction Data* has a database, *The Powder Diffraction File* [9], in which there is an extensive record of patterns. Furthermore, X-rays have high penetrating power; therefore, this technique is not limited to the surface planes of the sample.

Debye-Scherrer equation was used to obtain the structural parameter's values from the XRD spectrum [10]:

$$L_{c(002),a(100)} = \frac{K \cdot \lambda}{\beta_{c(002),a(100)} \cdot cos(\theta)} \qquad (2.7)$$

Where $\beta_{c(002),\ a(100)}$ is the full width at half maximum of the symmetrically shaped (002) and (100) diffraction peaks, and K is the shape factor equal to 0.89 and 1.84 for L_c (stack height of microcrystallite) and L_a (width of microcrystalline) respectively, depending on the peak employed.

A D-Max Rigaku diffractometer equipped with a Cu rotating anode was used for the XRD diffractograms presented in this study. The equipment was operated at a voltage of 40 kV and intensity of 80 mA. In addition, a graphite monochromator was used to select the Cu Kα radiation (λ=0.15418 nm). The analyses were performed with a scanning angle 2θ between 5 and 30º, at a rate of 0.03°/s. The data were processed using the High-Spore Plus program. All the analyses were performed using the X-ray Diffraction Service, belongs to the National Facility ELECMI ICTS, node "Laboratorio de Microscopias Avanzadas (LMA)" at the University of Zaragoza.

2.6.2. Transmission electron microscopy (TEM)

Transmission electron microscopy (TEM) is a technique that allows to obtain images at the nanometre scale, providing information about the structure and morphology of a solid.

To obtain a TEM image, a beam of electrons is directed onto a small amount of the solid. The electrons interact with the sample in three ways: absorption, scattering, or passing through the sample without interaction. The latter formed a TEM image. Additionally, some electron microscopes are equipped with energy-dispersive X-ray spectroscopy (EDX) detectors, which collect scattered electrons and provide information regarding the atomic composition of the sample [11]. In conventional TEM mode the image is generated, in the diffraction plane, only with the transmitted electron beam, since the size of the lens aperture does not allow the diffracted electrons to pass through. In HRTEM mode, the size of the lens aperture allows the passage of certain diffracted electrons. These interact with the transmitted electron beam to form the image. For this reason, the resolution obtained in HRTEM mode is almost atomic and obviously higher than in conventional TEM mode. Despite the excellent resolution of the HRTEM mode, the electromagnetic lenses generate defects, such as spherical and chromatic aberrations, which are visible in the image formed. To minimise these defects, transmission microscopes have been developed with aberration correction systems, allowing them to work in the sub-1 Å scale [12].

The images shown in this work were obtained using three different microscopes. Conventional TEM was carried out using a Tecnai T20, equipped with a LaB6 gun capable of operating in the 80-200 kV range, and a Veleta 2k × 2k CCD camera. A FEI Tecnai F30 equipped with a field emission gun (FEG) and a SuperTwin® objective lens, which allows a resolution of 0.19 nm, which operates at 200 and 300 kV. As it has a scanning module, it can work in TEM mode and in scanning-transmission mode (STEM). It is equipped with a High Angle Annular Detector (HAADF) for Z-contrast imaging. It is also equipped with an EDAX spectrometer for X-ray microanalysis and a Gatan Tridiem Energy Filter for electron energy loss spectroscopy (EELS) and energy filtered imaging (EFTEM). Combined with the STEM mode it allows to obtain chemical composition maps and profiles. For TEM mode imaging the microscope has the Gatan Ultrascan CCD 2k x 2k camera. Both of the microscopes belong the National Facility ELECMI ICTS, node “Laboratorio de Microscopias Avanzadas (LMA)” at the University of Zaragoza. And finally, high-resolution transmission electron microscopy (HR-TEM) was performed using an FEI Titan Cube Themis 60−300 microscope (Cs = 0.001 mm and sub-angstrom resolution) operating at 200 kV with a camera length of 11.5 cm and an aberration correction of 60−300. This microscope also offers a Super

XG2 option in STEM mode, which was employed to acquire STEM images of the catalyst at 200 pA and a dwell time per pixel of 128 μs.

The images obtained allowed to analyse the morphology of the catalysts and the distribution of the metal nanoparticles on the supports. For this purpose, an image processing software (Scope Photo 3.0) was used to measure for each sample the size of 100-200 nanoparticles in different images of the same sample. The mean nanoparticle size ($\overline{d_P}$) was calculated using the Sauter diameter equation [13]:

$$\overline{d_P} = \frac{\sum n_i \cdot d_i^3}{\sum n_i \cdot d_i^2} \qquad (2.8)$$

where $\overline{d_P}$ is the mean particle diameter and n_i the number of particles of diameter d_i.

2.6.3. Nitrogen adsorption analysis

The determination of the textural properties of the samples was realize by the adsorption of N_2 technique, that is based on the adsorption of N_2 on the surface of a solid sample. At a constant temperature below the critical temperature of the gas, the volume of gas adsorbed per mass of adsorbent depends on the relative pressure of the gas. The adsorption isotherm of a material can be obtained by plotting the volume of gas adsorbed per mass of solid against relative pressure. The numerical data for the desired textural properties were obtained by performing a series of mathematical analyses.

The Brunauer–Emmett–Teller (BET) method [14] was used to calculate the specific surface area. The method is based on Langmuir's theory on monolayer adsorption, extending it to multilayer adsorption. It is based on the following assumptions:

a) Adsorption can occur in multiple layers, with adsorbed molecules in the first layer serving as adsorption sites for the next layer of molecules.

b) The adsorption capacity of the centres does not depend on the occupancy of neighbouring centres. All adsorption centres were equivalent.

c) Except for the first layer, the heats of adsorption are equal.

Based on these assumptions, the following equation was formulated.

$$\frac{p}{\left[V\left(p^0 - p\right)\right]} = \frac{1}{V_m C} + \frac{C-1}{V_m C} \cdot \frac{p}{p^0} \qquad (2.9)$$

Where V is the volume of gas adsorbed at a pressure p, p^0 is the saturation pressure and V_m is the volume of the monolayer (the first layer adsorbed on the surface of the sample). Finally, C is an empiric constant that depends on the interaction between adsorbate and adsorbent. This equation can be graphically represented as a straight line, and the slope and intercept can be used to obtain the values of V_m and C. Usually, the application of the linearization of the adsorption isotherm is only valid in the range of p/p^0 = 0.05-0.20. From V_m, Avogadro's number and the diameter of the molecule, the specific surface area can be calculated.

The Brunauer-Emmett-Teller (BET) specific surface areas were measured from the adsorption branches in the relative pressure range of 0.01–0.10. The volume of micropores was calculated using the t-plot method developed by Lippens and de Boer [15]. The mean pore size was obtained by the method developed by Horvath and Kawazoe (HK)[16], based on the previous statistical analyses of Everett and Powl on the confinement of a fluid in a pore [17]. The HK method is an improvement over previously developed models because it takes into account that the adsorption potential varies as the pore size decreases.

Nitrogen adsorption–desorption isotherms were obtained at 77 K using a TriStar 3000 instrument (Micromeritics Instrument Corp) from the Institute of Nanoscience and Materials of Aragon (INMA) at the University of Zaragoza.

2.6.4. Temperature programmed reduction (TPR)

Temperature programmed reduction (TPR) is a material characterization process commonly used in catalysis studies to examine the surface chemistry of metals and metal oxides under varying thermal conditions. The test consists of a reduction reaction of a sample with a gas flow of H_2 diluted with an inert gas (N_2 in our case), with a constant increase in the temperature of the reaction. The measurement of the H_2 concentration at the reactor outlet allows knowing the H_2 consumed for the reduction of the sample. The plot of H_2 consumption versus time or temperature allows to know the reduction temperature of the different species present in the sample, also providing information on the interaction between them.

The analyses were performed using Quanchrome Instruments (TPR) equipment with a thermal conductivity detector (TCD) from the Institute of Nanoscience and Materials of Aragon (INMA) at the University of Zaragoza. The selected reduction temperature

range was from room temperature to 900 °C at a heating rate of 10 °C/min and total gas flow rate of 20 NmL/min (5% H_2/95% N_2).

2.6.5. Atomic absorption spectroscopy (AAS)

The composition of the catalysts was determinate by atomic absorption spectroscopy (AAS), elemental analysis method with good sensitivity in parts per million (ppm). The technique is based in two steps: conversion of an analyte into atomic vapour (atomization), and adsorption of radiation by these free atoms. The atoms absorb a specific wavelength based on the unique configuration of the electrons in the outer shell of the atom. In this technique a detector measures the photons emitted by the light source at the specific wavelength, this ray is interrupted by the absorption of some photons by the sample. Because absorbance is directly proportional to the concentration of the analyte in the sample, it can be obtained the concentration of specific elements depending on the wavelength of the source. The relation of the absorbance and the concentration is calculated with a calibration curve using patron solutions with known concentration of the analyte [18]. To measure the metallic content of the solid samples, it was necessary to dissolve them in an aqueous solution. Approximately 25 mg of the solid sample was stirred in 25mL of an aqua regia solution (chloride acid and nitric acid in a 3:1 ratio) for 24h. A flame was used to vaporise the solution, break the chemical bonds of the analyte, and become free atom vapour. A specific wavelength was used with hollow-cathode lamps to obtain absorption lines for each element.

The analyses were performed using a VARIAN atomic absorption spectrophotometre (SpectraA 110 model) equipped with an automatic dilution system (SIPS). The equipment programming and control were carried out using SPECTRAA 110 v.2.20 software.

2.6.6. Temperature programmed desorption coupled to a mass spectrometer (TPD-MS)

Superficial functional groups were studied using temperature-programmed desorption coupled to a mass spectrometer. The analysis was performed using ChemBet PULSAR equipment from Quantachrome, connected to a ThermoStar mass spectrometer from Balzers instruments. First, 40 mg of the sample was reduced at 250ºC with a total flow of 25 NmL/min of a H_2/He mixture with 20% H_2 to simulate the pre-reduction step performed on the catalysts before its introduction into the CSRN reactor. After cooling

to the ambient temperature, the sample was heated with a flow of 20 NmL/min of He to 900ºC at 10ºC/min and remained at that temperature for 30 min. The evolution of the desorbed species was followed by TCD, and signals with m/z values of 2, 15, 28, 30, and 44, related to H_2, CH_4, CO, NO, and CO_2, respectively, were obtained using a mass spectrometer. From the data obtained with the mass spectrometer we did a qualitative analysis of the compounds adsorbed on the surface of the catalyst, based on the bibliography. And from the signal of the TCD we obtained quantitative data of the CO_2 and CO desorbed per gram of sample, which is a proxy measure of two groups of compounds adsorbed on the catalyst.

2.6.7. Raman spectroscopy (Raman)

Raman spectroscopy is a non-destructive technique that allows the determination of the atomic structure of a sample. Raman spectroscopy is based on the dispersion of a monochromatic beam whose range extends from near ultraviolet light to near infrared light. When this beam interacts with the sample, it leads to the excitation of the sample and posterior emission of another photon with the same energy as the original one, and the sample returns to the same energy level as before the excitation. This phenomenon is called elastic dispersion or Rayleigh dispersion and is the most frequent one. However, at a much lower frequency, the molecule does not return to its previous state, and the emitted photons have different energies; this phenomenon is called Raman dispersion. When the photons emitted have less energy than the original, the wavelength is higher, and the frequency is smaller; this Raman dispersion is called Stokes. However, when the molecule ends at a lower energy level, the emitted photon has a smaller wavelength and higher frequency; this Raman dispersion is called anti-Stokes [19].

The analyses were performed using a WiTec Alpha300 confocal Raman microscope with a 532 nm laser excitation beam from the Institute of Nanoscience and Materials of Aragon (INMA) at the University of Zaragoza. The intensity ratios of the bands D (~1350 cm^{-1}), G (~1580 cm^{-1}) and 2D (~2690 cm^{-1}) characteristic of the carbon materials from different sample spots (three spectra) were obtained. From these values we calculated the relation *R* from the intensities of the bands D and G (I_G/I_D), that represent the defects present in the carbon, higher values can be translated as more

ordered carbon. From these results we obtained the value of the size of the crystalline layer of carbon, L_a [20]:

$$L_a = 4.35 \cdot R \qquad 2.10$$

2.6.8. X-ray photoelectron spectroscopy (XPS)

X-ray photoelectric spectroscopy, or XPS, is a surface analysis technique that allows the chemical composition of a material to be analyzed.

It consists of the emission of X-rays from the emitting source to the sample. These X-rays, when absorbed by the sample, excite the electrons of the atoms in the sample and are emitted outwards (photoelectrons). The binding energy (Eb) of these photoelectrons can be known thanks to the Equation 2.11:

$$E_b = h \cdot \nu - E_k - W \qquad 2.11$$

Where $h \cdot \nu$ is the energy of the beam emitted to the sample, E_k is the kinetic energy of the emitted photoelectron and W is the work function of the spectrometer. This binding energy is what identifies the atom and its electronic state, since its binding energy varies depending on whether it is bonded to another atom.

With this technique it is possible to know the elements that constitute the first 10 micrometers of a material and their relative percentage composition, with the exception of the atoms of hydrogen (H) and helium (He), which have a very low intensity signal in relation to the rest of the elements. Being two elements that only have electrons in their valence band, their energy is very low and therefore outside the range.

As the energy of the electrons varies when they are shared between two elements, the oxidation state of these elements can be known. Thus, if an electron from a carbon atom is bonded to an oxygen atom it will have a slightly different binding energy than if that same electron is bonded to another carbon [21].

Spectra were obtained from a Kratos Axis ULTRA spectrometer using non-monochromatic Al Kα radiation (hν = 1486.7 eV). All spectra were analyzed in the CASA® XPS software by applying a Shirley-type background which belongs to the National Facility ELECMI ICTS, node “Laboratorio de Microscopias Avanzadas (LMA)” at the University of Zaragoza.

2.7. References

[1] J.K. Chinthaginjala, L. Lefferts, Support effect on selectivity of nitrite reduction in water, Appl Catal B 101 (2010) 144–149. https://doi.org/10.1016/j.apcatb.2010.09.023.

[2] P. Xu, S. Agarwal, L. Lefferts, Mechanism of nitrite hydrogenation over Pd/γ-Al2O3 according a rigorous kinetic study, J Catal 383 (2020) 124–134. https://doi.org/10.1016/j.jcat.2020.01.003.

[3] T. Salmi, J. Warna, T. Maunulas, I. Turunen, Kinetics of nitrate reduction reactor, Chem Eng Sci 49 (1994) 5763–5773. https://doi.org/https://doi.org/10.1016/0009-2509(94)00331-9.

[4] I. Mikami, Y. Sakamoto, Y. Yoshinaga, T. Okuhara, Kinetic and adsorption studies on the hydrogenation of nitrate and nitrite in water using Pd-Cu on active carbon support, Appl Catal B (2003). https://doi.org/10.1016/S0926-3373(03)00021-3.

[5] S.D. Ebbesen, B.L. Mojet, L. Lefferts, In situ ATR-IR study of nitrite hydrogenation over Pd/Al2O3, J Catal 256 (2008) 15–23. https://doi.org/10.1016/j.jcat.2008.02.013.

[6] R. Zhang, D. Shuai, K.A. Guy, J.R. Shapley, T.J. Strathmann, C.J. Werth, Elucidation of Nitrate Reduction Mechanisms on a Pd-In Bimetallic Catalyst using Isotope Labeled Nitrogen Species, ChemCatChem 5 (2013) 313–321. https://doi.org/10.1002/cctc.201200457.

[7] R. Brunet Espinosa, D. Rafieian, R.S. Postma, R.G.H. Lammertink, L. Lefferts, Egg-shell membrane reactors for nitrite hydrogenation: Manipulating kinetics and selectivity, Appl Catal B 224 (2018) 276–282. https://doi.org/10.1016/j.apcatb.2017.10.058.

[8] M. Faraldos Izquierdo, S. Pérez Ferreras, Difracción de rayos X, in: M. Faraldos Izquierdo, C. Goberna (Eds.), Técnicas de Análisis y Caracterización de Materiales, 3rd ed., 2021: pp. 489–560.

[9] International Centre of Diffraction Data, (2023).

[10] M. Deraman, N.E.S. Sazali, M.F.Y.M. Hanappi, N.S.M. Tajuddin, E. Hamdan, M. Suleman, M.A.R. Othman, R. Omar, M.A. Hashim, N.H. Basri, N.S.M. Nor, B.N.M.

Dolah, A.M. Noor, M.R.M. Jasni, Graphene/semicrystalline-carbon derived from amylose films for supercapacitor application, in: J Phys Conf Ser, Institute of Physics Publishing, 2016. https://doi.org/10.1088/1742-6596/739/1/012085.

[11] I. Díaz, L. Pascual, Microscopía electrónica de materiales, in: M. Faraldos, C. Goberna (Eds.), Técnicas de Análisis y Caracterización de Materiales, 3rd ed., 2021: pp. 563–591.

[12] F. Cazaña, Síntesis y aplicaciones de nuevos materiales carbonosos: Carbón biomórfico y Grafeno, (2016) 293.

[13] G. Bergeret, P. Gallezot, Particle Size and Dispersion Measurements, in: G. Ertl, H. Knözinger, J. Weitkamp (Eds.), Handbook of Heterogeneous Catalysis, Wiley-VCH, Weinheim, 1997.

[14] S. Brunauer, P.H. Emmett, E. Teller, Adsorption of Gases in Multimolecular Layers, 1938. https://pubs.acs.org/sharingguidelines.

[15] B.C. Lippens, J.H. de Boer, Studies on pore systems in catalysts: V. The t method, J Catal 4 (1965) 319–323. https://doi.org/http://dx.doi.org/10.1016/0021-9517(65)90307-6.

[16] G. Horvath, K. Kawazoe, Method for the Calculation of Effective Pore Size Distribution in Molecular Sieve Carbon, Journal of Chemical Engineering of Japan 16 (1983) 470–475. https://doi.org/https://doi.org/10.1252/jcej.16.470.

[17] D.H. Everett, J.C. Powl, Adsorption in Slit-like and Cylindrical Micropores in the Henry's Law Region, Journal of the Chemical Society, Faraday Transactions 1 72 (1976) 619–636.

[18] R. Garcia, A.P. Báez, Analysis of High Solid Content in Biological Samples by Flame Atomic Absorption Spectrometry., INTECH Open Access Publisher, Pakistan, 2012.

[19] M.A. Bañares Gonzalez, V. Calvino Casilda, A. Serrano-Lotina, Espectroscopía Raman, in: M. Faraldos, C. Goberna (Eds.), Técnicas de Análisis y Caracterización de Materiales, 3rd ed., 2021: pp. 191–219.

[20] TUINSTRA F, KOENIG JL, RAMAN SPECTRUM OF GRAPHITE, Journal of Chemical Physics 53 (1970) 1126–1130. https://doi.org/10.1063/1.1674108.

[21] S.G. Booth, A.M. Tripathi, I. Strashnov, R.A.W. Dryfe, A.S. Walton, The offset droplet: a new methodology for studying the solid/water interface using x-ray photoelectron spectroscopy, Journal of Physics: Condensed Matter 29 (2017) 454001. https://doi.org/10.1088/1361-648X/aa8b92.

3. KINETIC MODEL OF CSRN

3.1. Reaction mechanism

The reaction mechanism of the catalytic selective reduction of nitrates (CSRN) was described by Vorlop and Tacke (1989) [1] and is still the most accepted reaction scheme. Based on this mechanism, Prüssen and Vorlop [2] proposed a scheme as shown in Figure 3.1., where there are multiple consecutive reduction steps using a reduction agent and employing bimetallic catalysts with an active phase with a noble metal (typically Pd or Pt) and a promoter metal (typically Cu, Sn, or In) over a support.

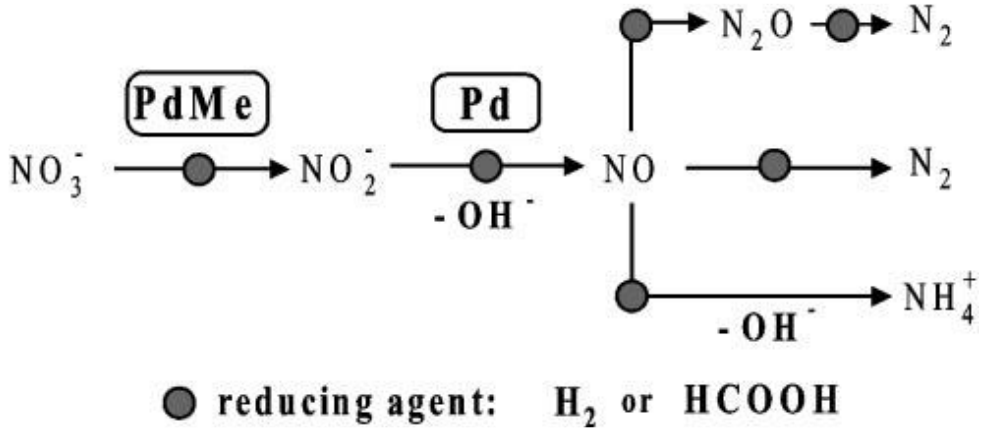

Figure 3.1 *Reaction scheme proposed by Prüssen and Vorlop [2].*

In the first step, nitrates (NO_3^-) are adsorbed over the promoter metal and then reduced to nitrites (NO_2^-). This promoter metal is regenerated through the spill-over of the hydrogen (H_2) chemisorbed on the noble metal. Then, NO_2^- is desorbed from the promoter metal and adsorbed by the noble metal, where the rest of the process takes place. In the following steps, NO_2^- is reduced to NO, an intermediate molecule. Finally, NO can be transformed into molecular nitrogen (N_2) or ammonium (NH_4^+). Alternatively, NO may become N_2O and transform into N_2. This reaction may occur on monometallic catalysts, where the support acts as the promoter metal (for example, Pd/SnO_2).

In order to identify the oxidation of the metals during a reaction, Edelmann et al. [3] performed an X-Ray Absorption Spectroscopy (XAS) study “in-situ”, using 3 catalysts: Cu/Al_2O_3, Pd/Al_2O_3 and $PdCu/Al_2O_3$. They reported how Pd was reduced in Pd/Al_2O_3 and $PdCu/Al_2O_3$ catalysts. In contrast, Cu was completely oxidised during the reaction in Cu/Al_2O_3 and partially oxidised in the bimetallic catalyst $PdCu/Al_2O_3$.

In the Figure 3.2. it can be seen the reaction scheme is based on the oxidation of metals in the catalyst during CSRN. In Scheme 1, Epron et al. [4] proposed the reduction of

NO_3^- through a redox reaction with the promoter metal, copper, in this case, oxidising Cu^0 to Cu^{2+} and reducing NO_3^- to the intermediate species NO_2^- or directly to N_2 and NH_4^+. And the role of the noble metal (Pd) is the adsorption of H_2 and the regeneration of Cu. However, reduction of NO_2^- can occur in Cu or Pd. Barrabes et al. (2006) [5] added a second step of nitrite reduction based on their results of XPS, as shown in Figure 3.2. (Scheme 2). In contrast to Scheme 1, the reduction of NO_2^- occurs only in noble metals (Pd or Pt), oxidising this metal in the process (Pd^{2+} or Pt^{2+}). This noble metal is regenerated through hydrogen, which adsorbs onto its metal state. Gao et al.[6] also guessed that the reduction of NO_3^- occurs in the promoter metal nano particles. In their study, a Pd-Cu/TiO_2 catalyst was used, and they reported that NO_3^- was adsorbed in Cu_2O which is activated (Cu*) by the spill-over hydrogen from Pd. For this reason, in strongly acidic solutions, the reduction of Cu_2O to Cu^0 is inhibited, as is the NO_3^- reduction.

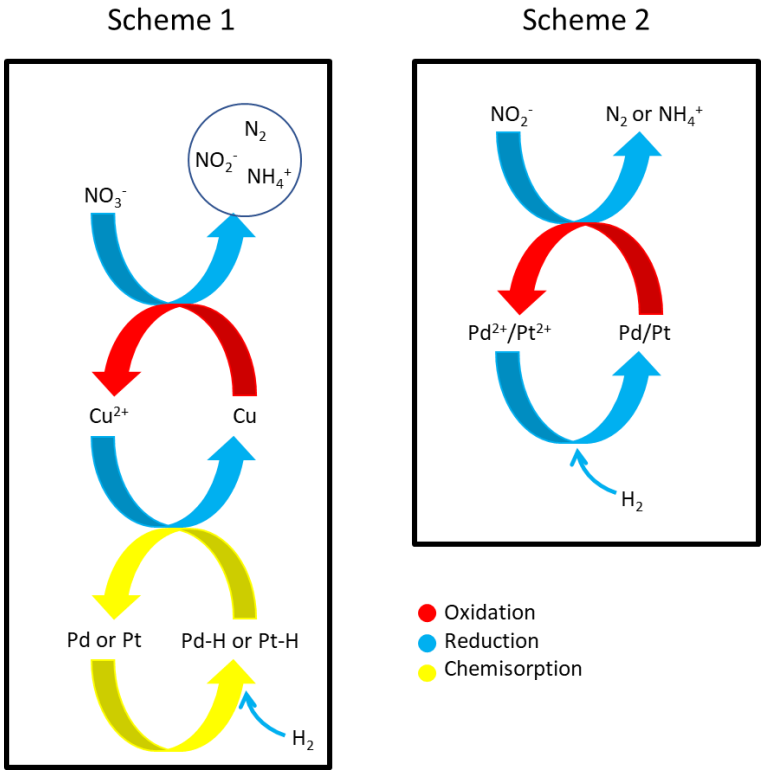

Figure 3.2 *Metal redox reactions and active sites in CSRN. Scheme 1, proposed by Epron et al. [4], and Scheme 2, modified by Barrabés et al. [5]*

Warna et al. [7] proposed a mechanism that considers the formation and subsequent hydrogenation of the intermediate compound NO* (*adsorbed) as the most important step in the CSRN, owing to their direct influence on the formation of the final products (NH_4^+ and N_2). Barbier et al. [8] and Horold et al. [9] also guessed the importance of

this intermediate compound, according to these authors, the reactions that take place at the liquid-solid interface are:

$$H_2 + 2^* \leftrightarrow 2H^* \qquad \text{eq.(i)}$$

$$NO_3^- + H^* \rightarrow NO_2^* + OH^- \qquad \text{eq. (ii)}$$

$$NO_2^* \leftrightarrow NO_2 + ^* \qquad \text{eq. (iii)}$$

$$2NO_2 + 2OH^- \rightarrow NO_2^- + NO_3^- + H_2O \qquad \text{eq. (iv)}$$

$$NO_2^- + H^* \rightarrow NO^* + OH^- \qquad \text{eq. (v)}$$

$$NO_2^* + H^* \rightarrow NO^* + OH^* \qquad \text{eq. (vi)}$$

$$NO^* + 2H^* \rightarrow NH^* + OH^* + ^* \qquad \text{eq. (vii)}$$

$$2NH^* \rightarrow N_2 + 2H^* \qquad \text{eq. (viii)}$$

$$NH^* + H^* \rightarrow NH_2^* + ^* \qquad \text{eq. (ix)}$$

$$NH_2^* + H^* \rightarrow NH_3^* + ^* \qquad \text{eq. (x)}$$

$$NH_3^* \rightarrow NH_3 + ^* \qquad \text{eq. (xi)}$$

$$NH_3 + H_2O \rightarrow NH_4^+ + OH^- \qquad \text{eq. (xii)}$$

$$OH^* + H^* \rightarrow H_2O + 2^* \qquad \text{eq. (xiii)}$$

Where * are the vacancies on the surface of the catalyst and X* is the compound adsorbed on the surface of the catalyst. The equations used are as shown in Figure 3.3.

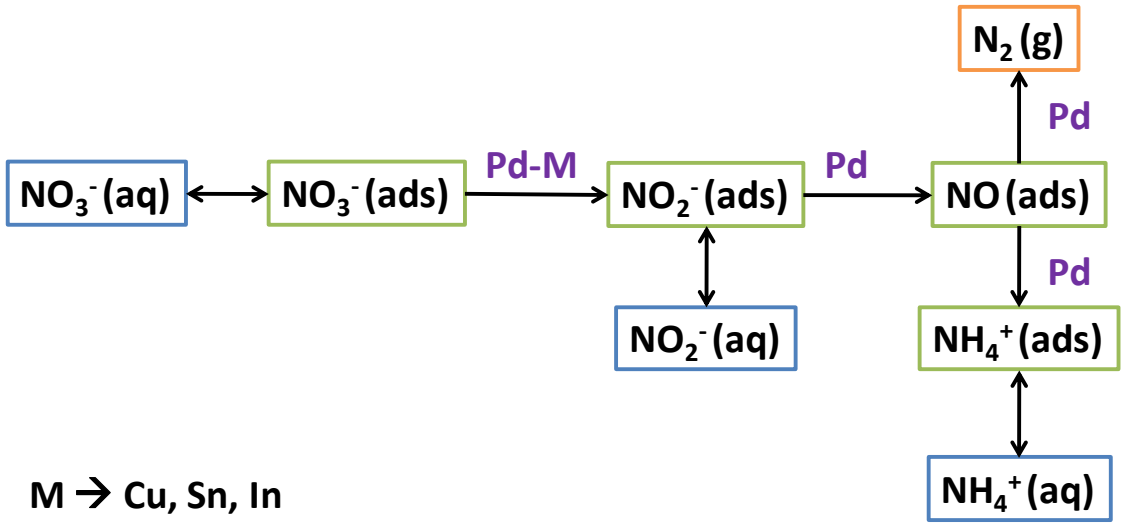

Figure 3.3 *The reaction scheme for the CSRN by Warna et al. [7].*

First, H_2 is adsorbed on the noble metal (eq.(i)), as shown in Fig. 3.4 where the adsorption and reaction of H_2 proposed by Prüssen and Vorlop [2] are presented. Subsequently, the adsorbed hydrogen (H*) reacts with NO_3^- to form NO_2* (eq.(ii)). This reaction takes place in the bimetallic particle (Pd-Me), whereas the following reaction takes place in the noble metal (Pd). The equation (iii) shows the equilibrium between the adsorbed NO_2* and the NO_2, this NO_2 reacts with OH^- present in the solution and becomes NO_2^-. NO_2^- is reduced by H* to form NO* (eq(vi)). There are two pathways for the reduction of NO*.

a) NO* reacts with H*, becomes NH*, and subsequently dissociates in N_2 (eqs. vii-viii).
b) The NO* reacts successively with H* till NH_4^+ (eqs. ix-xii)

Finally, the adsorbed compounds, OH* and H*, may react to form H_2O (eq. xiii).

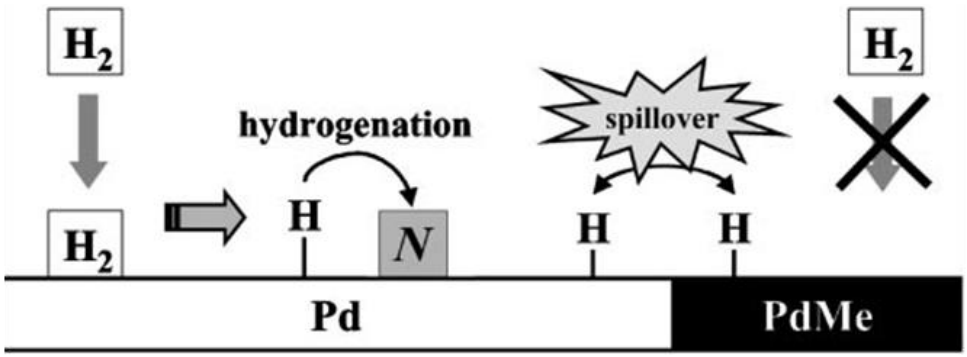

Figure 3.4 *Adsorption and reaction scheme for hydrogen on the surfaces of Pd and PdCu by Prüsse and Vorlop [2].*

Later, Ilinitch et al. [10] doubted the formation of N_2 from the dissociation of NH*, as stated by the model of Wärna et al. [7] (eqs. vii-viii). Alternatively, they proposed a mechanism for the formation of N_2 from a combination of two N* atoms (ec(xv)), which was explained previously by Barbier et al. [8]. In addition, the formation of NH* to form NH_3 would result from the hydrogenation of N*, as shown in eq. xvi, instead of eq. vii. The subsequent hydrogenation of NH* follows the same path as that proposed by Wärna et al. eqs. ix-xii. This mechanism was corroborated by Rahkamaa et al. [11] throw FTIR and the use of a metallic monolith of Pd as catalyst.

$$NO^* \rightarrow N^* + O^* \qquad \text{eq. (xiv)}$$

$$N^* + N^* \rightarrow N_2 + 2^* \qquad \text{eq. (xv)}$$

$$N^* + H^* \rightarrow NH^* \qquad \text{eq. (xvi)}$$

Various authors [1,8,12] added another mechanism to that proposed by Wärna et al., where it is said that the N* produced may react with NO* to produce N_2O.

$$N^* + NO^* \rightarrow N_2O \qquad \text{eq. (xvii)}$$

Fan et al. [13] considered a different origin for the formation of N_2. They hypothesised that N_2 originated from a direct reaction between NO* and H* to form N*. This N* reacts with other NO* and becomes N_2 (eqs. xviii-xix). Regarding NH4 + formation, they supported the model proposed by Ilinitch et al. However, they disagree with Barbier et al. regarding the formation of N_2O, which was not observed when using $PdSn/Al_2O_3$ catalysts.

$$NO^* + H^* \rightarrow N^* + OH^* \qquad \text{eq. (xviii)}$$

$$N^* + NO^* \rightarrow N_2 + O^* + ^* \qquad \text{eq. (xiv)}$$

Yoshinaga et al. [14] studied the influence of the active sites on the selectivity toward the final products. For this purpose, they studied their XRD results. In the proposed model, as shown in Fig. 3.5. studied three different catalysts, PdCu/active carbon, with different amounts of Cu: a) 5%Pd, b) 5%Pd-0.6%Cu, and c) 5%Pd-3%Cu. They proposed two different methods of NO_2^- reduction depending on the location of the absorption sites:

i) If it is adsorbed on the terrace surface of the Pd, where the hydrogenation is mild, the NO_2^- is more likely to product N_2, as shown in Figure 3.5.a

ii) If it is adsorbed on the edges of the nanoparticle are isolated between Cu atoms, it is more likely to produce NH_4^+, as shown in Figure 3.5.a and 3.5.c.

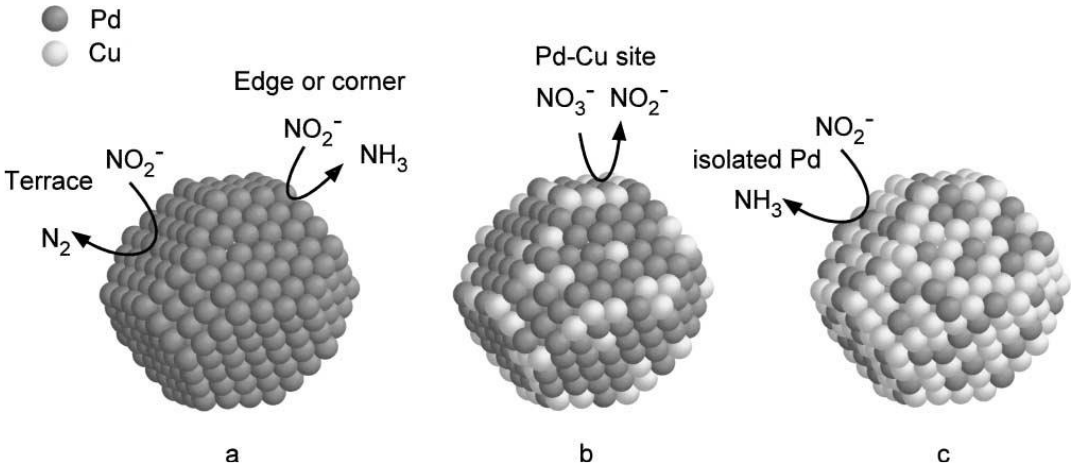

Figure 3.5. *Reaction scheme depending on the active sites where hydrogenation occurs for different catalyst loadings: (a) 5% Pd, (b) 5%Pd-0.6%Cu, and (c) 5%Pd-3%Cu proposed by Yoshinaga et al. [14]*

On the other hand, an increase in the quantity of Cu means a faster conversion of NO_3^-, but it produces an increase in the selectivity towards NH_4^+. They showed an increase in the selectivity towards N_2 for atomic relations lower than 1%. The authors think that due to the dispersion of Cu on the nanoparticles, the Pd atoms are more separated (Figure 3.5.c); therefore, the NO_2- adsorbed on Pd is also more separated, making the combination of two nitrogen atoms more unlikely and favouring the formation of NH_4^+. They also suggested that an increase in the Pd content produced a higher crystallisation of the nanoparticles and a higher N_2 selectivity. In 2007, Sá et al. [15] tested the relationship between the crystalline net and the N_2 selectivity. They poisoned the Pd sites with Bi, a geometrical poison in specific locations of the Pd net, but there weren't relevant changes in the N_2 selectivity.

3.2. Kinetic model of the catalytic selective reduction of nitrates

An important area to explore is the realization of exhaustive and realistic kinetic studies to elucidate the reaction mechanism, and through an adequate design of the catalyst and the operating conditions in the reactor, maximizing the selectivity of the reaction to N_2.

3.2.1. Type of kinetic models

3.2.1.1. Power-Law model

The power-law model has been used empirically because of its similarity to the kinetic equations used in homogeneous reactions for the hydrogenation of nitrates. In this case, the adsorption follows the Freund isotherm [16,17], and then the reaction rate of nitrates elimination, $(-r_{NO_3^-})$, can be expressed as:

$$(-r_{NO_3^-}) = -\frac{dC_{NO_3^-}}{C_{cat} \cdot dt} = k_p^{'} \cdot C_{NO_3^-}^{n} \tag{3.1}$$

Where, $C_{NO_3^-}$, is the concentration of nitrate, C_{cat} is the concentration of the catalyst, k_p is the intrinsic kinetic constant of nitrate reduction. The integration of the above expression allows to know the evolution of nitrate concentration over time. Thus, if the order of the reaction is one (n=1), we obtain the following exponential model:

$$C_{NO_3^-} = C_{NO_3^-,0} \cdot \exp(-k_p \cdot t) \quad ; \quad k_p = k_p^{'} \cdot C_{cat} \tag{3.2}$$

If $n \neq 1$, the following expression is obtained:

$$C_{NO_3^-} = \frac{C_{NO_3^-,0}}{(1 + k_{obs} \cdot t)^m} \tag{3.3}$$

Where k_{obs} and m are given by the following equations:

$$k_{obs} = (n-1) \cdot k_p \cdot C_{NO_3^-,0}^{(n-1)} \; ; \; m = 1/(n-1) \; ; \; k_p = k_p^{'} \cdot C_{cat} \tag{3.4}$$

If the order is higher than 1 (n>1), then the value of m is between zero and one (0<m<1), and k_{obs} has a positive value (hyperbolic model). If the order is between zero and one (0<n<1), then m and k_{obs} are negative (m<0; k_{obs}<0), resulting in a parabolic model. The exponential and hyperbolic models predict and end for nitrate concentration at infinite time. On the other hand, the parabolic model predicts a determinate time when the total conversion of nitrates is reached; this time can be calculated as:

$$\left(t_{final}\right)_{X_{NO_3^-}=1} = \frac{C_{NO_3^-,0}^{(1-n)}}{(1-n) \cdot k_p} \tag{3.5}$$

The usual way to calculate the kinetic parameters (k_p and n) is to convert them into the form of a linear equation:

$$\ln(-r_{NO_3^-}) = \ln(k_p) + n \cdot \ln(C_{NO_3^-}) \tag{3.6}$$

From this expression, the kinetic order can be calculated from the logarithmic derivative [18–20]

$$n = \frac{d(\log(-r_{NO_3^-}))}{d(\log(C_{NO_3^-}))} = \frac{d((-r_{NO_3^-})}{d(C_{NO_3^-})} \cdot \frac{C_{NO_3^-}}{(-r_{NO_3^-})} \tag{3.7}$$

Finally, the constant of reaction k_p is calculated as

$$k_p = \frac{(-r_{NO_3^-})}{C_{NO_3^-}^n} \tag{3.8}$$

In this equation, the value of the order n is obtained from Equation (3.7). If the catalyst is deactivated, the reaction rate decreases. Then, the activity of the catalyst, a, is the division of the reaction rate at time 0 and at a given time t:

$$a = \frac{(-r_{NO_3^-})_t}{(-r_{NO_3^-})_0} \tag{3.9}$$

The reaction rate was then calculated using the following expression:

$$(-r_{NO_3^-})_t = (-r_{NO_3^-})_0 \cdot a = k_p \cdot C_{NO_3^-}^n \cdot a \tag{3.10}$$

To calculate the activity of the catalyst over time, it was necessary to determine the deactivation rate. According to the model of Levenspiel, the deactivation can be calculated by a power type kinetic model [21,22]

$$-\frac{da}{dt} = k_d \cdot a^d \tag{3.11}$$

Where the terms k_d and d are the deactivation kinetic constant and the deactivation order, respectively. If k_d is constant, then equation can be integrated when d=1 and $d \neq 1$:

$$a = \exp(-k_d \cdot t) \quad ; \quad d = 1 \tag{3.12}$$

$$a = \frac{1}{(1 + (d-1) \cdot k_d \cdot t)^m} \quad ; \quad m = \frac{1}{d-1} \quad ; \quad d \neq 1 \tag{3.13}$$

For example, if *d=2*, the activity is derived from the following equation:

$$a = \frac{1}{1 + k_d \cdot t} \quad ; \quad d = 2$$

This model predicts that $d \geq 1$ the activity of the catalyst will be zero at t $\rightarrow\infty$, however, if the deactivation order takes values between 0 and 1, $0 < d < 1$, this model predicts that the activity of the catalyst will be cero in a finite time, given by:

$$t\big|_{a=0} = \frac{1}{(1-d) \cdot k_d} \tag{3.14}$$

The Levenspiel model predicts that the activity of a catalyst will reach zero. If the catalysts show residual activity (a_S) at high reaction times, the deactivation kinetics must be expressed as [23–27]

$$-\frac{da}{dt} = k_d \cdot (a - a_s)^d \tag{3.15}$$

$$-\frac{da}{dt} = k_d \cdot a^d - k_r \cdot (a^{d_m} - a) \tag{3.16}$$

Deactivation affects the prediction of Equations 3.1, 3.2, and 3.3. For example, considering the deactivation of the catalyst, when the reaction order is 1 (*n*=1) and the deactivation order is also 1 (*d*=1), the reaction rate can be expressed as

$$(-r_{NO_3^-}) = k_p \cdot C_{NO_3^-} \cdot \exp(-k_p \cdot t) \tag{3.17}$$

By integrating this equation, the result is:

$$C_{NO_3^-} = C_{NO_3^-,0} \cdot \exp\left(-\frac{k_p}{k_d} \cdot (1 - \exp(-k_d \cdot t)) \right) \tag{3.18}$$

This is a significant change from equation 3.2 for the same reaction order. If the deactivation is a second-order reaction (*d*=2) and following the previous procedure, the following equation is obtained:

$$C_{NO_3^-} = \frac{C_{NO_3^-,0}}{\left(1 + k_d \cdot t\right)^{k_p/k_d}} \tag{3.19}$$

This equation is analogous to Equation 3.3, despite the fact that the kinetic constants have completely different meanings. Thus, the exponent of the denominator is now the

division of the reaction and deactivation kinetic constants (k_p/k_d), and the observed kinetic constant coincides with the deactivation kinetic constant (k_d). This makes both models so similar that it is impossible to discern between them with only direct kinetic measures, so it is very difficult to detect deactivation of the catalyst in a discontinuous reactor of perfect mix. Nevertheless, when the catalyst is deactivated, the reaction rate can generally be expressed as

$$(-r_{NO_3^-}) = f_1(C_{NO_3^-}) \cdot f_2(t) \tag{3.20}$$

Therefore, if we proceed to calculate the observable reaction order under these conditions, applying the logarithmic derivative, equation 3.7, to equation 3.20, the following equation is obtained:

$$n = \left(\frac{df_1(C_{NO_3^-})}{d(C_{NO_3^-})} \cdot f_2(t) + f_1(C_{NO_3^-}) \cdot \frac{df_2(t)}{d(C_{NO_3^-})} \right) \cdot \frac{C_{NO_3^-}}{(-r_{NO_3^-})} \tag{3.21}$$

Combining this equation with equation 3.17, for first-order deactivation, the resulting observable kinetic reaction order is:

$$n = 1 + \frac{k_d}{k_p} \cdot \exp(k_d \cdot t) \tag{3.22}$$

For second-order deactivation;

$$n = 1 + \frac{k_d}{k_p} \tag{3.23}$$

In both cases, the apparent reaction kinetic order was higher than 1, and this kinetic order was proportional to deactivation, k_d. In the case of first-order deactivation, the kinetic order increased over time. In conclusion, this equation shows that by analysing the evolution of nitrate concentration over time with a power-type model, a high reaction order is obtained, and deactivation of the catalysts can be achieved. However, this must be confirmed using other methods.

3.2.1.2. Langmuir-Hinshelwood type model.

Most of the models employed were of the Langmuir-Hinshelwood (L-H) type [8,25,33]. In this type of model, it is assumed that the adsorption of nitrates follows the Langmuir

isotherm [16,17]. Therefore, they are adsorbed on the same type of active site, obtaining the following expression:

$$(-r_{NO_3^-}) = \frac{k \cdot K_{NO_3^-} \cdot C_{NO_3^-} \cdot \sqrt{K_{H_2} \cdot C_{H_2}}}{1 + K_{NO_3^-} \cdot C_{NO_3^-} + \sqrt{K_{H_2} \cdot C_{H_2}} + \sum K_i \cdot C_i} \tag{3.24}$$

If the concentration of hydrogen is constant, equation (3.24) can be expressed as

$$(-r_{NO_3^-}) = \frac{k_1 \cdot C_{NO_3^-}}{1 + K'_{NO_3^-} \cdot C_{NO_3^-}} \tag{3.25}$$

Where the lumped parameters k_1 and $K'_{NO_3^-}$ are given by the following equations:

$$k_1 = \frac{k \cdot K_{NO_3^-} \cdot \sqrt{K_{H_2} \cdot C_{H_2}}}{1 + \sqrt{K_{H_2} \cdot C_{H_2}} + \sum K_i \cdot C_i} \tag{3.26}$$

$$K'_{NO_3^-} = \frac{K_{NO_3^-}}{1 + \sqrt{K_{H_2} \cdot C_{H_2}} + \sum K_i \cdot C_i} \tag{3.27}$$

If we assume that there is more than one active site, mono and bimetallic, adsorbing the nitrates in the bimetallic sites, and the remaining species are adsorbed in the monometallic sites, the L-H equation obtained is

$$(-r_{NO_3^-}) = \frac{k \cdot K_{NO_3^-} \cdot \sqrt{K_{H_2} \cdot C_{H_2}} \cdot C_{NO_3^-}}{\left(1 + K_{NO_3^-} \cdot C_{NO_3^-}\right) \cdot \left(1 + \sqrt{K_{H_2} \cdot C_{H_2}}\right)} \tag{3.28}$$

As in the earlier case, if the hydrogen concentration is constant during the reaction, the equation can be simplified as:

$$(-r_{NO_3^-}) = \frac{k_1 \cdot K_{NO_3^-} \cdot C_{NO_3^-}}{1 + K_{NO_3^-} \cdot C_{NO_3^-}} \tag{3.29}$$

Where k_1 is given by:

$$k_1 = \frac{k \cdot \sqrt{K_{H_2} \cdot C_{H_2}}}{\left(1 + \sqrt{K_{H_2} \cdot C_{H_2}}\right)} \tag{3.30}$$

If we integrate equation (3.28), we obtain the evolution along time of the nitrate concentration in a mixed-flow bath reactor:

$$\ln\left(\frac{C_{NO_3^-,0}}{C_{NO_3^-}}\right) + K_{NO_3^-}\cdot\left(C_{NO_3^-,0} - C_{NO_3^-}\right) = k_1 \cdot K_{NO_3^-}\cdot t \tag{3.31}$$

This equation is implicit in the concentration of nitrates; thus, its application for the calculation of kinetic parameters requires the use of iterative numerical methods or the consideration of the reaction time as the dependent variable. However, this expression can be linearised to yield the following expression:

$$\frac{\ln\left(\frac{C_{NO_3^-,0}}{C_{NO_3^-}}\right)}{(C_{NO_3^-,0} - C_{NO_3^-})} = -K_{NO_3^-} + k_1 \cdot K_{NO_3^-}\cdot\frac{t}{(C_{NO_3^-,0} - C_{NO_3^-})} \tag{3.32}$$

This equation can be represented as a straight line which slope is $k_1 \cdot K'_{NO_3^-}$, and which value at t=0 is negative, $-K_{NO_3^-}$. Thus, it was easier to obtain the kinetic parameters of this model. Equation 3.31 can be also linearised as:

$$\frac{\ln\left(\frac{C_{NO_3^-,0}}{C_{NO_3^-}}\right)}{t} = k_1 \cdot K_{NO_3^-} - K_{NO_3^-}\frac{(C_{NO_3^-,0} - C_{NO_3^-})}{t} \tag{3.33}$$

In this case, the slope is $-K_{NO_3^-}$ and the value at t=0 is $k_1 \cdot K'_{NO_3^-}$. If we calculate the apparent reaction order for model L-H, equation 3.28, using equation 3.7, we obtain:

$$n = \frac{1}{1 + K_{NO_3^-}\cdot C_{NO_3^-}} \tag{3.34}$$

Therefore, in the L-H model, the reaction order is between 0 and 1 ($0<n<1$). If there is strong adsorption or the nitrate concentration is high, the order will be close to 0, and in the opposite case, the order will tend to 1.

If the catalyst suffers deactivation, the kinetics of the process will follow equation 3.9, and can be combined with equation (3.28) to add the activity to the nitrate reduction rate:

$$(-r_{NO_3^-})_t = (-r_{NO_3^-})_0 \cdot a = \left(\frac{k_1 \cdot K_{NO_3^-} \cdot C_{NO_3^-}}{1 + K_{NO_3^-} \cdot C_{NO_3^-}} \right) \cdot a \tag{3.35}$$

In addition to the power-type model, this equation can be integrated into various deactivation kinetic models. Therefore, if we assume a first-order kinetic deactivation (d=1), equation 3.11, the integration of equation 3.35 is

$$t = -\frac{1}{k_d} \left(\ln \left(1 + \frac{k_1 \cdot K_{NO_3^-}}{k_d} \left(\ln \left(\frac{C_{NO_3^-,0}}{C_{NO_3^-}} \right) + K_{NO_3^-} \cdot \left(C_{NO_3^-,0} - C_{NO_3^-} \right) \right) \right) \right) \tag{3.36}$$

In the case of second-order deactivation kinetics, the result is

$$t = -\frac{1}{k_d} \left(1 - \exp \left(-\frac{k_1 \cdot K_{NO_3^-}}{k_d} \left(\ln \left(\frac{C_{NO_3^-,0}}{C_{NO_3^-}} \right) + K_{NO_3^-} \cdot \left(C_{NO_3^-,0} - C_{NO_3^-} \right) \right) \right) \right) \tag{3.37}$$

In the same way than equation 3.31, this equation is implicit in the nitrate concentration, but, in this case, this equation can't be linearized. On the other hand, if we calculate the apparent kinetic orders of the reaction using equation 3.21 and 3.35 for the cases where d=1 and d=2, we obtain the following equations:

$$n = \frac{1}{1 + K_{NO_3^-} \cdot C_{NO_3^-}} + \frac{k_d \cdot (1 + K_{NO_3^-} \cdot C_{NO_3^-}) \cdot \exp(k_d \cdot t)}{k_1 \cdot K_{NO_3^-}} \quad ; \quad d = 1 \tag{3.47}$$

$$n = \frac{1}{1 + K_{NO_3^-} \cdot C_{NO_3^-}} + \frac{k_d \cdot (1 + K_{NO_3^-} \cdot C_{NO_3^-})}{k_1 \cdot K_{NO_3^-}} \quad ; \quad d = 2 \tag{3.48}$$

As before, deactivation increases the apparent kinetic order of the equation, compared with equation 3.34. This difference was greater depending on k_d.

3.2.2. Preliminary models of CSRN reaction.

A way to increase the knowledge of the reaction mechanism is the use of kinetic studies that throw an optimum catalyst design and operational conditions of the reactions to maximise the selectivity towards nitrogen.

The first studies on the kinetics and mechanism of selective catalytic reduction of nitrates were conducted by Tacke and Vorlop (1993) [28]. These authors determined the

kinetics of nitrate and nitrite reduction for a Pd5-Cu1.25/Al_2O_3 catalyst using a power kinetic model (equations 3.49 and 3.50). They obtained reaction orders of 0.7 with regard to the nitrates, and independent of the partial pressure of hydrogen(*b*=0) for values higher than 1 bar:

$$(-r_{NO_3^-})_t = k_{NO_3^-} C_{NO_3^-}^a C_{H_2}^b \tag{3.49}$$

$$(-r_{NO_2^-})_t = k_{NO_2^-} C_{NO_3^-}^c C_{H_2}^d \tag{3.50}$$

Wärna et al (1994)[7] developed a Langmuir-Hinshelwood (L-H) kinetic model applied to monolithic reactors. Based on this model, nitrite, ammonium, and nitrogen formation rates were calculated using the following equations:

$$(r_{N_2})_t = \frac{k_{N_2} \cdot C_{NO_3^-} \cdot \sqrt{C_{H_2}}}{1 + K_{NO_3^-} \cdot C_{NO_3^-} \cdot \sqrt{C_{H_2}}} \tag{3.51}$$

$$(r_{NH_3})_t = \frac{k_{NH_3} \cdot C_{NO_3^-} \cdot \sqrt{C_{H_2}}}{\left(1 + K_{NO_3^-} \cdot C_{NO_3^-} \cdot \sqrt{C_{H_2}}\right)^2} \tag{3.52}$$

$$(r_{NO_2^-})_t = k_{NO_2^-} C_{NO_2^-} \cdot \frac{k_{NH_3} \cdot C_{NO_3^-} \cdot \sqrt{C_{H_2}}}{1 + K_{NO_3^-} \cdot C_{NO_3^-} \cdot \sqrt{C_{H_2}}} \tag{3.53}$$

They calculated the nitrate disappearance rate using the balance of matter.

$$(-r_{NO_3^-})_t = -2(r_{N_2}) - (r_{NO_2^-}) - (r_{NH_4^+}) \tag{3.54}$$

Pintar et al. (1996) [29] developed a L-H kinetic model based on the reaction mechanism proposed to analyse the results obtained from a Pd-Cu/Al_2O_3 catalyst. This mechanism indicates that NO_3^- and H_2 have non-competitive adsorption on different active sites. Nitrates were adsorbed on the bimetallic Pd–Cu sites, and hydrogen was adsorbed on the monometallic Pd. According to this model, the rate of NO3- disappearance is given by the following equation:

$$(-r_{NO_3^-}) = -\frac{dC_{NO_3^-}}{C_{cat} \cdot dt} = \frac{k \cdot K_{NO_3^-} \cdot C_{NO_3^-} \cdot K_{H_2}^n \cdot C_{H_2}^n}{(1 + K_{NO_3^-} \cdot C_{NO_3^-}) \cdot (1 + K_{H_2}^n \cdot C_{H_2}^n)} \tag{3.55}$$

After integration and linearisation of the earlier expression, the following equation is obtained:

$$\frac{\ln\left(C_{NO_3^-,0}/C_{NO_3^-}\right)}{(C_{NO_3^-,0}-C_{NO_3^-})}=-K_{NO_3^-}+\frac{k\cdot K_{NO_3^-}\cdot C_{NO_3^-}\cdot K_{H_2}^n\cdot C_{H_2}^n}{1+K_{H_2}^n\cdot C_{H_2}^n}\cdot\frac{t}{(C_{NO_3^-,0}-C_{NO_3^-})} \quad (3.56)$$

Using Equation 3.8, the kinetic parameters were obtained through linear regression. Using different partial pressures of hydrogen, between 0.09 bar and 0.46 bar, they found a reaction order of *n*=1/2 with respect to the hydrogen. This confirms the dissociative adsorption of hydrogen on the Pd sites. In addition, they performed the reaction at different temperatures (280 and 293 K) to calculate the apparent activation energy (22 kJ/mol) and chemisorption adsorption heat (47 kJ/mol) of nitrates. In addition, these authors found that the catalytic activity was not influenced by the intermediate species (for example, NO_2^-) or the final products (i.e. NH_4^+), but is highly influenced by pH. Considering the effect of pH, Glass et al. (1998) [30] developed a model that adjusts the results to a kinetic reaction order of zero. Lecloux [31] and Mikami et al. [32] employed the same model and obtained reaction orders for hydrogen pressure of hydrogen, 0.34 and 0.2-0.3, respectively. The reason for this low reaction kinetic order was the adsorption of H_2 at different active sites than NO_3^- and NO_2^-, as previously reported by Pintar et al. [29], and the quick dissociative adsorption of H_2, which reached equilibrium on the surface of the catalyst. The tests of Mikami et al. [32] with PdCu supported on active carbon resulted in a reaction order of 0.2 for [NO_3^-] and 1 for [NO_2^-]. They justified this difference with the difference in the strong adsorption of the nitrates on the active site in comparison with the nitrites under the same conditions. These results are similar to those reported by Tacke and Vorlop [28].

Regarding catalyst deactivation, Pintar and Bercic (1998) [33] studied the deactivation of nitrites using catalysts $PdCu/Al_2O_3$. These authors proposed different kinetic models, aside from the L-H model, assuming the dissociative adsorption of hydrogen [29,34]. To calculate the concentration of hydrogen in the liquid phase, expressed as the molar fraction, they proposed the use of the correlation proposed by Fogg and Gerrard [35]:

$$\ln(x_{H_2})=-125{,}939+\frac{5528{,}45}{T}+16{,}8893\cdot\ln(T) \quad (3.57)$$

Considering that the concentration and liquid phase are proportional to the partial pressure of the gas phase y_{H_2}, the concentration of H_2, in mg/L, is calculated as:

$$C_{H_2} = 1000 \cdot y_{H_2} \cdot \frac{x_{H_2}}{1 - x_{H_2}} \cdot \rho_{H_2} \cdot \frac{PM_{H_2}}{PM_{H_2O}} \tag{3.58}$$

The deactivation of the catalyst is thought to be due to the preferential adsorption of OH^- ions on the Pd surface instead of NO_2^- [33,36]. Chaplin et al. [37] considered the deactivation by adsorption competition with other ions, the developed a kinetic model which includes the adsorption of different ions:

$$(r_{NO_3^-})_t = \frac{k_{NO_3^-} \cdot K_{NO_3^-} \cdot C_{NO_3^-}}{1 + K_{NO_3^-} \cdot C_{NO_3^-} + \sum K_i \cdot C_i} \tag{3.59}$$

The values of the kinetic constants of adsorption, K_i, decreased in the following order: $SO_4^{2-} < HCO_3^- < Cl^- <$ humic acid $< SO_3^{2-} <$ HS.

Fan et al. [13]with a $PdCu/Al_2O_3$ catalyst and Soares et al. [38] with a PdCu/CNT catalyst developed mechanistic models based in the reduction of the NO_3^- ions assuming a few premises:

(i) The reduction of NO_3^- occurs at the PdCu sites through a redox reaction.
(ii) The adsorption of NO_3^- at these sites was rapid and reached equilibrium.
(iii) The regeneration of the metallic oxide is fast and is produced by the spill-over of hydrogen from the noble metal.

They also considered other aspects related to the reduction of NO_2^-:

(i) The adsorption of nitrites occurs on monometallic noble metal sites.
(ii) The adsorption/desorption of H_2 and NO_2^- was fast and in a state of quasi-equilibrium.
(iii) The reduction steps were irreversible.
(iv)The desorption of the final product was rapid.

With these premises and considering the balances of the mono-and bimetallic sites, these authors developed an equation for the nitrate reduction rate:

$$(r_{NO_3^-})_t = \frac{k_{NO_3^-} \cdot K_{NO_3^-} \cdot C_{NO_3^-}}{1 + K_{NO_3^-} \cdot C_{NO_3^-}} \cdot \theta_*^{Bi} \tag{3.60}$$

Where θ_*^{Bi} is the fraction of bimetallic sites available, and the summarize of this value and the fraction of bimetallic sites with NO_3^- adsorbed ($\theta_{NO_3^-}^{Bi}$) is equal to 1. Regarding the monometallic sites (θ_*^{Mono}) the equations are:

$$1 = \theta_H^{Mono} + \theta_{NO_2^-}^{Mono} + \theta_{NO}^{Mono} + \theta_N^{Mono} + \theta_*^{Mono} \tag{3.61}$$

$$(r_{NO_2^-}) = \frac{k_{NO_3^-} \cdot K_{NO_3^-} \cdot C_{NO_3^-}}{1 + K_{NO_3^-} \cdot C_{NO_3^-}} \cdot \theta_*^{Bi} - k_1 \cdot \theta_{NO_2^-}^{Mono} \cdot \theta_{H_2}^{Mono} \tag{3.62}$$

$$(r_{N_2}) = k_3 \cdot \theta_N^{Mono} \cdot \theta_{NO}^{Mono} \tag{3.63}$$

$$(r_{NO_4^+}) = k_4 \cdot \theta_N^{Mono} \cdot \theta_H^{Mono} \tag{3.64}$$

Simulation with this model [13] allowed the author to conclude that the presence of external diffusional resistance increases the selectivity towards the formation of NH_4^+. They also concluded that the lowest Pd/Me ratio resulted in a higher N_2 selectivity.

3.2.2.1. General kinetic model.

A kinetic global kinetic model for catalytic selective nitrate reduction was developed based on the reaction mechanism (Figure 3.6) previously explained by Warna et al. [7] and other previous studies [7,13,29,38–40].

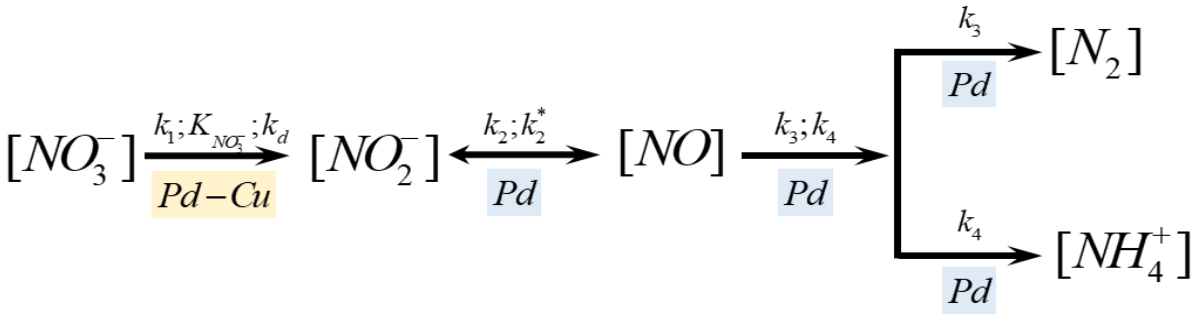

Figure 3.6 *Reaction scheme for the selective catalytic reduction of nitrates on a Pd-Cu catalyst.*

In addition, the following assumptions were made for the development of the kinetic model:

(i) The reduction of nitrate to nitrite occurs in the bimetallic sites (i.e. Pd-Me) through a reversible redox process. This is the only reaction that occurs in this type of bimetallic sites.

(ii) These sites can suffer deactivation over time owing to the adsorption of the OH^- ions formed in the reaction.

(iii) The reduction of NO_2^- to NO species occurs at monometallic sites (i.e. Pd).

(iv) The hydrogenation of NO species occurs through a parallel process, producing molecular N_2, which is transferred directly to the gas phase or NH_4^+ through successive hydrogenations.

Based on the previous considerations and the reaction mechanism considered, the proposed kinetic model can be expressed according to the following differential equations of the formation and disappearance rates of the species involved in the reaction (NO_3^-, NO_2^-, NO, N_2, and NH_4^+):

$$\left(-r_{NO_3^-}\right)_t = \frac{1}{\rho_{cat}} \cdot \left(\frac{dC_{NO_3^-}}{dt}\right) = \frac{k_1 \cdot K_{NO_3^-} \cdot C_{NO_3^-}}{1 + K_{NO_3^-} \cdot C_{NO_3^-}} \cdot a \tag{3.65}$$

$$\left(r_{NO_2^-}\right)_t = \frac{1}{\rho_{cat}} \cdot \left(\frac{dC_{NO_2^-}}{dt}\right) = \frac{k_1 \cdot K_{NO_3^-} \cdot C_{NO_3^-}}{1 + K_{NO_3^-} \cdot C_{NO_3^-}} \cdot a - k_2 \cdot C_{NO_2^-} + k_2 * \cdot C_{NO} \tag{3.66}$$

$$\left(r_{NO}\right)_t = \frac{1}{\rho_{cat}} \cdot \left(\frac{dC_{NO}}{dt}\right) = k_2 \cdot C_{NO_2^-} - \left(k_2 * + k_4\right) \cdot C_{NO} - k_3 \cdot \left(C_{NO}\right)^2 \tag{3.67}$$

$$\left(r_{N_2}\right)_t = \frac{1}{\rho_{cat}} \cdot \left(\frac{dC_{N_2}}{dt}\right) = k_3 \cdot \left(C_{NO}\right)^2 \tag{3.68}$$

$$\left(r_{NH_4^+}\right)_t = \frac{1}{\rho_{cat}} \cdot \left(\frac{dC_{NH_4^+}}{dt}\right) = k_4 \cdot C_{NO} \tag{3.69}$$

In these equations, there are represented the kinetic constants related to nitrate elimination (k_1), nitrite elimination (k_2), formation of nitrites from specie NO (k_2^*), N_2 (k_3) and NH_4^+ (k_4) formation. $K_{NO_3^-}$ is the nitrate adsorption constant on the catalyst. The deactivation rate of the catalyst has been calculated by the following differential equation:

$$(r_d) = \frac{1}{\rho_{cat}} \cdot \frac{-da}{dt} = k_d \cdot C_{OH^-}; a = \frac{(-r_{NO_3^-})_t}{(-r_{NO_3^-})_0} \tag{3.70}$$

Where k_d is the constant related to the catalyst activity. On the other hand, when more ions are present in the solution, the nitrate rate equation changes, and the adsorption of the different ions must be taken into consideration. To take into consideration, the contribution of the different ions on the solution we have created an apparent adsorption constant (K_{obs}):

$$(-r_{NO_3^-}) = \frac{k_1 K_{NO_3^-} C_{NO_3^-}}{1 + K_{NO_3^-} C_{NO_3^-} + \sum K_i C_i} = \frac{k_1 K_{obs} C_{NO_3^-}}{1 + K_{obs} C_{NO_3^-}}$$
$$K_{obs} = \frac{K_{NO_3^-}}{1 + \sum K_i C_i} \tag{3.71}$$

In this equation, K_i and C_i are he kinetic constant and the concentration of the other ions present in the solution. This apparent adsorption constant was used in the test of the influence of the ions.

The resolution of the above kinetic equations considers also the nitrogen balance, which can be expressed as:

$$C_{N_2} + C_{NO} = C_{NO_3^-;0} - C_{NO_3^-} - C_{NO_2^-} - C_{NH_4^+} \tag{3.72}$$

The parameters, k_1, $K_{NO_3^-}$, k_2, k_2*, k_3 and k_4, are estimated by numerical integration of the experimental concentrations vs. time data. The maximized objective function is the Model Selection Criteria, *MSC*, [41–43], defined as:

$$MSC = \ln\left(\frac{1}{1-R^2}\right) - \left(\frac{2p}{n-p}\right) \tag{3.73}$$

In this expression, p represents the number of parameters ($p=6$) and n represents the number of experimental points in each experiment and R^2 is de coefficient of correlation.

3.2.2.2. Kinetic model of the adsorption of ammonium.

As mentioned, ammonium ions are an undesired subproduct of the nitrate reduction, with legal limit of 0.5ppm in drinkable water [44,45]. In order to eliminate the ammonium formed during the reaction, in this work, we have used an adsorption process employing protonic exchange resins (Amberlite H^+). In a first step, we have tested the resins in a simulated adsorption test that will simulate and adsorption of the ammonium after reaction. In this case we measured the diminution of NH_4^+ over time as it is adsorbed on the resin. In a second test, we tested the use of the resins during the reaction, so the ammonium is adsorbed while the nitrates are reduced, and new ammonium is formed.

The adsorption models which describe the elimination of ammonium by resins are mostly based in the Langmuir isotherm [46–48] or Freundlich isotherm [18,49], but in this work we have also used the Temkin model [50,51].

In the ammonium adsorption experiment the concentration of ammonium adsorbed on the resins ($C^S_{NH_4^+}$), expressed in mmol/g resin, can be calculated from the ammonium concentration in the liquid phase, $C^l_{NH_4^+}$ expressed in mmol/L:

$$C^S_{NH_4^+} = \frac{C^l_{NH_4^+,0} - C^l_{NH_4^+}}{C_R} \tag{3.74}$$

Where C_R is the concentration of resin used in the experiment in g of resin/L. If the process follows a Langmuir model, the concentration of ammonium in equilibrium between the solid phase and the liquid phase comes from the equation:

$$\theta_{NH_4^+} = \frac{C^s_{NH_4^+}}{C^{sat,s}_{NH_4^+}} = \frac{K_{NH_4^+} \cdot C^{l,*}_{NH_4^+}}{1 + K_{NH_4^+} \cdot C^{l,*}_{NH_4^+}} \tag{3.75}$$

In this equation, $K_{NH_4^+}$ is the kinetic constant related with the adsorption of ammonium in the resin, $C^{Sat}_{NH_4^+}$ is the maximum concentration of ammonium that the resin can adsorb, in mmol/g of resin; $C^{l,*}_{NH_4^+}$ is the concentration of ammonium in the liquid phase that is in equilibrium with the ammonium on the solid phase, $C^S_{NH_4^+}$. From this expression $C^{l,*}_{NH_4^+}$ can be calculated as:

$$C_{NH_4^+}^{l,*} = \frac{\theta_{NH_4^+}}{K_{NH_4^+} \cdot (1 - \theta_{NH_4^+})} \tag{3.76}$$

If it is used the Freundlich model, the concentration of ammonium in equilibrium between the solid phase and the liquid phase is given by:

$$\theta_{NH_4^+} = \frac{C_{NH_4^+}^{s}}{C_{NH_4^+}^{sat,s}} = k_{NH_4^+} \cdot \left(C_{NH_4^+}^{l,*} \right)^{\gamma} \tag{3.77}$$

$k_{NH_4^+}$ and γ (0< γ <1) are constants of the Freundlich model, and are constants related to the surface characteristics of the adsorbent [50,51]. From this expression $C_{NH_4^+}^{l,*}$ can be calculated as:

$$C_{NH_4^+}^{l,*} = \left(\frac{\theta_{NH_4^+}}{k_{NH_4^+}} \right)^{1/\gamma} \tag{3.78}$$

Finally, if the process is modelled with the Temkin model, the concentration of ammonium in equilibrium between the solid and liquid phases is given by:

$$\theta_{NH_4^+} = \frac{C_{NH_4^+}^{s}}{C_{NH_4^+}^{sat,s}} = \frac{1}{f} \cdot \ln\left(1 + K_{NH_4^+}^{0} \cdot C_{NH_4^+}^{l,*}\right) \tag{3.79}$$

$K_{NH_4^+}^{0}$ is the constant of adsorption when the adsorption surface is empty ($\theta_{NH_4^+}$ =0) and f is a term that depends on the adsorption heat range on the resin surface [50,51]. From this expression $C_{NH_4^+}^{l,*}$ can be calculated as:

$$C_{NH_4^+}^{l,*} = \frac{\exp(f \cdot \theta_{NH_4^+}) - 1}{K_{NH_4^+}^{0}} \tag{3.80}$$

For the experiments that the resin is added after the reaction, the rate of the transference of the ammonium from the liquid phase to the solid phase, $J_{NH_4^+}$, in mmol/L·min, can be calculated:

$$J_{NH_4^+} = \frac{dC_{NH_4^+}^{l}}{dt} = -(K_L \cdot a) \cdot (C_{NH_4^+}^{l} - C_{NH_4^+}^{l,*}) \tag{3.81}$$

In this expression, $K_L.a$ is the global coefficient of ammonium transfer between the liquid phase and resin. On the other hand, considering the equation 3.74, and the three adsorption models (equations 3.76; 3.78 and 3.80), $C^{l,*}_{NH_4^+}$ can be calculated for each model using the following equation:

Langmuir isotherm:

$$C^{l,*}_{NH_4^+} = \frac{C^{l}_{NH_4^+,0} - C^{l}_{NH_4^+}}{K_{NH_4^+} \cdot (C_R \cdot C^{Sat}_{NH_4^+} - (C^{l}_{NH_4^+,0} - C^{l}_{NH_4^+}))} \tag{3.82}$$

Freundlich isotherm:

$$C^{l,*}_{NH_4^+} = \left(\frac{C^{l}_{NH_4^+,0} - C^{l}_{NH_4^+}}{k_{NH_4^+} \cdot C_R \cdot C^{Sat}_{NH_4^+}} \right)^{1/\gamma} \tag{3.83}$$

Temkin isotherm:

$$C^{l,*}_{NH_4^+} = \frac{1}{K^0_{NH_4^+}} \cdot \left(\exp\left(f \cdot \frac{C^{l}_{NH_4^+,0} - C^{l}_{NH_4^+}}{C_R \cdot C^{Sat}_{NH_4^+}} \right) - 1 \right) \tag{3.84}$$

The numerical resolution of equation (3.81), along with equations (3.82), (3.83), or (3.84), allows us to obtain the evolution of the concentration of ammonia in both the liquid and resin over time. By fitting the data of ammonium concentration in the liquid phase over time using nonlinear regression, the global ammonium transfer coefficient ($K_L.a$) and the thermodynamic parameters of the three models, namely $K_{NH_4^+}$ (Langmuir), $k_{NH_4^+}$ and γ (Freundlich); $K^0_{NH_4^+}$ and f (Temkin), were calculated. In this fitting process, the minimised objective function is the sum of squared residuals, *SSR*:

$$SSR = \sum_{i,n} \left(C^{l,\exp}_{NH_4^+} - C^{l,cal}_{NH_4^+} \right)^2 \tag{3.85}$$

Finally, when the addition of the resins occurs during the reaction is taking place, the adsorption of ammonium is produced at the same time as its formation. For this reason, equation 3.69 have to be modified considering a second term related to the adsorption of ammonium over the resins, resulting in the following equation:

$$(r_{NH_4^+})_t = k_4 \cdot C_{NO} - (K_L a) \cdot (C^{l}_{NH_4^+} - C^{l,*}_{NH_4^+}) \tag{3.86}$$

From the results of the combined use of ion exchange resin with the catalyst 1%Pd0.4%Cu/Al_2O_3, for the elimination of ammonium in the liquid phase in the experiments of CNSR in combination with the cationic resin, can be calculated the values $C^{l,*}_{NH_4^+}$ using the three adsorption models proposed: Langmuir, Freundlich and Temkin. The results indicate the all these adsorption models can be simplified to a linear isotherm of the form:

$$C^{l,*}_{NH_4^+} = \frac{C^{s}_{NH_4^+}}{C_R \cdot k} \tag{3.87}$$

Combining now equations 3.86 and 3.87, the rate of ammonium in the liquid phase is obtained as follows:

$$(r_{NH_4^+})_t = k_4 \cdot C_{NO} - (K_L a) \cdot \left(C^{l}_{NH_4^+} - \frac{C^{S}_{NH_4^+}}{k \cdot C_R} \right) \tag{3.88}$$

This equation was used instead of equation 3.69 in the global kinetic model. Because the constant $K_L.a$ was calculated in the adsorption tests, the number of kinetic parameters calculated using the global kinetic model is the same.

3.3. References

[1] K.D. Vorlop, T. Tacke, First steps towards noble-metal catalyzed removal of nitrate and nitrite from drinking water, Chemieingenieurtechnik 61 (1989) 836–837. https://doi.org/10.1002/cite.330611023.

[2] U. Prüsse, K.D. Vorlop, Supported bimetallic palladium catalysts for water-phase nitrate reduction, J Mol Catal A Chem 173 (2001) 313–328. https://doi.org/10.1016/S1381-1169(01)00156-X.

[3] A. Edelmann, W. Schießer, H. Vinek, A. Jentys, Oxidation state of bimetallic PdCu catalysts during liquid phase nitrate reduction, 2000.

[4] F. Epron, F. Gauthard, C. Pinéda, J. Barbier, Catalytic Reduction of Nitrate and Nitrite on Pt-Cu/Al2O3 Catalysts in Aqueous Solution: Role of the Interaction between Copper and Platinum in the Reaction, J Catal 198 (2001) 309–318. https://doi.org/10.1006/jcat.2000.3138.

[5] N. Barrabés, J. Just, A. Dafinov, F. Medina, J.L.G. Fierro, J.E. Sueiras, P. Salagre, Y. Cesteros, Catalytic reduction of nitrate on Pt-Cu and Pd-Cu on active carbon using continuous reactor: The effect of copper nanoparticles, Appl Catal B 62 (2006) 77–85. https://doi.org/10.1016/j.apcatb.2005.06.015.

[6] W. Gao, N. Guan, J. Chen, X. Guan, R. Jin, H. Zeng, Z. Liu, F. Zhang, Titania supported Pd-Cu bimetallic catalyst for the reduction of nitrate in drinking water, Appl Catal B 46 (2003) 341–351. https://doi.org/10.1016/S0926-3373(03)00226-1.

[7] T. Salmi, J. Warna, T. Maunulas, I. Turunen, Kinetics of nitrate reduction reactor, Chem Eng Sci 49 (1994) 5763–5773. https://doi.org/https://doi.org/10.1016/0009-2509(94)00331-9.

[8] J. Barbier Jr, F. Marsollier, D. Duprez, Reduction of nitrates by dihydrogen in CeO2 and Rh/CeO2 catalysts, Appl Catal A Gen 90 (1992) 11–23.

[9] S. H&old, K.-D. Vorlop, T. Tacke', M. Sellb, Development of catalysts for a selective nitrate and nitrite removal from drinking water, Elsevier Science Publishers B.V, 1993.

[10] O.M. Ilinitch, F. Petrus Cuperus, L. V Nosova, E.N. Gribov, Catalytic membrane in reduction of aqueous nitrates: operational principles and catalytic performance, 2000.

[11] K. Rahkamaa, T. Salmi, R. Keiski, J. Warna, Y. Zhou, Transient reduction kinetics of NO over Pd-based metallic monoliths, Chem Eng Sci 56 (2001) 1395–1401.

[12] F. Gauthard, F. Epron, J. Barbier, Palladium and platinum-based catalysts in the catalytic reduction of nitrate in water: Effect of copper, silver, or gold addition, J Catal 220 (2003) 182–191. https://doi.org/10.1016/S0021-9517(03)00252-5.

[13] X. Fan, C. Franch, E. Palomares, A.A. Lapkin, Simulation of catalytic reduction of nitrates based on a mechanistic model, Chemical Engineering Journal 175 (2011) 458–467. https://doi.org/10.1016/j.cej.2011.09.069.

[14] Y. Yoshinaga, T. Akita, I. Mikami, T. Okuhara, Hydrogenation of nitrate in water to nitrogen over Pd-Cu supported on active carbon, J Catal 207 (2002) 37–45. https://doi.org/10.1006/jcat.2002.3529.

[15] J. Sá, J. Montero, E. Duncan, J.A. Anderson, Bi modified Pd/SnO2 catalysts for water denitration, Appl Catal B 73 (2007) 98–105. https://doi.org/10.1016/j.apcatb.2006.06.012.

[16] M. Boudart, G. Djega-Mariadassou, Kinetics of heterogeneous catalytic reactions, Priceton Univ. Press, Princeton, New Jersey (USA), 1984.

[17] M.A. Vannice, W.H. Joyce, Kinetics of catalytic reactions, Springer, 2005.

[18] Q. Du, S. Liu, Z. Cao, Y. Wang, Ammonia removal from aqueous solution using natural Chinese clinoptilolite, Sep Purif Technol 44 (2005) 229–234. https://doi.org/10.1016/j.seppur.2004.04.011.

[19] P. Stoltze, Microkinetic simulation of catalytic reactions, Prog Surf Sci 65 (2000) 65–150. https://doi.org/https://doi.org/10.1016/S0079-6816(00)00019-8.

[20] S.A. Regenhardt, C.I. Meyer, A.F. Trasarti, A. Monzón, T.F. Garetto, Catalytic oxidation of carbon tetrachloride on metal exchanged Y-zeolite, Chemical Engineering Journal 198–199 (2012) 18–26. https://doi.org/10.1016/j.cej.2012.05.055.

[21] S. Szépe, O. Levenspiel, Catalyst deactivation, in: Proceedings of the Fourth European Symposium on Chemical Reactive Engeenering, Pergamon Press, Brussels, NY, 1971: pp. 265–276.

[22] A. Monzón, E. Romeo, A. Borgna, Relationship between the kinetic parameters of different catalyst deactivation models, Chemical Engineering Journal 94 (2003) 19–28. https://doi.org/10.1016/S1385-8947(03)00002-0.

[23] C.I. Meyer, A.J. Marchi, A. Monzon, T.F. Garetto, Deactivation and regeneration of Cu/SiO2 catalyst in the hydrogenation of maleic anhydride. Kinetic modeling, Appl Catal A Gen 367 (2009) 122–129. https://doi.org/10.1016/j.apcata.2009.07.041.

[24] T.F. Garetto, C.I. Vignatti, A. Borgna, A. Monzón, Deactivation and regeneration of Pt/Al2O3 catalysts during the hydrodechlorination of carbon tetrachloride, Appl Catal B 87 (2009) 211–219. https://doi.org/10.1016/j.apcatb.2008.09.005.

[25] A. Monzón, E. Romeo, A. Borgna, Relationship between the kinetic parameters of different catalyst deactivation models, Chemical Engineering Journal 94 (2003) 19–28. https://doi.org/10.1016/S1385-8947(03)00002-0.

[26] T.F. Garetto, A. Borgnau, A. Monzon, Modelling of sintering kinetics of naphtha-reforming Pt/Al2O3-CI catalysts, Journal of the Chemical Society, Faraday Transactions 92 (1996) 2637–2640. https://doi.org/DOI https://doi.org/10.1039/FT9969202637.

[27] A. Borgna, T.F. Garetto, A. Monzon, C.R. Apestegufa, Deactivation Model with Residual Activity to Study Thioresistance and Thiotolerance of Naphtha Reforming Catalysts, J Catal 146 (1994) 69–81. https://doi.org/https://doi.org/10.1016/0021-9517(94)90009-4.

[28] T. Tacke, K.-D. Vorlop, Kinetische Charakterisierung von Katalysatoren zur selektiven Entfernung von Nitrat und Nitrit aus Wasser, Chemie Ingenieur Technik 65 (1993) 1500–1502. https://doi.org/10.1002/cite.330651216.

[29] A. Pintar, J. Batista, J. Levec, T. Kajiuchi, Kinetics of the catalytic liquid-phase hydrogenation of aqueous nitrate solutions, Appl Catal B 11 (1996) 81–98. https://doi.org/10.1016/S0926-3373(96)00036-7.

[30] C. Glass, J. Silverstein, Denitrification Kinetics of high nitrate concentration water: pH effect on inhibition and nitrite accumulation., Water Res 32 (1998) 831–839. https://doi.org/https://doi.org/10.1016/S0043-1354(97)00260-1.

[31] A.J. Lecloux, Chemical, biological and physical constrains in catalytic reduction processes for purification of drinking water, Catal Today 53 (1999) 23–34. https://doi.org/10.1016/S0920-5861(99)00100-5.

[32] I. Mikami, Y. Sakamoto, Y. Yoshinaga, T. Okuhara, Kinetic and adsorption studies on the hydrogenation of nitrate and nitrite in water using Pd-Cu on active carbon support, Appl Catal B 44 (2003) 79–86. https://doi.org/10.1016/S0926-3373(03)00021-3.

[33] A. Pintar, G. Berčič, J. Levec, Catalytic liquid-phase nitrite reduction: kinetics and catalyst deactivation, AIChE Journal 44 (1998) 2280–2292. https://doi.org/10.1002/aic.690441017.

[34] Z. Knor, Chemisorption of Dihydrogen, in: Catalysis, Springer Berlin Heidelberg, Berlin, Heidelberg, 1982: pp. 231–280. https://doi.org/10.1007/978-3-642-93223-6_5.

[35] P.G.T. Fogg, W. Gerrard, Solubility of gases in liquids, Chichester-New York–Brisban, 1990.

[36] A. Pintar, M. Šetinc, J. Levec, Hardness and salt effects on catalytic hydrogenation of aqueous nitrate solutions, J Catal 174 (1998) 72–87. https://doi.org/10.1006/jcat.1997.1960.

[37] B.P. Chaplin, E. Roundy, K.A. Guy, J.R. Shapley, C.I. Werth, Effects of natural water ions and humic acid on catalytic nitrate reduction kinetics using an alumina supported Pd-Cu catalyst, Environ Sci Technol 40 (2006) 3075–3081. https://doi.org/10.1021/es0525298.

[38] O.S.G.P. Soares, X. Fan, J.J.M. Órfão, A.A. Lapkin, M.F.R. Pereira, Kinetic modeling of nitrate reduction catalyzed by Pd-Cu supported on carbon nanotubes, Ind Eng Chem Res 51 (2012) 4854–4860. https://doi.org/10.1021/ie202957v.

[39] A.S.G.G. Santos, J. Restivo, C.A. Orge, M.F.R. Pereira, O.S.G.P. Soares, Nitrate Catalytic Reduction over Bimetallic Catalysts: Catalyst Optimization, C (Basel) 6 (2020) 78. https://doi.org/10.3390/c6040078.

[40] O.M. Ilinitch, L. V Nosova, V. V Gorodetskii, V.P. Ivanov, S.N. Trukhan, E.N. Gribov, S. V Bogdanov, F.P. Cuperus, Catalytic reduction of nitrate and nitrite ions by hydrogen: investigation of the reaction mechanism over Pd and Pd-Cu catalysts, J Mol Catal A Chem 158 (2000) 237–249. https://doi.org/https://doi.org/10.1016/S1381-1169(00)00070-4.

[41] G. Schwarz, Estimating the Dimension of a Model, 1978.

[42] S.L. Sclove, Application of model-selection criteria to some problems in multivariate analysis, Psychometrika 52 (1987) 333–343. https://doi.org/10.1007/BF02294360.

[43] T. Teräsvirta, I. Mellin, Model Selection Criteria and Model Selection Tests in Regression Models, 1986.

[44] World Health Organisation (WHO), Nitrate and Nitrite in Drinking Water,ackground Document for the Development of WHO Guidelines for Drinking-water Quality, 2016.

[45] European Union, Directive 2020/2184 of the European Parliament and of the Council of 16 December 2020 on the quality of water intended for human consumption, 2020.

[46] R. Malekian, J. Abedi-Koupai, S.S. Eslamian, S.F. Mousavi, K.C. Abbaspour, M. Afyuni, Ion-exchange process for ammonium removal and release using natural Iranian zeolite, Appl Clay Sci 51 (2011) 323–329. https://doi.org/10.1016/j.clay.2010.12.020.

[47] R. Leyva-Ramos, J.E. Monsivais-Rocha, A. Aragon-Piña, M.S. Berber-Mendoza, R.M. Guerrero-Coronado, P. Alonso-Davila, J. Mendoza-Barron, Removal of ammonium from aqueous solution by ion exchange on natural and modified chabazite, J Environ Manage 91 (2010) 2662–2668. https://doi.org/10.1016/j.jenvman.2010.07.035.

[48] A. Thornton, P. Pearce, S.A. Parsons, Ammonium removal from solution using ion exchange on to MesoLite, an equilibrium study, J Hazard Mater 147 (2007) 883–889. https://doi.org/10.1016/j.jhazmat.2007.01.111.

[49] Y.F. Wang, F. Lin, W.Q. Pang, Ammonium exchange in aqueous solution using Chinese natural clinoptilolite and modified zeolite, J Hazard Mater 142 (2007) 160–164. https://doi.org/10.1016/j.jhazmat.2006.07.074.

[50] M.A. Vannice, W.H. Joyce, Kinetics of catalytic reactions, New York: Springer, 2005.

[51] M. Boudart, G. Djéga-Mariadassou, Kinetics of heterogeneous catalytic reactions , Princeton University Press, 2014.

4. PERFORMANCE OF CATALYSTS PdCu SUPPORTED OVER Al_2O_3 ON THE CSNR

4.1. Introduction

The use of appropriate models for describing the reaction network and catalyst deactivation [1,2] will allow the correct selection, design, and optimisation of the type of reactor, mode of operation, and type of contact between phases to purify the wastewater to the required level. Given that the conversion and selectivity obtained in the operation depend on both the catalyst properties and operating conditions, in the present study, we investigated how the catalyst composition, catalyst concentration, stirring rate, and ions present in the water and CO_2 flow as a pH buffer influence the selective reduction of nitrates in a batch reactor using a Al_2O_3 supported catalyst.

Furthermore, the kinetic model developed in Chapter 3, has been modified and applied to include the effect of the adsorption phenomena that occurs in presence of the cationic resin Amberlite H^+.

4.2. Catalyst characterization

4.2.1. Textural properties- N_2 adsorption isotherm

Table 4.1 lists the textural properties of the prepared catalysts and supports. The BET area of the catalysts (around 200 m^2/g) was slightly lower than the BET area of the support (225 m^2/g) owing to the effect of the calcination step and the occupation of the pores by the metal. Consequently, the pore volume (V_{pore}) also decreased. In addition, these values did not change after the reaction, indicating that the structural properties of the catalysts did not change during the reaction. The average pore diameter of the catalysts was 7.5 nm. The metallic content of the catalysts was measured by atomic absorption to obtain Pd and Cu contents very close to the nominal metal values.

Table 4.1 *The textural properties of the catalysts and support were calculated from the N_2 isotherm.*

Catalyst	***BET area (m^2/ g)***	***Pore size (nm)***	***Pore volume (cm^3/g)***
Al_2O_3	*225*	*7*	*0.41*
0.25Pd0.4Cu/Al_2O_3	*195*	*8*	*0.38*
0.5Pd0.4Cu/Al_2O_3	*209*	*7*	*0.39*
0.75Pd0.4Cu/Al_2O_3	*200*	*7*	*0.37*
1Pd0.4Cu/Al_2O_3	*191*	*8*	*0.36*

4.2.2. X-Ray Diffraction (XRD)

Figure 4.1 shows the XRD diffractograms of the Al_2O_3 support and catalyst 1Pd0.4Cu/Al_2O_3, fresh and after the reaction. The peaks present in the diffractograms correspond to the Al_2O_3 pattern, with no peaks related to the active species of the catalyst owing to their low content of Pd and Cu, small particle size, and good dispersion. Similar diffractograms were obtained for the other catalysts (Figure. 4.2). No changes were observed in the structure of the support owing to the reaction.

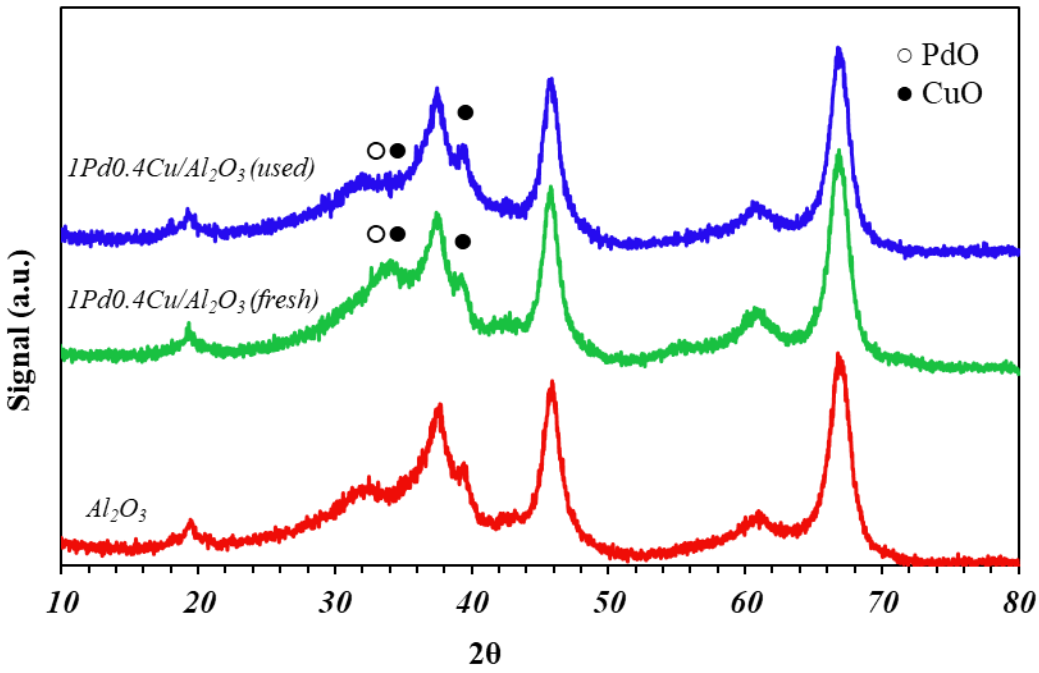

Figure 4.1 *XRD diffractograms of Al_2O_3, 1Pd0.4Cu/Al_2O_3 (fresh) and 1Pd0.4Cu/Al_2O_3 (used).*

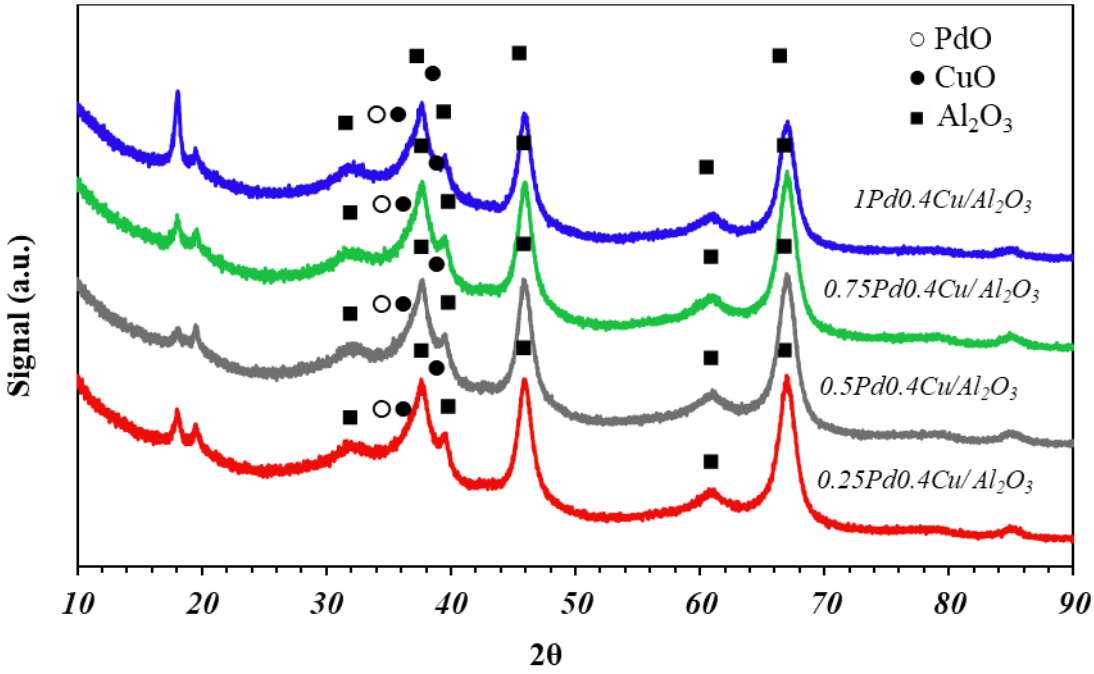

Figure 4.2 *XRD diffractograms 1Pd0.4Cu/Al_2O_3, 0.75Pd0.4Cu/Al_2O_3, 0.5Pd0.4Cu/Al_2O_3 and 0.25Pd0.4Cu/Al_2O_3.*

4.2.3. Transmission Electron Microscopy (TEM)

Figure 4.3 shows HAADF-STEM images of 1Pd0.4Cu/Al_2O_3, 0.75Pd0.4Cu/Al_2O_3, 0.5Pd0.4Cu/Al_2O_3, and 0.25Pd0.4Cu/Al_2O_3. A blurred white mass corresponding to the alumina support and white dots corresponding to the nanoparticles can be observed in the image. As can be observed, the nanoparticles are well dispersed, and there is an increase in the number of nanoparticles with higher content of Pd. In the histograms of the particle size (Figure 4.4), measured with the HAADF-STEM images, we observed that most nanoparticles on the catalysts were in the range of 3–5 nm, with a common mean particle size of approximately 5 nm, regardless of the Pd loading. EDS analysis (Figure 4.5 and 4.6) of the synthesised catalysts corroborated the XRD and TEM results, showing how metals (green dots=Pd, Red dots= Cu) were well dispersed on the surface of the catalysts, regardless of the Pd load used (Figure 4.6). Cu is deposited in the first impregnation step of the synthesis method, and its dispersion on the surface of the support is very good. Pd was added during the second impregnation and calcined at a higher temperature, forming the main bulk of the nanoparticles observed in the HAADF.

Additionally, the images indicate an excellent interaction between Pd and Cu, which allows the quick regeneration of Cu through H_2 chemisorbed on Pd (Figure 4.5). This was probably responsible for the high activity of the catalysts. However, EDX analysis showed no difference in the Pd/Cu ratio of the nanoparticles of the catalysts with different amounts of Pd (Table 4.2). This implies that an increase in Pd following the synthesis method employed in this study does not increase the Pd/Cu ratio in the nanoparticles. Taking into consideration this Pd/Cu ratio and the nanoparticle size of the catalysts observed by TEM, it can be said that successive incipient wetness impregnation allowed an increase in the Pd loading of the catalysts, maintaining the nanoparticle size and the relation of both metals in the nanoparticle. Considering the highly dispersed Cu on the surface of the catalysts and that the nanoparticle size did not change significantly between the catalysts, the increase in Pd was translated as an increase in the number of nanoparticles, as can be observed in Figure 4.3.

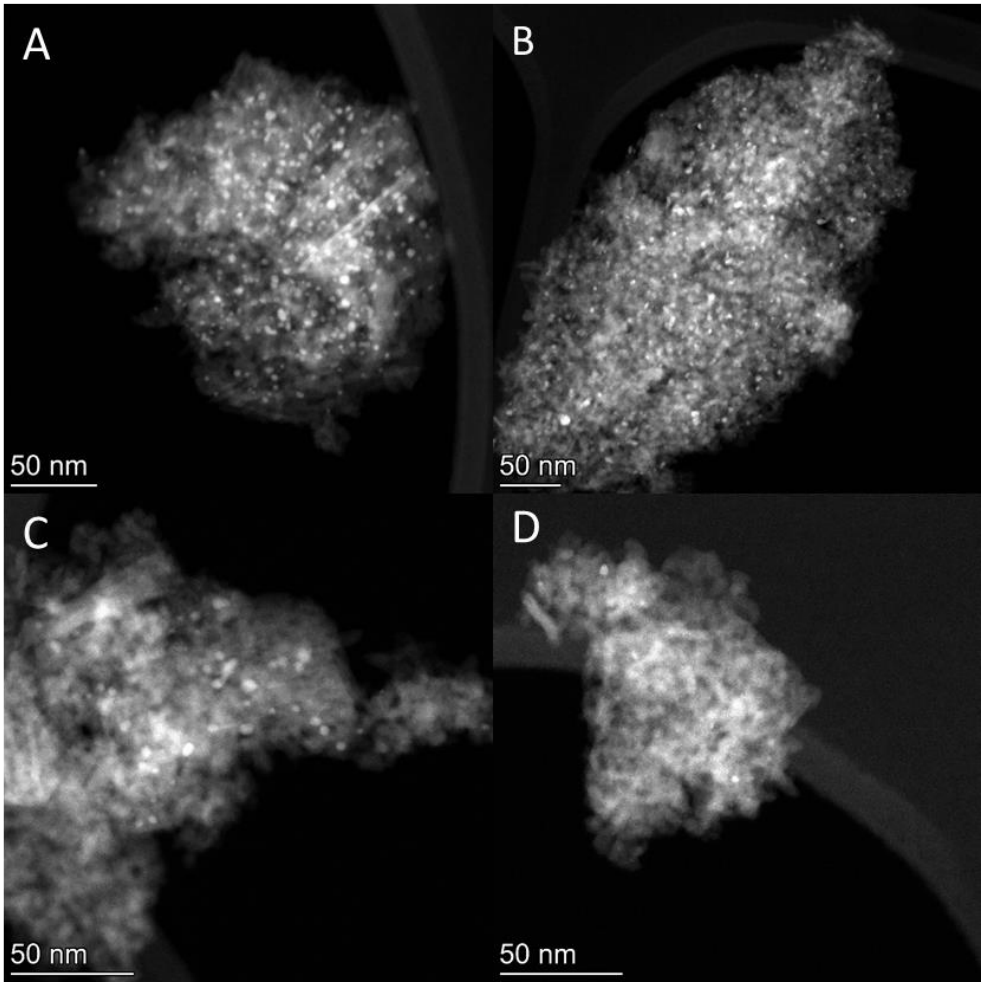

Figure 4.3 *HAADF-TEM images of 1Pd0.4Cu/Al_2O_3catalyst (A), 0.75Pd0.4Cu/Al_2O_3 (B), 0.5Pd0.4Cu/Al_2O_3 (C) and 0.25Pd0.4Cu/Al_2O_3 (D).*

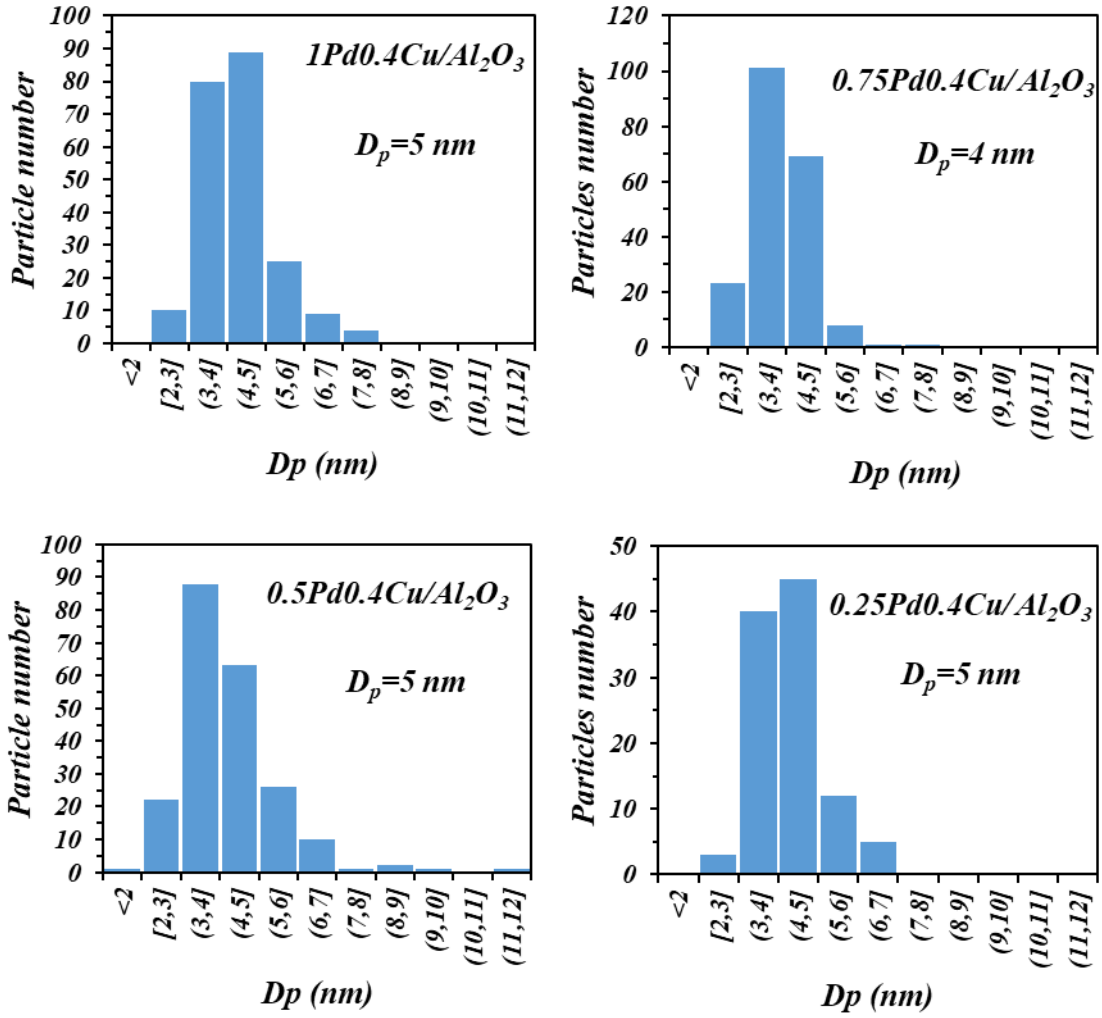

Figure 4.4 *Particle size distribution measured from the TEM images of the catalysts.*

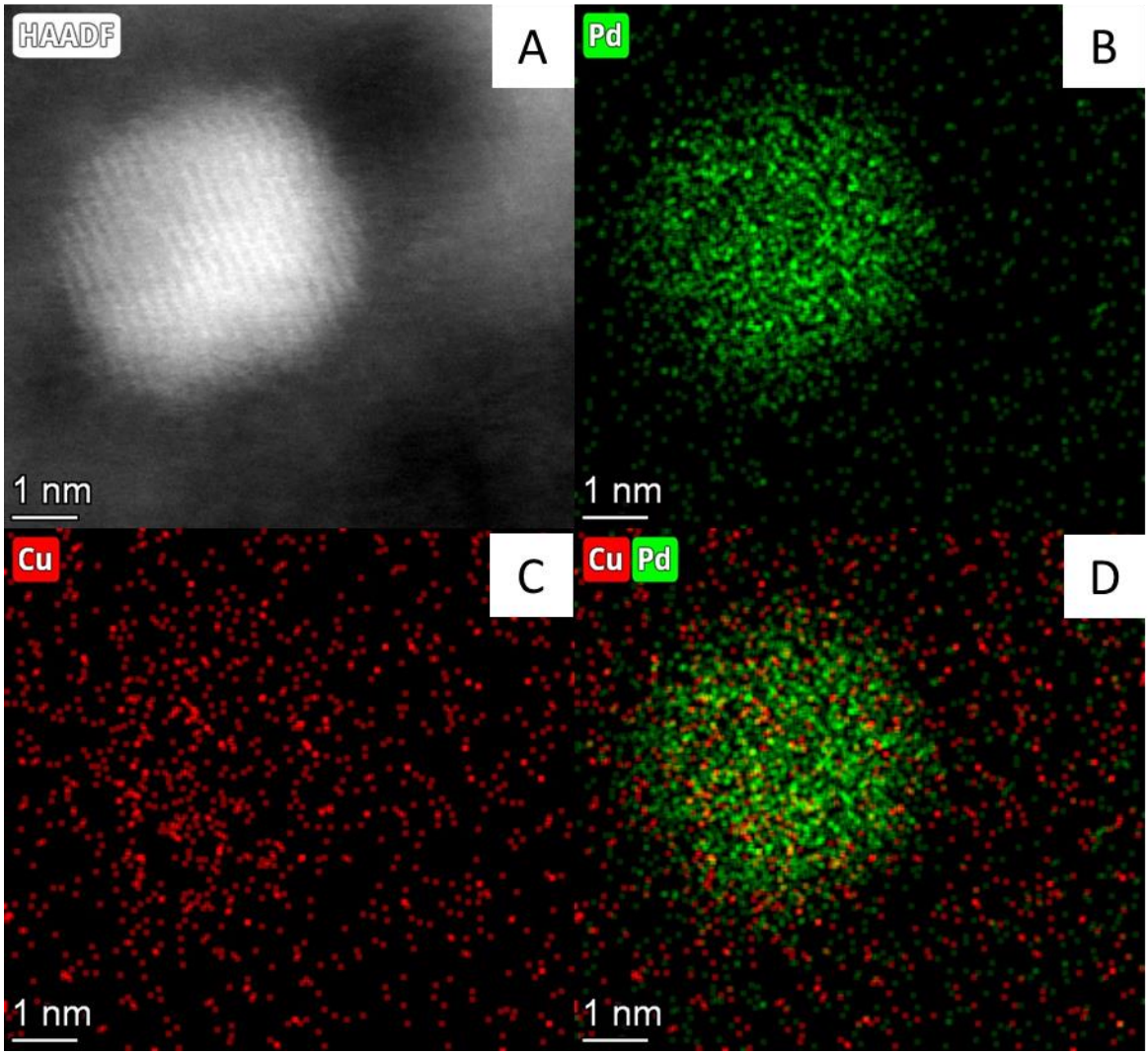

Figure 4.5 *HR-TEM images of 1Pd0.4Cu/Al_2O_3 catalyst: (A) HAADF image, EDS analysis of Pd (B, green), Cu (C, green) and PdCu (D).*

Table 4.2 *Mean Pd/Cu ratio at the nanoparticles of the different catalysts measured by EDX.*

Catalysts	***Pd%***	***Cu%***
1Pd0.4Cu0.4/Al_2O_3	*87.3*	*12.8*
0.75Pd0.4Cu0.4/Al_2O_3	*87.9*	*12.1*
0.5Pd0.4Cu0.4/Al_2O_3	*81.3*	*18.3*
0.25Pd0.4Cu0.4/Al_2O_3	*86.9*	*13.1*

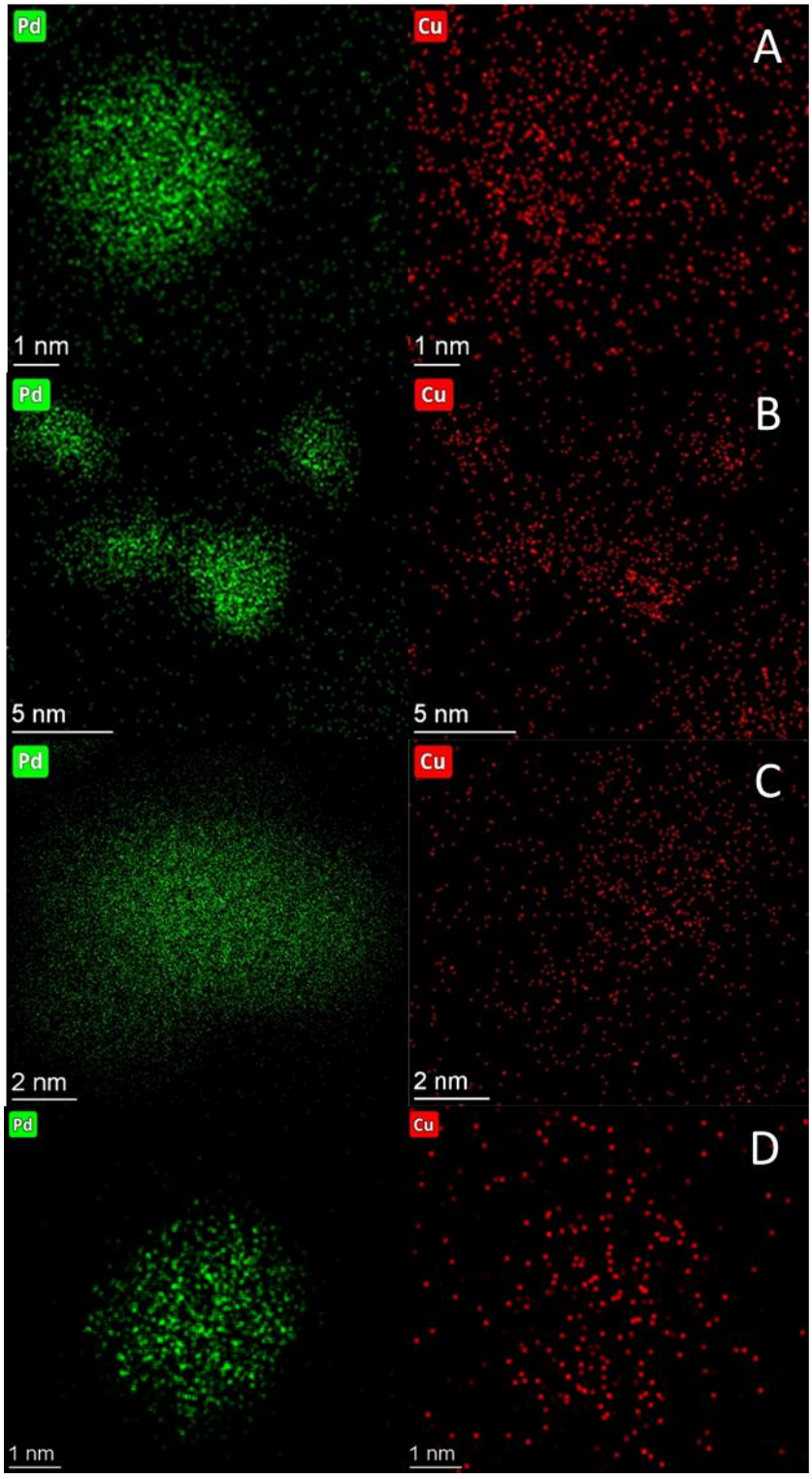

Figure 4.6 *EDS analysis of the HR-TEM images of the different catalyst: 1Pd0.4Cu/Al_2O_3 (A), 0.75Pd0.4Cu/Al_2O_3 (B), 0.5Pd0.4Cu/Al_2O_3 (C) and 0.25Pd0.4Cu/Al_2O_3 (D) (Pd: green; Cu: red).*

4.2.4. Temperature Programmed Reduction (TPR)

Temperature-programmed reduction of the catalysts (Figure 4.7) was realised with the aim of determining the reducibility and interactions between the active metals of the catalysts. The TPR profile of the monometallic catalyst Cu/Al_2O_3 (not shown) shows a peak at 553 K, related to the reduction of the CuO species [3]. On the other hand, the monometallic Pd catalysts show a peak at approximately 373 K, which is attributed to the reduction of the PdO species. The addition of Cu to the catalysts modified their reduction profile. Sá et al. [4] observed how the peat at 400K can be assigned to the reduction of mixed Pd-Cu oxidized species, with a reduction of the reduction temperature of the copper oxides due to the spill-over hydrogen adsorbed on the Pd. This singular reduction peak in the temperature between CuO and PdO indicates good contact between Cu and Pd [4]. Furthermore, it can be observed that hydrogen consumption decreases when metallic load of Pd diminishes but the reduction temperature does not vary significantly.

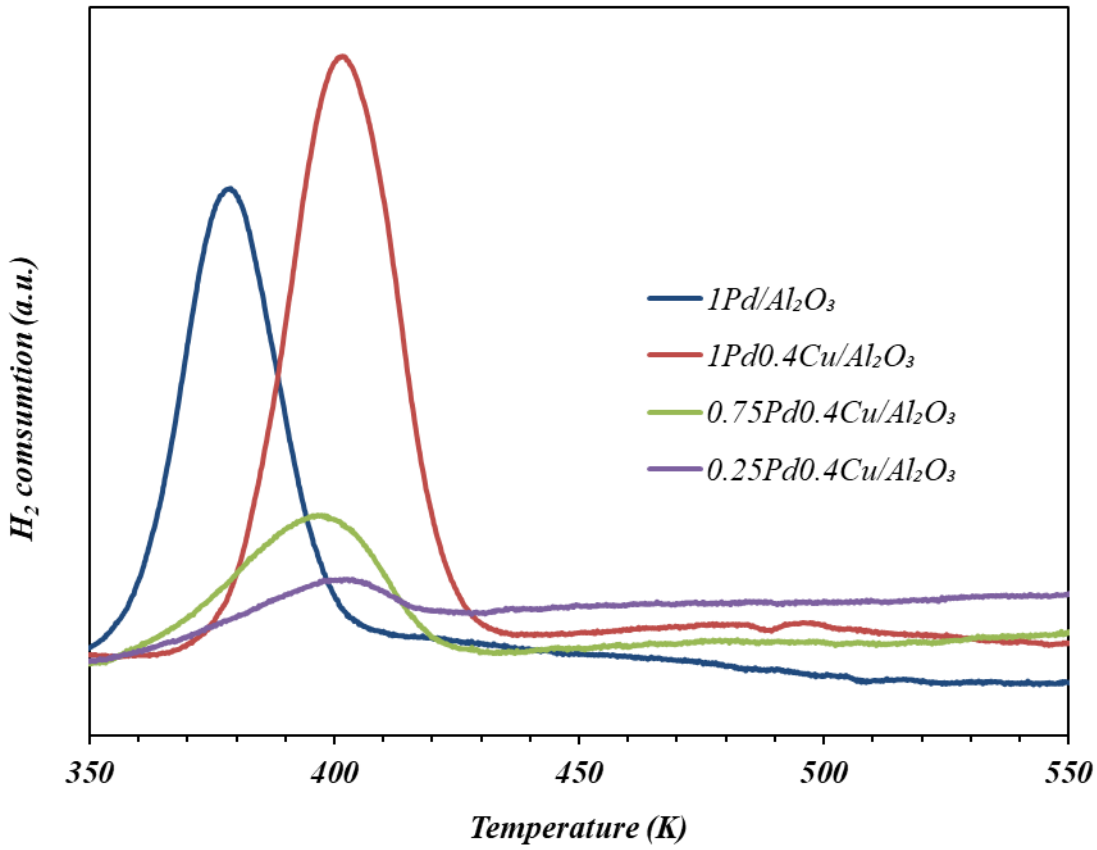

Figure 4.7 *TPR profiles of the fresh catalysts with different Pd load and without Cu.*

4.3. Catalytic tests:

4.3.1. Influence of stirring rate

The nitrate conversions obtained at different agitation rates of the aqueous solution are shown in Figure 4.8 Experiments were performed using 1Pd0.4Cu/Al_2O_3. The operational variables were 1 g $_{catalyst}$/L and 100 ppm initial nitrate concentration. It can be observed that the total conversion is obtained in all the experiments. However, this transformation was slower when the stirring rate was lower. The nitrate conversion rate increased when the agitation rate increased but reached a maximum at 900 rpm. This effect can be explained by considering that diffusional restrictions of hydrogen occur at low agitation rates, producing low adsorption of the gas on the active sites of the catalyst, and consequently, lower reaction rates. When the agitation rate is high (above 900 rpm), there are no diffusional restrictions, and consequently, the rate of transformation of nitrates is constant.

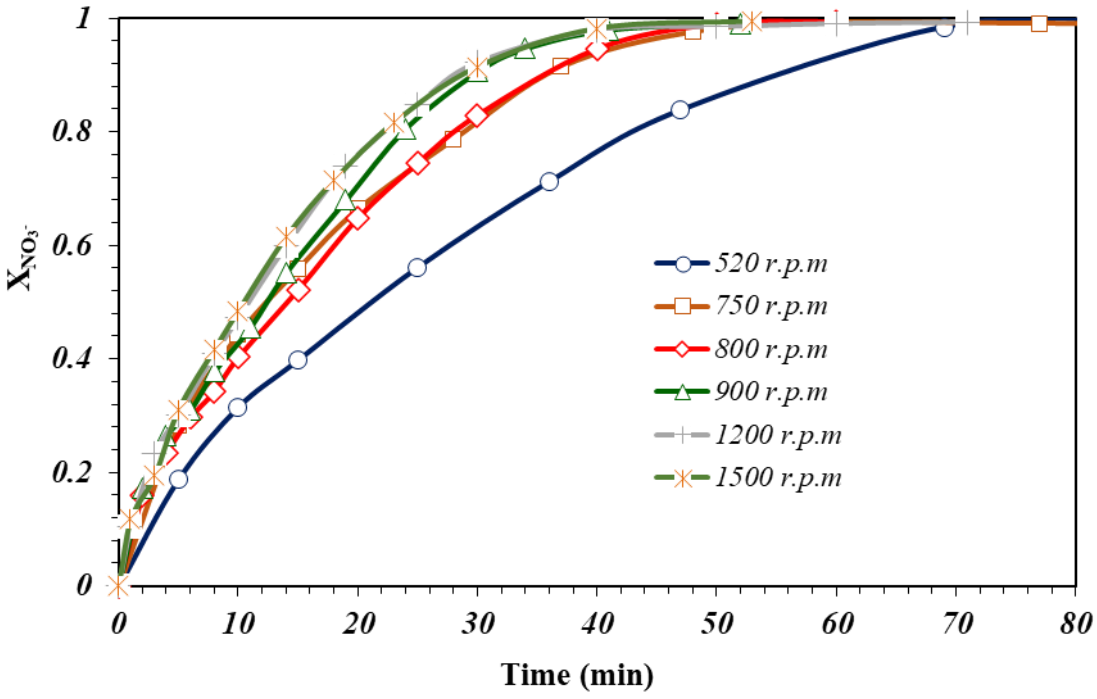

Figure 4.8 *Influence of stirring rate on the evolution of nitrate conversion along time.*

As shown in Figure 4.9, a low selectivity towards nitrite was observed for all the experiments and over all the reactions. In addition, nitrites are desorbed and reabsorbed in the proximity of the nanoparticles; therefore, the transference improvement from higher agitation does not significantly affect it. At the end of the reaction, the nitrite concentration was below the legal limit for all the experiments.

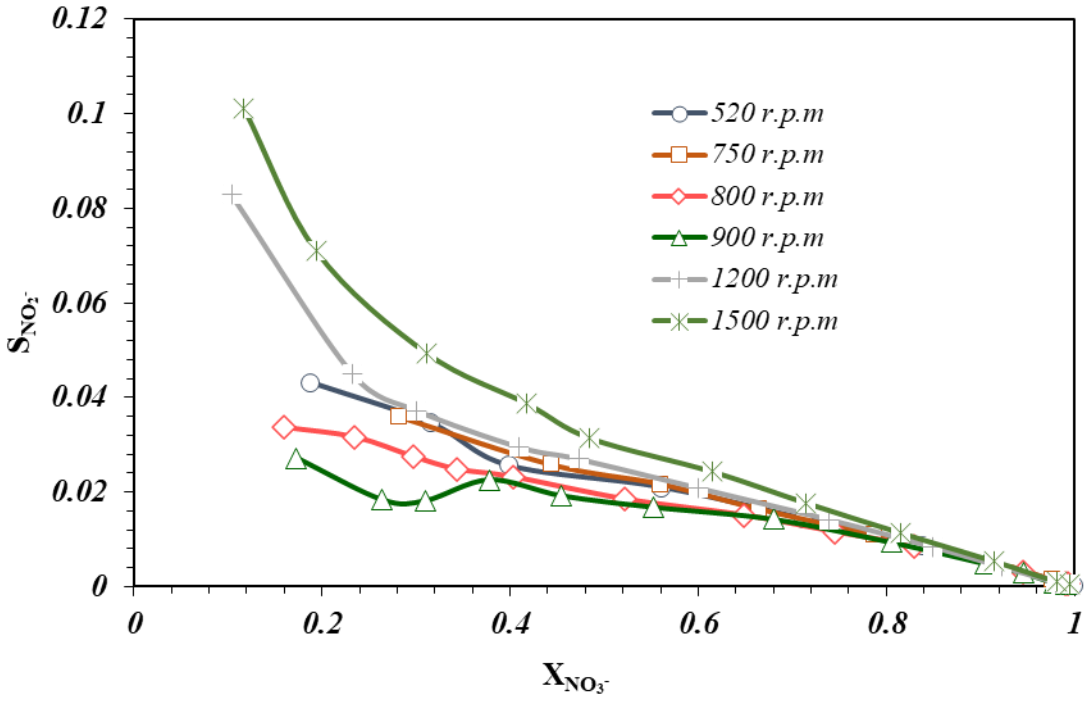

Figure 4.9 *Nitrite selectivity vs. nitrate conversion plots at the different stirring rates used.*

In this case, a clear tendency was not observed regarding the selectivity to ammonium versus nitrate conversion in the experiments (Figure 4.10). To appreciate the effect of agitation on the production of ammonium, the ammonium yield is shown in Figure 4.11. Two zones can be distinguished: when the stirring rate was low (520-750 rpm), slow nitrate conversion and low ammonium selectivity were observed. On the other hand, fast nitrate conversion and high selectivity to ammonium were observed at high agitation rates, which led to high ammonium yields. Considering these results, it can be concluded that agitation rate is an operational variable which is able to modulate the conversion and selectivity of the CSRN reaction [5–8]. As can be seen, the agitation grade also produced a change in the selectivity to N_2. When the agitation rate was low (520-750 rpm), the selectivity for ammonium was lower, reaching N_2 selectivity values of 88% at 750 rpm. This agrees with the literature, where a lower quantity of hydrogen adsorbed on the active sites, in relation to the N species adsorbed, increases the probability of the interaction between two N-species, which leads to N_2 formation instead of over-hydrogenation towards NH_4^+ [5–9]. In this study, 750 rpm was selected for subsequent studies. At this rate, the conversion is fast enough, which avoids undesired long reaction times for complete nitrate elimination, and selectivity to ammonium is adequate, obtaining values of 12%.

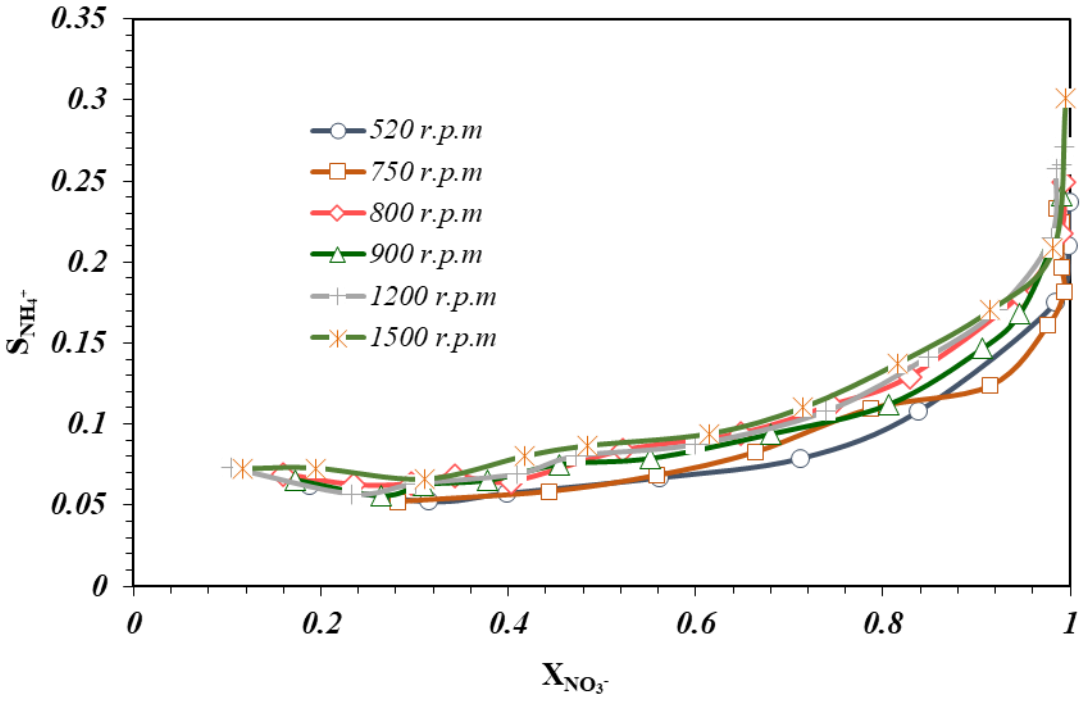

Figure 4.10 *Ammonia selectivity vs. nitrate conversion plots at the different stirring rates used.*

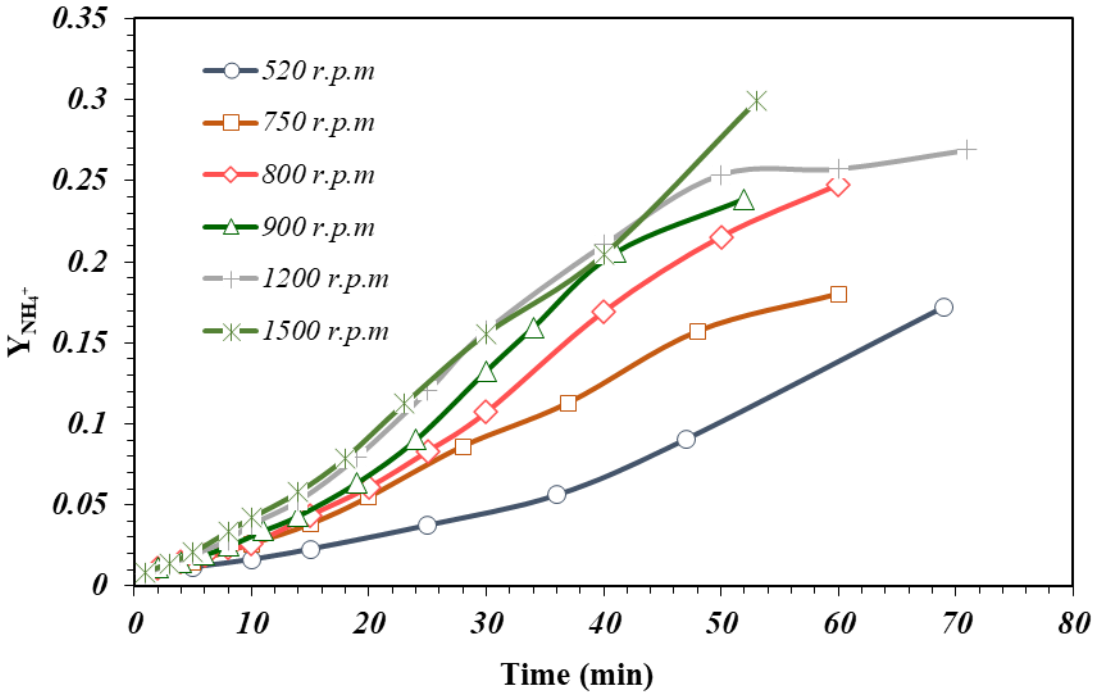

Figure 4.11 *Influence of stirring rate on the evolution of ammonia yield a long time.*

However, as shown in Figure 4.10, with the aim of optimizing the operational conditions for the future implementation of the process, it is also important to select an adequate reaction time. When the nitrate conversion was near 100%, there was a significant increase in the selectivity towards ammonium in all the experiments (Figure 4.10). As previously mentioned, the relationship between the N species and hydrogen on the surface of the nanoparticles is related to the selectivity towards N_2 or NH_4^+. At the end of the reaction, nitrates are almost completely reduced, so the density of the N-species, obtained from the reduction of these nitrates, is low, while the flow of hydrogen is constant during all the experiments, meaning that the quantity of hydrogen available is not reduced. Therefore, in this case, the N/H ratio on the nanoparticles is smaller and, consequently, the chances of ammonium formation are higher. Therefore, it was important to complete the reaction before this rapid increase.

The experimental results of this study were fitted with a kinetic model to deepen and quantify the influences observed on conversion and selectivity.

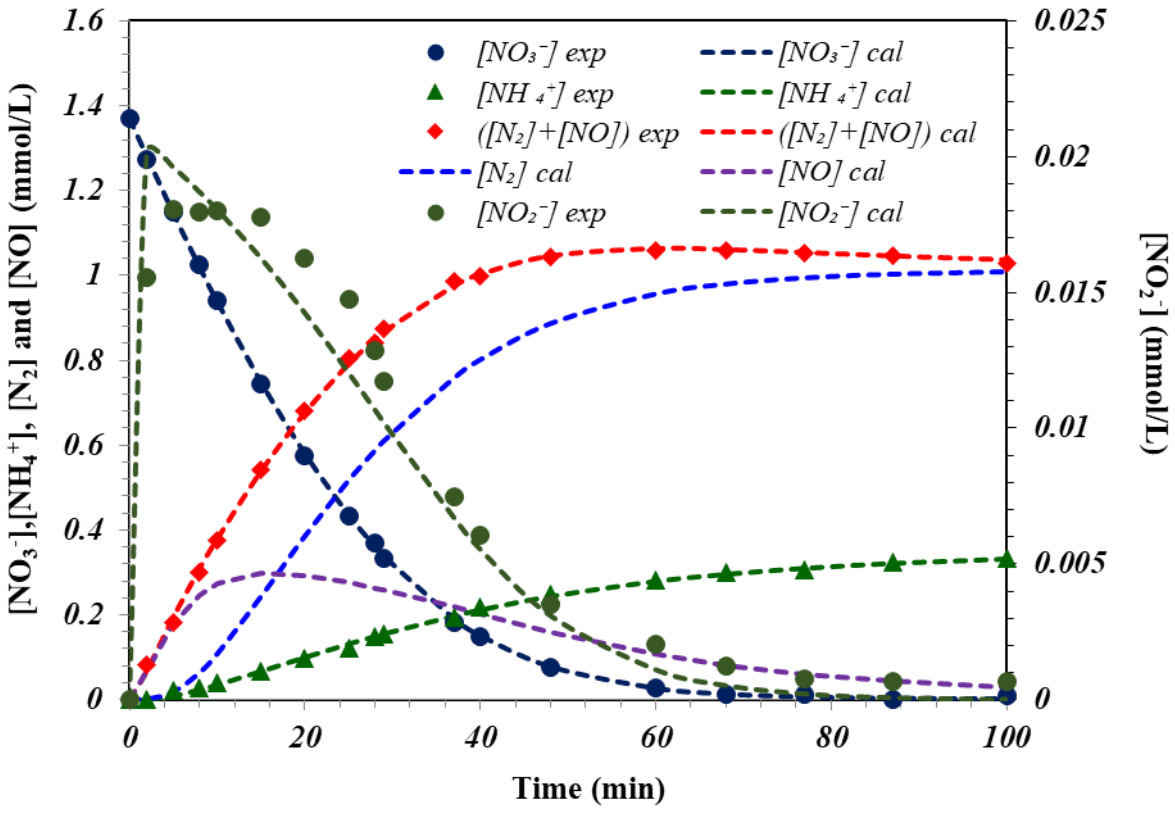

Figure 4.12 *Evolution along time of the different species considered. Dots (experimental values) dashed lines (model predictions).*

As an example, Figure 4.12 shows the evolution of nitrate, nitrite, nitrogen, and ammonium concentrations with reaction time using an agitation speed of 750 rpm, as well as the fitting of these curves using the kinetic model. As expected, nitrates were continuously consumed during the reaction until complete elimination. The nitrite concentration was very low during the reaction, reaching a maximum, followed by a decrease, associated with their rapid adsorption on the catalyst surface and subsequent conversion to NO. This indicates that the conversion of NO_3^- to NO_2^- is the limiting step of the CSRN reaction. Ammonium and nitrogen concentrations, as products of the reaction, increased until the reactants were almost completely converted.

Besides, as can be observed in Figure 4.12, the model fits the experimental results very satisfactorily, obtaining fitted values very close to the experimental ones. Furthermore, the model also predicts the concentrations of the intermediate species, NO.

Global fitting was realised by numerical integration of all experimental concentrations versus time data of the study, maximising the model selection criteria as an objective function, as mentioned above. The global MSC value obtained was 20.3, indicating a very good fit. In the fitting of this and the rest of the studies, k_2* was considered zero because experiments do not present residual concentrations of nitrites and are therefore irrelevant in these conditions, the contribution of the transformation of NO to nitrites. As mentioned before, the kinetic constant k_d was designated as 0 too, due to because no deactivation is observed.

In addition, K_{obs}, a constant related to the adsorption of nitrates on the catalyst surface, was maintained at a constant value in the fitting because it was considered that changes in agitation rate do not influence this adsorption.

The kinetic parameters are presented in Table 4.3. The kinetic constant related to the hydrogenation of nitrates to nitrites, k_1, increases with an increase in the agitation rate owing to the diminution of the diffusional restrictions and, consequently, the presence of a greater quantity of reactive and hydrogen adsorbed on the catalyst, which favours the transformation of nitrates to nitrites. At high agitation rates, this constant tends to a constant value because it reaches a state in which there are no diffusional restrictions. The constant related to the reduction of nitrites to NO, k_2, tends to increase until 900 rpm, when the diffusional restriction is negligible, from which it tends to decrease. Comparing k_1 and k_2, k_2 is one order of magnitude higher than k_1, indicating that the

conversion of NO_3^- to NO_2^- is the limiting step, as mentioned above. On the other hand, $k_3 \cdot \overline{NO} / k_4$ represent the tendency of the catalyst to produce N_2 or NH_4^+, having higher values related with higher selectivity towards N_2. The mean $k_3 \cdot \overline{NO} / k_4$ relation of this experiments shows two zones, low agitation rates (520-750 rpm) have higher mean $k_3 \cdot \overline{NO} / k_4$ values and high agitation rates have lower values, therefore the reaction of NO to nitrogen favoured over the reaction to ammonium at low agitation rates and corroborating the two zones related to the control of selectivity with this operating variable commented previously.

Table 4.3 *Values of the kinetic parameters for the CSRN under different stirring rates using 1 g/L of catalyst 1Pd0.4Cu/Al_2O_3 and 100ppm of initial nitrate concentration.*

Stirring speed (r.p.m.)	***520***	***750***	***800***	***900***	***1200***	***1500***
k_1 (NO_3^-) (mol.g.L^{-1}.min^{-1})	*0.04 ± 0.001*	*0.053 ± 0.001*	*0.061 ± 0.001*	*0.07 ± 0.002*	*0.079 ± 0.003*	*0.08 ± 0.003*
K_{obs} (NO_3^-)* (mol^{-1})	*2.572 ± 0.201*					
k_2 (NO_2^-) (g.L^{-1}.min^{-1})	*1.727 ± 0.265*	*2.147 ± 0.344*	*2.996 ± 0.421*	*4.131 ± 0.863*	*3.043 ± 0.717*	*2.38 ± 0.47*
k_3 (N_2) (g.mol^{-1}.L^{-1}.min^{-1})	*0.032 ± 0.005*	*0.34 ± 0.043*	*0.046 ± 0.006*	*0.044 ± 0.008*	*0.102 ± 0.016*	*0.036 ± 0.009*
k_4 (NH_4^+) (g.L^{-1}.min^{-1}.)	*0.008 ± 0.0003*	*0.023 ± 0.001*	*0.014 ± 0.001*	*0.015 ± 0.001*	*0.02 ± 0.001*	*0.016 ± 0.001*
$k_3 \cdot \overline{NO} / k_4$	*2.032*	*2.849*	*1.571*	*1.524*	*2.002*	*1.228*

*This value was considered constant for all experimental tests in this study

4.3.2. Influence of metallic content concentration of the catalyst

To study the influence of the metal loading of the catalyst, four catalysts, 1Pd0.4Cu/Al_2O_3, 0.75Pd0.4Cu/Al_2O_3, 0.5Pd0.4Cu/Al_2O_3, and 0.25Pd0.4Cu/Al_2O_3, were tested with 100 ppm of initial nitrates, 1 $g_{catalyst}$/L, and a stirring rate of 750 rpm. Figure 4.13 shows the nitrate conversion over time for a series of synthesised catalysts. As can be seen, higher Pd concentrations led to faster nitrate conversion. 0.25Pd0.4Cu/Al_2O_3 was the least active catalyst in this study and did not completely

eliminate the initial nitrate concentration after 470 min of reaction. As mentioned, it is assumed that nitrate hydrogenation occurs in the bimetallic active sites of the catalyst, where nitrates are adsorbed and converted to Cu nanoparticles, and H_2 is absorbed on Pd nanoparticles, allowing the regeneration of the oxidised Cu sites to its metallic state. The TEM images show that the catalysts have approximately the same Pd/Cu ratio in the nanoparticles, good contact between both metals, and the same nanoparticle size. Therefore, the increase in Pd translates to an increase in the number of bimetallic nanoparticles (Figure 4.2). Therefore, fewer nanoparticles led to a slower reduction in nitrates.

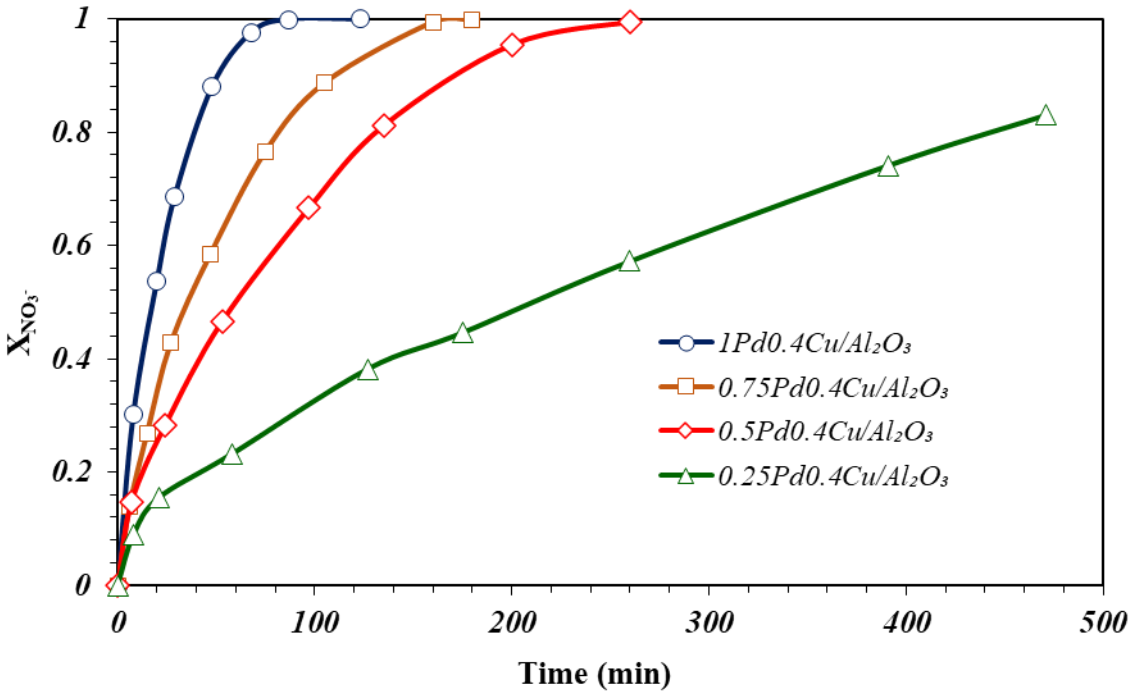

Figure 4.13 *Influence of the Pd content on the evolution along time of the nitrate conversion.*

With respect to the formation and transformation of nitrites to the intermediate species NO (Figure 4.14), the increase in the Pd concentration in the catalyst improves the reaction rate of nitrite reduction owing to an increase in the active sites of Pd in the catalyst, where this reaction takes place. On the other hand, the selectivity to N_2 or NH_4^+ did not show a determinate pattern in the Pd concentration (Figure 4.15). The characterisation results indicated that the nanoparticle size of the catalysts and the Pd/Cu ratio were not significantly affected by the increase in Pd concentration (Figure 4.6 and Table 4.2). For this reason, it is produced an increase in the available active sites with the increase in Pd and, consequently, the increase in the nitrite elimination

reaction and the non-variation of the selectivity observed. 1Pd0.4Cu/Al_2O_3 is the most active catalyst, reaching the total conversion of nitrates after 60 min of reaction and the selectivity to ammonium is low, 14%. Consequently, this catalyst was used in the remaining studies.

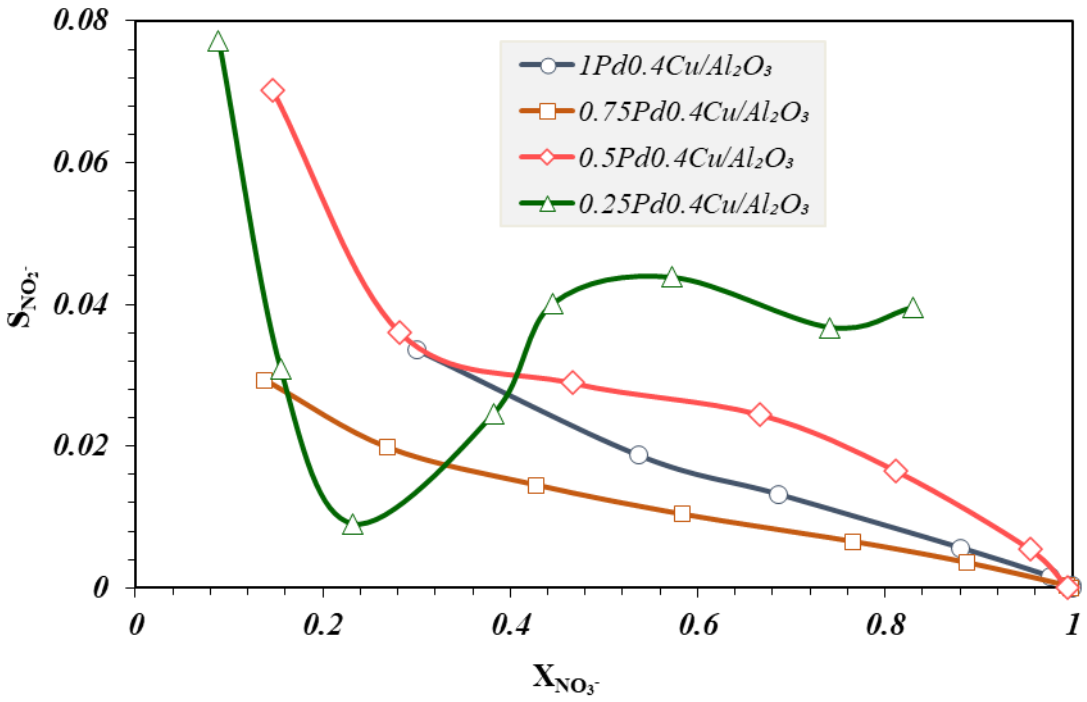

Figure 4.14 *Influence of the Pd content on the evolution of nitrite selectivity along time.*

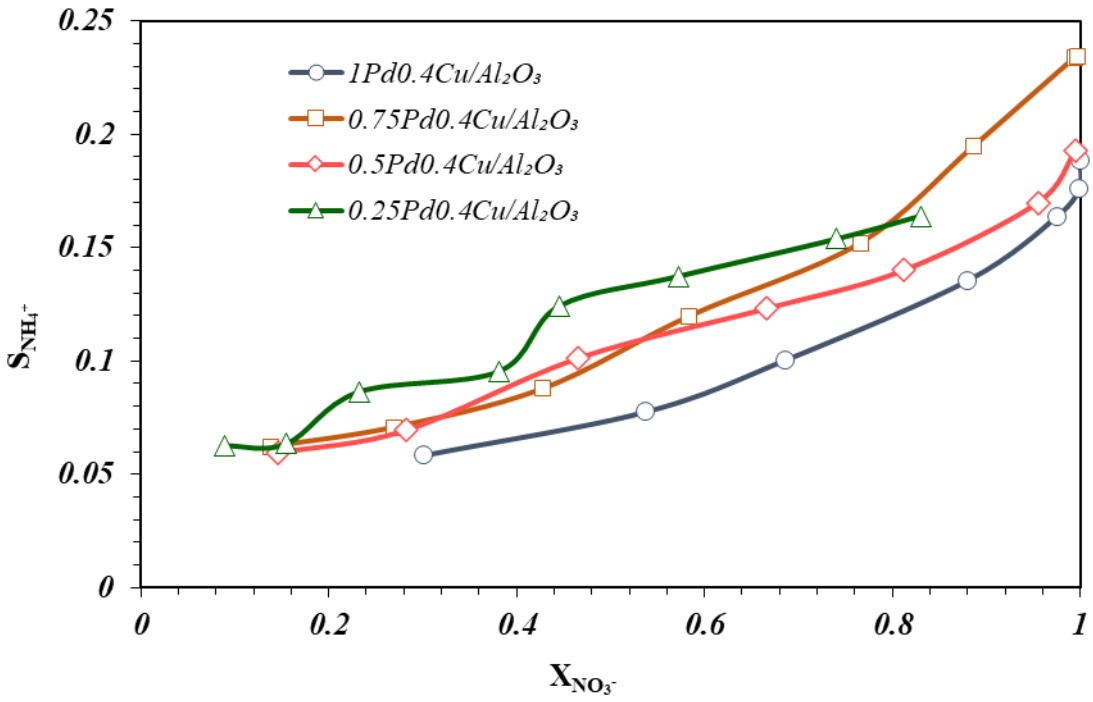

Figure 4.15 *Ammonia selectivity vs. nitrate conversion plots at the different Pd content used.*

The parameters obtained for the fitting in this study are listed in Table 4.4. The global MSC value was 19.4. As expected, and corroborating the experimental results, k_1 and k_2, related to nitrate and nitrite conversion, respectively, increased with increasing Pd content due to the increase in available active sites of the catalysts to carry out both reactions. K_{obs} was considered constant for these fittings since it was checked to be unaffected by the variation in catalyst composition. By the other hand, the ratio $k_3 \cdot \overline{NO} / k_4$, which represent the intrinsic selectivity towards nitrogen or ammonium, doesn't show a determinate tendency, and similar values have been obtained in the adjustment. This corroborates that the selectivity towards the final product of the reaction was not affected by the change in the composition of the catalyst, since similar particle size distributions were achieved regardless of its composition.

Table 4.4. Values of the kinetic parameters for the CSRN for different Pd loads using 1 g/L of catalyst at 750 r.p.m. and 100ppm of nitrate initial concentration.

Pd concentration	***1%***	***0.75%***	***0.50%***	***0.25%***
k_1 (NO_3^-) ($mol.g.L^{-1}.min^{-1}$)	*0.072 ± 0.001*	*0.029 ± 0.0016*	*0.017 ± 0.0005*	*0.005 ± 0.0003*
K_{obs} (NO_3^-) * (mol^{-1})	*1.344 ± 0.053*			
k_2 (NO_2^-) ($g.L^{-1}.min^{-1}$)	*2.233 ± 0.204*	*1.977 ± 1.0154*	*0.42 ± 0.0453*	*0.08 ± 0.009*
k_3 (N_2) ($g.mol^{-1}.L^{-1}.min^{-1}$)	*0.325 ± 0.025*	*0.111 ± 0.0345*	*0.484 ± 0.2165*	*0.5 ± 0.748*
k_4 (NH_4^+) ($g.L^{-1}.min^{-1}$.)	*0.022 ± 0.001*	*0.01 ± 0.0014*	*0.013 ± 0.0028*	*0.008 ± 0.005*
$k_3 \cdot \overline{NO} / k_4$	*3.549*	*2.861*	*3.961*	*3.987*

*This value was considered constant for all experimental tests in this study.

4.3.3. Influence of catalyst load

This series of experiments was designed with the aim of studying the deactivation of the catalyst during the reaction, which is difficult to study because of the discontinuous configuration of the experimental system. The experiments were performed at an agitation rate of 750 rpm and an initial nitrate concentration of 100 ppm. In addition to

the previous studies, the feed flow was 250 NmL/min for H_2 and 250 NmL/min for CO_2, and the catalyst load was varied from 0.25 to 2 g/L.

Figure 4.16 shows the nitrate conversion versus the time of reaction normalised with the ratio of $g_{catalyst/Lsolution}$ used in each experiment. As can be seen, the trend and the normalised values of nitrate conversion are practically the same regardless of the concentration of the catalyst used, which indicates that it does not suffer deactivation during the reaction. As expected, greater quantities of catalyst led to faster elimination of nitrates, but the nitrate hydrogenation rate per gram of catalyst was very similar in all cases [10]. In Figure 4.17, it can be seen that as well as the NO_3^- conversion when we represent NO_2^- selectivity over time normalised with the ratio $g_{catalyst}/L_{solution}$, there is no significant difference between the different catalyst loads. In addition, the selectivity of the reaction was not affected, as shown in Figure 4.18, the graph does not show a trend.

A concentration of 1 g/L was chosen as the optimum because the reaction time for nitrate elimination was adequate and the reproducibility of the experiments was good with 1 g of the catalyst.

To corroborate and quantify these results, fitting of the experiments was performed. The values of the kinetic parameters are listed in Table 4.5 and the global MSC value obtained was 20.28. k_1 shows a small decrease at higher catalysts loads, while the rest remain mostly constant. The $k_3 \cdot \overline{NO} / k_4$ don't show a big difference.

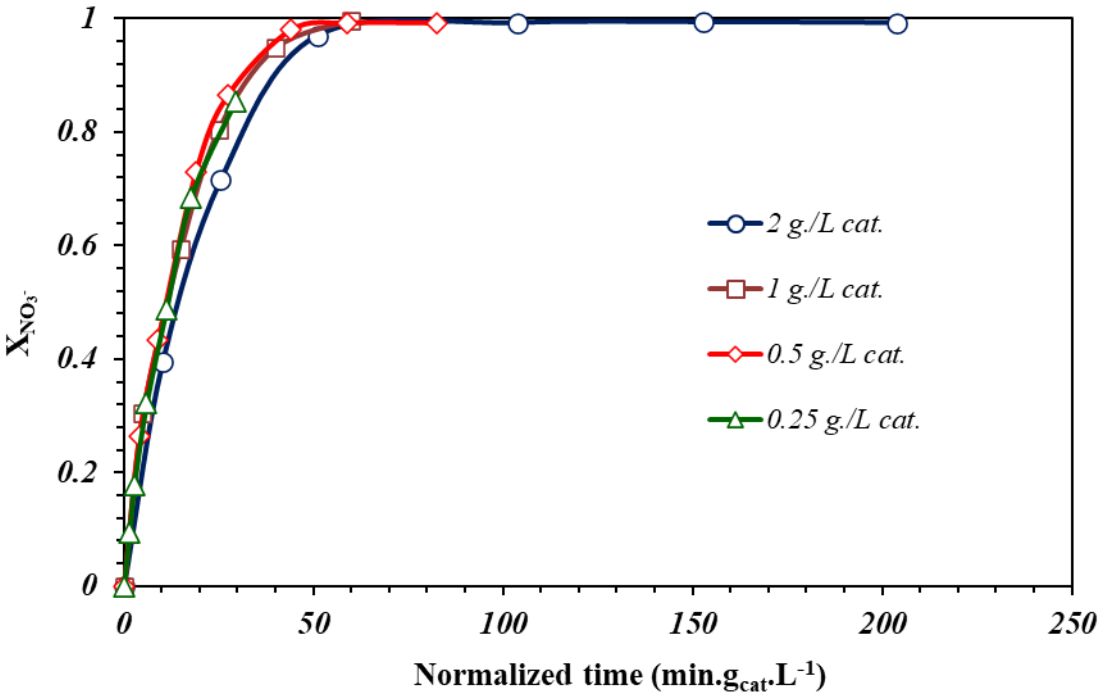

Figure 4.16 *Evolution of nitrate conversion vs. normalized time.*

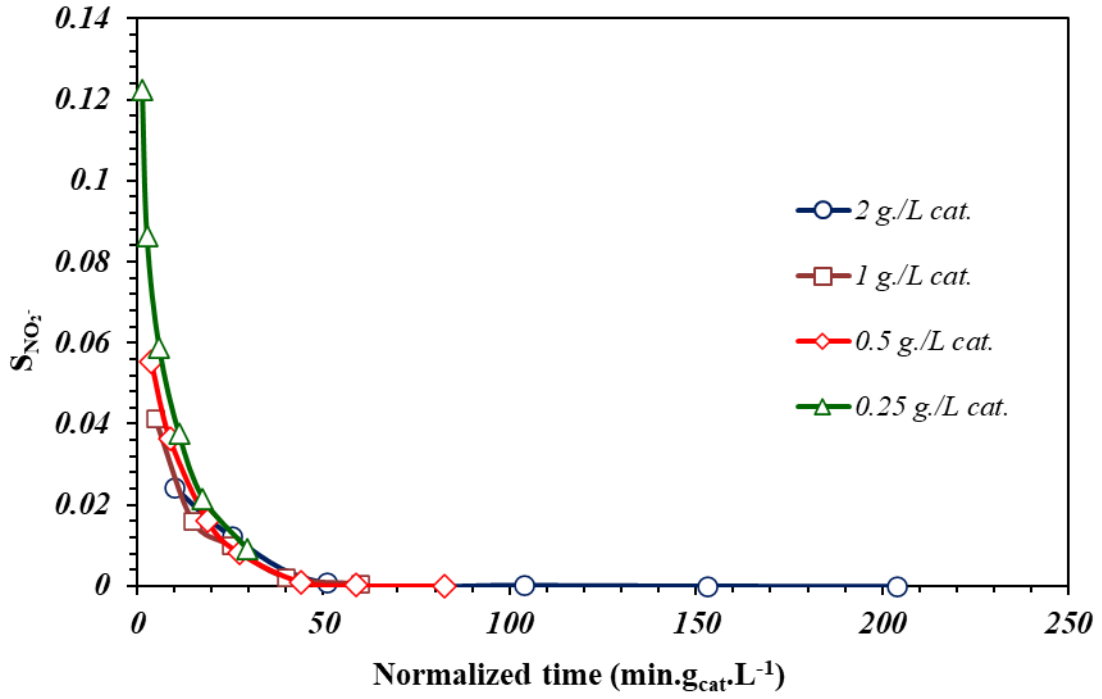

Figure 4.17 *Influence of the catalyst concentration on the evolution of nitrite selectivity along normalized time.*

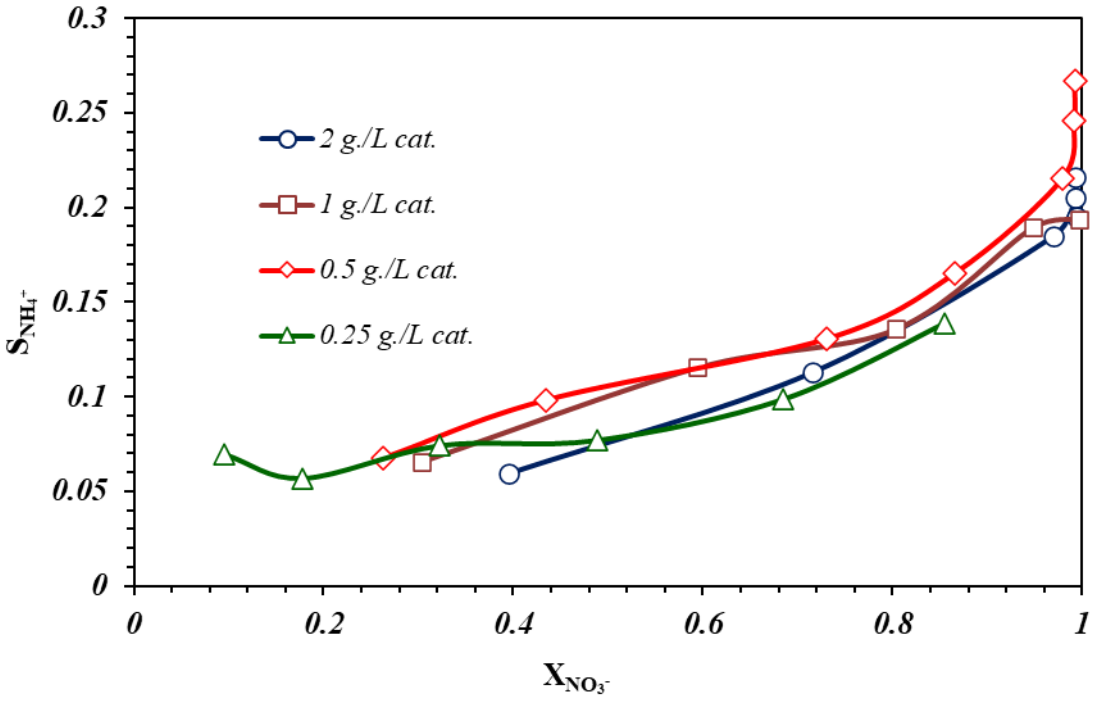

Figure 4.18 *Ammonia selectivity vs. nitrate conversion plots at the different catalyst concentrations used.*

Table 4.5 *Values of the kinetic parameters by catalyst load for the CSRN with different catalyst loads of catalyst 1Pd0.4Cu/Al_2O_3, with a stirring rate of 750 rpm. and 100ppm of nitrate initial concentration.*

Catalyst load	***0.25 g_{cat}/L***	***0.50 g_{cat}/L***	***1 g_{cat}/L***	***2 g_{cat}/L***
k_1 (NO_3^-) ($mol.g.L^{-1}.min^{-1}$)	*0.155 ± 0.001*	*0.151 ± 0.001*	*0.11 ± 0.001*	*0.092 ± 0.005*
K_{obs} (NO_3^-) * (mol^{-1})	*1.451 ± 0.112*			
k_2 (NO_2^-) ($g.L^{-1}.min^{-1}$)	*3.446 ± 0.082*	*4.046 ± 0.144*	*3.578 ± 0.205*	*3.914 ± 1.372*
k_3 (N_2) ($g.mol^{-1}.L^{-1}.min^{-1}$)	*0.447 ± 0.045*	*0.387 ± 0.012*	*0.517 ± 0.024*	*0.517 ± 0.095*
k_4 (NH_4^+) ($g.L^{-1}.min^{-1}.$)	*0.034 ± 0.001*	*0.045 ± 0.001*	*0.036 ± 0.001*	*0.032 ± 0.003*
$k_3 \cdot \overline{NO} / k_4$	*4.078*	*2.660*	*3.497*	*3.592*

*This value was considered constant for all experimental tests in this study.

4.3.4. Influence of the relationship between CO_2 and H_2

The nitrate conversion over time obtained using a feed flow composed of different ratios hydrogen/ carbon dioxide (H_2/CO_2) can is shown in Figure 4.19 The total feed flow was maintained at 900 NmL/min, whereas the H_2/CO_2 ratio varied with increasing CO_2 and reducing H_2 in the flow. In this way, we have four tests: no CO_2, a relation of 1/1, 1/2, and 1/3. The catalyst was deactivated when CO_2 was not introduced and did not achieve total conversion of the nitrates. In the presence of CO_2, it can be observed that there is an optimum H_2/CO_2 ratio of 1/2 which leads to faster conversion of nitrates; however, in the cases of 1/1 and 1/2, there is no significant difference, with a slightly faster conversion in the case of 1/2. This is because of the role of CO_2 as a pH controller and how CO_2 reacts in water and with the hydroxide ions formed during CSRN, as follows:

$$CO_2 + H_2O \rightarrow HCO_3^- + H^+$$
$$OH^- + H^+ \rightarrow H_2O$$

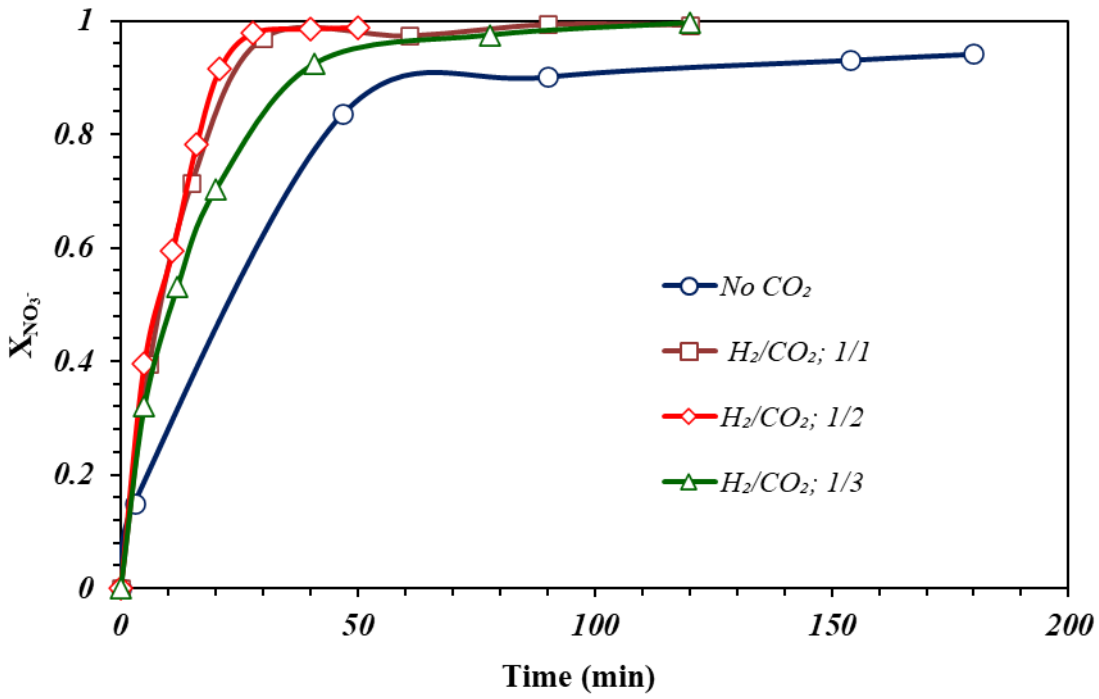

Figure 4.19 *Influence of H_2/CO_2 relation at the feed flow on the evolution of nitrate conversion along time.*

This cleans the Pd active sites, avoiding the adsorption of OH^- ions on the active sites of the catalyst and eventually hinders the regeneration of Cu. In addition, the presence of these OH^- ions adsorbed on the catalyst produces a negative charge [11,12], which

means that the negative ions are repelled and therefore, the reaction does not take place, which can be observed in the deactivation of the catalyst when no CO_2 is added to the reaction. On the other hand, in the case of the 1/3 test, the nitrate reduction is slowed owing to the production of high quantities of bicarbonate which are adsorbed on the nitrate active sites and decrease the nitrate conversion ratio [11]. This is because there is an optimum of nitrate conversion around 1/1 and 1/2 where there is a neutralisation of the OH^-, avoiding its adsorption on Pd which enhances the regeneration of Cu and a lack of HCO_3^- which hinders the adsorption of NO_3^-.

The final pH values of each test (Table 4.6) show how an increase in the H_2/CO_2 ratio leads to a higher pH, which strongly affects the absence of CO_2 at a pH of 10. This value shows how some carbon dioxide can significantly neutralise the hydroxides formed during the reaction.

Table 4.6 *The pH values for different H_2/CO_2 relations in the feed flow using 2 g/L of the catalyst at 750 rpm. and 100ppm of nitrate initial concentration.*

H_2/CO_2	***Final pH***
No CO_2	*10*
1/1	*5.5*
1/2	*5*
1/3	*4.5*

This effect was also observed during the transformation of nitrites. Figure 4.20 shows the NO_2^- selectivity versus the nitrate conversion. It can be observed that the selectivity was much higher when CO_2 was not fed. Therefore, as mentioned above, deactivation of the active sites due to the adsorption of OH^- hinders the adsorption of NO_2^- on the Pd and its conversion to NO. This eventually produces a negative charge on the catalysts which also repels NO_3^-.

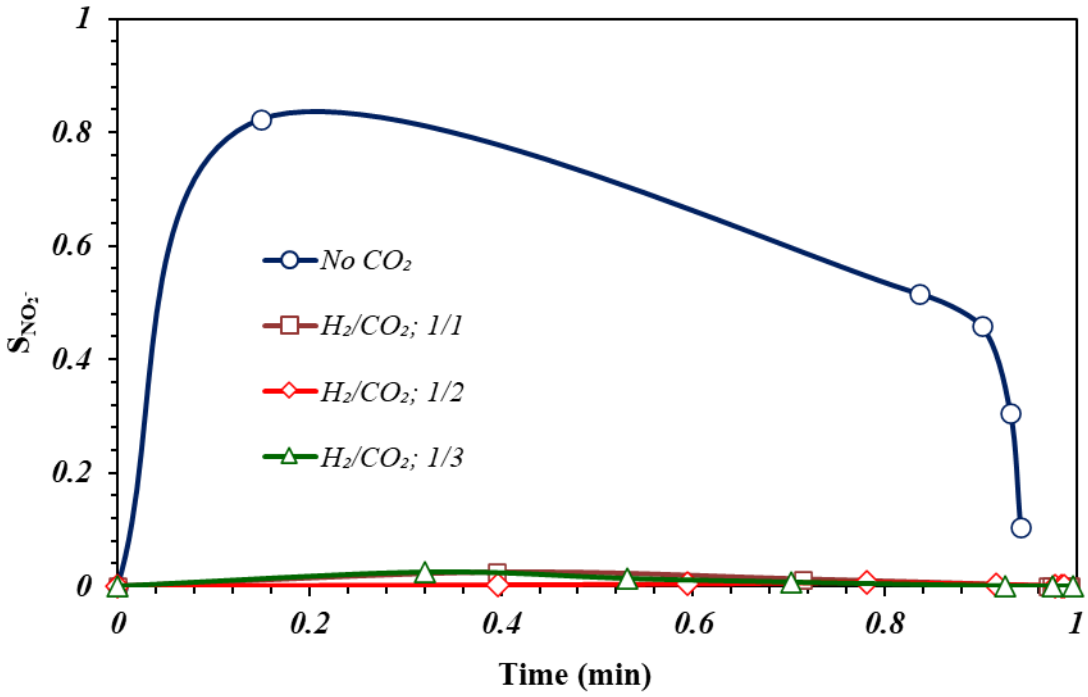

Figure 4.20 *Influence of H_2/CO_2 relation at the feed flow on the evolution of nitrite selectivity along time.*

With respect to the selectivity to NH_4^+, lower H_2/CO_2 ratios reduced the selectivity to NH_4^+ (Figure 4.21). As mentioned previously, the selectivity towards N_2 or NH_4+ is related to the quantity of NO_2^- adsorbed on the Pd active sites in relation to the adsorbed hydrogen. Higher quantities of CO_2 improved the neutralisation of OH^- and enhanced the adsorption of NO_2^-, increasing the ratio of N species adsorbed on its surface. On the other hand, the presence of bicarbonates doesn't affect the adsorption of NO_2^- like it happened to NO_3^- due to the different absorption sites for NO_2^- and NO_3^-, Pd and Cu respectively, been the bicarbonates been adsorbed only in the Cu sites. For this reason, higher relations of CO_2 improve the adsorption of NO_2^- and the selectivity towards N_2 [5–9].

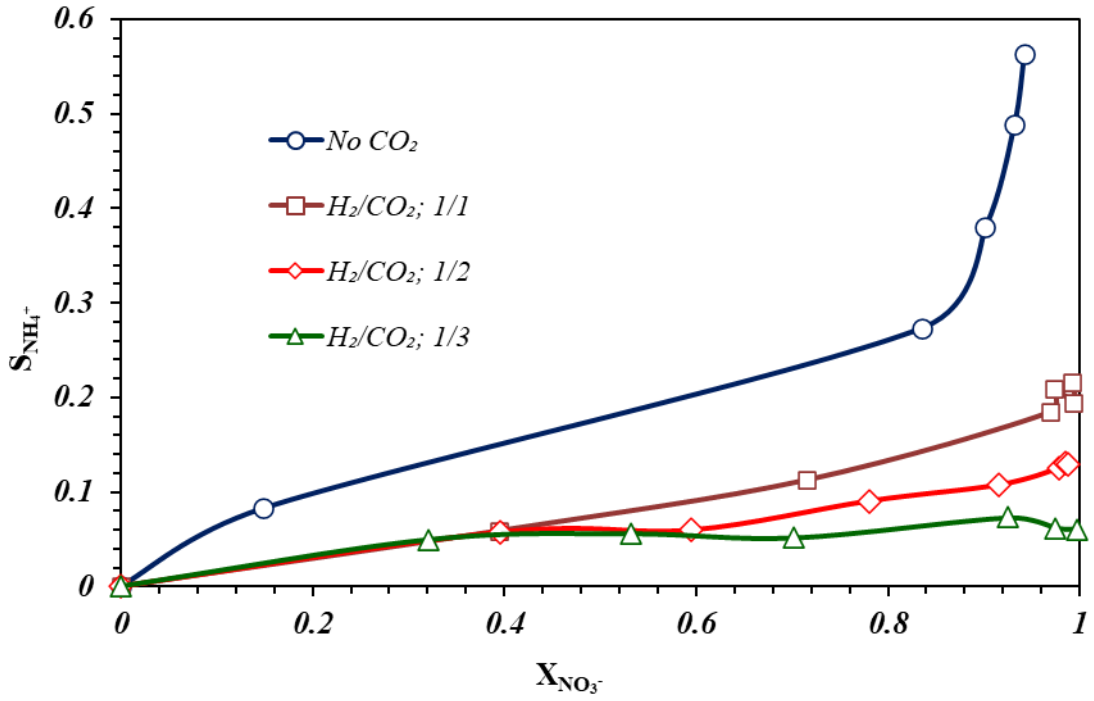

Figure 4.21 *Ammonia selectivity vs. nitrate conversion plots with different H_2/CO_2 relations at the feed flow.*

Table 4.7 *Values of the kinetic parameters for the CSRN for different H_2/CO_2 relations in the feed flow using 2 g/L of catalyst at 750 rpm. and 100ppm of nitrate initial concentration.*

H_2/CO_2	No CO_2	1/1	1/2	1/3
k_1 (NO_3^-) ($mol.g.L^{-1}.min^{-1}$)	3.491 ± 0.584	0.089 ± 0.007	0.094 ± 0.005	0.087 ± 0.026
K_{obs} (NO_3^-) (mol^{-1})	0.013 ± 0.0002	2.645 ± 0.642	2.657 ± 0.431	2.615 ± 0.318
k_1* ($g.L^{-1}.min^{-1}$)	0.046	0.235	0.249	0.227
k_2 (NO_2^-) ($g.L^{-1}.min^{-1}$)	0.012 ± 0.001	3.864 ± 2.559	12.755 ± 16.545	4.92 ± 10.175
k_3 (N_2) ($g.mol^{-1}.L^{-1}.min^{-1}$)	5.055 ± 0.652	1.292 ± 0.55	2.025 ± 0.11	0.63 ± 0.258
k_4 (NH_4^+) ($g.L^{-1}.min^{-1}$.)	0.253 ± 0.016	0.06 ± 0.014	0.05 ± 0.021	0.011 ± 0.002
k_d ($g.L^{-1}.min^{-1}$.)	0.078 ± 0.023	0	0	0
$k_3 \cdot \overline{NO} / k_4$	0.379	1.022	3.553	5.575

The parameters obtained for the fitting of this study are listed in Table 4.7, and the global MSC value obtained was 15.5. As mentioned before, due to the deactivation of the test without CO_2, we used the model with deactivation (k_d). In previous experiments,

there was no variation in the adsorption of nitrates (K_{obs}); therefore, we could compare the intrinsic nitrate conversion to the kinetic constant k_1. In this case, we can see that the test without CO_2 has a much higher value for the kinetic constant k_1, but it has a K_{obs}, two order of magnitude inferior to the rest of tests. In this case, due to the variation of K_{obs}, we used k_1^*, the product of k_1 by K_{obs}, to compare the intrinsic nitrate conversion. We can see that there is a maximum for k_1^* at the 1/2 H_2/CO_2 relation, but there is no significant difference between tests 1/1 and 1/3. On the other hand, it can be observed that the test without CO_2, despite having a higher k_1, has the lowest k_1^* owing to the low adsorption of nitrates. The test with no CO_2 is the only one which shows deactivation, k_d, which is the reason why the experimental test does not achieve total conversion of nitrates. Regarding the nitrite conversion, it can be observed that the test without CO_2 has the lowest k_2, and the 1/2 test shows the highest k_2, in agreement with the experimental results. At last, it can be seen how when CO_2 is added the ($k_3 \cdot \overline{NO} / k_4$) increase significantly and higher relation of CO_2 increase gradually the selectivity towards N_2.

4.3.5. Influence of ions on water

Finally, to have an approach to the reaction in a real situation, the reaction was carried out using distilled water, mineral water, and tap water. The experimental conditions were 1 g $_{catalyst}$/L, 100 ppm initial nitrate concentration, stirring at 750 rpm, and 500 NmL/min total flow (1/1 H_2/CO_2). In Figure 4.22, it can be observed that tap water has lower activity than mineral water and distilled water; similarly, in the same way mineral water has a lower activity than distilled water.

Table 4.8 *Ionic concentrations of the water samples.*

	Distilled water	***Mineral water***	***Tap water***
Conductivity (µS/cm)	*<1*	*513*	*653*
Calcium (mg/L)	-	*60.0*	*64.1*
Chloride (mg/L)	-	*8.3*	*94.9*
Sulphates (mg/L)	-	*21.8*	*88.8*
Sodium (mg/L)	-	*4.8*	*66.9*
Magnesium (mg/L)	-	*26.7*	*11.3*

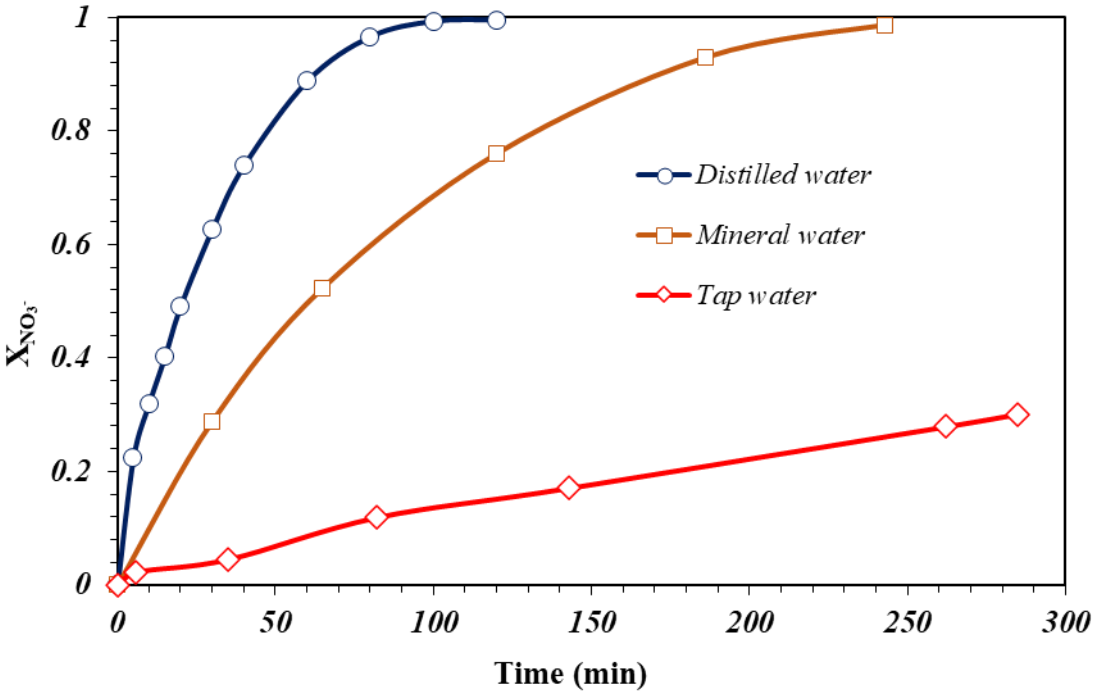

Figure 4.22 *Influence of ion in the water on the evolution of nitrate conversion along time.*

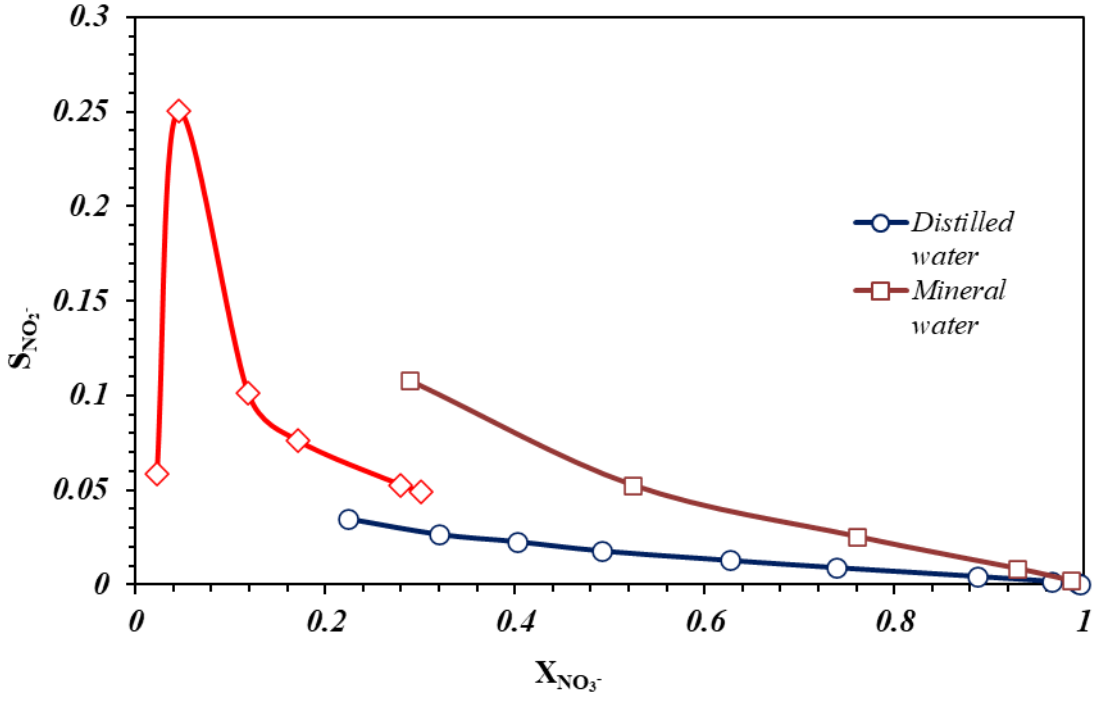

}

Figure 4.23 *Influence of ion in the water on the evolution of nitrate conversion along time.*

Regarding the conductivity of this different water in Table 4.8 (653 µS/cm for tap water, 513 µS/cm for mineral water, and lower than 1 µS/cm for distilled water), which is related to the quantity of ions in the water, a higher concentration of ions is related to a lower nitrate conversion rate. This slower nitrate conversion may be due to the competitive adsorption of the anions present in mineral and tap water with NO_3^-. In contrast, NO_2^- selectivity did not change significantly between the different tests (Figure 4.23), indicating that competitive adsorption only occurs with NO_3^- and has little to no effect on the adsorption of NO_2^-. These results are in accordance with those reported by Chaplin et al. [11].

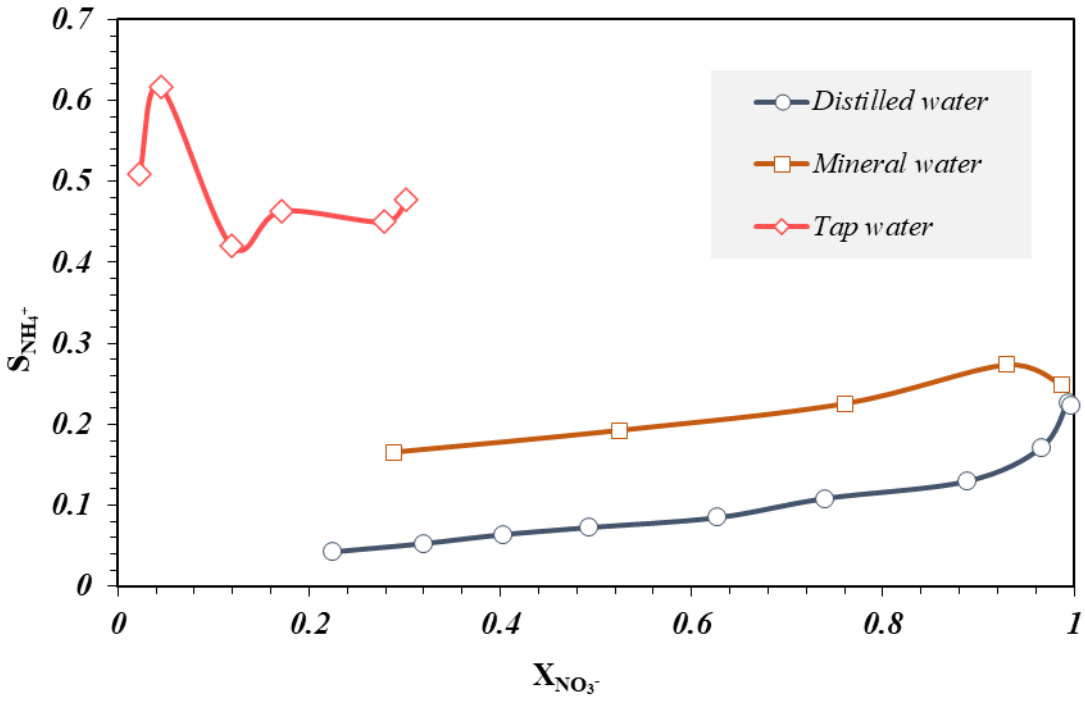

Figure 4.24 *Ammonia selectivity vs. nitrate conversion plots with different ion concentration in the water*

In Figure 4.24, which shows the selectivity towards NH_4^+ versus the nitrate conversion, it can be observed that tap water has a much higher NH_4^+ production than mineral and distilled water, and following the tendency of nitrate conversion, mineral water has higher selectivity to ammonium than distilled water. In a previous study, it was found that higher concentrations of chlorides and sulphates were related to higher NH_4^+ selectivity. This is due to the phenomenon, previously mentioned, of a competitive adsorption of this anions and the NO_2^-, resulting in a reduction of the relation N/H on the surface of the Pd and an increase in the formation of NH_4^+ [11–13].

As can be observed in Table 4.8, the concentrations of chlorides and sulphates followed the same tendency as the selectivity towards ammonium, which was higher in the following order: tap water, mineral water, and distilled water.

Table 4.8 *Ionic concentrations of the water samples.*

	Distilled water	***Mineral water***	***Tap water***
Conductivity (µS/cm)	*<1*	*513*	*653*
Calcium (mg/L)	-	*60.0*	*64.1*
Chloride (mg/L)	-	*8.3*	*94.9*
Sulphates (mg/L)	-	*21.8*	*88.8*
Sodium (mg/L)	-	*4.8*	*66.9*
Magnesium (mg/L)	-	*26.7*	*11.3*

As previously mentioned, the kinetic constant for the adsorption calculated in this case is an apparent kinetic constant which considers the presence of other ions (K_{obs}), and k_d was considered to be 0. The global MSC value obtained was 21.04. As shown in Table 4.9, k_1^* had higher values when water with lower conductivity was used (distilled water > mineral water > tap water). The value of k_1^* when water with more ions is used, the difference between distilled water and mineral or tap water, is much larger than the difference between mineral and tap water. On the other hand, the experimental results show a tendency for the disappearance of nitrites. However, in the results of k_2, a lower conductivity in water means an increase in k_2. Finally, $k_3 \cdot \overline{NO} / k_4$ shows the same trend that the rest of parameters, being higher when the water has lower conductivity.

Table 4.9 Values of the kinetic parameters for CSRN for different water samples using 1 g/L of catalyst at 750 rpm. and 100ppm of nitrate initial concentration.

Water	***Distilled***	***Mineral***	***Tap***
k_1 (NO_3^-) $(mol.g.L^{-1}.min^{-1})$	*0.069 ± 0.001*	*0.015 ± 0.001*	*0.079 ± 0.001*
K_{obs} (NO_3^-) (mol^{-1})	*1.451 ± 0.057*	*1.798 ± 0.363*	*0.016 ± 0.0002*
$k1^*$ $(g.L^{-1}.min^{-1})$	*0.100*	*0.028*	*0.001*
k_2 (NO_2^-) $(g.L^{-1}.min^{-1})$	*2.236 ± 0.205*	*0.207 ± 0.045*	*0.078 ± 0.016*
k_3 (N_2) $(g.mol^{-1}.L^{-1}.min^{-1})$	*0.323 ± 0.024*	*17.176 ± 0.802*	*32.072 ± 2.039*
k_4 (NH_4^+) $(g.L^{-1}.min^{-1}.)$	*0.022 ± 0.001*	*0.123 ± 0.003*	*0.178 ± 0.006*
$k_3 \cdot \overline{NO} / k_4$	*3.097*	*2.014*	*0.849*

4.4. Combination of ion exchange resin with 1%Pd0.4%Cu/Al_2O_3.

4.4.1. Isotherm adsorption

To study the kinetics of Amberlite IR120 H^+ in the adsorption of NH_4^+ formed during CSNR, we performed a study of NH_4^+ removal with different amounts of resin. Amberlite IR 120 H^+ is sulfonated polystyrene cross-linked with divinylbenzene, and the active site is a cationic site on the sulfonated group, which can be exchanged for another cationic species [14]. Adsorption isotherm was obtained following the method described in Section 2.4.3. To model the adsorption, we employed equation 3.81, as shown in Section 3.1.2.2. to calculate the rate of transfer of ammonium from the liquid to the solid phase.

$$J_{NH_4^+} = \frac{dC^l_{NH_4^+}}{dt} = -(K_L \cdot a) \cdot (C^l_{NH_4^+} - C^{l,*}_{NH_4^+}) \qquad (3.81)$$

Three different models were employed to calculate the ammonium concentration at equilibrium in the liquid phase ($C^{l,*}_{NH_4^+}$): Langmuir, Freundlich and Temkin. The

equations for each model are presented in Section 3.1.2.2. and correspond to Equations 3.82, 3.83, and 3.84, respectively. the three models adjust the experimental data perfectly. The maximum capacity of Amberlite IR120 H^+ for NH_4^+ retention was also evaluated using the Langmuir equation, obtaining a $C_{NH_4^+}^{Sat}$ of 57.27 mmol/g of resin. To compare the different models, we compared the concentration of liquid ammonium, $C_{NH_4^+}^{l}$, with that of liquid ammonium at equilibrium, $C_{NH_4^+}^{l,*}$.

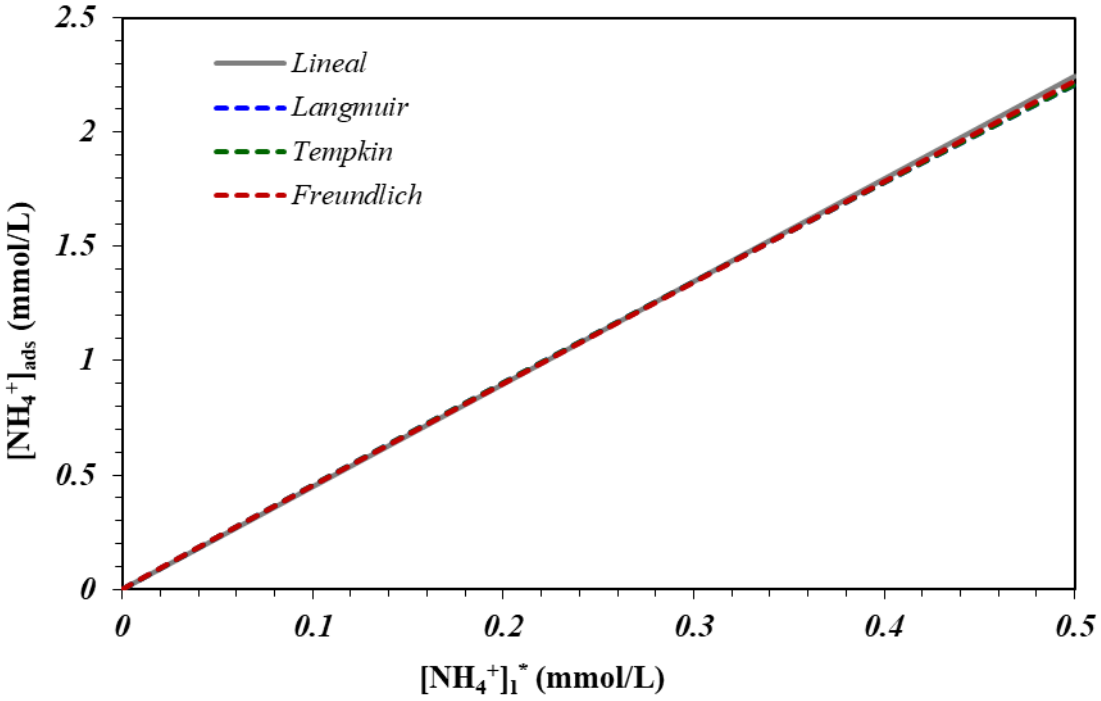

Figure 4.25 *[NH_4^+] adsorbed versus [NH_4^+] on equilibrium in the liquid phase ($C_{NH_4^+}^{l,*}$) calculated by the Langmuir, Tempkin, Freundlich and Lineal models.*

In Figure 4.25, it can be observed that the three models mentioned before coinciding with a straight line for the ammonium concentrations in this study. For this reason, we simplified the calculation of $C_{NH_4^+}^{l,*}$ to a linear model (Equation 3.87), which also fits the experimental data perfectly. This correlation between the four models was also supported by the similarity of the calculated value of the global coefficient of ammonium transfer between the liquid phase and the resin ($K_L.a$), as shown in Table 4.10.

Table 4.10 *Value of the kinetic constant $K_L.a$ for the Langmuir, Tempkin, Freundlich and Lineal models, and each resin concentration tested.*

	$K_L.a$ (min^{-1})			
CR (g. resin/L)	***Langmuir***	***Temkin***	***Freundlich***	***Lineal***
0.08	*0.003*	*0.003*	*0.003*	*0.003*
0.16	*0.0042*	*0.0042*	*0.0042*	*0.0042*
0.24	*0.0052*	*0.0052*	*0.0052*	*0.0053*
0.32	*0.0062*	*0.0062*	*0.0062*	*0.0062*
0.4	*0.007*	*0.007*	*0.007*	*0.007*
0.8	*0.0108*	*0.0108*	*0.0108*	*0.0108*
1.2	*0.014*	*0.014*	*0.014*	*0.014*
1.6	*0.0169*	*0.0169*	*0.0169*	*0.017*
3.2	*0.027*	*0.027*	*0.027*	*0.0271*
4.8	*0.0357*	*0.0357*	*0.0357*	*0.0357*
6.4	*0.0436*	*0.0436*	*0.0436*	*0.0436*
8	*0.0509*	*0.0509*	*0.0509*	*0.051*
9.6	*0.0579*	*0.0579*	*0.0578*	*0.0579*

4.4.2. Influence of the resin quantity in combination with the CSNR

To test the combination of the influence of the concentration of resins (0, 2, 4, 5, and 6 g of resin Amberlite H^+) on the CSNR employing a 1%Pd-0.4%Cu/Al_2O_3 catalyst was studied. Tests were performed following the method described in Section 2.4.3. Figure 4.26 shows the evolution of the conversion of nitrates over time for the combination of the catalyst with different amounts of the Amberlite H^+ resin. It can be observed that higher quantities of resins negatively influence the conversion of nitrates, although in all cases, the nitrates are completely at 70 min.

Figure 4.27 shows the selectivity towards nitrite over nitrate. In this image, a low selectivity towards nitrite can be observed for all reactions, but 5 g of resin and 6 g of resin cases should be highlighted because of their especially low selectivity. As explained previously, the OH^- formed during the reaction tend to be adsorbed on the surface of the Pd and hinders the adsorption of other species like nitrites or hydrogen. In these cases, the high loaded resins test shows lower selectivity to nitrites because the Pd nanoparticles in these experiments have a lower amount of adsorbed OH^- and allow the adsorption of nitrites. This is because during the adsorption of NH_4^+ by the resins, they release H^+ which neutralises the OH^- formed. This can be seen in Figure 4.28, which

shows the evolution of pH with respect to nitrate conversion for the tests with different amounts of resin.

The ammonium yield over time is shown in Figure 4.29. In this figure, it can be observed that higher loads of resin are related to lower ammonium on the liquid phase, as expected owing to the higher adsorption of ammonium formed on the cationic resins.

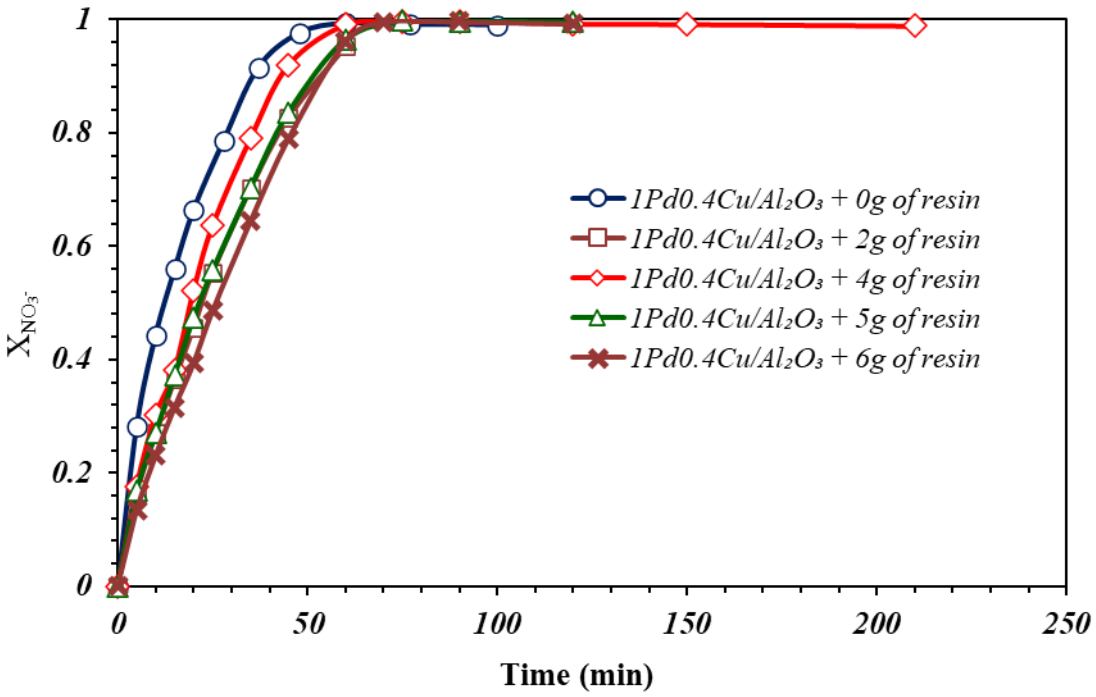

Figure 4.26 *Influence of the quantity of resin on the evolution of nitrate conversion along time.*

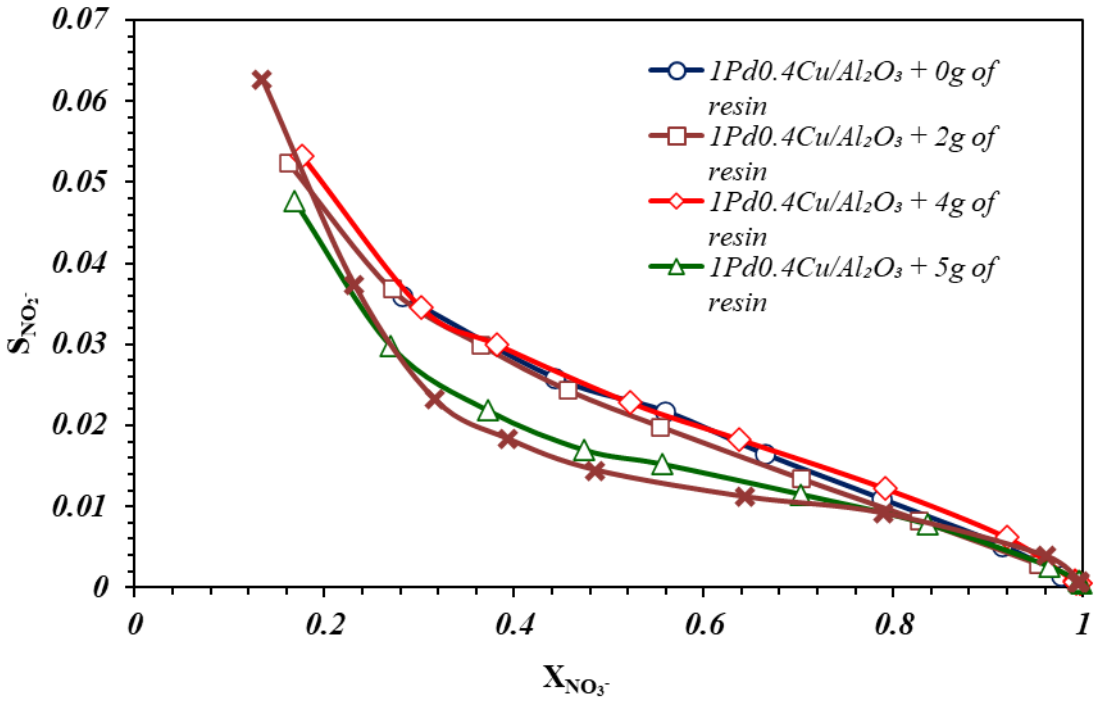

Figure 4.27 *Nitrite selectivity vs. nitrate conversion plots for different quantities of resin.*

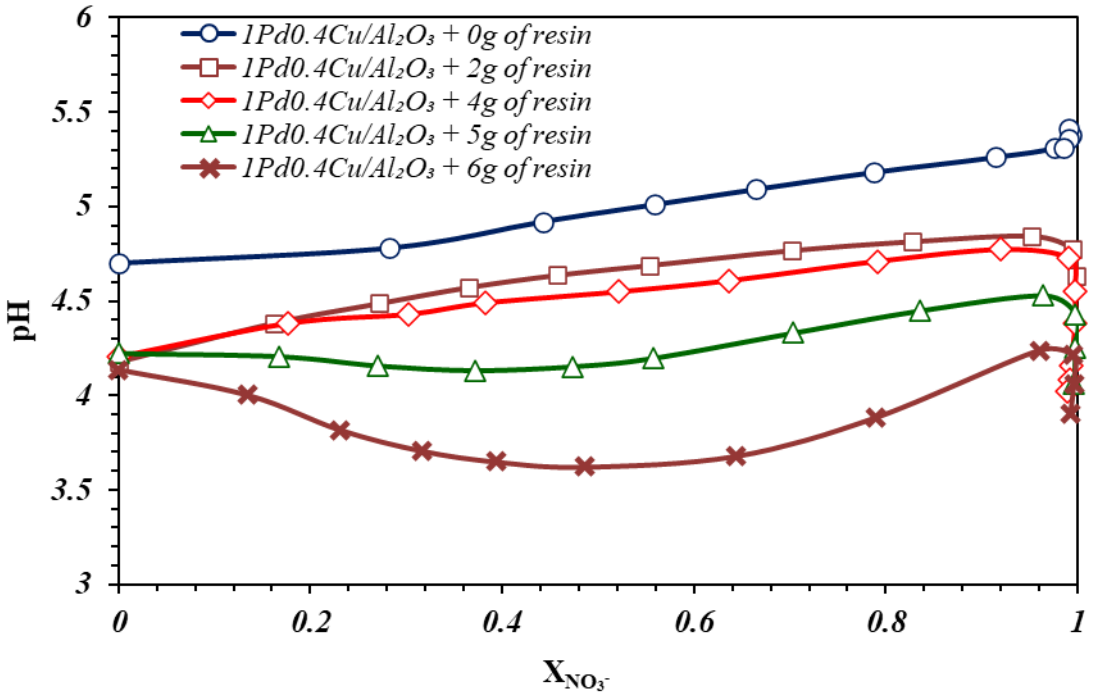

Figure 4.28 *Evolution of the pH on the reaction over nitrate conversion for different quantities of resin.*

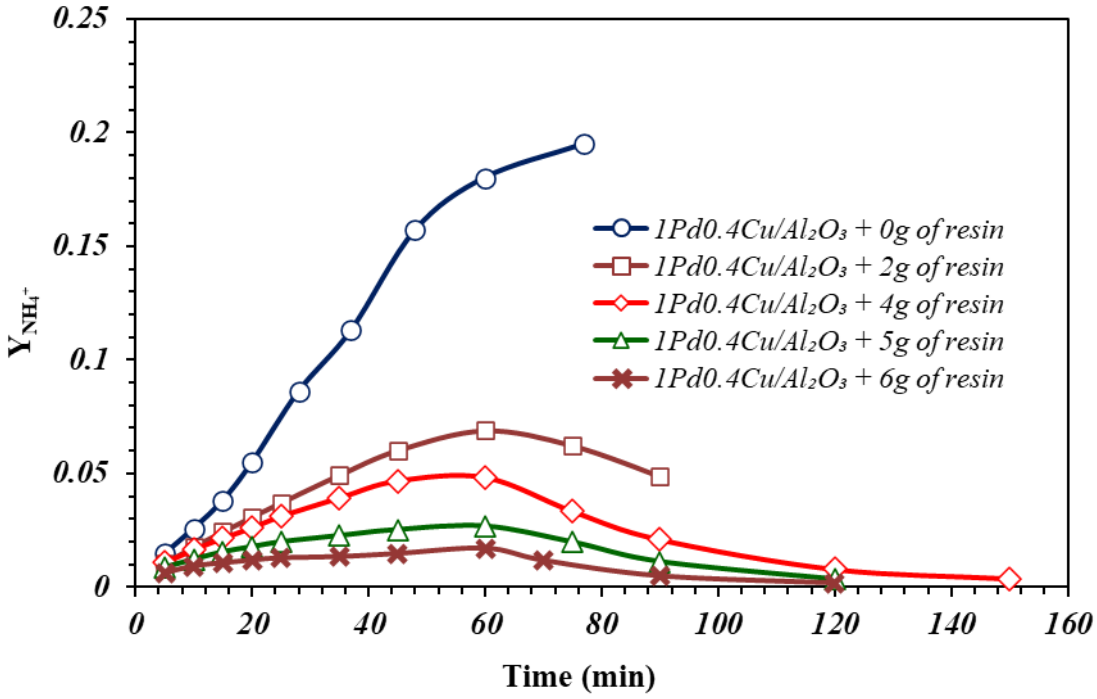

Figure 4.29 *Evolution of the ammonium yield over time for different quantities of resin.*

But when we look at the Table 4.11. where the kinetic constants of the model of the reaction in combination with the adsorption of ammonium on the resin, showed on the sections 3.1.2.1. and 3.1.2.2. It can be observed that by maintaining $K_L.a$, the global coefficient of ammonium transfer between the liquid phase between the liquid phase and the resin, from the isotherms of absorption from the preview section, the $k_3 \cdot \overline{C_{NO}} / k_4$ relation increases. This means that there is a synergic effect; the cationic resin Amberlite H^+ not only adsorbed NH_4^+, but also neutralised the OH^- formed during the reaction, as previously explained. For this reason, the concentration of adsorbed N species on the surface of Pd increases and favours the formation of N_2 [6,8,11–13,15–19]. Regarding the kinetic constants k_1 and $K_{NO_3^-}$, it can be observed that the presence of resins decreases the constant k_1 but increases the adsorption constant $K_{NO_3^-}$. This is related to the quicker conversion start of the catalyst without resin, but a better performance of the catalysts with resin near full conversion thanks to a better adsorption. The lower $K_{NO_3^-}$ but higher k_1 of this test means that for higher concentrations of NO_3^-, the catalyst alone converts the nitrates faster than when there is resin present; however, when the concentration of nitrates is low, better adsorption of nitrates due to the resins improves the overall rate of nitrate conversion.

Table 4.11 *Values of the kinetic parameters for the CSRN using 1Pd0.4Cu/Al_2O_3 for each quantity of Amberlite H^+ added.*

	0g resin	***2g resin***	***4g resin***	***5g resin***	***6g resin***
k_1 (NO_3^-) (mol.g.L^{-1}.min^{-1})	0.374 ± 0.145	0.061 ± 0.004	0.062 ± 0.003	0.061 ± 0.004	0.038 ± 0.001
K_{obs} (NO_3^-) (mol^{-1})	0.181 ± 0.083	1.31 ± 0.185	1.903 ± 0.259	1.331 ± 0.201	3.875 ± 0.591
k_2 (NO_2^-) ($g.L^{-1}.min^{-1}$)	2.872 ± 1.334	2.059 ± 0.811	2.195 ± 0.753	2.557 ± 1.094	2.386 ± 1.169
k_3 (N_2) ($g.mol^{-1}.L^{-1}.min^{-1}$)	0.078 ± 0.025	0.317 ± 0.034	0.466 ± 0.044	1.61 ± 0.514	80.604 ± 37.108
k_4 (NH_4^+) ($g.L^{-1}.min^{-1}$.)	0.01 ± 0.002	0.014 ± 0.001	0.016 ± 0.001	0.019 ± 0.003	0.086 ± 0.02
$K_L.a$ (min^{-1})	0	0.027 ± 0.003	0.044 ± 0.004	0.051 ± 0.01	0.058 ± 0.016
$k_3 \cdot \overline{NO} / k_4$	3.071	4.463	5.839	8.031	14.448

4.5. Conclusions

All Pd-Cu/Al_2O_3 tested catalysts were active in catalytic nitrate reduction, achieving a higher selectivity toward nitrogen than ammonium. The catalysts used in this work had a similar metallic particle size, despite the increase in the metallic content, meaning that the successive wetness impregnation of 0.4Cu before Pd favoured the good dispersion of this second metal and promoted the formation of more nanoparticles between 3 and 5 nm over the alumina. It can also be concluded that higher agitation rates during reaction makes the external diffusion of hydrogen towards the catalyst easier. However, higher concentrations of hydrogen lead to higher ammonium selectivity due the over-

hydrogenation as a consequence of the lower density of adsorbed N-species and a higher H/N ratio on the Pd nanoparticle surface. As expected, the catalyst load increase does not affect the selectivity of the process, and it can be assumed that there is no deactivation due to the agreement between the different nitrate rates of elimination per gram of catalyst. In addition, the flow of CO_2 is necessary to avoid deactivation of the catalyst by OH^- reversible poisoning. Higher flowrates of CO_2 can improve the selectivity towards N_2 at the expense of losing some of the nitrate conversion rate.

In the case of treatment of tap water, nitrate conversion and selectivity to N2 decrease owing to the presence of large quantities of competitive ions in the water. Therefore, although real water treatment remains unachieved, further research is required to achieve this.

The catalytic hydrogenation treatment in combination with the adsorption with the cationic resin Amberlite H^+ shows a notorious improvement in the selectivity to NH_4^+. This fact is due to the in-situ adsorption of the NH_4^+ produced, and to the enhancement of the intrinsic selectivity towards N_2, due to a better control of the pH.

These results indicate that, in addition to the catalyst composition, the operational conditions play a key role in achieving high activity for selective catalytic nitrate reduction and low selectivity towards NH_4^+. Other operational conditions will be investigated in future research. In all the cases, the developed kinetic model allows to attain an excellent fitting of the experimental results. This model provides an insight into the evaluation of the intrinsic kinetics of the SCRN, achieving a better understanding of the mechanism involved during this process.

4.6. References

[1] X. Fan, C. Franch, E. Palomares, A.A. Lapkin, Simulation of catalytic reduction of nitrates based on a mechanistic model, Chemical Engineering Journal 175 (2011) 458–467. https://doi.org/10.1016/j.cej.2011.09.069.

[2] O.S.G.P. Soares, X. Fan, J.J.M. Órfão, A.A. Lapkin, M.F.R. Pereira, Kinetic modeling of nitrate reduction catalyzed by Pd-Cu supported on carbon nanotubes, Ind Eng Chem Res 51 (2012) 4854–4860. https://doi.org/10.1021/ie202957v.

[3] J. Batista, A. Pintar, D. Mandrino, M. Jenko, V. Martin, XPS and TPR examinations of γ-alumina-supported Pd-Cu catalysts, Appl Catal A Gen 206 (2001) 113–124. https://doi.org/10.1016/S0926-860X(00)00589-5.

[4] J. Sá, H. Vinek, Catalytic hydrogenation of nitrates in water over a bimetallic catalyst, Appl Catal B 57 (2005) 247–256. https://doi.org/10.1016/j.apcatb.2004.10.019.

[5] S. Hörold, K.D. Vorlop, T. Tacke, M. Sell, Development of catalysts for a selective nitrate and nitrite removal from drinking water, Catal Today 17 (1993) 21–30. https://doi.org/10.1016/0920-5861(93)80004-K.

[6] A. Pintar, J. Batista, J. Levec, Potential of mono- and bimetallic catalysts for liquid-phase hydrogenation of aqueous nitrite solutions, Water Science and Technology 37 (1998) 177–185. https://doi.org/10.1016/S0273-1223(98)00248-0.

[7] J.K. Chinthaginjala, L. Lefferts, Support effect on selectivity of nitrite reduction in water, Appl Catal B 101 (2010) 144–149. https://doi.org/10.1016/j.apcatb.2010.09.023.

[8] Y. Matatov-Meytal, V. Barelko, I. Yuranov, M. Sheintuch, Cloth catalysts in water denitrification. I. Pd on glass fibers, Appl Catal B 27 (2000) 127–135. https://doi.org/10.1016/S0926-3373(00)00141-7.

[9] Y. Yoshinaga, T. Akita, I. Mikami, T. Okuhara, Hydrogenation of nitrate in water to nitrogen over Pd-Cu supported on active carbon, J Catal 207 (2002) 37–45. https://doi.org/10.1006/jcat.2002.3529.

[10] P. Xu, S. Agarwal, L. Lefferts, Mechanism of nitrite hydrogenation over Pd/γ-Al2O3 according a rigorous kinetic study, J Catal 383 (2020) 124–134. https://doi.org/10.1016/j.jcat.2020.01.003.

[11] B.P. Chaplin, E. Roundy, K.A. Guy, J.R. Shapley, C.I. Werth, Effects of natural water ions and humic acid on catalytic nitrate reduction kinetics using an alumina supported Pd-Cu catalyst, Environ Sci Technol 40 (2006) 3075–3081. https://doi.org/10.1021/es0525298.

[12] A. Pintar, M. Šetinc, J. Levec, Hardness and salt effects on catalytic hydrogenation of aqueous nitrate solutions, J Catal 174 (1998) 72–87. https://doi.org/10.1006/jcat.1997.1960.

[13] D.T. González, J.A. Baeza, L. Calvo, M.A. Gilarranz, Influence of bicarbonate, other anions and carbon dioxide in the activity of Pd-Cu catalysts for nitrate reduction in drinking water, Journal of CO2 Utilization 72 (2023). https://doi.org/10.1016/j.jcou.2023.102494.

[14] M.A. El-Ghobashy, M.M. Khamis, A.S. Elsherbiny, I.A. Salem, Selective removal of ammonia from wastewater using Cu(II)-loaded Amberlite IR-120 resin and its catalytic application for removal of dyes, Environmental Science and Pollution Research (2023). https://doi.org/10.1007/s11356-023-25677-3.

[15] J. Sá, J. Montero, E. Duncan, J.A. Anderson, Bi modified Pd/SnO2 catalysts for water denitration, Appl Catal B 73 (2007) 98–105. https://doi.org/10.1016/j.apcatb.2006.06.012.

[16] J.K. Chinthaginjala, L. Lefferts, Support effect on selectivity of nitrite reduction in water, Appl Catal B 101 (2010) 144–149. https://doi.org/10.1016/j.apcatb.2010.09.023.

[17] S. Hörold, K.D. Vorlop, T. Tacke, M. Sell, Development of catalysts for a selective nitrate and nitrite removal from drinking water, Catal Today 17 (1993) 21–30. https://doi.org/10.1016/0920-5861(93)80004-K.

[18] Y. Yoshinaga, T. Akita, I. Mikami, T. Okuhara, Hydrogenation of nitrate in water to nitrogen over Pd-Cu supported on active carbon, J Catal 207 (2002) 37–45. https://doi.org/10.1006/jcat.2002.3529.

[19] C. Franch, R.G.H. Lammertink, L. Lefferts, Partially hydrophobized catalyst particles for aqueous nitrite hydrogenation, Appl Catal B 156–157 (2014) 166–172. https://doi.org/10.1016/j.apcatb.2014.03.020.

5. PERFORMANCE OF CATALYSTS PdSn SUPPORTED OVER Al_2O_3 ON THE CSNR

5.1. Introduction

Tin is another widely used promoter in bimetallic catalysts for nitrate elimination by CSRN. In this section, different series of PdSn catalysts supported on Al_2O_3 have been synthesized with the aim of elucidating the influence of the composition and operating conditions of the catalyst synthesis process (order of impregnation of active phases, %wt.Pd, %wt.Sn and influence of the reduction temperature), as well as the different operating reaction variables (like feed composition and ions in water), on the activity and selectivity in the selective catalytic reduction of nitrates. The catalysts presented in this paragraph have been presented in Chapter 2, Table 2.1.

5.2. Catalyst Characterization

5.2.1. Textural properties- N_2 adsorption isotherm

Table 5.1 *Textural properties of the catalysts and support obtained by nitrogen adsorption-desorption isotherms.*

Sample	BET area (m^2/ g)	Pore size (nm)	Pore volume (cm^3/g)
Al_2O_3	225	7	0.41
1Pd0.6Sn/ Al_2O_3	201 (fresh) 200 (used)	7	0.34-0.36
1Pd1.2Sn/Al_2O_3	197 (fresh) 195 (used)	7	0.34-0.36
1.2Pd1.2Sn/ Al_2O_3	200 (fresh) 197 (used)	7	0.34-0.36
4Pd1.2Sn/ Al_2O_3	180 (fresh) 180 (used)	7	0.34-0.36

Table 5.1 summarizes the textural properties of the support material, γ-alumina, and of a series of PdSn/Al_2O_3 catalysts with different compositions of Sn and Pd. The data were obtained for the fresh catalysts and after been used in reaction. For these latter ones, the

catalysts were recovered after nitrate reduction reaction by filtration and subsequent drying at 100 °C for 12 h.

As can be observed, BET surface area of all the synthetized catalysts is lower than that of the Al_2O_3 support. This loss of surface area is originated mainly from pores plugging due to the impregnation process, being the most important reduction exhibited by 4Pd1.2Sn/Al_2O_3, the catalyst with the highest metal content of the series studied, decreasing the surface area by 20 % and the pore volume by 12 %. However, it can also be observed that even with a decrease in pore volume, the pore size was not affected.

On the other hand, the surface area before and after the reaction did not undergo significant changes for any catalyst, which implies that there were no structural alterations in the materials during the reaction.

5.2.2. Transmission Electron Microscopy (TEM)

Figures 5.1, 5.2 and 5.3 show the TEM images or STEM-EDS images, as well as the histogram of the comparative distributions of the impregnation order, Sn content variation and Pd content variation respectively.

Figure 5.1 shows the STEM-EDS image of the 1Pd0.4Sn/Al_2O_3 and 0.4Sn1Pd/Al_2O_3 catalyst, as well as the average size and the distribution size of the metallic particles. On the STEM-EDS images it is possible to distinguish a more greyish area corresponding to the alumina support and some white dots corresponding to the Pd and Sn nanoparticles. From these images we can say that there is a good dispersion of the nanoparticles on the support, and we could measure the nanoparticles diameter. The catalyst 1Pd0.4Sn/Al_2O_3 was synthetized by impregnating first with Sn and calcined for 12 h in an open-air oven at 350°C for 12 h at a heating rate of 5°C/min . Afterwards, it was impregnated with Pd calcined for 12 h in an open-air oven at 500°C for 12 h at a heating rate of 5°C/min as explained in Chapter 2, Section 2.2.1 and Table 2.1. The catalyst 0.4Sn1Pd /Al_2O_3, was prepared with the same methodology but in reverse order of impregnation. This difference in the synthesis process of the catalysts has led to a better dispersion of the metal in this second case, obtaining an average particle size of 8 nm for the first catalyst and 5 nm in the case in which the Sn is impregnated in a first step. Additionally, the particle size distribution is much broader for the catalyst 0.4Sn1Pd/Al_2O_3, with particles of up to 15 nm. Therefore, the impregnation order of

the active phases is an important factor in order to obtain a good dispersion of the metals, which is in concordance with the results observed in bibliography [1]. In view of these results and the activity results discussed later, the rest of the catalysts were synthesized by impregnating Sn in a first stage.

Figure 5.2 shows the average particle size and its distribution for the catalysts 1Pd1.2Sn/Al_2O_3 and 1Pd2.5Sn/Al_2O_3. As can be observed comparing this data with catalyst 1Pd0.4Sn/Al_2O_3, from Figure 5.1 an increase in Sn content produces a reduction in the average particle size from 5nm to 3nm.

In the study of PdCu catalysts, section 4.1.2.1, it was observed that using the same synthesis process, copper was widely dispersed on the support, while palladium formed bigger nanoparticles that combined with Cu. In this case, similarly, it is assumed that Sn is widely dispersed on the support and the increase of tin content facilitates a greater number of anchoring points for the Pd, which results in better dispersion of the Pd and a reduction in particle size.

Figure 5.2 also shows the comparative of catalyst 1Pd1.2Sn/Al_2O_3 which was reduced before reaction at 250ºC and 1Pd1.2Sn/Al_2O_3_Tr550 which was reduced at 550ºC. Comparing both TEM images and particle size distribution it can be observed the sintering of the nanoparticles and the wider distribution of the nanoparticle size due to higher reduction temperatures at 550ºC.

Finally, a series of catalysts with a constant quantity of Sn of 1.2% wt. and different percentages of Pd, from 0.6 to 4% wt., were analyzed by microscopy (Figure 5.3 and catalyst 1Pd1.2Sn/Al_2O_3 from Figure 5.2). An increase in the Pd content produce an increase in the nanoparticle size, being especially significant in the 4Pd1.2Sn/Al_2O_3 catalyst, where also the distribution of particle sizes is much wider and displaced to higher particle diameter.

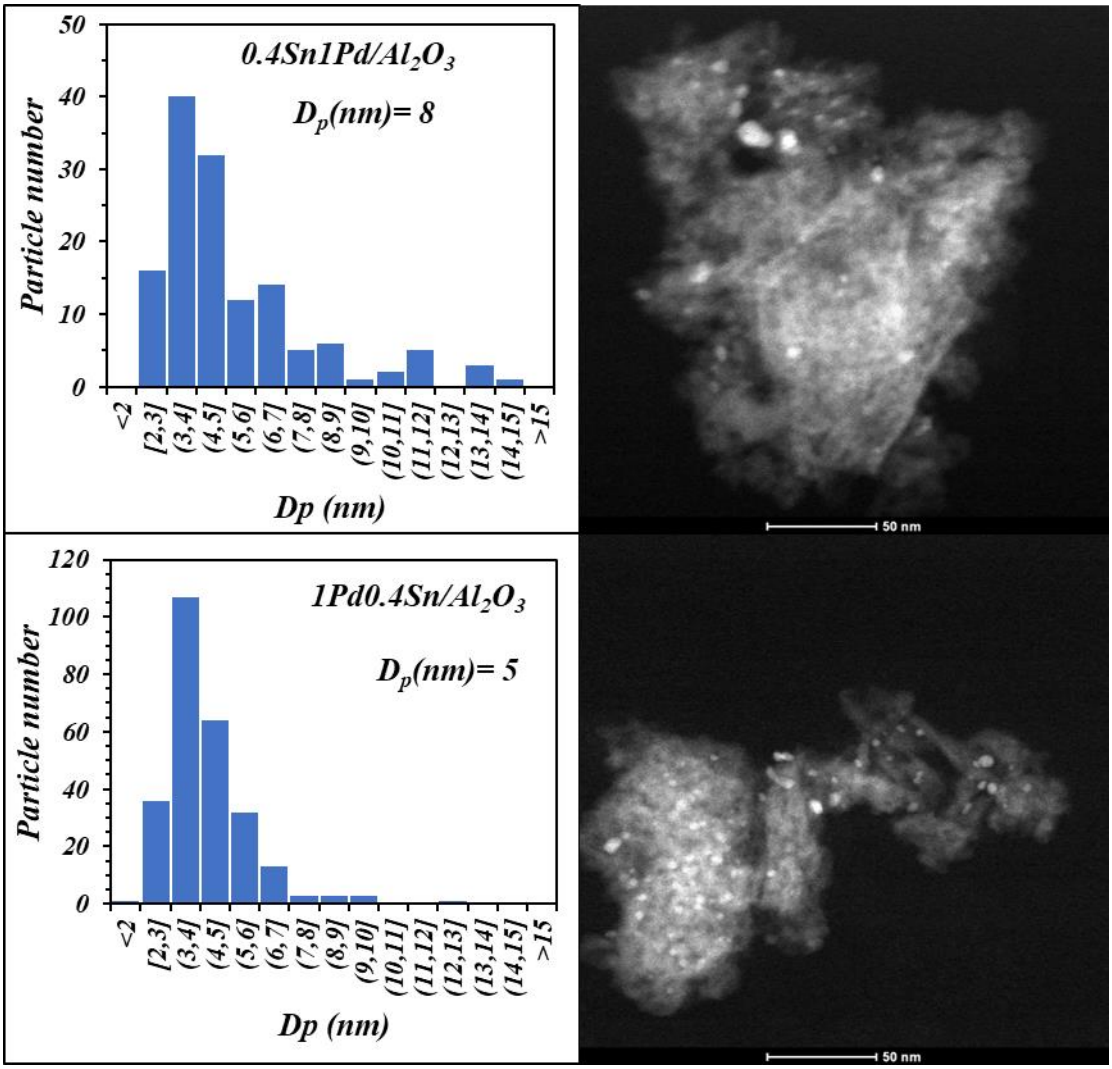

Figure 5.1 *STEM-EDS images and histograms of the nanoparticle size distribution of the catalysts 0.4Sn 1Pd/Al_2O_3 and 1Pd0.4Sn/Al_2O_3.*

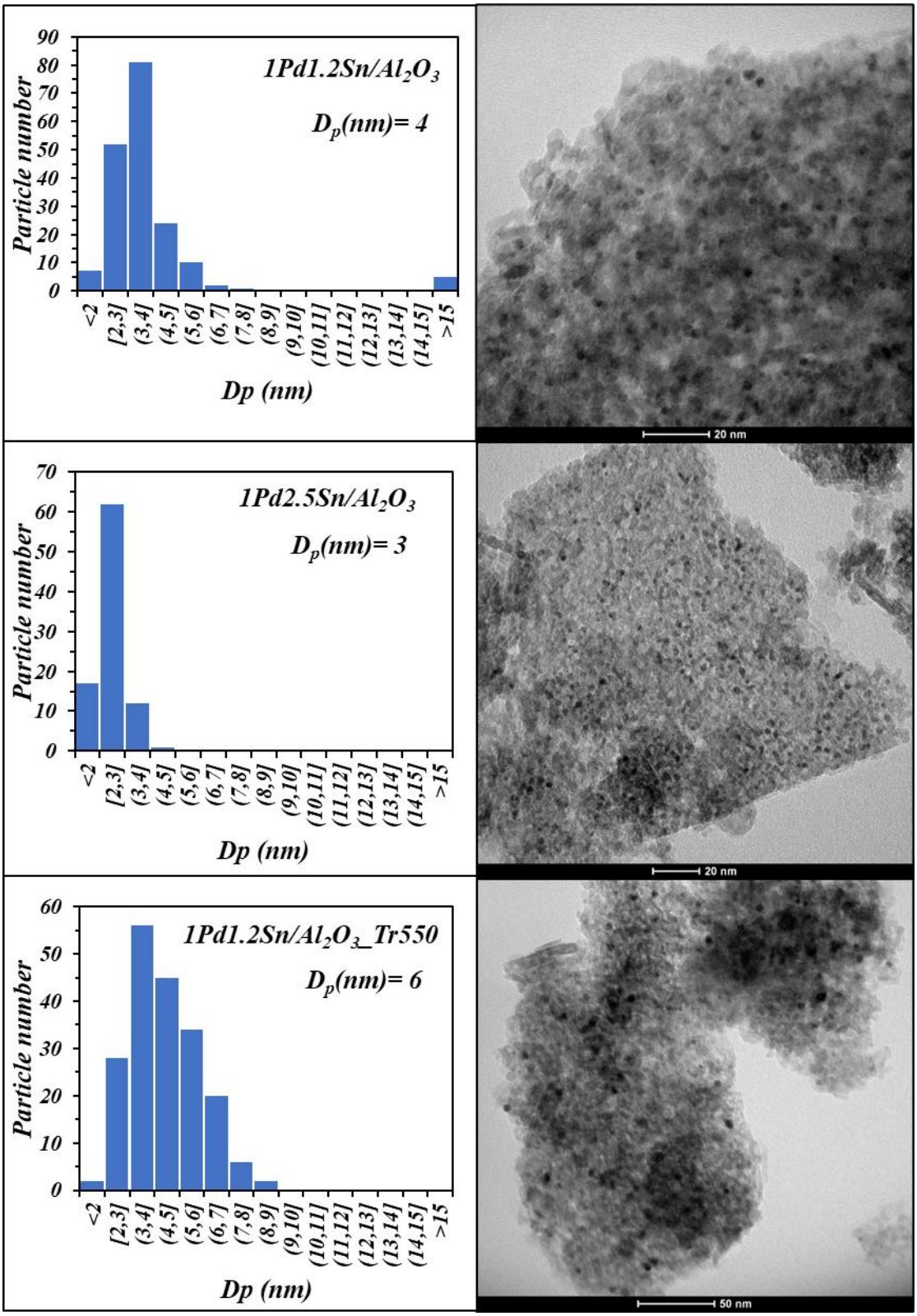

Figure 5.2 *TEM images and histograms of the nanoparticle size distribution of the $PdSn/Al_2O_3$ catalysts with different amount of Sn reduced at 250ºC and the catalyst $1Pd1.2Sn/Al_2O_3$ reduced at 550ºC.*

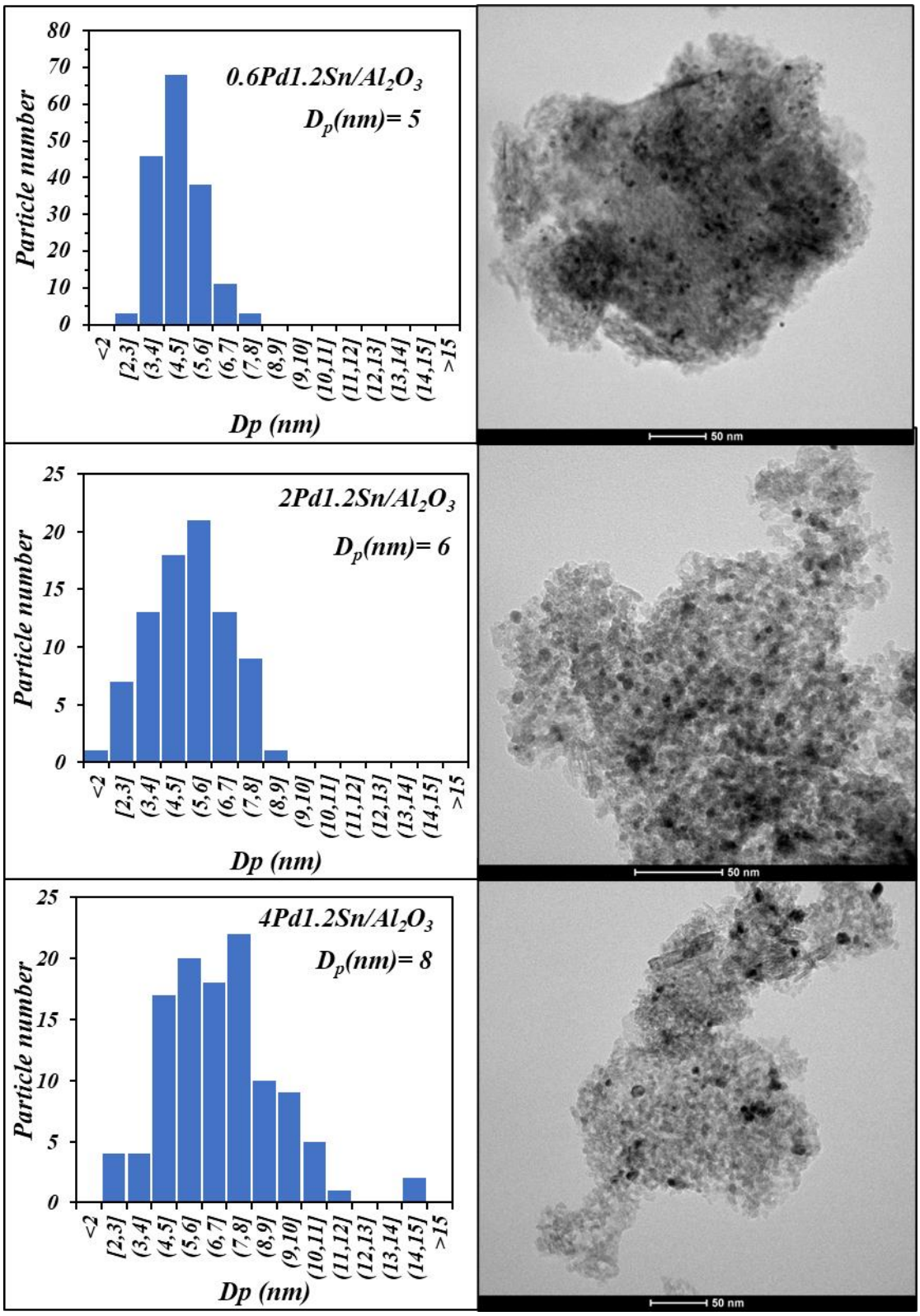

Figure 5.3 *TEM images and histograms of the nanoparticle size distribution of the $PdSn/Al_2O_3$ catalysts with different amount of Pd.*

5.2.3. X-Ray Diffraction (XRD)

Figure 5.4 shows the XRD spectra corresponding to the Al_2O_3 support and the fresh catalysts 1Pd0.4Sn/Al_2O_3, 1Pd1.2Sn/Al_2O_3 and 4Pd1.2Sn/Al_2O_3. As can be observed, the diffractograms present the peaks corresponding to the γ-alumina main diffractions at 2θ = 37.6, 39.5, 45.9 and 67.0 in all cases [2]. With respect to the active phase, peaks from tin species are not observed for the 1Pd0.4Sn/Al_2O_3 and 1Pd1.2Sn/Al_2O_3 catalysts, because the low content and high dispersion of the metals. For the catalyst with the highest Pd content (4 %), peaks at 2θ= 34; 42; 54.9 and 60.3º (ref. patrons: JPCDS 01-085-0624) associated with PdO are observed. The active phase is in oxidized form due to the sample is before activation and reaction.

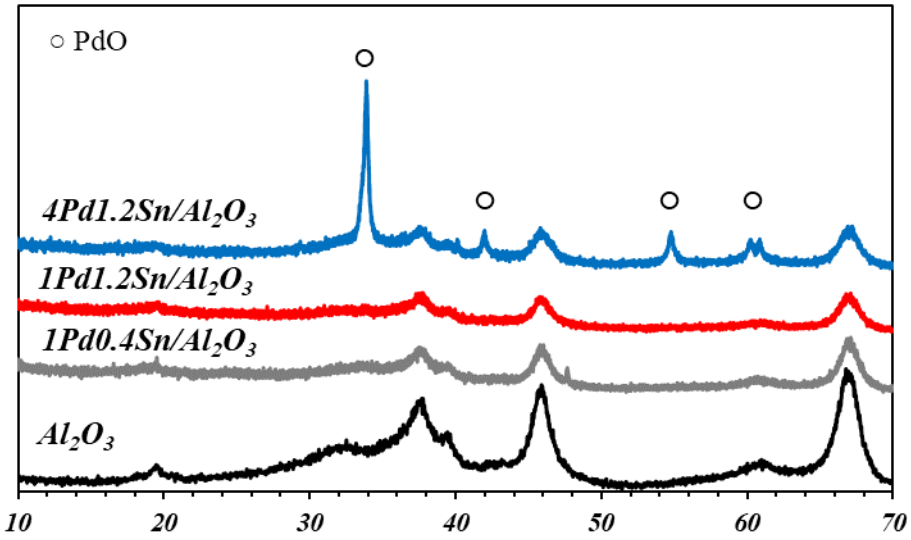

Figure 5.4 *XRD patterns for the Al_2O_3 support and the catalysts: 1Pd0.4Sn/Al_2O_3, 1Pd1.2Sn/Al_2O_3 and 4Pd1.2Sn/Al_2O_3.*

5.2.4. X-Ray Photoelectron Spectroscopy (XPS)

In order to obtain information about the oxidation state of the active phases, X-ray photoelectron spectroscopy studies of samples after reaction were performed. The results obtained are summarised in Table 5.2.

All catalysts show a Pd/Sn atomic ratio lower than the nominal one, showing that the surface of the catalysts is enriched in Sn, which can indicate that Sn species are better dispersed on the Al_2O_3 surface and Pd is found forming larger particles. The catalyst where this effect is greater is Pd1Sn0,4 /Al_2O_3. These results corroborate the assumption made in the TEM results.

Deconvolution of the core-level spectra of Pd3d and Sn3d orbital evidence the existence of zerovalent and electrodeficient Pd and Sn species. In the case of Pd spectra, four main bands were observed for Pd $3d_{5/2}$, which can be attributed to Pd^0, PdO, Pd-Sn alloy and $AlPd_xO$. The Sn spectra (Sn $3d_{5/2}$) presented three peaks, corresponding to zerovalent Sn species (Sn^0), electrodeficient Sn species (SnO_2) and Pd-Sn. Table 5.2 collects the relative distribution (%) of the reduced and oxidized species for both metals.

As commented, the results evidence the presence of Sn and Pd species with different oxidation states after reaction. In the case of Pd, the predominant species were Pd^0 and a strong alloy Pd-Sn, which remains after reaction. On the other hand, Sn is mainly found in Sn–Pd alloy or in oxidized state, except for the $4Pd1.2Sn/Al_2O_3$ catalyst, which presented a high concentration of zerovalent Pd on the catalyst surface along with the lowest concentration of oxidized Sn. This fact could be associated with the high availability of active sites (Pd^0) for initial H_2 activation ($Pd^0 + H_2 \rightarrow Pd\text{-}2H_{ads}$), and consequently SnO/SnO_2 rejuvenation to Sn^0 by H_{ads} [3]. This catalyst also showed the specie AlPdxO, which indicates a high interaction of Pd with the support.

Table 5.2 *XPS results for $PdSn/Al_2O_3$ catalysts after reaction.*

Catalyst	**Pd/Sn (nominal)**	**Pd/Sn**	**Pd $3d_{5/2}$**				**Sn $3d_{5/2}$**		
			$AlPd_xO$	**Pd (0)**	**Pd-Sn**	**Pd (II)**	**Sn (0)**	**Pd-Sn**	**Sn (IV)**
$Pd4Sn1.2/Al_2O_3$	3.7	2.4	18%	72%	--	10%	9%	91%	--
$Pd1Sn1,2/Al_2O_3$	0.92	0.47	--	51%	49%	--	-	74%	26%
$Pd0,6Sn1,2/Al_2O_3$	0.55	0.3	--	61%	39%	--	--	73%	27%
$Pd1Sn0,8/Al_2O_3$	1.25	0.86	--	33%	67%	--	--	76%	24%
$Pd1Sn0,4/Al_2O_3$	2.79	0.72	--	40%	60%	--	--	58%	42%

5.2.5. Temperature Programmed Reduction (TPR)

Figure 5.5 shows the hydrogen consumption profiles for the catalysts Pd1Sn0.2/Al_2O_3, Pd1Sn1/Al_2O_3 and Pd1Sn1.2/ Al_2O_3. In all cases, several peaks of hydrogen consumption at different temperatures are presented, which are associated with the reduction of the different species present in the catalysts. The peak observed from 106 to 111 ºC corresponds to Pd reduction. It appears at temperatures a little higher than the peaks associated with the reduction of Pd, probably due to the contact with Sn [4–6]. In the higher temperature range, from 330 to 487 ºC, a broad band of hydrogen consumption is found, forming approximately 3 peaks at 330, 420 and 487ºC. According to the literature [4–6], in bimetallic catalysts PdSn, the reduction peaks at temperatures below 400 ºC (temperature required for the reduction of SnO_2 to Sn0) indicate the reduction of Sn species in contact with Pd, so the TPR results indicate the existence of Pd-Sn interaction. These results corroborate de XPS analysis commented.

An increase in catalyst loading (%Sn) does not imply modifications in the temperature ranges of the hydrogen consumption peaks.

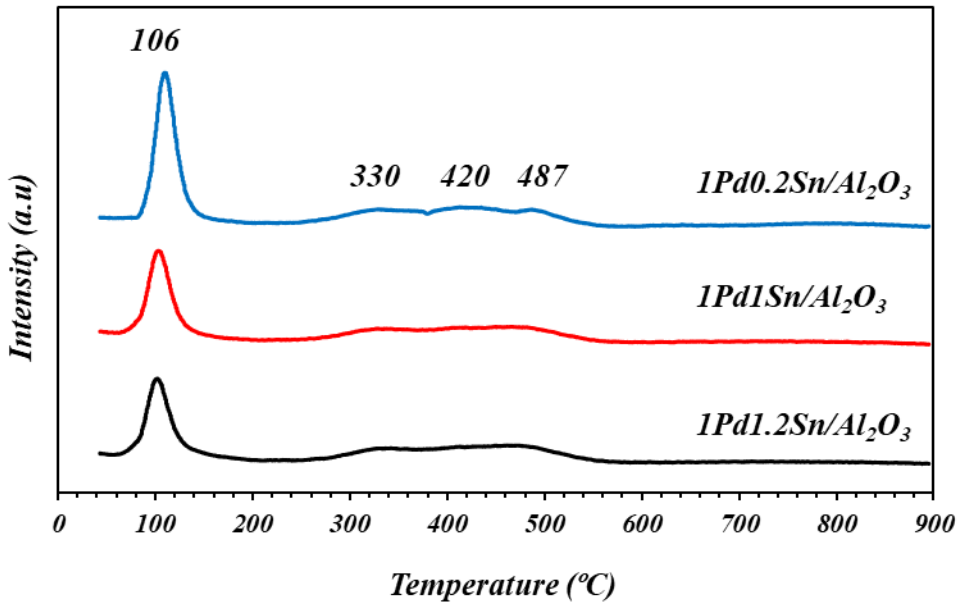

Figure 5.5 *TPR image of the catalyst 1Pd1.2Sn/Al_2O_3, 1Pd1Sn/Al_2O_3 and 1Pd0.2Sn/Al_2O_3.*

5.3. Catalytic tests

5.3.1. Influence of the impregnation order of the metals

The effect of the conditions used in the preparation method was investigated in this study, more specifically, the effect of the order of impregnation of the metals on the synthesis of the catalyst. For this purpose, two catalysts with a metal content of 1% wt. Pd and 0.4% wt. Cu were synthesised varying the impregnation method. The catalyst 1Pd0.4Sn/Al_2O_3 was synthesized by impregnating the support with tin, followed by calcination in air at 350ºC. After this, impregnation with palladium and final calcination at 500ºC were carried out (as explained in Chapter 2, Section 2.2.1). On the other hand, 0.4Sn1Pd/Al_2O_3 was prepared by reversing the impregnation order, first Pd impregnation and calcination at 350ºC was realized and afterwards Sn impregnation and calcination at 500ºC. The catalysts were reduced at 250ºC in H_2 atmosphere with a flow of 100mL/min. The reaction operational variables were: 1 g.cat./L; initial nitrate concentration of 100 ppm; reaction flow of 200 mL/min CO_2 and 100 mL/min H_2; stirring rate of 750 r.p.m.

The nitrate conversion along reaction time is showed in the Figure 5.6. It can be observed that 1Pd0.4Sn/Al_2O_3 reached total conversion in less than 150 minutes. On the other hand, when Pd is impregnated first the reaction took much longer, not reaching total conversion after 450 minutes of reaction. As commented in characterization results, the obtained average and nanoparticle size distribution is smaller (5 nm) and narrower for the catalyst 1Pd0.4Sn/Al_2O_3. Therefore, a better dispersion of the metals on the support was achieved by impregnating Sn in a first step, which produces a greater existence of active centres and better contact between active phases and, consequently, higher rate of nitrate the activity when the impregnation order was varied.

Regarding to the selectivity to NO_2- (Figure 5.7), elimination of nitrites is very fast in both cases, especially for nitrate conversions higher than 0.4, showing very low selectivity to this intermediate product. Furthermore, in this study, it is worth highlighting that nitrites were not completely eliminated at the end of the reaction, even when nitrates had been completely removed in the case of the catalyst 1Pd0.4Sn/ Al_2O_3. In this case, the importance of the reaction of formation of NO_2^- from NO has to be considerate, as explained in Chapter 3, section 3.1.1.

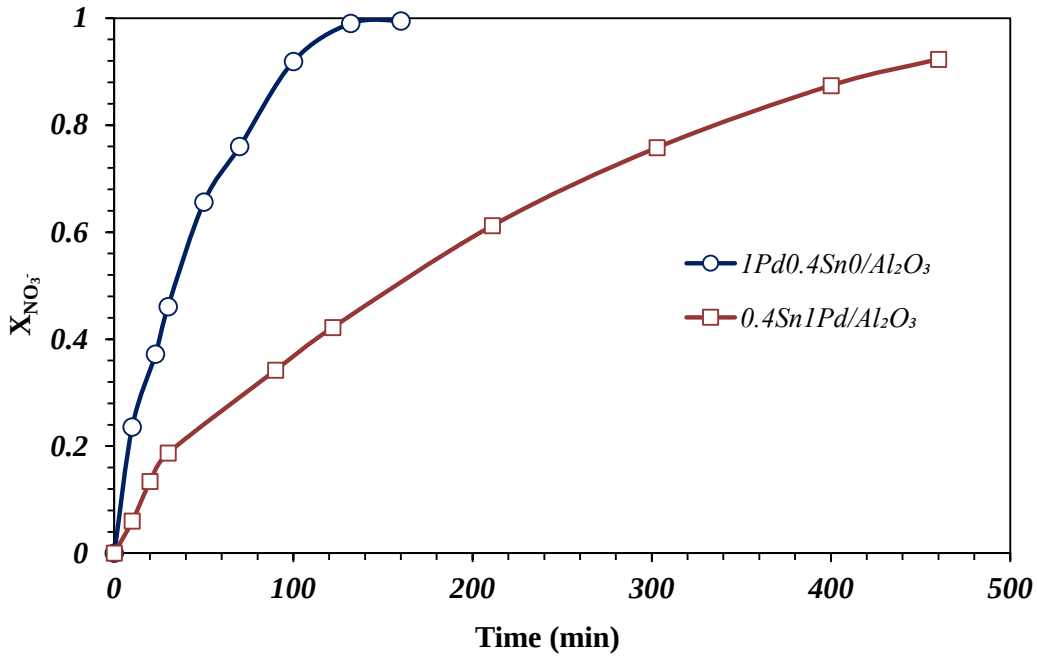

Figure 5.6 *Nitrate conversion over time for the catalyst impregnated with Sn first ($1Pd0.4Sn/Al_2O_3$) and the catalyst impregnated with Pd first ($0.4Sn1Pd/Al_2O_3$)*

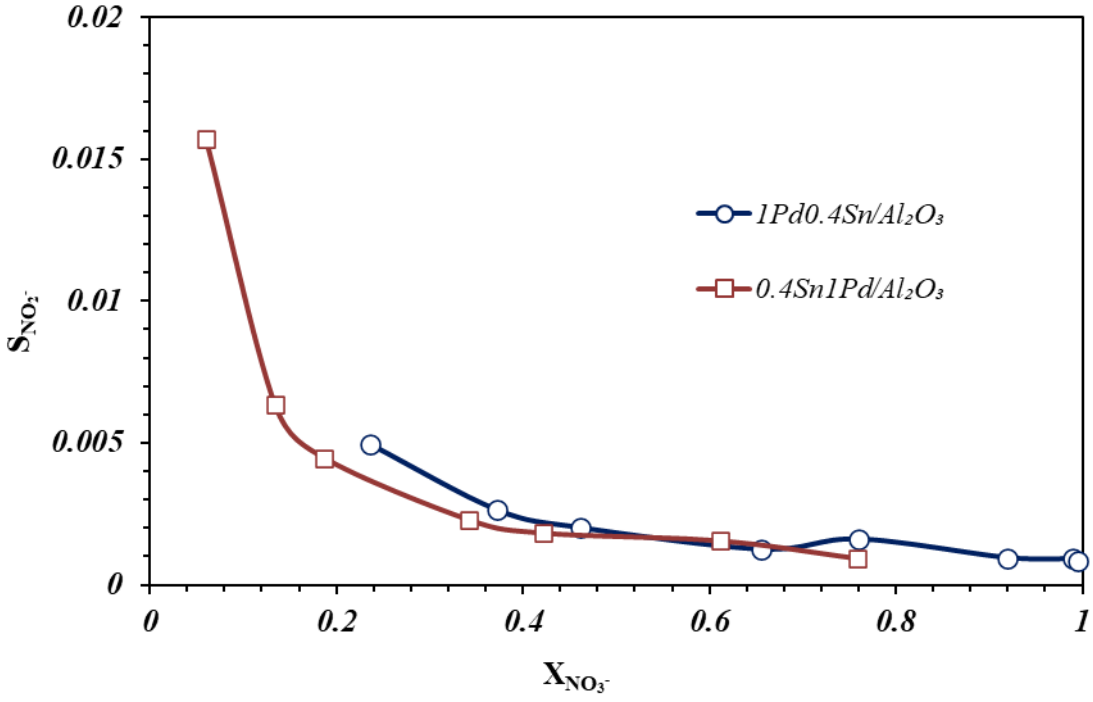

Figure 5.7 *Nitrite selectivity versus nitrate conversion for the catalyst impregnated with Sn first ($1Pd0.4Sn/Al_2O_3$) and the catalyst impregnated with Pd first ($0.4Sn1Pd/Al_2O_3$)*

Finally, the evolution of the selectivity to ammonium can be observed in Figure 5.8. $1Pd0.4Sn/Al_2O_3$, in which Sn was impregnate in the first step, showed a higher selectivity to ammonium than $0.4Sn1Pd/ Al_2O_3$. XPS results, shown in Table 5.2, indicate that for all samples synthesized following this protocol, the catalyst surface is

enriched in Sn above the nominal value of the catalyst. This fact can indicate the partial encapsulation of Pd, metal where the conversion to final reaction products carry out, resulting in a lower density of adsorbed nitrogen species on the catalyst surface, which favours selectivity to ammonium.

This may be due to a higher surface covered by the Pd on the catalyst because it was impregnated in a second step, which enhance the adsorption of H_2 to an extent where the N/H ratio decrease and, in consequence the selectivity towards N_2 [7].

The obtained experimental data were fitted with the kinetic model obtaining very satisfactory results, as can be observed in Figure 5.9. The model fits perfectly the experimental data of the reagents and products of the reaction. It can be observed how the nitrates are consumed until their complete conversion and nitrogen and ammonium increase their value progressively.

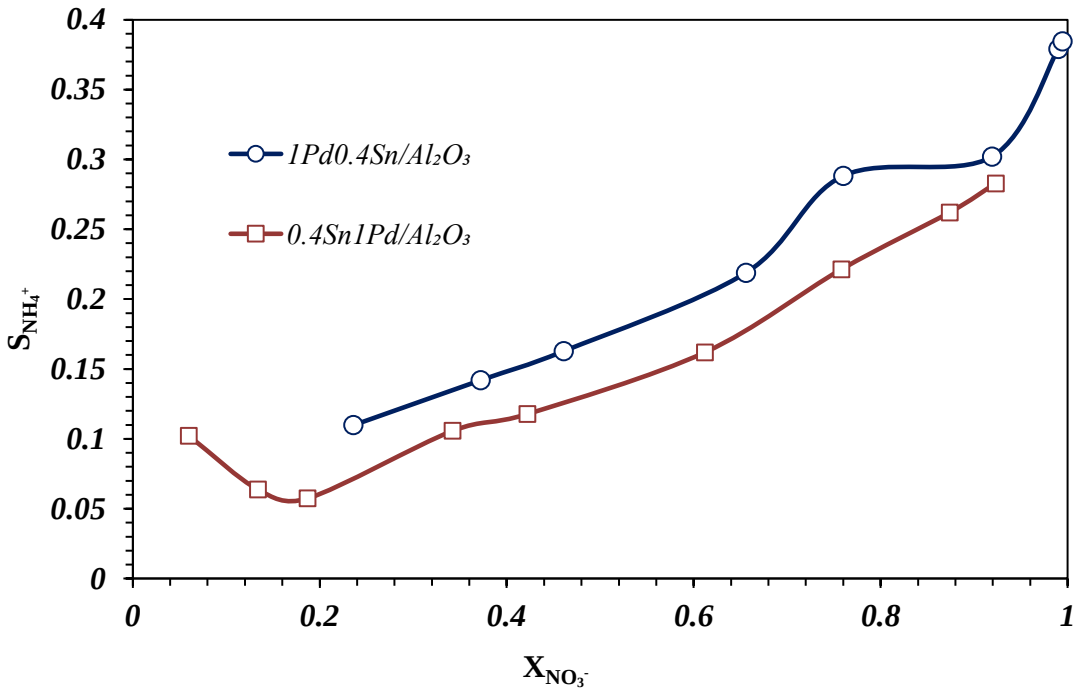

Figure 5.8 *Ammonium selectivity versus nitrate conversion for the catalyst impregnated with Sn first (1Pd0.4Sn/Al_2O_3) and the catalyst impregnated with Pd first (0.4Sn1Pd/Al_2O_3)*

Table 5.3 shows the values of the kinetic constants calculated from the fittings of the experiments. In this case, the fittings considerate k_2* to take into account the presence of residual nitrites. As can be seen in the results, the change in the catalyst synthesis method modifies its structure, which produces changes in k_1, constant related to nitrate elimination reaction and in the adsorption constant. Due to the difference of the K_{ads} it

was decided to compare the nitrate reduction using the product of k_1 and K_{ads}, k_1^*. Looking at table 5.3 it can clearly be observed that k_1^* of the catalyst $1Pd0.4Sn/Al_2O_3$ is six times higher than the one of $0.4Sn1Pd/Al_2O_3$. Meaning that the overall conversion of nitrate is faster for the catalyst $1Pd0.4Sn/Al_2O_3$, as it was observed on the experimental data. Comparing the results of k_1 and k_2 it can be observed how k_2 is three orders of magnitude higher then k_1, meaning that the conversion of nitrites is much faster than the conversion of nitrates. Finally, the relation $k_3 \cdot \overline{[NO]}/k_4$, whose higher values indicate higher selectivity to N_2, shows, as well as the experimental data, that the catalyst firstly impregnated with Pd obtain lower selectivity towards NH_4^+.

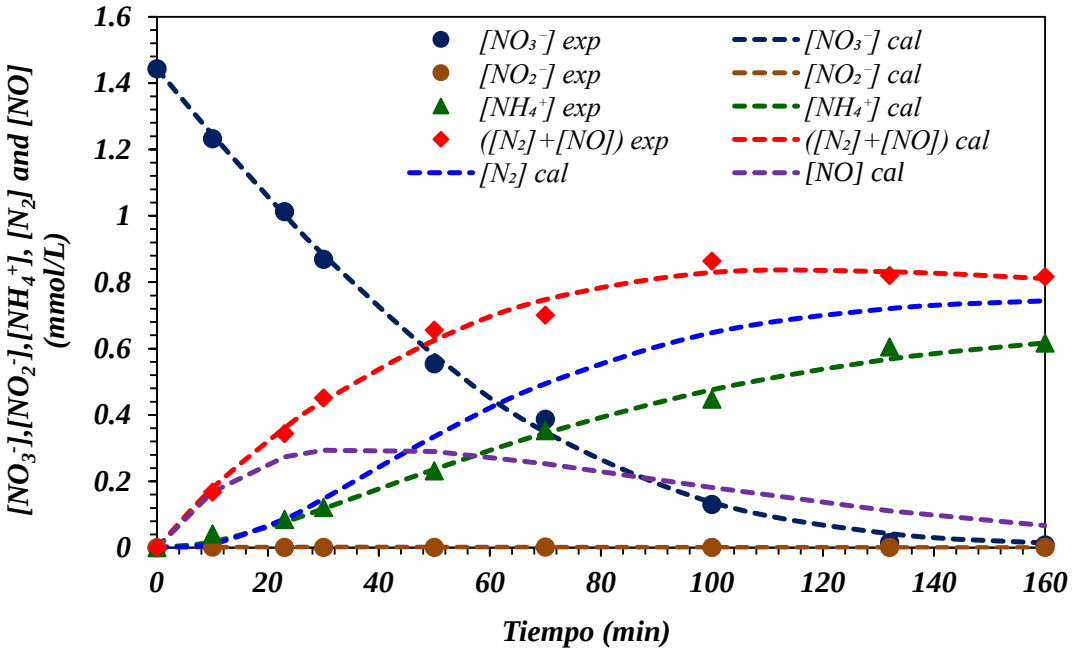

Figure 5.9 *Comparation of the evolution of nitrate (NO_3^-), nitrite (NO_2^-), nitrogen (N_2), nitrogen oxide (NO) and ammonia (NH_4^+) concentrations between experimental and calculated results over time of the catalyst impregnated with Sn first ($1Pd0.4Sn/Al_2O_3$).*

Table 5.3 *Values of the kinetic parameters for the CSRN for the catalyst with different impregnation order.*

Catalyst	***1Pd0.4Sn/Al₂O₃***	***0.4Sn1Pd/ Al₂O₃***
$k_1 (NO_3^-)$ $(mol.g.L^{-1}\cdot min^{-1})$	*0.019 ± 0.002*	*0.013 ± 0.0018*
$K_{ads} (NO_3^-)$ (mol^{-1})	*4.057 ± 1.281*	*0.523 ± 0.1079*
k_1^*	*0.410*	*0.007*
$k_2 (NO_2^-)$ $(g.L^{-1}\cdot min^{-1})$	*29.228 ±14.239*	*9.264 ± 51.7628*
$k_2^* (NO_2^-)$ $(g.L^{-1}.min^{-1})$	*0.138 ± 0.005*	*0.024 ± 0.0018*
$k_3 (N_2)$ $(g.mol^{-1}.L^{-1}\cdot min^{-1})$	*0.024 ± 0.001*	*0.009 ± 0.004*
$k_4 (NH_4^+)$ $(g.L^{-1}\cdot min^{-1})$	*0.019 ± 0.002*	*0.002 ± 0.0003*
$k_3 \cdot \overline{[NO]}/k_4$	*0.957*	*1.467*

5.3.2. Influence of the tin load on the catalyst

In order to optimize the quantity of Sn loaded on the catalyst we performed a study maintaining constant the load of Pd on 1% a varying the mass percentage of Sn: 0.2%, 0.4%, 0.8%, 1.2%, 2% and 2.5%. The condition of the operations is explained in section 2.2.1. The catalysts were reduced at 250ºC in a with a H_2 flow of 100ml/min. The operational variables were 1 g.cat./L and 100 ppm initial nitrate concentration, a flow of 200 mL/min CO_2 and 100 mL/min H_2, and a stirring rate of 750 r.p.m.

The nitrate conversion over reaction time for the catalysts with different amount of Sn can be observed in Figure 5.10. The increase of the content of Sn in the catalyst sped up the nitrate conversion, attaining a maximum when the weight percentage of Sn was of 2%. The catalyst 1Pd2Sn/Al_2O_3 achieved total conversion in around 50 min. However, a greater increase in the amount of Sn decreased the activity. As observed in the characterization results, the increase in the amount of Sn in the catalyst improves the dispersion of the active phase, obtaining smaller particle sizes. Furthermore, the XPS

characterization results also corroborate good contact between metals, with a high proportion of the two metals in alloy form in the catalysts studied in this series (Table 5.2). All of these factors produced faster nitrate reduction because, as explained before, the nitrate adsorption takes place on the promoter metal, Sn in this case, so, the increase in Sn produces an increment in active sites for the adsorption and transformation of nitrates [8–10]. In the case of the catalyst with the highest amount of Sn, 1Pd2.5Sn, the decrease in activity could be due to partial Pd encapsulation. Similar results were published by Hamid et al. [11], in which a decrease in NO_3^- reduction was observed with high Sn:Pd ratios, explaining that this fact may have been due to the overlap of the Sn particles on the Pd surface. Besides, the catalysts show an enrichment of Sn on the catalyst surface, as can be seen in the XPS results, Table 5.2, decreasing the superficial Pd/Sn ratio compared to the nominal one and corroborating the overlap/encapsulation effect. If this effect is very elevated, the reaction can be hindered since in this stage Pd assumes the role of regenerating the oxidized Sn to its metallic state, necessary for the reduction of nitrates. Therefore, a significant reduction of the noble metal sites for the adsorption of H_2 with respect to the promoter metal can lead to a reduction in the reaction rate [11–13].

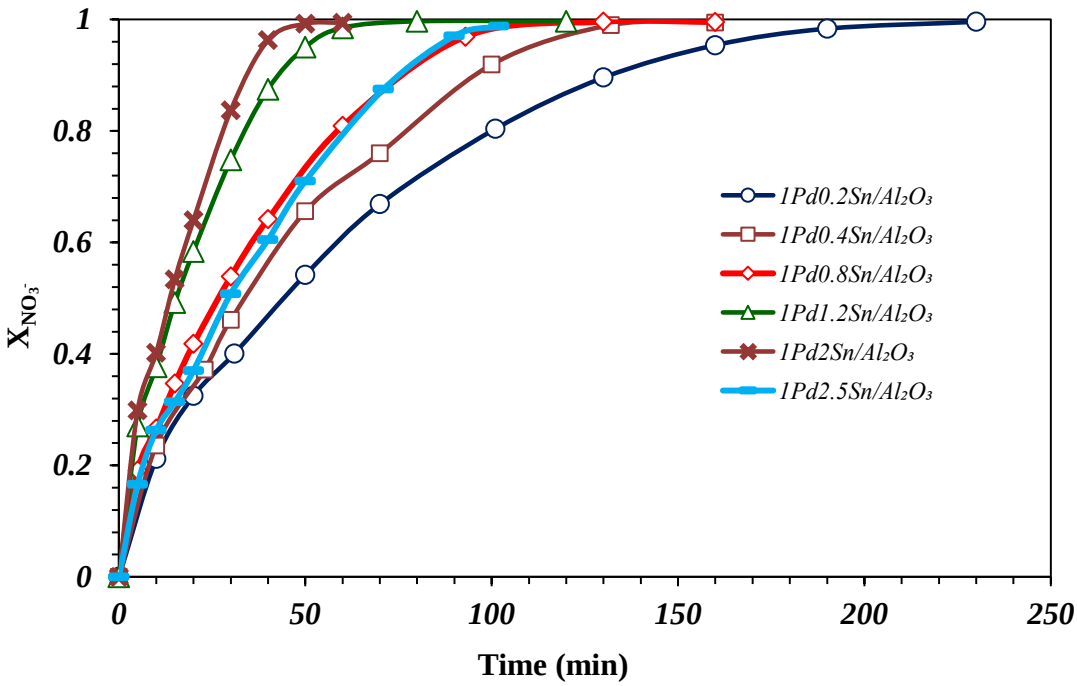

Figure 5.10 *Nitrate conversion over time for the catalysts with 1%Pd and various %wt. of Sn.*

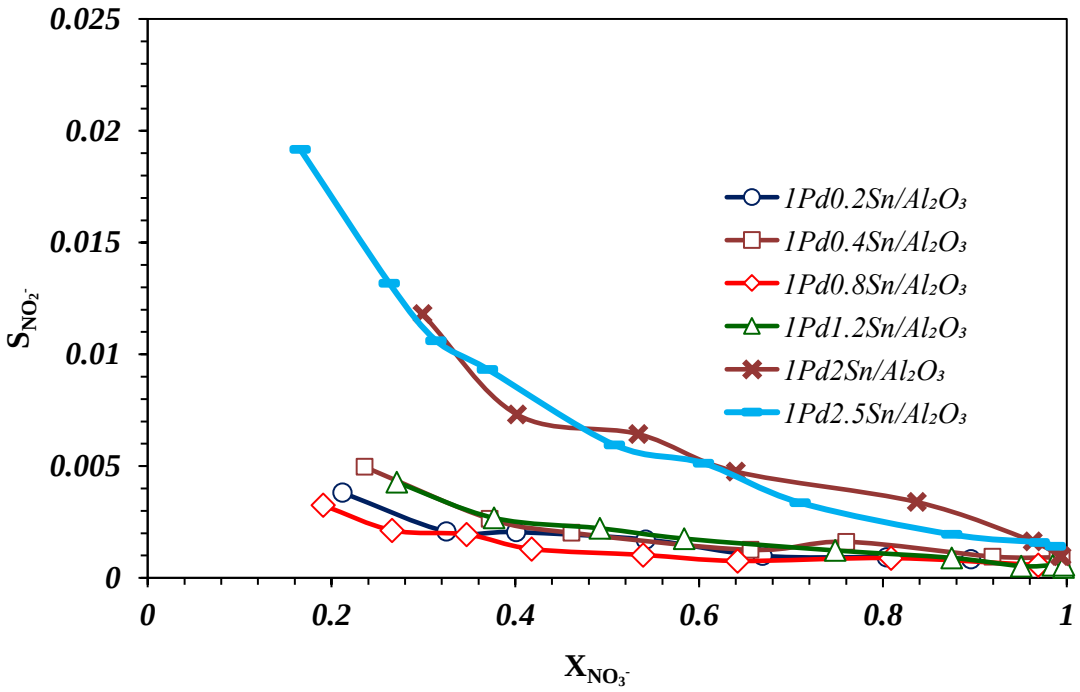

Figure 5.11 *NO_2^- selectivity versus NO_3^-conversion. Catalysts: 1%Pd and various %wt. of Sn.*

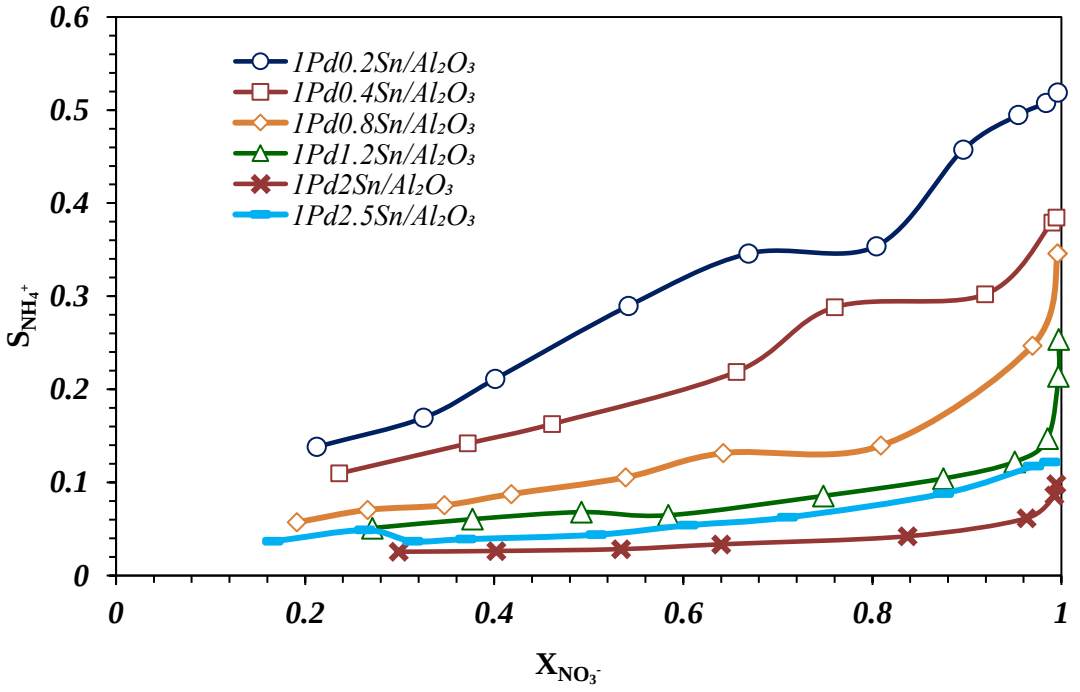

Figure 5.12 *NH_4^+ selectivity versus NO_3^-conversion. Catalysts: 1%Pd and various %wt. of Sn.*

With respect to nitrite reduction (Figure 5.11), the selectivity was very low for all the catalysts tested, even compared with $PdCu/Al_2O_3$, below 2% in all cases and for all conversions. The catalysts 1Pd2Sn and 1Pd2.5Sn showed slightly higher selectivity to this intermediate product.

Finally, ammonium selectivity can be observed in Figure 5.12. The results show a similar trend to that observed for nitrate conversion. High loads of promoter metal reduced the selectivity to NH_4^+, attaining a minimum at 2% wt. of Sn.

This minimum may be due to the $1Pd2Sn/Al_2O_3$ catalyst achieving the best balance between all the opposing factors that occur when increasing the Sn content in the catalyst. On the one hand, the introduction of increasing amounts of Sn in the catalyst produces a better dispersion of the metals, reducing the metallic particle size, improving contact between phases and increasing the conversion to nitrates, as commented before. On the other hand, this increase of Sn content decreases the proportion of Pd on the surface (Table 5.2) [12], potentially hindering the reaction steps that occur on the noble metal and varying the N/H ratio adsorbed on the surface, and, in consequence, the ammonium selectivity [14–18]. Related to this, another variable factor in this study is the formation of the alloy of Pd-Sn. Yoshinaga et al. [18] suggested that a dilution of Pd takes place during alloying. This leads to an increment in the number of isolated Pd atoms, which are suggested to be active sites for the ammonium formation. In other work [19] , it was demonstrated that the selectivity to ammonium is higher when the noble metal is isolated, because as the noble metal is very active for hydrogenation reactions the nitrite ions are deeply hydrogenated into ammonium [19]. Therefore, in this case, it seems that $1Pd2Sn/Al_2O_3$ catalyst shows an optimum amount of PdSn alloy, which allows good contact between phases but without favoring the formation of ammonium.

The results of the kinetic constants of the reaction obtained from the fittings of these experiments can be observed in Table 5.4. For these fittings, K_{ads} was considered constant because it was observed that there was no variation due to the catalyst composition. The kinetic constant related to nitrate elimination, k_1, increase with the load of Sn, attaining a maximum at 2% wt. of Sn, following the trend of the experimental data. Regarding at the kinetic constant related with the reduction of NO_2^- to NO, k_2, it can be observed that the value for the catalysts with 2 and 2.5% wt. of Sn are lower than the rest of catalysts, matching the difference observed in the

experimental results, which showed a higher selectivity to NO_2^- for these catalysts. Finally, the relation $k_3 \cdot \overline{[NO]}/k_4$ shows an augment when the percentage of Sn increases, i.e. higher selectivity towards N_2, until attaining a maximum for the catalyst with 2% wt. of Sn, which is the same trend that was observed on the experimental data.

The results of the kinetic constants of the reaction obtained from the fittings of these experiments can be observed in Table 5.4. For these fittings, K_{ads} was considered constant because it was observed that there was no variation due to the catalyst composition. The kinetic constant related to nitrate elimination, k_1, increase with the load of Sn, attaining a maximum at 2% wt. of Sn, following the trend of the experimental data. Regarding at the kinetic constant related with the reduction of NO_2^- to NO, k_2, it can be observed that the value for the catalysts with 2 and 2.5% wt. of Sn are lower than the rest of catalysts, matching the difference observed in the experimental results, which showed a higher selectivity to NO_2^- for these catalysts. Finally, the relation $k_3 \cdot \overline{[NO]}/k_4$ shows an augment when the percentage of Sn increases, i.e. higher selectivity towards N_2, until attaining a maximum for the catalyst with 2% wt. of Sn, which is the same trend that was observed on the experimental data.

Table 5.4 *Values of the kinetic parameters for the CSRN. Catalysts: 1%Pd and various %wt. of Sn.*

Tin concentration	***0.2 %***	***0.4 %***	***0.8 %***	***1.2 %***	***2 %***	***2.5 %***
k_1 (NO_3^-) $(mmol.g.L^{-1}.min^{-1})$	*0.014 ± 0.002*	*0.019 ± 0.002*	*0.026 ± 0.002*	*0.041 ± 0.002*	*0.050 ± 0.019*	*0.025 ± 0.001*
K_{ads} (NO_3^-) $(mmol^{-1})$	*4.057 ± 1.281*					
k_2 (NO_2^-) $(g.L^{-1}.min^{-1})$	*35.005 ± 13.234*	*29.228 ± 14.239*	*46.687 ± 18.564*	*25.338 ± 13.669*	*8.53 ± 9.609*	*4.422 ± 1.954*
k_2* (NO_2^-) $(g.L^{-1}.min^{-1})$	*0.014 0.002*	*0.019 ± 0.002*	*0.026 ± 0.002*	*0.026 ± 0.002*	*0.05 ± 0.002*	*0.025 0.001*
k_3 (N_2) $(g.mmol^{-1}.L^{-1}.min^{-1})$	*0.132 ± 0.002*	*0.138 ± 0.005*	*0.019 ± 0.008*	*0.027 ± 0.01*	*0,015 ± 0.014*	*0.005 0.002*
k_4 (NH_4^+) $(g.L^{-1}.min^{-1})$	*0.033 ± 0.011*	*0.024 ± 0.001*	*0.009 ± 0.001*	*0.008 ± 0.001*	*0.004 ± 0.001*	*0.003 0.001*
$k_3 \cdot \overline{[NO]}/k_4$	*0.455*	*0.957*	*0.908*	*1.483*	*2.586*	*1.094*

5.3.3. Influence of the palladium load on the catalyst

With the aim of evaluating the influence of the load of the noble metal in the catalyst, a series of catalysts was prepared maintaining the load of Sn at 1.2% w.t. and modifying Pd load (0.6, 1, 2 and 4 % wt.). The concentration of 1.2% wt. of Sn was considered as a good balance between nitrate conversion rate and low ammonium selectivity with respect to the total amount of metal loaded in the catalyst, as observed in previous section.

These catalysts were prepared using the synthesis conditions explained in section 2.2.1. of the Experimental chapter. As well as the previous catalysts, the samples were reduced at 250ºC in a with a H_2 flow of 100ml/min. The reaction operational variables were: 1 g.cat./L; initial nitrate concentration of 100 ppm; reaction flow of 200 mL/min CO_2 and 100 mL/min H_2; stirring rate of 750 r.p.m.

The nitrate conversion along reaction time can be observed in the Figure 5.13. The increase in the Pd content decreased the nitrate reduction time, going from 100 minutes necessary to convert all the nitrates using the catalyst with 0.6% wt. of Pd, to less than 30 minutes with the catalyst with 4% wt. of Pd. The increase in Pd load produces an increase in the number of active sites available for the reaction, showing a greater Pd/Sn surface ratio (Table 5.2) despite that the particle size formed increased slightly (Figure 5.2 and 5.3). Furthermore, PdSn alloy is formed in all catalysts (Table 5.2), which favors the nitrate elimination reaction. During this conversion, if accessible Pd active sites are low or the contact between metals is bad, it results in limited Sn regeneration, leading to slower nitrate conversion [20]. In conclusion, a greater amount of palladium in the catalyst increased the nitrate conversion rate due to the formation of higher quantity of active sites and a good contact between metallic phases.

With respect to the nitrite selectivity (Figure 5.14), it can be observed that the selectivity is very low for all the experiments, i.e. the elimination of nitrites is very fast, and there are no large differences between the different catalysts. It is slightly higher for the 0.6Pd1.2Sn catalyst due to its low Pd content, as already occurred in the nitrate elimination step. Finally, the ammonium selectivity versus nitrate conversion can be observed in Figure 5.15. The results don't show a trend with respect to the Pd loading. All catalysts achieved very good results in selectivity to nitrites and nitrogen due to good dispersion of the metals in all cases.

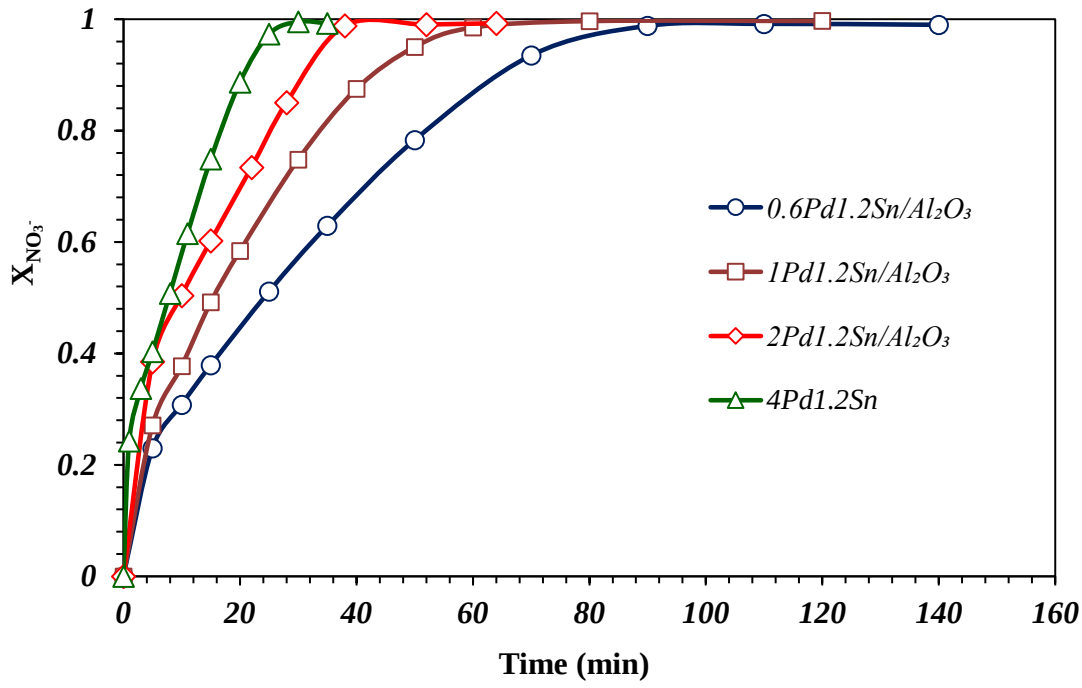

Figure 5.13 *Nitrate conversion over time for the catalysts with 1.2%Sn and various %wt. of Pd.*

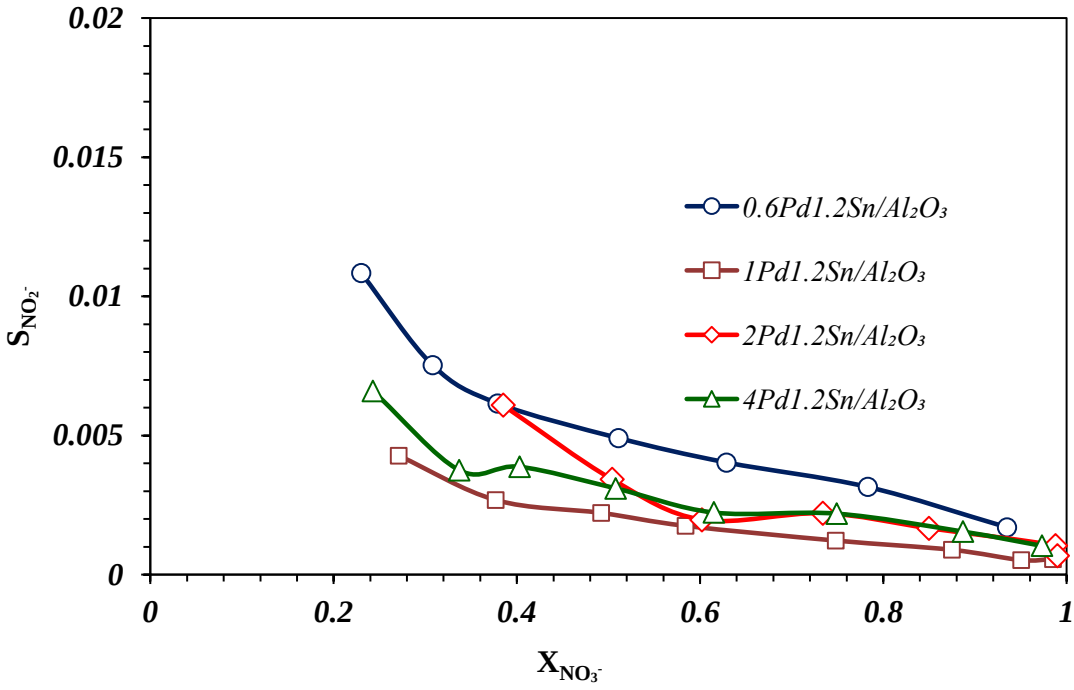

Figure 5.14 *NO_2^- selectivity versus NO_3^- conversion. Catalysts:1.2%Sn and various %wt. of Pd*

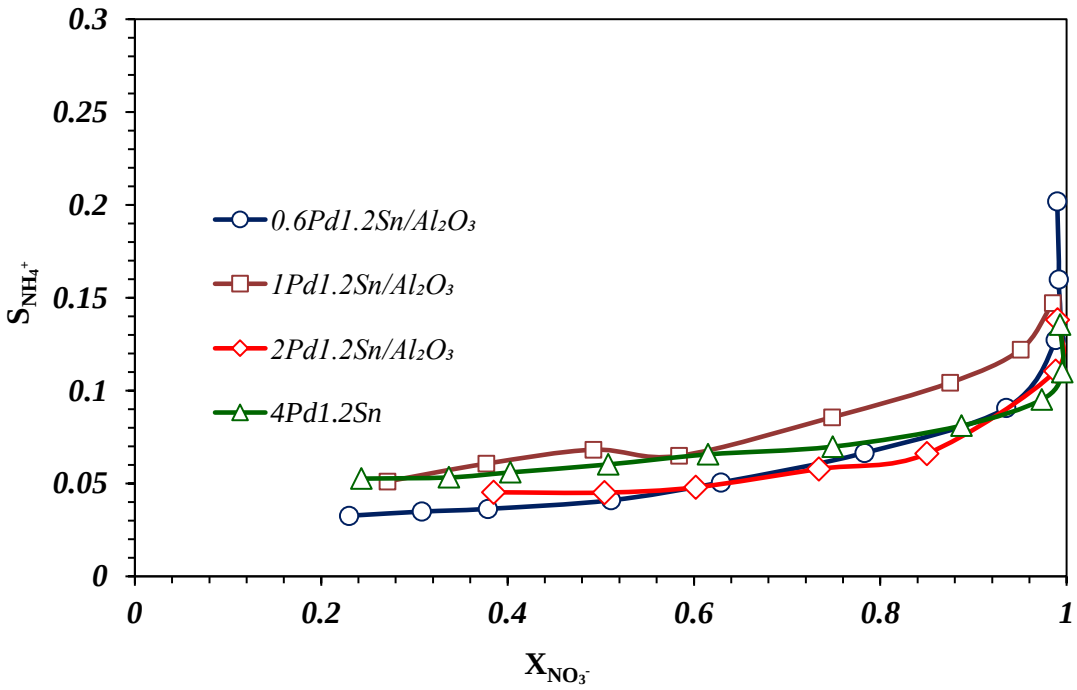

Figure 5.15 *NH_4^+ selectivity versus NO_3^- conversion. Catalysts:1.2%Sn and various %wt. of Pd*

Taking this into account, the catalyst with 1%wt. of Pd was chosen as the best compromise between the yield achieved by the catalyst and its price. This catalyst with 1%Pd instead of the catalyst 0.6%Pd the reaction time is reduced in 40 minutes approximately. On the other hand, when we employ the 2%Pd catalyst instead of the 1%Pd catalyst the reaction comes to an end only 15 min earlier, even when we doubled the amount of Pd.

As in the previous study, the presence of residual nitrites is observed, so k_2^* will be greater than 0, and there is no deactivation of the catalyst, meaning k_d is equal to 0. In table 5.5, the values of the constants and their error for the different Pd concentrations are shown. As expected, and according to the experimental data, k_1 increases with increasing Pd. The parameter K_{ads} was considered constant as it was found to be unaffected by the variation of the catalyst composition. The constant k_2 is much higher than k_1, corroborating that nitrite removal is faster than nitrate conversion, with nitrate decomposition being the limiting step in the process. The relation $k_3 \cdot \overline{[NO]}/k_4$ seems to increase with the increase on the Pd content, but this is not observed on the experimental data, so this virtual tendency may be due to error on the calculated data.

Table 5.5 *Values of the kinetic parameters for the CSRN for the catalyst with with 1.2%Sn and various %wt. of Pd.*

Pd concentration	***0.6%***	***1%***	***2%***	***4%***
k_1 (NO_3^-) $(mol.g.L^{-1}.min^{-1})$	0.027 ± 0.0006	0.041 ± 0.001	0.049 ± 0.002	0.079 ± 0.003
K_{ads} (NO_3^-) (mol^{-1})	4.057 ± 0.529			
k_2 (NO_2^-) $(g.L^{-1}.min^{-1})$	6.259 ± 6.251	25.338 ± 46.374	16.67 ± 22.07	35.909 ± 65.16
k_2^* (NO_2^-) $(g.L^{-1}.min^{-1})$	0.009 ± 0.032	0.026 ± 0.148	0.025 ± 0.126	0.086 ± 0.289
k_3 (N_2) $(g.mol^{-1}.L^{-1}.min^{-1})$	0.005 ± 0.002	0.027 ± 0.005	0.03 ± 0.004	0.12 ± 0.063
k_4 (NH_4^+) $(g.L^{-1}.min^{-1})$	0.003 ± 0.0002	0.008 ± 0.0005	0.008 ± 0.001	0.015 ± 0.002
$k_3 \cdot \overline{[NO]}/k_4$	1.002	1.550	1.839	3.367

5.3.4. Influence of water composition

After carrying out the optimization of the catalyst composition, the influence of different reaction variables, such as the water composition, was analyzed. The experiments for this study were realized with a constant flow of H_2 of 100mL/min and a flow of CO_2 of 0, 200 or 400 mL/min (H_2/CO_2 ratio: ½ and ¼ respectively). The catalyst used was 1Pd1.2Sn, which was reduced at 250ºC in H_2 atmosphere. The rest of the operational conditions were the same as the previous experiments: 1 g.cat./L, 100 ppm of initial nitrate concentration and stirring rate of 750 r.p.m.

The pH of the solution was measured during the reaction. In absence of CO_2, the pH increased abruptly at the beginning of the reaction and after was constant around a value of 9. On the other hand, when CO_2 was fed, regardless of the flow used, the pH was practically constant, slowly increasing from 4 till 5. As commented in Section 4.1.3.4, the CO_2 introduced into the reaction has the objective of buffering the increase in pH produced by the OH^- ions formed as a product of the reaction. CO_2 reacts with water

producing carbonic acid, which partially dissociates in bicarbonate and H^+ ions, which react with the OH^- produced during the reaction, transforming them into water.

The evolution of the nitrate conversion over time for the different flows of CO_2 can be observed in Figure 5.16. Nitrate conversion was similar for all the experiments the 20 first minutes approximately. At higher conversions, the experiment without CO_2 slowed down due to the non-neutralization of the OH^- formed, which produced the increase of the pH of the solution. These ions adsorbed on the Pd surface hinder the adsorption of H2, deactivating the catalyst. Besides, this fact also produces the negatively charge of the surface of the catalyst, also hindering the adsorption of the NO_3^- [21,22]. In these conditions, the catalyst did not achieve total nitrate conversion after 250 min of reaction. On the other hand, the experiments with different flow of CO_2, 200 and 400mL/min, had very similar behavior during all reaction, reaching complete conversion at around 60min. The experiment with H_2/CO_2 ratio of ½ was slightly faster, probably due to the higher concentration of H_2 present in the feed, which allowed a faster regeneration of the promoter metal and nitrate conversion. This effect can also be observed in the test without CO_2, which is the most active at the beginning of the reaction. However, this effect is lost due to the deactivation suffered for the catalyst. The presence of CO_2 strongly affects the selectivity to NO_2^-, as can be observed in Figure 5.17. When CO_2 was not introduced in the alimentation, the nitrite elimination rate was low, observing high nitrite selectivities. As commented before, the OH^- formed during the reaction are preferable adsorbed on the surface of the Pd, hindering the adsorption of NO_2^- and resulting on an accumulation in the solution of this intermediate product formed in the previous step of reaction [15–18,23]. On the other hand, the increase in the concentration of CO_2 in the alimentation did not affect significantly NO_2^- selectivity, being very low due to a very rapid conversion of the nitrites to the final products of the reaction.

Finally, the selectivity to NH_4^+ was also affected by the composition of the water, as can be observed in Figure 5.18. Ammonia selectivity showed high values, up to almost 40% at the end of the reaction when CO_2 was not introduced in the feed. As mentioned before, the adsorption of nitrites is hindered by the adsorbed OH^-, so the density of N species on the surface of the catalyst is lower, i.e. the N/H relation on surface is low, which favours the formation of ammonium [15–18,23]. The selectivity to the final reaction products is also affected by the concentration of CO_2 introduced in the feed.

The higher the concentration, within the range studied, the lower the selectivity to ammonium.

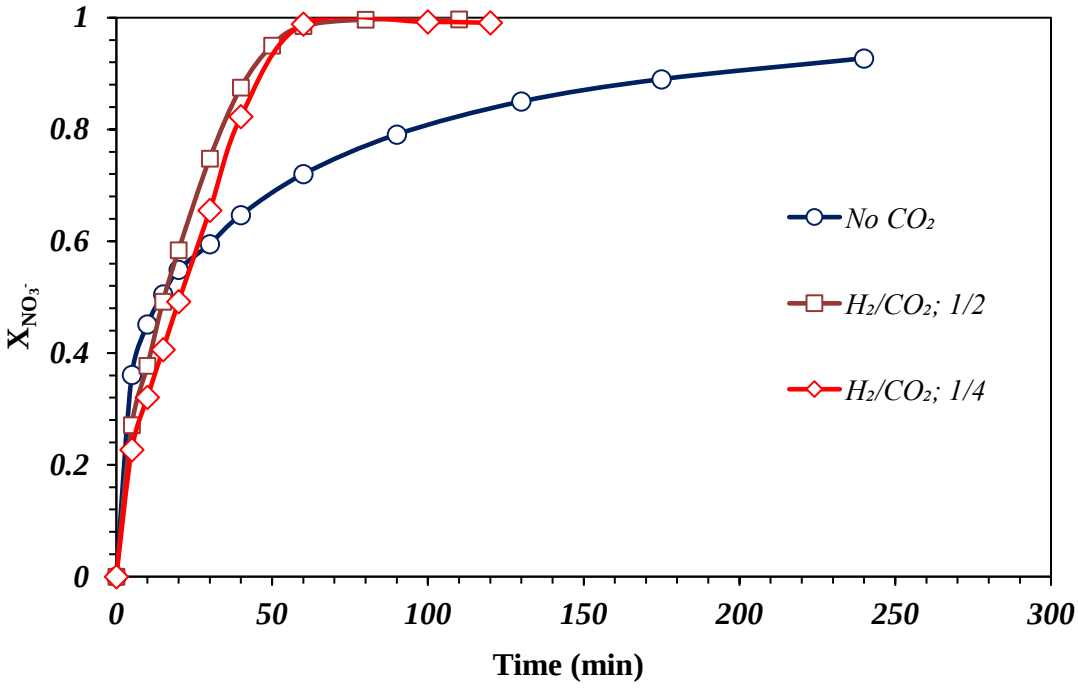

Figure 5.16 *Nitrate conversion over time for the catalyst 1Pd1.2Sn/Al_2O_3 with different H_2/CO_2 ratio feed composition.*

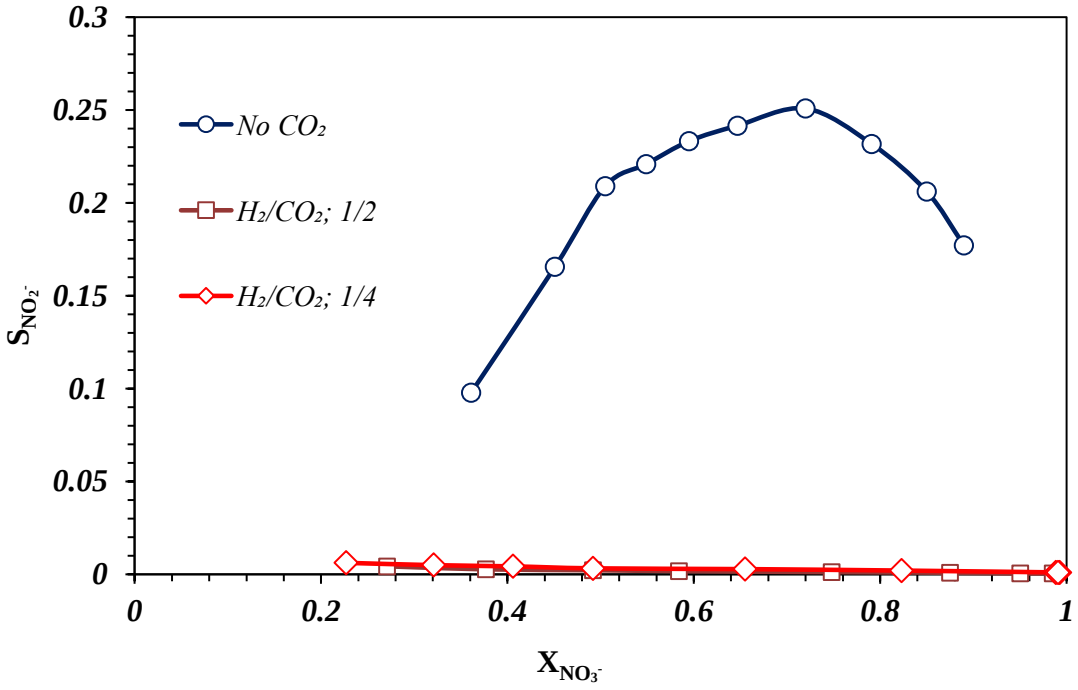

Figure 5.17 *Nitrite selectivity versus nitrate conversion for the catalyst 1Pd1.2Sn/Al_2O_3 with different H_2/CO_2 ratio feed composition.*

This fact can be due to greater cleaning of the surface of OH^- ions and to the competition between CO_2 and H_2 adsorption when CO_2 concentration increases, which produces two effects: a slight decrease in the activity, as commented before; and a lower concentration of hydrogen ions adsorbed on the surface, which prevents the formation of ammonium [13].

The experimental results of this study were fitted with the kinetic model, showing a good fitting with a global MSC value of 14.8. The values of the kinetic constants can be observed in the Table 5.6. In this case, k_2^* was introduced in the adjustment in order to take into account the presence of nitrites at the end of the experiments. In addition, the constant k_d was also considered for the experiment without CO_2, due to the catalyst deactivation observed in the experiment.

The use of the model considering a more kinetic constant produces a change in the weight that the model gives to the constants, which makes the values of the rest of the constants difficult to compare with the other experiments. In order to overcome this mathematical factor, the product of k_1 and K_{ads}, k_1^*, was compared.

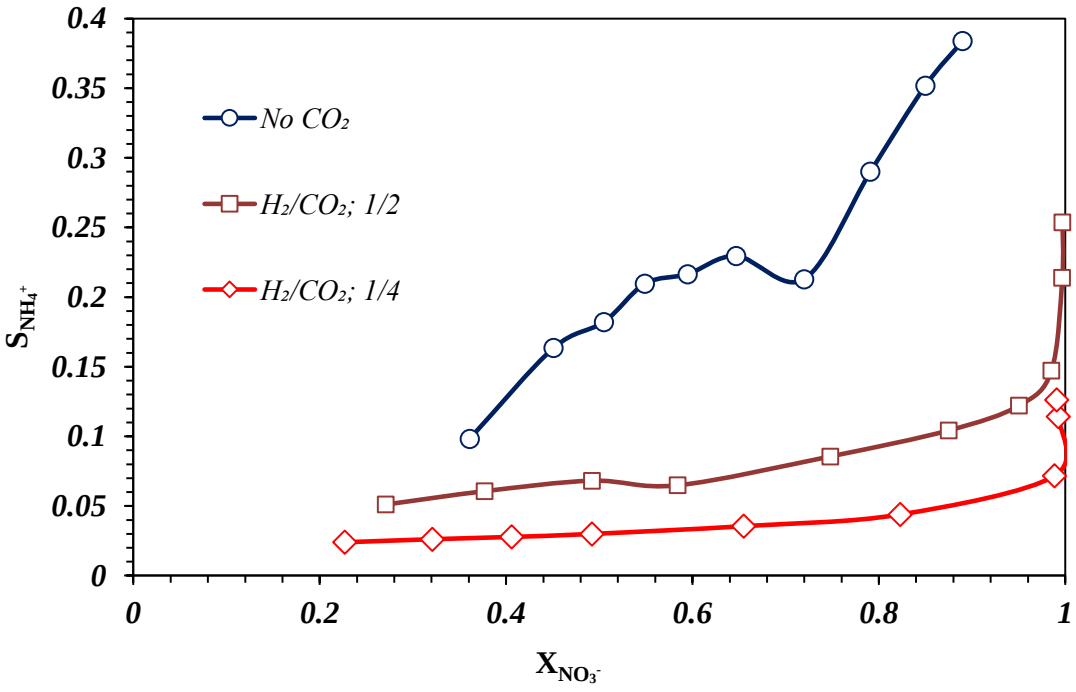

Figure 5.18 *Ammonium selectivity versus nitrate conversion for the catalyst 1Pd1.2Sn/Al_2O_3 with different H_2/CO_2 ratio feed composition.*

Table 5.6 *Values of the kinetic parameters for the CSRN for the catalyst 1Pd1.2Sn/Al_2O_3 with different H_2/CO_2 ratio feed composition.*

CO_2 feed	***No CO_2***	***200mL/min***	***400mL/min***
k_1 (NO_3^-) ($mol.g.L^{-1}.min^{-1}$)	*1.272 ± 0.073*	*0.041 ± 0.001*	*0.038 ± 0.001*
K_{ads} (NO_3^-) (mol^{-1})	*0.012 ± 0.001*	*4.057 ± 0.466*	
k_1* (NO_3^-) ($g.L^{-1}.min^{-1}$)	*0.015*	*0.167*	*0.152*
k_2 (NO_2^-) ($g.L^{-1}.min_{-1}$)	*1.621 ± 0.165*	*25.338 ± 7.221*	*18.172 ± 9.737*
k_2* (NO_2^-) ($g.L^{-1}.min^{-1}.$)	*6.845 ± 3.09E-7*	*0.026 ± 0.001*	*0.044 ± 0.001*
k_3 (N_2) ($g.mol^{-1}.L^{-1}.min^{-1}$)	*0.161 ± 0.068*	*0.027 ± 0.005*	*0.02 ± 0.008*
k_4 (NH_4^+) ($g.L^{-1}.min^{-1}.$)	*0.056 ± 0.006*	*0.008 ± 0.0005*	*0.003 ± 0.0004*
$k_3 \cdot \overline{[NO]}/k_4$	*0.175*	*1.550*	*3.697*

This constant represents the global constant of the nitrate elimination reaction. As can be observed, its value is very lower for the experiment without CO_2 fed, which causes a low nitrate elimination rate. Regarding the tests with different amounts of CO_2 were, the value is slightly higher for the case of 200 ml/min of CO_2 due to the higher concentration of hydrogen in the feed, which favors its adsorption, as mentioned above. With respect to the nitrite removal step, the overall rate of this step, taking into account the forward and reverse reaction, k_2 and k_2^*, is much lower for the case in which the feed does not contain CO_2, since that k_2 takes much lower values and k_2^* much higher. This fact leads to the high concentrations of nitrites in solution observed in this experiment. Finally, the ratio $k_3 \cdot \overline{[NO]}/k_4$ is higher when the CO_2 flow rate increases, corroborating the experimental data.

5.3.5. Influence of the reduction temperature.

The effect of the reduction temperature of the catalyst is evaluated in this section. For this purpose, the reduction pre-reaction temperature of the catalyst 1Pd1.2Sn/Al_2O_3 was varied from 250 to 550ºC in H_2 flow of 100mL/min. The rest of the operational conditions were the same as the previous experiments: 1 g.cat/L, 100 ppm of initial nitrate concentration and stirring rate of 750 r.p.m.

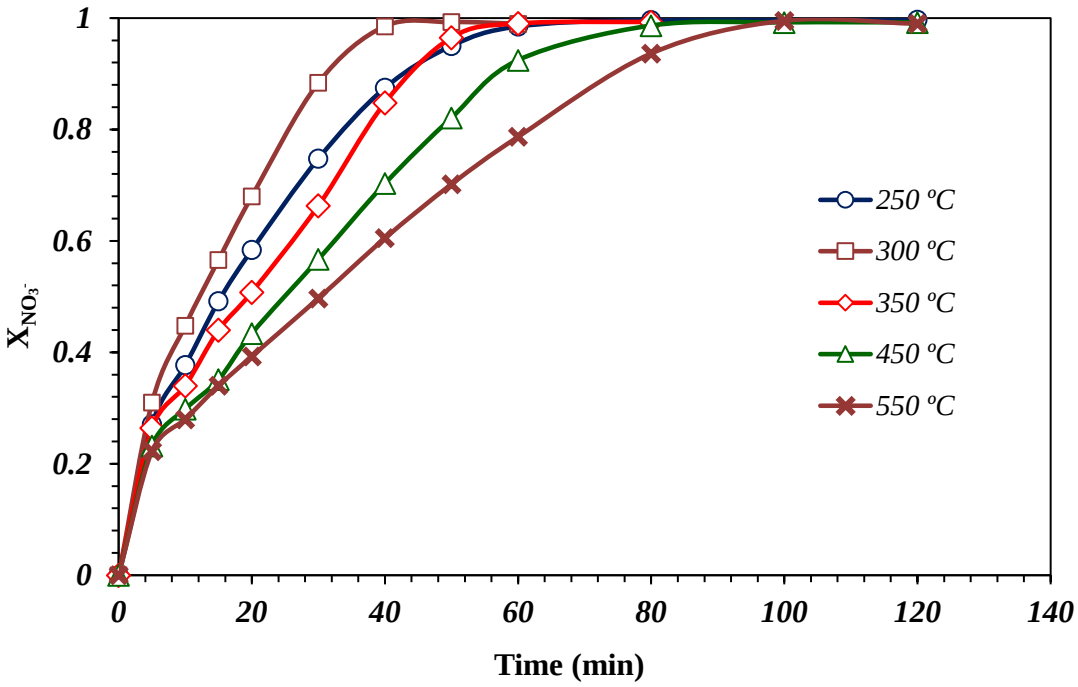

Figure 5.19 *Nitrate conversion over time for the catalyst 1Pd1.2Sn/Al_2O_3 at different reduction temperatures.*

As can be observed in Figure 5.19, the rate of nitrate elimination over time changed when the catalyst was reduced at different temperature, observing a maximum in the activity at 300ºC. The increase in the reduction temperature favours the formation of the active phases of Pd and Sn for the reaction. Elevated temperatures can help reduce Sn species, which, as can be seen in the TPR results, Figure 5.5, are reduced at temperatures above 300ºC. However, high temperatures can also produce the sintering of the nanoparticles, decreasing the activity. Another factor to take into account is the formation of the alloy of Pd-Sn. Alloying of metals may result in important changes in the activity and selectivity of the catalyst [24], Soaeres et al. [28] observed that nitrate reduction is highly influenced by the preparation conditions, being the formation of alloys a severe limitation for this reaction. In order to obtain high activities, the metals

must be in close contact but not alloyed because the alloy reduces the active sites for the nitrate reduction [25]. However, Batista et al. [26] and Deganello et al.[27] observed similar performances for nitrate reduction using alloyed or non-alloyed Pd–Cu. In the PdSn catalysts studied in this work, the formation of the alloy seems to be favorable, showing high activity and low selectivities to ammonium. Therefore, in this case, the maximum in activity can be due to the better balance between reduction of the metallic species, sintering and the formation of an adequate amount of the PdSn alloy. Besides, high amounts of PdSn alloy can increase the number of isolated Pd related with the formation of NH_4^+ [28]. Observing the evolution of the selectivity to nitrites (Figure 5.20), it can be observed as the selectivity shown for the catalyst in all the conditions tested was very low, less than 1% in all cases. The catalyst reduced at 250ºC showed the lowest selectivity value.

In Figure 5.21 it can be observed the selectivity towards ammonium for the different reduction temperatures. In this case, it can be observed a minimum around 300-350ºC. As well as was explained in other sections, this may be due to a higher concentration of NO resulting from the conversion of nitrates but the same Pd active surface to convert this NO into the final products [12], in the case of the catalyst reduced at 300ºC. Another factor may be that the increase of the nanoparticle size due to the sintering increase the Pd on the terrace of the nanoparticle related with the formation of N_2 instead of the Pd in the corners, related with isolated Pd and the formation of NH_4^+[18]. But, with the increase of temperature over 350º, the quantity of Pd forming an alloy is increased and incrementing the number of isolated Pd related with the formation of NH_4^+[28].

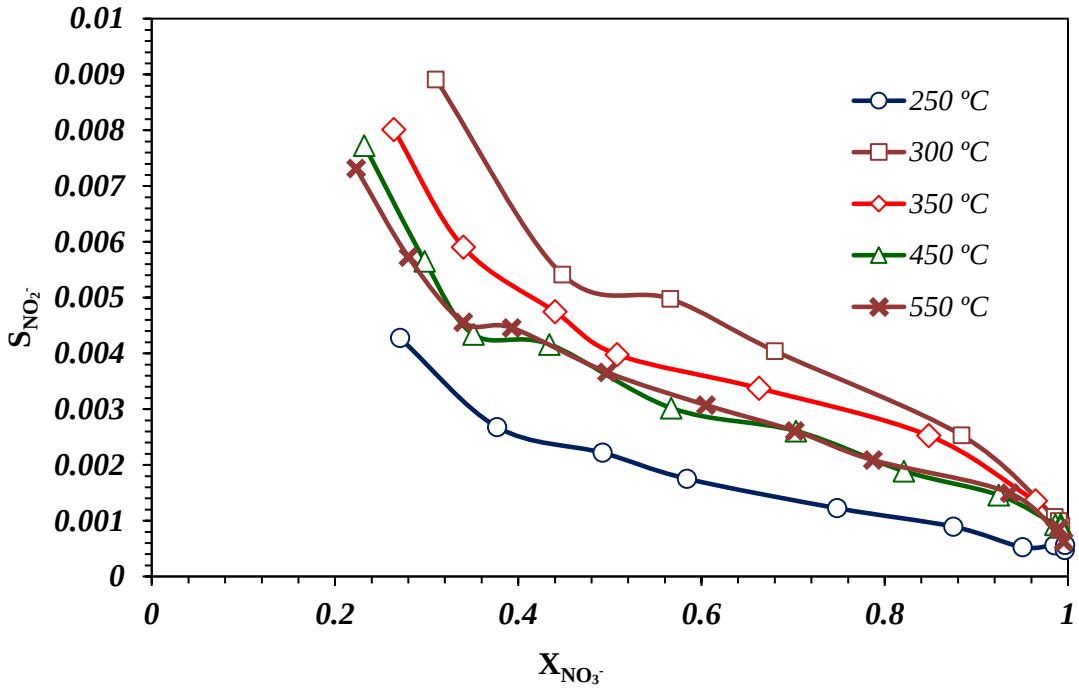

Figure 5.20 *Nitrite selectivity versus nitrate conversion for the catalyst 1Pd1.2Sn/Al_2O_3 at different reduction temperatures.*

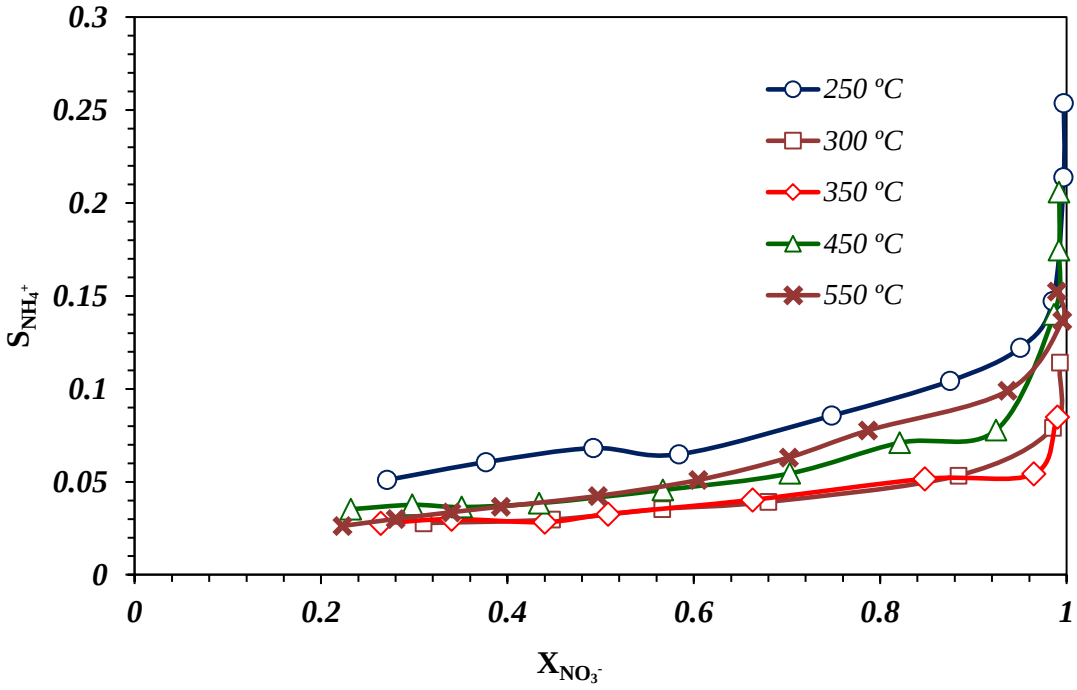

Figure 5.21 *Ammonium selectivity versus nitrate conversion for the catalyst 1Pd1.2Sn/Al_2O_3 at different reduction temperatures.*

As well as in previous studies, it was employed the global nitrate conversion k_1^* to compare the different tests. It can be observed a maximum at 300ºC which agree with the experimental data as the experiment with the faster nitrate conversion. In the case of the relation $k_3 \cdot \overline{[NO]}/k_4$, the higher value corresponds to the reduction at 350ºC in agreement with the experimental data, although it can't be observed the clear tendency observed on the experimental data (Table 5.7).

Table 5.7 *Values of the kinetic parameters for the CSRN for the catalyst 1Pd1.2Sn/Al_2O_3 reduced a different temperature.*

Reduction Temp.	***250 ºC***	***300ºC***	***350ºC***	***450ºC***	***550ºC***
k_1 (NO_3^-) (mol.g.L^{-1}.min^{-1})	*0.041 ± 0.001*	*0.044 ± 0.001*	*0.035 ± 0.001*	*0.024 ± 0.001*	*0.021 ± 0.0002*
K_{ads} (NO_3^-) (mol^{-1})	*4.057 ± 0.472*	*9.461 ± 1.36*	*7.726 ± 1.808*	*7.318 ± 2.555*	*6.517 ± 0.453*
k_1^* (NO_3^-) (g.L^{-1}.min^{-1})	*0.167*	*0.416*	*0.268*	*0.174*	*0.134*
k_2 (NO_2^-) (g.L^{-1}.min^{-1})	*25.338 ± 46.374*	*18.412 ± 14.986*	*18.287 ± 37.398*	*19.907 ± 59.854*	*25.086 ± 17.599*
k_2^* (NO_2^-) (g.L^{-1}.min^{-1})	*0.026 ± 0.148*	*0.056 ± 0.06*	*0.057 ± 0.156*	*0.057 ± 0.203*	*0.092 ± 0.068*
k_3 (N_2) (g.mol^{-1}.L^{-1}.min^{-1})	*0.027 ± 0.005*	*0.011 ± 0.007*	*0.025 ± 0.025*	*0.009 ± 0.008*	*0.014 ± 0.003*
k_4 (NH_4^+) (g.L^{-1}.min^{-1}.)	*0.008 ± 0.0005*	*0.005 ± 0.0005*	*0.004 ± 0.001*	*0.004 ± 0.0007*	*0.004 ± 0.0002*
$k_3 \cdot \overline{[NO]}/k_4$	*1.550*	*1.365*	*3.722*	*1.177*	*2.040*

5.3.6. Influence of ions on water

The effect of the presence of different ions in the reaction solution was evaluated in this study. Distilled and tap water from Casablanca deposit in Zaragoza, with a conductivity of 635 and 7,68 μS/cm respectively, were used and compared in reaction. The conductivity of tap water is mainly due to the presence of cations (Ca^{2+}, Na^{+}) and anions (Cl^{-}, SO_4^{2-}), among others (see Table 4.8). In both cases, nitrates were added just before the start of the reaction. The catalyst used was: 1%Pd1.2%Sn and the conditions of reduction/reaction were: reduction temperature of 350ºC, 1 g.cat./L, 100 ppm of initial nitrate concentration, 200 mL/min of CO_2 and 100 mL/min of H_2 and stirring rate of 750 r.p.m.

The conversion of nitrates over time for the experiments carried out with the two solutions is shown in the Figure 5.22. Nitrate reduction was much faster when distilled water was used, achieving complete conversion at approximately 60 minutes of reaction, practically half the time that in the case of tap water. The competitive adsorption of the other anions presents in the solution with the nitrates for the active sites of the catalyst slowed down the reaction when tap water was used [29]. The presence of other ions in the solution also had an impact in the nitrite selectivity, as can be observed in Figure 5.23. The selectivity was higher when the experiment was realized with tap water. Both tests follow the same tendency, with higher NO_2^{-} selectivity at the beginning of nitrate conversion. The experiment realized with tap water showed higher selectivity to this intermediate product. The bibliography suggests that the anions present in the solution are adsorbed on the metals and probably negatively charge the surface of the catalyst, hindering the adsorption of the NO_2^{-} on the Pd active sites and slowing down their conversion [21]. This effect can also be observed in the selectivity to NH_4^{+} (Figure 5.24). The selectivity was higher for the experiment realized with tap water. The density of nitrogen species adsorbed on the catalyst surface is lower due to the competition in the adsorption with other ions present in the solution and the slow nitrite elimination, reducing therefore the relation N/H on the catalyst surface and, in consequence, favouring the formation of ammonium, i.e. the selectivity to NH_4^{+} [21,22,30].

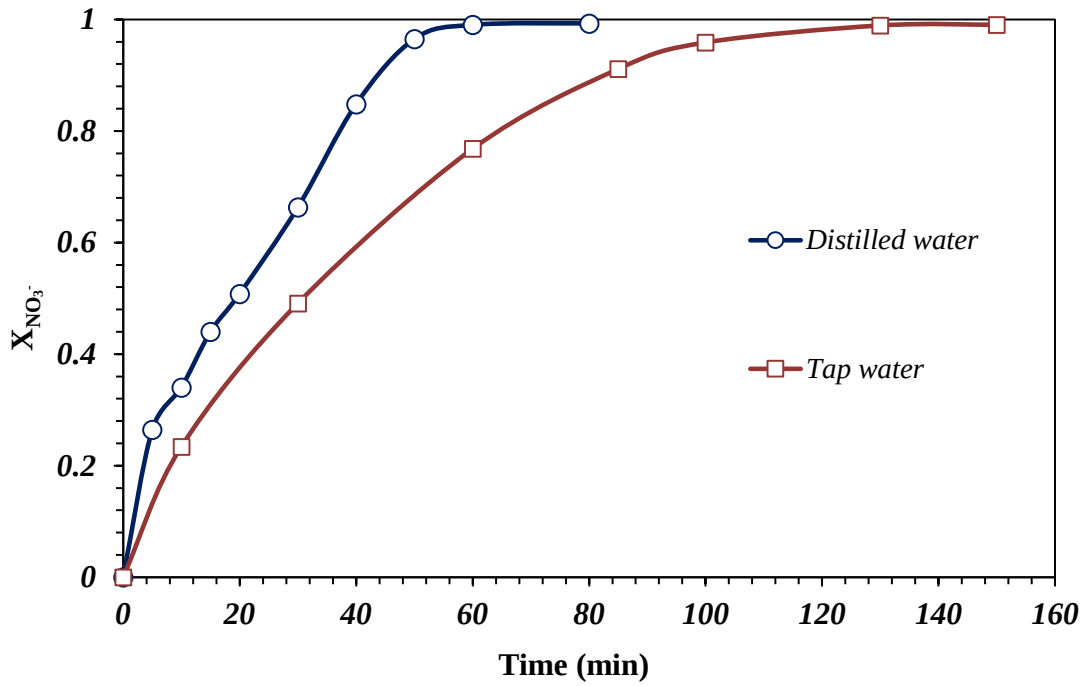

Figure 5.22 *Nitrate conversion over time for the catalyst 1Pd1.2Sn/Al_2O_3 without other ions (distilled water) and in the presence of ions different than nitrates (tap water).*

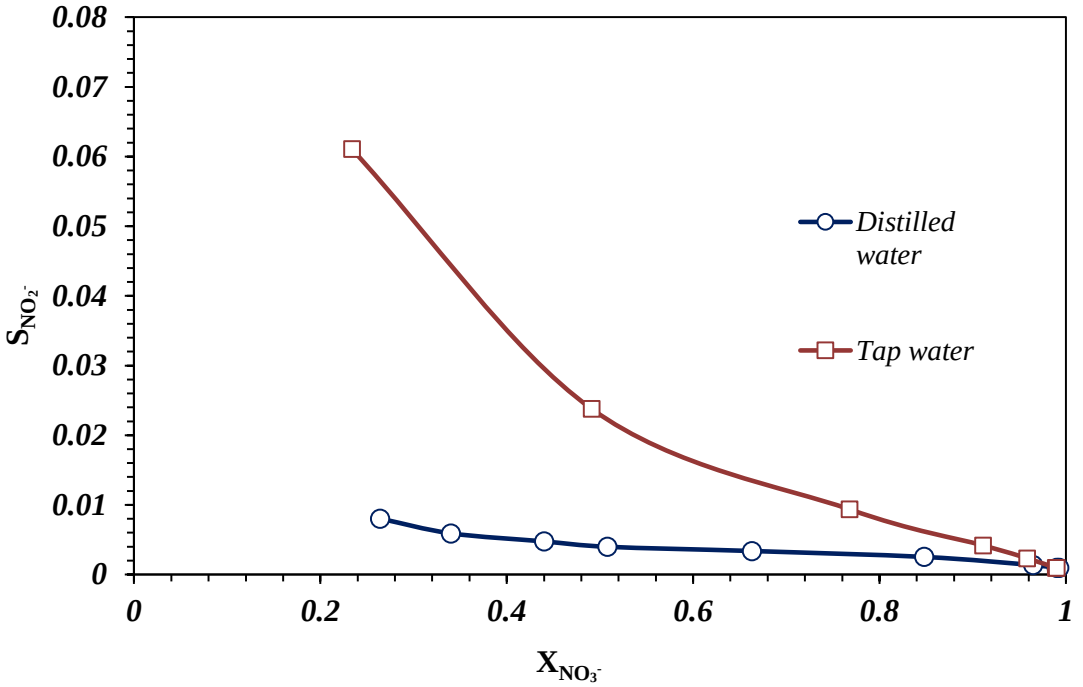

Figure 5.23 *Nitrite selectivity versus nitrate conversion for the catalyst 1Pd1.2Sn/Al_2O_3 without other ions (distilled water) and in the presence of ions different than nitrates (tap water).*

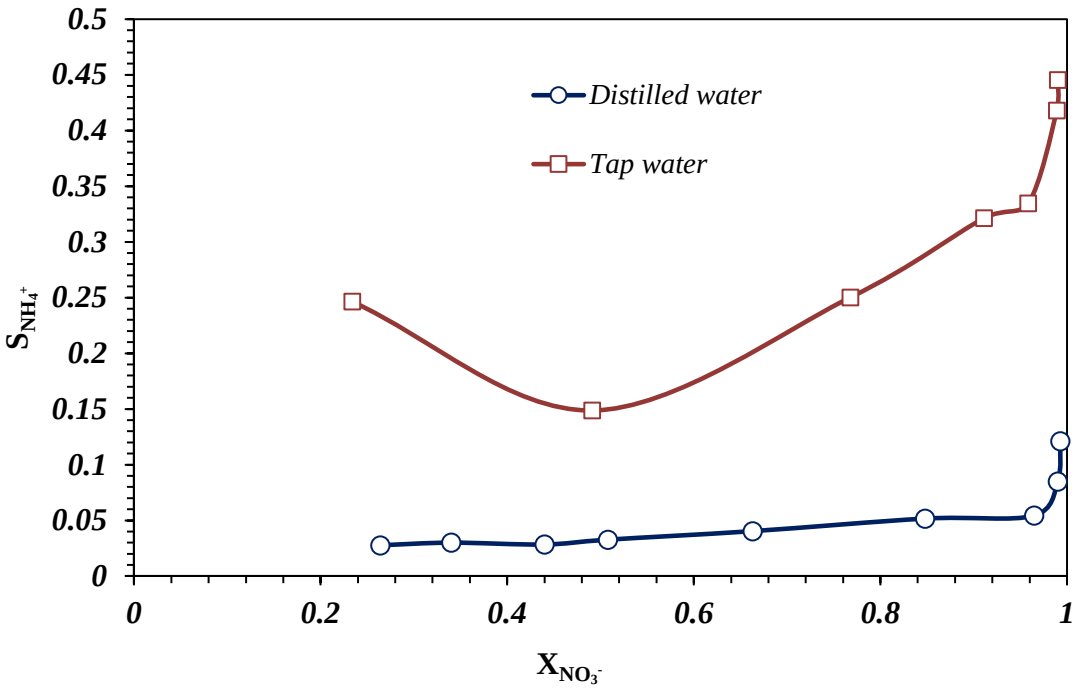

Figure 5.24 *Ammonium selectivity versus nitrate conversion for the catalyst 1Pd1.2Sn/Al_2O_3 without other ions (distilled water) and in the presence of ions different than nitrates (tap water).*

Table 5.8 presents the values of the kinetic constants obtained from the fitting of the experiments realised in different aqueous media. In both experiments, residual nitrites remained at the end of the reaction, being therefore k_2^* taken into account in the adjustment. On the other hand, k_d, constant related with catalyst deactivation, was considered 0. Analysing the obtained results, k_1, is similar for both experiments. However, the K_{ads} is almost double in the case of distilled water, which reflects the competition for the active sites of the catalysts due to the presence of other ions in tap water. Consequently, k_1^*, related to the global constant of the step of nitrate elimination, and calculated as the product of K_{ads} and k_1, is higher when the reaction is carried out using distilled water, making the nitrate elimination reaction in this medium faster, as observed in the experimental results.

A similar effect is observed in the reaction of transformation of NO_2^- to NO. k_2, kinetic constant related to nitrite elimination rate, is much lower when the experiment is realized in tap water than that for distilled water, in accordance with experimental data, where the selectivity to nitrites was higher in tap water due to the slower rate of nitrite disappearance caused by ion adsorption on the active sites of Pd. Finally, the relation $k_3 \cdot \overline{[NO]}/k_4$ is also lower for tap water, corroborating that the rate of nitrogen

formation with respect to ammonium is lower, and therefore the observed selectivity to ammonium is higher, which corroborates the experimental results.

Table 5.8 *Values of the kinetic parameters for the CSRN for the catalyst 1Pd1.2Sn/Al_2O_3 without other ions (distilled water) and in the presence of ions different than nitrates (tap water).*

Water	***Distilled***	***Tap***
k_1 (NO_3^-)	0.050 ±	0.045 ±
$(mmol.g.L^{-1}.min^{-1})$	0.007	0.01
K_{ads} (NO_3^-)	1.977 ±	0.935 ±
$(mmol^{-1})$	0.521	0.459
k_1^*	0.099	0.042
k_2 (NO_2^-)	11.593 ±	1.076 ±
$(g.L^{-1}.min^{-1})$	4.357	0.694
k_3 (N_2)	0.004 ±	0.011 ±
$(g.mmol^{-1}.\ L^{-1}.min^{-1})$	0.002	0.005
k_4 (NH_4^+)	0.003 ±	0.010 ±
$(g.L^{-1}.min^{-1})$	0.001	0.001
k_2^* (NO_2^-)	0.016 ±	0.045 ±
$(g.L^{-1}.min^{-1})$	0.007	0.01
$k_3 \cdot \overline{[NO]}/k_4$	1.160	0.544

5.4. Conclusions

The PdSn catalysts synthetized have been active in the catalytic reduction of nitrates and have shown high selectivity for nitrogen.

The impregnation order influences the dispersion and the size of the nanoparticles, obtaining smaller particle sizes impregnating the promoter of the metal first. It was also observed that the increase in the content of promoter metal don't increase the particle

size significantly, meanwhile, the increase of the noble metal load considerably enlarges the particle size.

The catalyst synthesis protocol affects the activity and selectivity by the $PdSn/Al_2O_3$ catalysts. The catalyst prepared by impregnating the support with tin, followed by calcination in air atmosphere at 350ºC and after this, impregnation with palladium and final calcination at 500ºC, significantly increases activity due to a decrease in the average particle size. This fact increases the number of active sites and better contact between active phases. Although the selectivity to ammonium is slightly increased using this catalyst, the reaction yield obtained is much higher.

The increase in the weight percentage of Sn in the catalysts leads to a better dispersion of the metals, reducing the metallic Pd particle size, which improves the contact between phases and in consequence the nitrate elimination rate. However, this increase of Sn content also decreases the proportion of Pd on the surface, even encapsulation of Pd may occur, which can hinder the reaction conversion and the selectivity to nitrogen by varying the N/H ratio adsorbed on the surface. The change in the Sn content also varies the quantity of PdSn alloy formed, which also can affect the selectivity of the process. The optimal trade-off between all these factors was found in the catalyst with a content of Sn of 2% wt.

The increase in the weight percentage of Pd in the catalyst causes an increase in the number of active sites available for the reaction, showing a greater Pd/Sn surface ratio despite that the particle size formed increased slightly. These effects produce an increase in the nitrate elimination rate without significant changes in ammonium selectivity. Therefore, a compromise can be achieved between the amount of Pd, considering the considerable cost increase of the catalyst and the improvement in activity, by selecting the catalyst with 1% wt. of Pd as the optimal choice.

The presence of CO_2 in the alimentation is essential to prevent catalyst deactivation. The neutralization of the OH^- ions formed in reaction is necessary to avoid the adsorption of these ions on the Pd surface, hindering the adsorption of H_2, which deactivate the catalyst, and charging negatively the surface of the catalyst, also hindering the adsorption of the NO_3^-. Moreover, the adsorption of nitrites is also hindered by the adsorbed OH^-, showing high selectivity to this compound, and leading to lower density of N-species adsorbed on the surface of the catalyst, i.e. low N/H relation on surface, which favors the formation of ammonium. On the other hand,

higher CO_2 flow rates further prevent ammonium formation without significantly affecting the activity or acidity of the reaction.

Reduction temperature is the key factor to achieved good reduction of the active metals, avoid sintering and optimize the quantity of metallic alloy. Elevated temperatures can help reduce Sn species but also can produce the sintering of the nanoparticles, decreasing the activity. Another factor to take into account is the formation of the alloy of Pd-Sn. In the PdSn catalysts studied in this work, the formation of the alloy seems to be favourable, but high amounts of PdSn alloy can increase the number of isolated Pd related with the formation of NH_4^+. The optimal reduction temperature found was of 300ºC for 1Pd1.2Sn catalyst.

The presence of other ions in the reaction solution, due to the use of tap water as reaction medium, leads to a decrease in catalytic activity and an increase in ammonium formation, similar to what observed with the PdCu catalyst. The anions present in the solution are adsorbed on the metals and probably negatively charge the surface of the catalyst, hindering the adsorption of the NO_2^- on the Pd active sites and slowing down their conversion. In consequence, the density of N-species adsorbed on the catalyst surface is low, in addition to the competition in the adsorption with other ions present in the solution. All these factors reduce the ratio N/H on the catalyst surface, and therefore the formation of ammonium is favoured. Therefore, the use of these catalysts in a real-world situation has not yet been achieved, and further research is required.

Finally, the model proposed adjusts the experimental data very satisfactorily, which has allowed to obtain the kinetic parameters involved in the process, a better understanding of the mechanisms that that take place in the reaction, allowing the quantification of the effect of all the variables studied.

5.5. References

[1] J. Batista, A. Pintar, J.P. Gomilšek, A. Kodre, F. Bornette, On the structural characteristics of-alumina-supported Pd-Cu bimetallic catalysts, 2001.

[2] Z. Wang, W. Wu, X. Bian, Y. Wu, Synthesis and characterization of amorphous Al2O3 and γ-Al2O3 by spray pyrolysis, Green Processing and Synthesis 5 (2016) 305–310. https://doi.org/10.1515/gps-2015-0128.

[3] I. Sanchis, J.J. Rodriguez, A.F. Mohedano, E. Diaz, N-doped activated carbon as support of Pd-Sn bimetallic catalysts for nitrate catalytic reduction, Catal Today 423 (2023). https://doi.org/10.1016/j.cattod.2023.01.018.

[4] P. Yan, L. Ma, S. Wang, L. Fang, X. Meng, X. Kong, S. Zhou, SnO2 modified intermetallic PdSn for selective hydrogenation of phenol to cyclohexanone with hydrogen donor, Chemical Engineering Journal 479 (2024). https://doi.org/10.1016/j.cej.2023.147794.

[5] A. Vicente, G. Lafaye, C. Especel, P. Marécot, C.T. Williams, The relationship between the structural properties of bimetallic Pd-Sn/SiO2 catalysts and their performance for selective citral hydrogenation, J Catal 283 (2011) 133–142. https://doi.org/10.1016/j.jcat.2011.07.010.

[6] R. Gavagnin, L. Biasetto, F. Pinna, G. Strukul, Nitrate removal in drinking waters: the effect of tin oxides in the catalytic hydrogenation of nitrate by Pd/SnO 2 catalysts, 2002.

[7] I. Sanchis, J.J. Rodriguez, A.F. Mohedano, E. Diaz, Activity and Stability of Pd Bimetallic Catalysts for Catalytic Nitrate Reduction, Catalysts 12 (2022). https://doi.org/10.3390/catal12070729.

[8] J. Jung, S. Bae, W. Lee, Nitrate reduction by maghemite supported Cu-Pd bimetallic catalyst, Appl Catal B 127 (2012) 148–158. https://doi.org/10.1016/j.apcatb.2012.08.017.

[9] Z. Gao, Y. Zhang, D. Li, C.J. Werth, Y. Zhang, X. Zhou, Highly active Pd-In/mesoporous alumina catalyst for nitrate reduction, J Hazard Mater 286 (2015) 425–431. https://doi.org/10.1016/j.jhazmat.2015.01.005.

[10] S. Jung, S. Bae, W. Lee, Development of Pd-Cu/hematite catalyst for selective nitrate reduction, Environ Sci Technol 48 (2014) 9651–9658. https://doi.org/10.1021/es502263p.

[11] S. Hamid, Y. Niaz, S. Bae, W. Lee, Support induced influence on the reactivity and selectivity of nitrate reduction by Sn-Pd bimetallic catalysts, J Environ Chem Eng 8 (2020). https://doi.org/10.1016/j.jece.2020.103754.

[12] G. Tokazhanov, E. Ramazanova, S. Hamid, S. Bae, W. Lee, Advances in the catalytic reduction of nitrate by metallic catalysts for high efficiency and N2 selectivity:

A review, Chemical Engineering Journal 384 (2020) 123252. https://doi.org/10.1016/j.cej.2019.123252.

[13] U. Prüsse, K.D. Vorlop, Supported bimetallic palladium catalysts for water-phase nitrate reduction, J Mol Catal A Chem 173 (2001) 313–328. https://doi.org/10.1016/S1381-1169(01)00156-X.

[14] S. H&old, K.-D. Vorlop, T. Tacke', M. Sellb, Development of catalysts for a selective nitrate and nitrite removal from drinking water, Elsevier Science Publishers B.V, 1993.

[15] A. Pintar, J. Batista, J. Levec, Potential of mono- and bimetallic catalysts for liquid-phase hydrogenation of aqueous nitrite solutions, Water Science and Technology 37 (1998) 177–185. https://doi.org/10.1016/S0273-1223(98)00248-0.

[16] J.K. Chinthaginjala, L. Lefferts, Support effect on selectivity of nitrite reduction in water, Appl Catal B 101 (2010) 144–149. https://doi.org/10.1016/j.apcatb.2010.09.023.

[17] Y. Matatov-Meytal, V. Barelko, I. Yuranov, M. Sheintuch, Cloth catalysts in water denitrification. I. Pd on glass fibers, Appl Catal B 27 (2000) 127–135. https://doi.org/10.1016/S0926-3373(00)00141-7.

[18] Y. Yoshinaga, T. Akita, I. Mikami, T. Okuhara, Hydrogenation of nitrate in water to nitrogen over Pd-Cu supported on active carbon, J Catal 207 (2002) 37–45. https://doi.org/10.1006/jcat.2002.3529.

[19] O.S.G.P. Soares, J.J.M. Órfão, M.F.R. Pereira, Bimetallic catalysts supported on activated carbon for the nitrate reduction in water: Optimization of catalysts composition, Appl Catal B 91 (2009) 441–448. https://doi.org/10.1016/j.apcatb.2009.06.013.

[20] A.S.G.G. Santos, J. Restivo, C.A. Orge, M.F.R. Pereira, O.S.G.P. Soares, Nitrate Catalytic Reduction over Bimetallic Catalysts: Catalyst Optimization, C (Basel) 6 (2020) 78. https://doi.org/10.3390/c6040078.

[21] B.P. Chaplin, E. Roundy, K.A. Guy, J.R. Shapley, C.I. Werth, Effects of natural water ions and humic acid on catalytic nitrate reduction kinetics using an alumina supported Pd-Cu catalyst, Environ Sci Technol 40 (2006) 3075–3081. https://doi.org/10.1021/es0525298.

[22] A. Pintar, M. Šetinc, J. Levec, Hardness and salt effects on catalytic hydrogenation of aqueous nitrate solutions, J Catal 174 (1998) 72–87. https://doi.org/10.1006/jcat.1997.1960.

[23] S. Hörold, K.D. Vorlop, T. Tacke, M. Sell, Development of catalysts for a selective nitrate and nitrite removal from drinking water, Catal Today 17 (1993) 21–30. https://doi.org/10.1016/0920-5861(93)80004-K.

[24] F. Epron, F. Gauthard, J. Barbier, Innuence of oxidizing and reducing treatments on the metal-metal interactions and on the activity for nitrate reduction of a Pt-Cu bimetallic catalyst, 2002.

[25] H. Berndt, I. Mönnich, B. Lücke, M. Menzel, Tin promoted palladium catalysts for nitrate removal from drinking water, 2001.

[26] J. Batista, A. Pintar, D. Mandrino, M. Jenko, V. Martin, XPS and TPR examinations of γ-alumina-supported Pd-Cu catalysts, Appl Catal A Gen 206 (2001) 113–124. https://doi.org/10.1016/S0926-860X(00)00589-5.

[27] F. Deganello, L.F. Liotta, A. Macaluso, A.M. Venezia, G. Deganello, Catalytic reduction of nitrates and nitrites in water solution on pumice-supported Pd-Cu catalysts, Appl Catal B 24 (2000) 265–273. https://doi.org/10.1016/S0926-3373(99)00109-5.

[28] O.S.G.P. Soares, J.J.M. Órfão, J. Ruiz-Martínez, J. Silvestre-Albero, A. Sepúlveda-Escribano, M.F.R. Pereira, Pd-Cu/AC and Pt-Cu/AC catalysts for nitrate reduction with hydrogen: Influence of calcination and reduction temperatures, Chemical Engineering Journal 165 (2010) 78–88. https://doi.org/10.1016/j.cej.2010.08.065.

[29] A.E. Palomares, C. Franch, A. Corma, Nitrates removal from polluted aquifers using (Sn or Cu)/Pd catalysts in a continuous reactor, Catal Today 149 (2010) 348–351. https://doi.org/10.1016/j.cattod.2009.05.013.

[30] D.T. González, J.A. Baeza, L. Calvo, M.A. Gilarranz, Influence of bicarbonate, other anions and carbon dioxide in the activity of Pd-Cu catalysts for nitrate reduction in drinking water, Journal of CO2 Utilization 72 (2023). https://doi.org/10.1016/j.jcou.2023.102494.

6. DEVELOPMENT OF CATALYSTS BASED ON PdCu AND SUPPORTED ON GRAPHITE FOR THE SELECTIVE REDUCTION OF NITRATES

6.1. Introduction

The current chapter presents a study of the selective reduction reaction of nitrates using PdCu-based catalysts supported on graphite. After the study and optimization of the type and concentration of the metallic active phases present in the catalysts and the optimal operating conditions used in reaction, aspects discussed in the previous chapter, this chapter study the catalyst optimization by changing the type of support. The selection of an appropriate support is very important in this process, as the catalyst's activity and selectivity can be influenced by the interaction between the active phases and the support. Many supports have been reported in literature, such as alumina [1–7], titanium oxide [2], anion exchange resins [8], active carbon [9,10], nanotubes [9,11], and graphene [12]. Carbon materials are versatile and exhibit notable features such as inertness, hydrothermal stability, and ease of recovering the metallic phase, among others [13]. Moreover, their physical and chemical properties can be tailored through various methods. Activated carbon has been widely used as a carbon support in catalytic NO_3^- reduction due to its large surface area; however, some Soares et al. [13] have reported that surface area does not always significantly influence activity. Carbon supports with a more ordered structure, such as graphite (G), carbon nanofibers (CNF), or carbon blacks, have been less studied, probably due to their lower surface area. However, these supports with a more ordered structure can facilitate mass transfer phenomena, impacting the activity and/or selectivity of the catalysts. In this study, a commercial graphite from Asbury Carbons® (GA) was selected as support because of its low price, easy availability, inertness, stability under reaction conditions, and large potential for functionalization and activation.

The selected graphite exhibits remarkably high specific surface area and hydrophilicity, great properties for its use as support (Chapter 2, Section 2.2.2). The catalysts were prepared by impregnating the graphite with a solution of the precursor metals following the instructions described in Chapter 2, Section 2.2.2. Besides, the support was modified by chemical (co-impregnation with urea or HNO_3 oxidation) and thermal (calcination under oxidising or reducing atmosphere) treatments, according to the experimental methodology explained in Chapter 2, Section 2.2.2. This section also presents the Table 2.2 with a compilation of the prepared catalysts. Therefore, this chapter shows firstly the influence of the different preparation methods used on the physicochemical properties of the catalysts (Section 5.2). After this, the influence of the

synthesis method on the activity and selectivity during the selective reduction reaction of nitrates is studied. The results are compared with those of the better Pd-Cu catalyst supported on γ-alumina obtained in Chapter 4. (Section 5.3). Additionally, and with the aim of better understand and quantify the influence of the different characteristics of the catalysts, the obtained experimental data were fitted to the kinetic model based on the main stages of the reaction mechanism explained in chapter 3, section 3.2.2.1.

6.2. Catalyst characterization

6.2.1. Atomic absorption spectroscopy (AA)

In order to determinate the metal content of the prepared catalysts, atomic absorption spectroscopy (AA) analyses were realized. The results indicated that the metal load of the catalyts was very close to the nominal load of 1% wt. Pd and 0.4% wt. Cu for all the synthesised catalysts. In addition, AA analysis of the aqueous solution after reaction were realised to study the possible lixiviation of the metals of the catalysts during the reaction. Palladium and copper were not detected, being the sensitivity of the equipment 0.1 ppm and 0.03 ppm respectively.

6.2.2. X-Ray Diffraction

Figure 6.1 shows the XRD diffractograms of the synthesised catalysts and of the support. It can be observed the characteristic peaks of graphite carbon (ref. patrons: JPCDS 01-086-2721) in all the samples, corresponding to the support. With respect to the active phases of the catalysts, a small peak corresponding to metallic Pd (ref. patrons: JPCDS 01-087-0639) is identified at 40.3° for all catalysts. In addition, PdO (ref. patron: JPCDS 01-085-0624) related peaks are present in the catalysts synthesised in oxidising atmosphere. The species related to Cu, metallic Cu and CuO were practically unidentifiable due to the low load of copper in the catalysts and, on the other hand, could be taken as an indication of a good metal dispersion on the support.

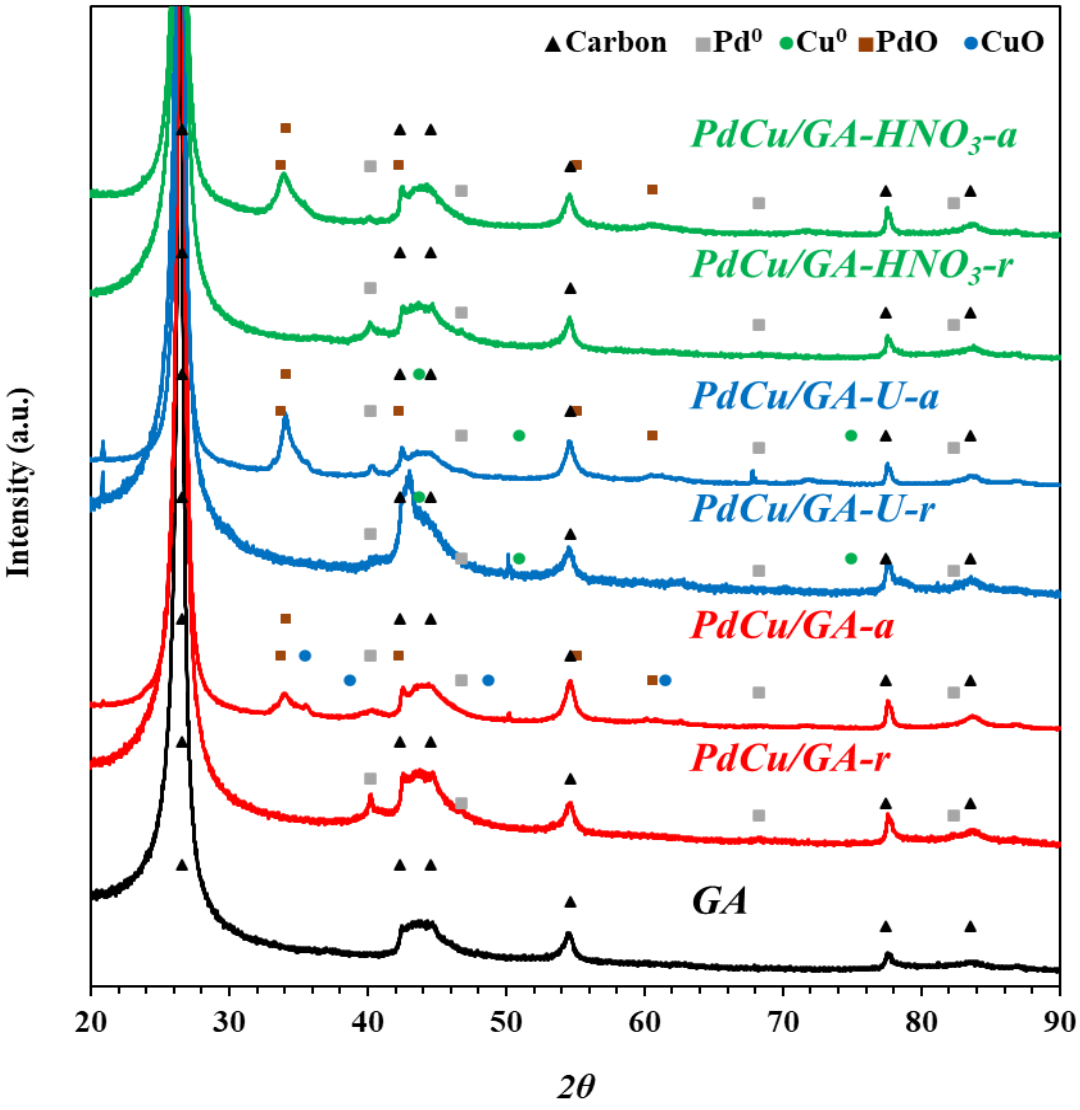

Figure 6.1 *XRD diffractograms of fresh catalysts with graphite support and graphite support.*

The XRD diffractogram of $PdCu/Al_2O_3$ catalyst can be observed in Figure 4.1 of chapter 4 Section4.2.3., where it can be observed the characteristic peaks of γ-alumina as well as the oxidised states of the Pd and the Cu. From these XRD we calculated the crystallite size along the *c* axis, L_c, and *a* axis, L_a, shown in Table 6.1. It can be observed that neither the oxidation with HNO_3 of the support without thermal treatment, nor thermal oxidation in air affects the L_c parameter. However, the combination of chemical treatment and synthesis in a reducing atmosphere yielded smaller values for L_c, indicating a more compact graphite. On the other hand, the combination of chemical treatment and synthesis in an oxidising atmosphere increases L_c value, widening the space between the layers [14]. Similarly, the size of the crystalline domain on the graphene layer, L_a, was reduced when the graphite was treated with HNO_3 or with the

process of catalyst synthesis with thermal treatment in reducing atmosphere or the combination of chemical treatment in reducing atmosphere. This is probable due to the increase of defects reducing the crystalline domain. However, the synthesis of catalyst in oxidizing atmosphere and especially its combination with urea treatment increased considerably the crystalline domain of the graphite. This effect is because the thermal treatment in oxidative atmosphere facilitates the decomposition of the defects present in the graphene layer of the edges instead of the more crystalline domains, and consequently it increases the overall crystalline domain, L_a [15].

Table 6.1 Structural parameters derived from Raman (R) and XRD (L_a and L_c) of the catalysts prepared and the supports.

Sample	***R(I_G/I_D)***	***L_a(nm)***	***L_c(nm)***
Graphite Asbury 4124	*3.47*	*50*	*15*
GA- HNO_3	*1.57*	*42*	*15*
PdCu/GA-r	*1.11*	*24*	*17*
PdCu/GA-a	*3.88*	*74*	*17*
PdCu/GA-U-r	*1.80*	*24*	*14*
PdCu/GA-U-a	*2.88*	*138*	*20*
PdCu/GA-HNO_3-r	*1.74*	*15*	*16*
PdCu/GA-HNO_3-a	*3.20*	*62*	*18*

6.2.3. Scanning Electron Microcopy (SEM)

SEM images of Figure 6.2 show the morphology of the graphite Asbury® 4124 selected as support compared with a more conventional graphite with a low surface area from the GK Advanced Metallurgical Group N.V. As can be observed, the graphite used as the support (GA) has smaller flakes with rougher surfaces and edges, this may explain the higher surface area commented in detail in section 6.2.6

.

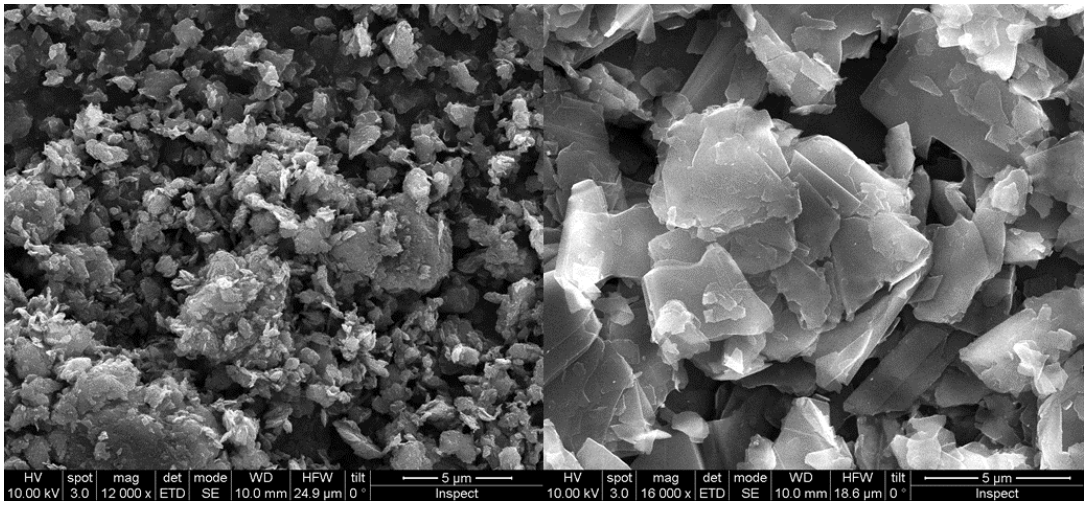

Figure 6.2 *SEM image of the graphite Asbury® 4124 used as support (left) and a conventional graphite from GK® UF4 (right).*

6.2.4. Transmission electron microscopy (TEM)

Nanoscale images of the synthesised catalysts, after reaction, were obtained using transmission electron microscopy (TEM) technique. The images show the laminar structure of the graphite and a very good dispersion of the nanoparticles on it, regardless of if the catalysts were synthesised in reducing (Figure 6.3 left) or oxidising atmosphere (Figure 6.3 right). The average diameter of the nanoparticles and their size distribution, both for the fresh catalysts and after the reduction stage, obtained from the TEM images and calculated as explained in Chapter 2, Section 2.6.2, are shown in Figure 6.4 (before reduction) and Figure 6.5 (after reduction).

The average size of the nanoparticles of the catalysts before reduction is very similar, ranged between 5-8 nm, except for the catalysts co-impregnated with urea (PdCu/GA-U-r and PdCu/GA-U-a), which show higher average particle size (13 and 10 nm respectively) (Figure 6.4). The atmosphere used in the synthesis method does not seems to affect the average size or its distribution, with very similar values being observed in each pair of catalysts where only the synthesis atmosphere changes. On the other hand, it can be observed that the chemical treatments realized widened the particle size distribution, resulting in higher particle sizes, especially in the case of the catalysts prepared by co-impregnation with urea.

On the other hand, looking at Figure 6.5 it can be observed how the average particle size of the catalysts PdCu/GA-a and the catalysts synthesized with urea (PdCu/GA-U-r and PdCu/GA-U-a) increased considerably. This effect may be because the reduction

step produces the decomposition/modification of the oxygenated functional groups initially formed on the carbon surface, as can be observed in the TPD results (Figure 6.6 and 6.7 and Table 6.3). With the removal/modification of these groups, the small, fixed metal particles become mobile on the support surface and consequently agglomerate into larger particles [16]. Furthermore, this effect may be more significant in the case of catalysts synthesized in oxidizing atmosphere since the active phase is in its oxidized state, as observed in the XRD results. Besides, the functional groups will be more modified when changing the type of atmosphere in which they were formed. Lastly, it is worth noting that the pre-treatment of the support with nitric acid has effectively prevented sintering during the reduction process.

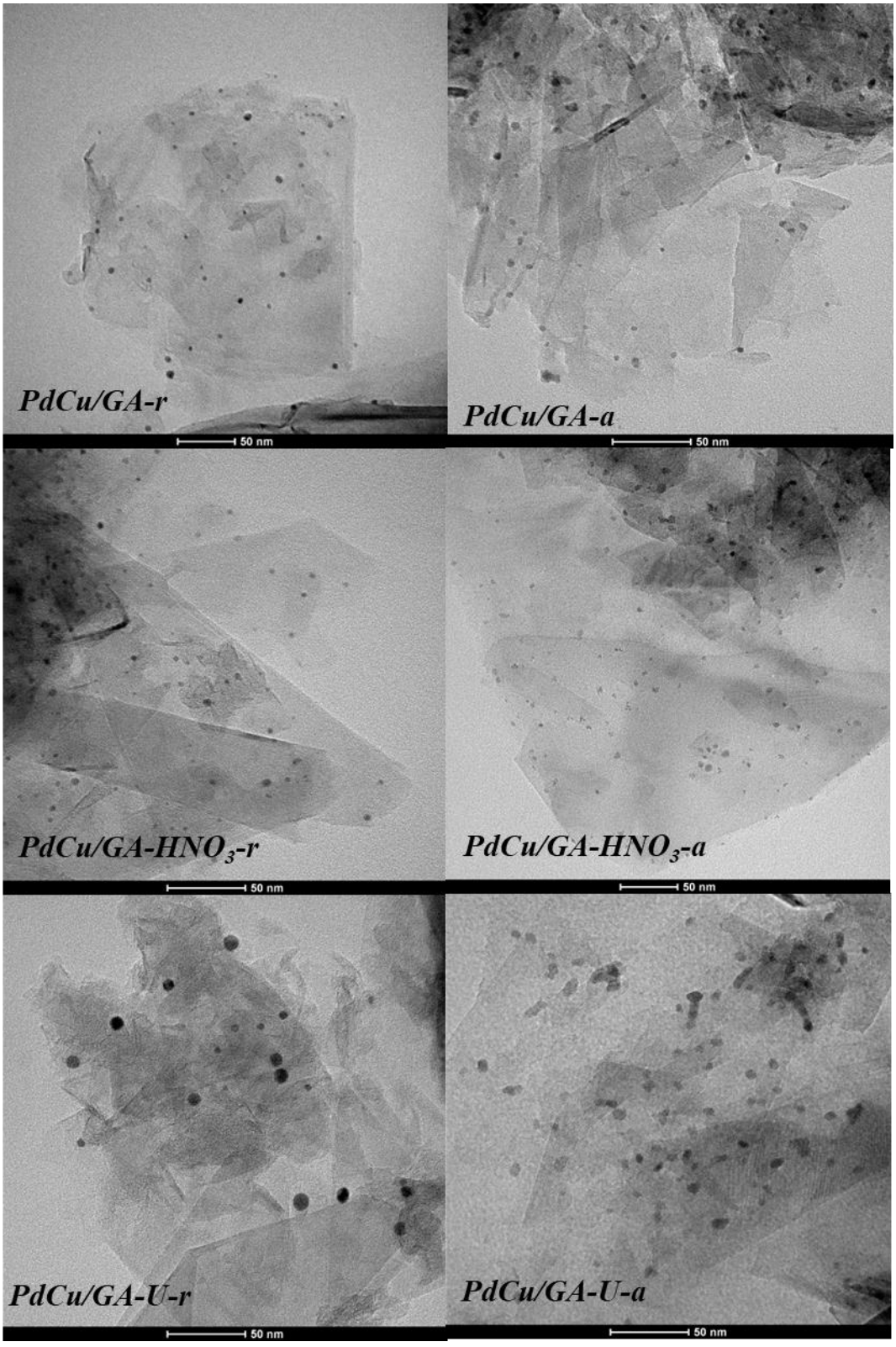

Figure 6.3 *TEM images of the catalysts synthetized in reducing atmosphere (left) and oxidizing atmosphere (right) after reduction.*

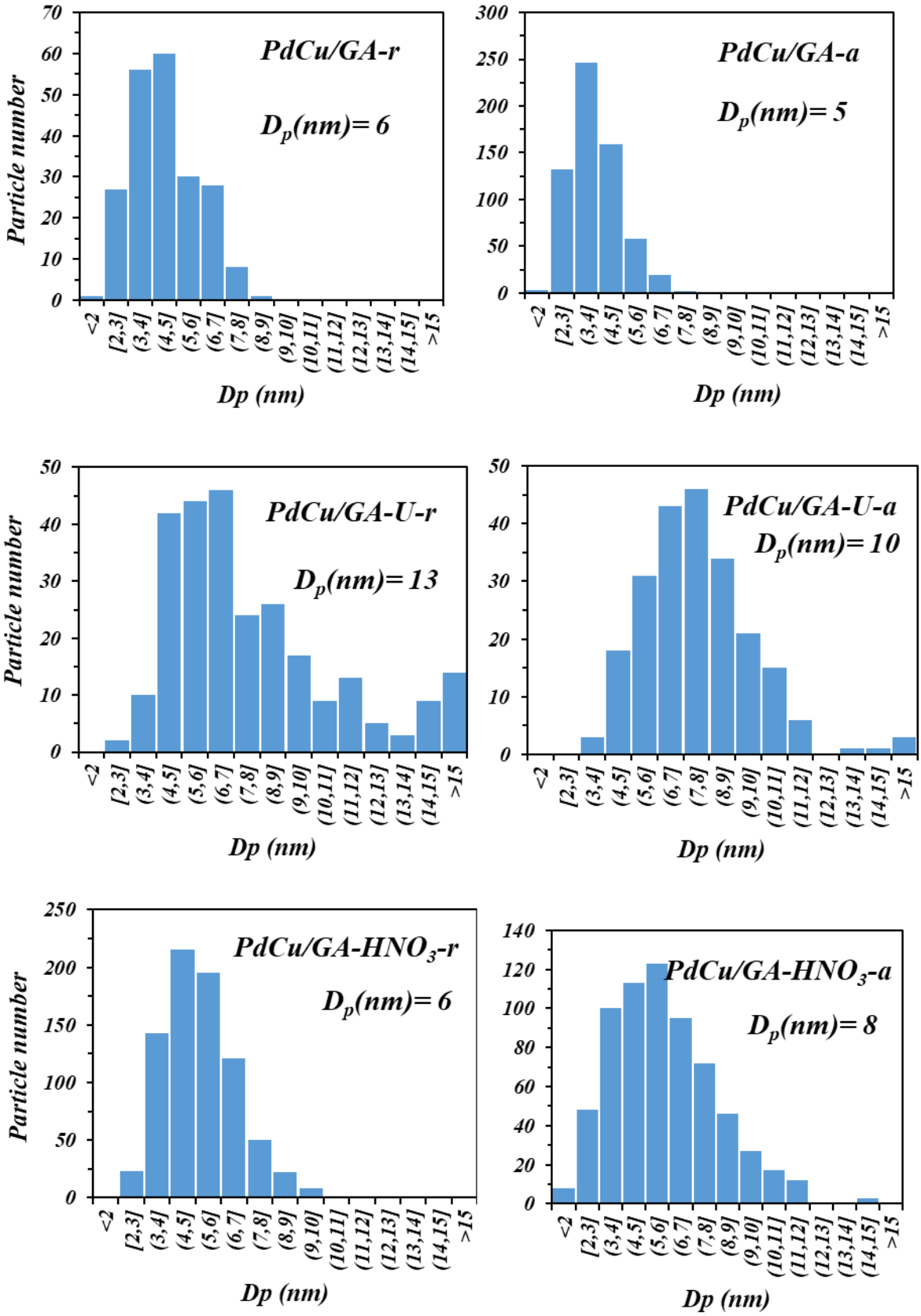

Figure 6.4 *Histograms of the nanoparticle size distribution of the graphite supported catalysts before reduction.*

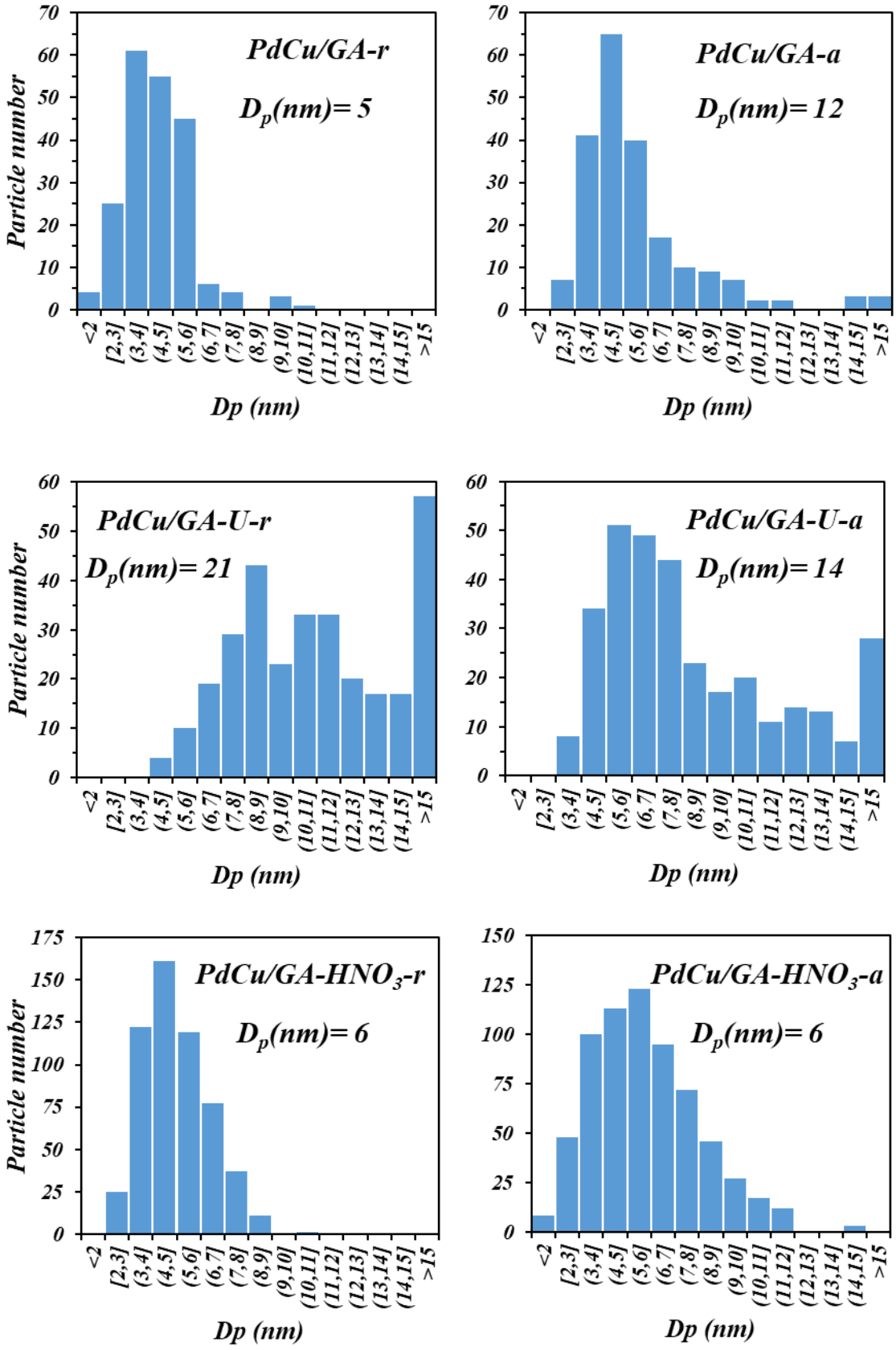

Figure 6.5 *Histograms of the nanoparticle size distribution of the graphite supported catalysts after reduction.*

6.2.5. High Resolution TEM

In the HRTEM images from Figure 6.6 it can be observed how the nanoparticles are mainly formed by Pd, in some cases like PdCu/GA-a and PdCu/GA-U-a the nanoparticles seems to have a more even proportion of Pd and Cu. As well as in $PdCu/Al_2O_3$ from chapter 4 there is Cu metal dispersed over the surface of the catalysts without forming agglomerations, but in this case, there can be observed also more quantity of Pd dispersed over the catalyst surface, probably due to the co-impregnation of both metals.

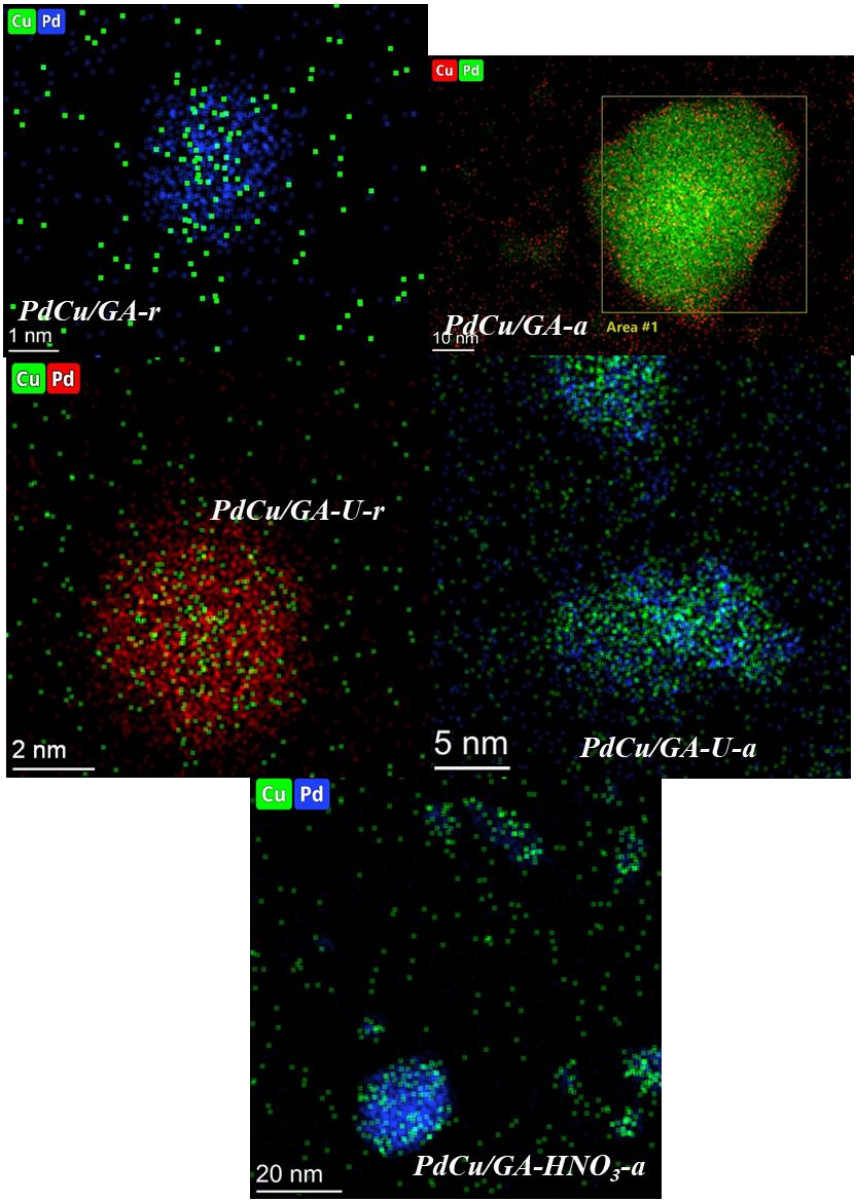

Figure 5.6 *HRTEM images of some of the graphite-based catalysts with dots of different colors which represents the atoms of Pd and Cu.*

6.2.6. Textural properties- N_2 Adsorption isotherms

The N_2 adsorption/desorption isotherms of the catalysts are shown in Figure 6.7. Their behaviour corresponds in all cases with isotherm type (IV) in the Brunauer classification [17]. The isotherms show a rapid increase in the quantity of N_2 adsorbed in the initial region of the curve at low relative pressures, followed by a gradual increase as the relative pressure rises, and a final larger increase when the relative pressure approaches 1, with hysteresis between the adsorption and desorption curves, which is typical of mesoporous materials [18]. This hysteresis is smaller in the catalysts synthesised in oxidising atmosphere than in their counterparts prepared in reducing atmosphere. This fact indicates that the pores present in PdCu/GA-a, PdCu/GA-U-a and PdCu/GA-HNO_3-a are more cylindrical and have more symmetrical adsorption and desorption than the conical pores of PdCu/GA-r, PdCu/GA-U-r and PdCu/GA-HNO_3-r.

Table 6.2 *Textural properties of the catalysts and support obtained by nitrogen adsorption-desorption isotherms.*

Sample	***BET area (m^2/ g)***	***Pore size (nm)***	***Pore volume (cm^3/g)***	***% microporosity***
Graphite Asbury 4124	*357*	*5*	*0.52*	*7 %*
GA- HNO_3	*344*	*6*	*0.43*	*7 %*
PdCu/GA-r	*294*	*9*	*0.48*	*3%*
PdCu/GA-a	*122*	*25*	*0.39*	-
PdCu/GA-U-r	*323*	*8*	*0.49*	*5%*
PdCu/GA-U-a	*102*	*26*	*0.36*	-
PdCu/GA-HNO_3-r	*302*	*9*	*0.48*	*4%*
PdCu/GA-HNO_3-a	*132*	*21*	*0.38*	-
PdCu/Al_2O_3	*191*	*7*	*0.36*	-

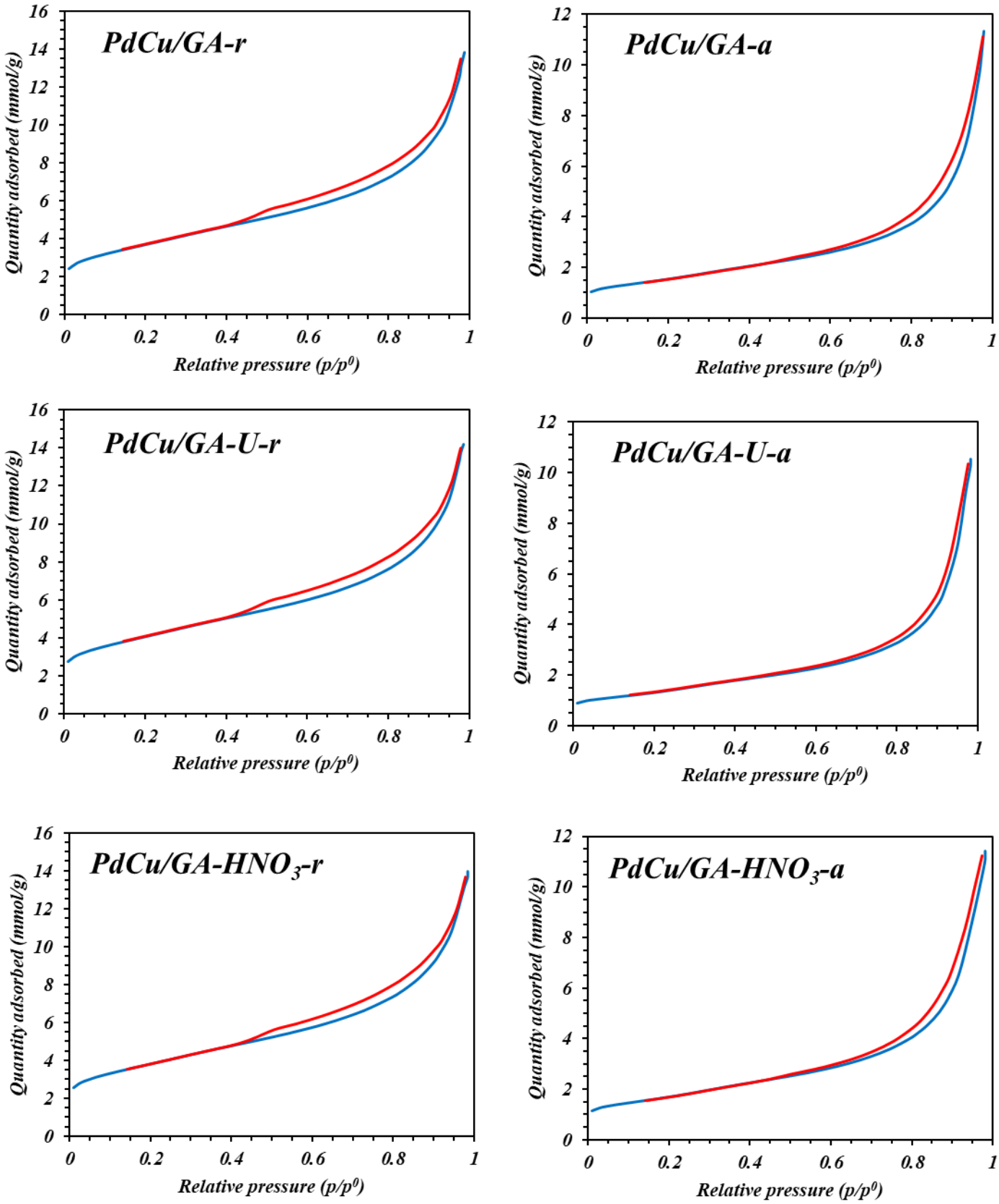

Figure 6.7 *N_2 adsorption (blue) and desorption (red) isotherm chart of the catalysts prepared in reducing atmosphere (left) and in oxidizing atmosphere (right).*

The textural properties of the catalysts obtained from N_2 adsorption isotherms are listed in Table 6.2. All catalysts showed a reduction in the BET area compared to the support owing to the occupation of the pores by the metal and the effect of the thermal decomposition step, which was more pronounced in the catalysts treated in oxidising atmosphere because of the partial combustion of the support produced during this treatment.

Analysing the different effects studied, it is worth noting that the change in the type of atmosphere used during synthesis significantly modified the BET area of the catalysts obtained, being of 294 m^2/g when the catalyst was synthesized in reducing atmosphere and of 122 m^2/g when it was synthesized in oxidizing atmosphere. Additionally, the pore size of the catalyst synthesized in air increased significantly and the microporosity present in the support was completely eliminated.

The chemical treatments performed did not significantly modify the textural properties of the catalysts, showing pore sizes and pore volumes very similar to the base catalysts PdCu/GA-a and PdCu/GA-r.

6.2.7. Raman spectroscopy

The diffractograms obtained by Raman spectroscopy for the support and the catalysts (Figure 5.8) show three characteristic peaks, typical of this kind of carbonaceous materials [20]: the D band at approximately 1350 cm^{-1} is related to in-plane heteroatoms in the graphitic structures, the G band at approximately 1580 cm^{-1} is related to the in-plane vibrations of aromatic carbons in the graphitic structure, and 2D (~2690 cm^{-1}) usually employed to calculate the number of layer for graphene or few layer graphite. Therefore, the G band is related to ordered carbon atoms, and the D band is related to defects in the structure [21]. The intensity ratio of these two peaks, I_G/I_D ratio, can be observed in Table 6.2.

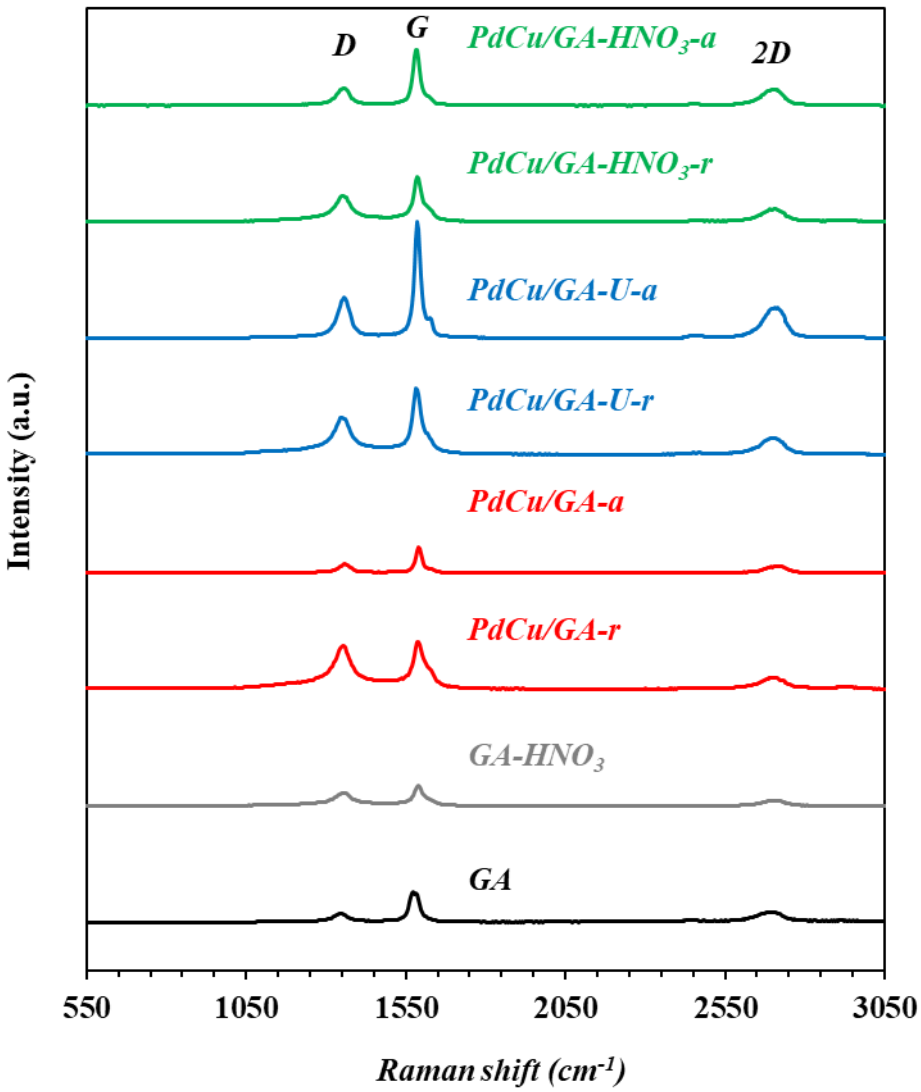

Figure 6.8 *Raman spectrum of the fresh catalysts with graphite support, modified graphite support with HNO_3 and graphite support.*

The catalyst synthesis process drastically decreases the I_G/I_D ratio of the graphite support when the process was carried out in reducing atmosphere. However, this ratio increases slightly when the treatment is realized in oxidizing atmosphere. This fact may be due to the partial oxidation of the support produced when the catalyst is thermally treated in air, reducing support defects by preferentially oxidizing the edges of the graphene layers, which exhibit more disordered phases. This effect can explain the increase in the I_G/I_D ratio. Contescu et al. [22] already demonstrated that the edges of cross-cut graphite are more disordered than its center. Consequently, the size of the carbon crystalline layer, La, increased for the PdCu/GA-a catalyst. This size is initially altered by defects in the carbon structure, so it increases as the disordered phases disappear when decomposed with air.

6.2.8. Temperature programmed desorption (TPD-MS)

The surface chemistry of the catalysts was analysed by TPD under an inert atmosphere of He coupled with mass spectrometry (TPD-MS), as explained in Chapter 2, section 2.6.6. In TPD tests carried out on carbon materials, the oxygen-containing groups decompose into CO_2 and CO. The main acidic groups typically found for carbon materials are carboxylic acids, carboxylic anhydrides and lactones and they decompose mainly to CO_2 at low temperature groups [9,23–25]. The basic groups decompose mainly into CO and are typically for this type of materials carboxylic anhydrides, phenols, carbonyls and quinone groups [9,23–25]. There may be also anhydride groups that release CO_2 and CO at the range of 400-660ºC [9,23–25].

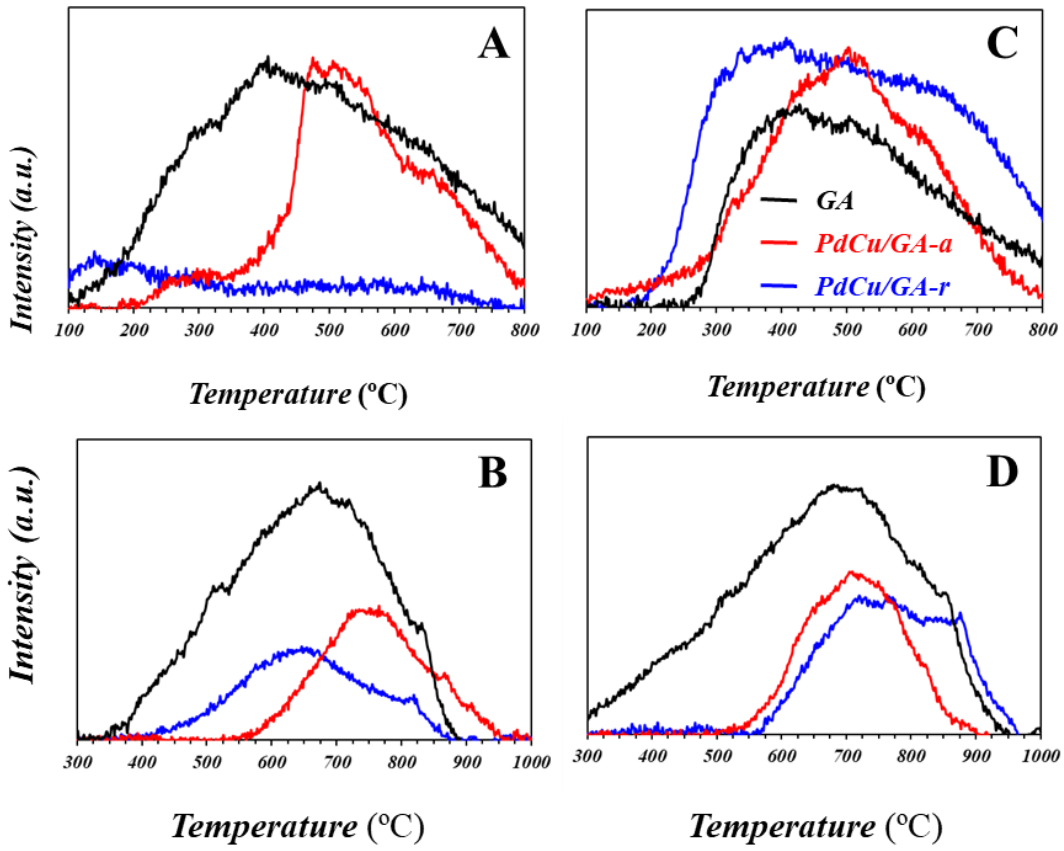

Figure 6.9 *PdCu/GA-r, PdCu/GA-a and graphite support (GA) TPD-MS desorption profiles of the catalysts before reduction (CO_2 (A); CO (B)) and after reduction (CO_2 (C); CO (D)).*

Figure 6.9 shows the CO and CO_2 desorption profiles obtained for the catalysts PdCu/GA-a and PdCu/GA-r compared with the support, before and after reduction step. The thermal treatment in reducing atmosphere decomposed all of the acid surface groups, showing almost no CO_2 desorbed compared to the support. Catalyst synthetized by treatment in oxidizing atmosphere showed a higher amount of CO_2 desorbed than the

catalyst thermally treated in a reducing atmosphere but in this case all the carboxylic acid groups (related with the CO_2 below 400ºC) were removed (Figure 6.9A). After reduction (Figure 6.9C), PdCu/GA-r catalyst showed an increased number of acid groups, particularly lactones released as CO_2 around 500ºC, surpassing the intensity of the CO_2 peak compared to that shown by the reduced support and the PdCu/GA-a. Carboxylic groups below 250ºC were desorbed for PdCu/GA-a, the support GA as expected by the thermal reduction. However, it can be observed how the few carboxylic groups present in the PdCu/GA-r were also desorbed, especially below 200ºC [9,25].

Looking at the basic groups, there is a change in the type of groups that desorb forming CO for the PdCu/GA-r catalyst before and after the catalyst reduction has been carried out. Before reaction, the catalyst shows CO at lower temperatures, associated with the presence of carboxylic anhydrides desorbed into CO_2 and CO around 500 ºC. After reduction, the peaks appear at higher temperatures associated with phenol and ether (around 700 ºC) and, carbonyl and quinones around (850ºC) (Figure 6.9B and 6.9D) [9,25]. However, there is no significant change in the CO desorbed for by the support and the catalyst PdCu/GA-a.

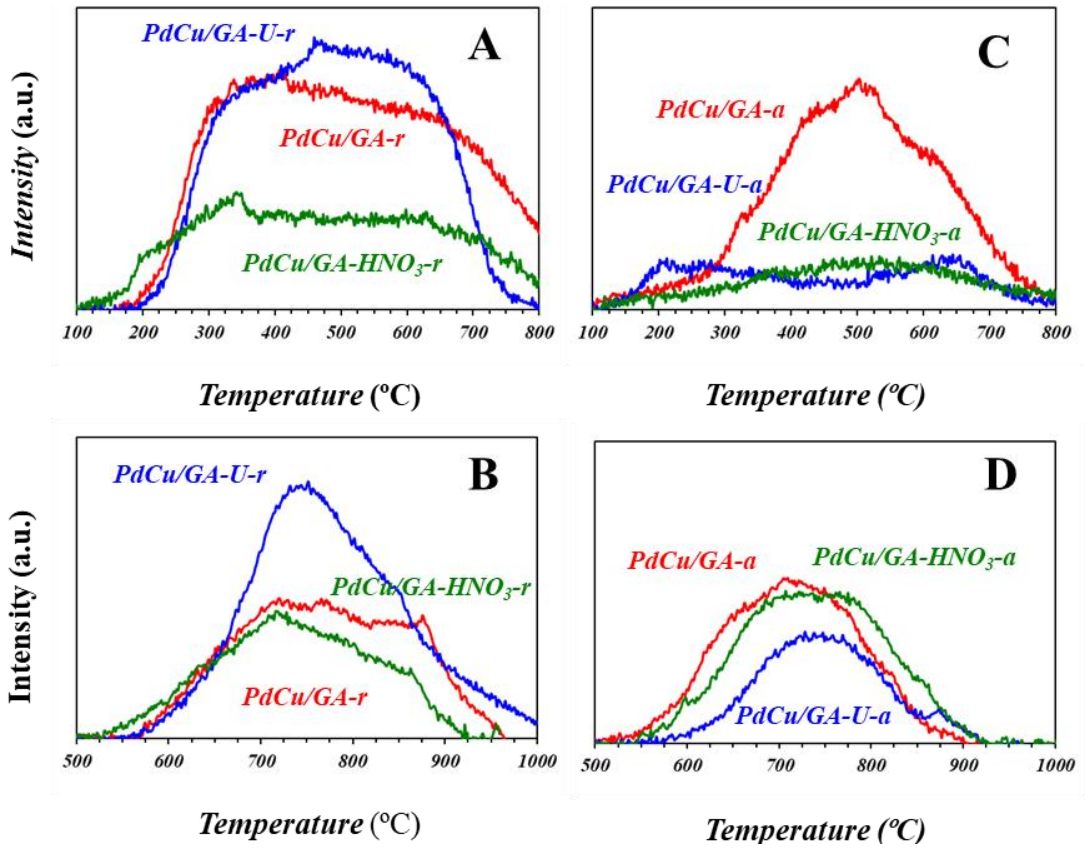

Figure 6.10 *TPD-MS desorption profiles by mass of the catalysts, after reduction with thermal treatment in reducing atmosphere (CO_2 (A); CO (B)) and in oxidizing atmosphere (CO_2 (C); CO (D)).*

TPD results obtained for the catalysts synthetized using different chemical treatments and after the reduction step can be observed in Figure 6.10. In general, the results show the disappearance of functional groups below 200ºC for the profile of CO_2, as expected due to the reduction temperature.

Analysing the effect of the different treatments realized, it can be seen, for the catalysts synthetized in reducing atmosphere, as the addition of urea led to an increase in the number of oxygenated groups on the surface, both acidic and basic, increasing the CO_2 and CO signal collected in the TPD tests with respect to that corresponding to the PdCu/GA-r catalyst (Figure 6.10A and B). The catalyst synthesized after treating the support with HNO_3 suffers a decrease in the acidic groups (Figure 6.10A), maintaining the basic groups, that is, those that are mostly decompose forming CO (Figure 6.10B).

After the synthesis of the catalysts in oxidizing atmosphere and the reduction step, a loss of acid groups is observed in both catalysts, PdCu/GA-HNO_3-a and PdCu/GA-U-a, with respect to the base catalyst PdCu/GA-a (Figure 6.10C), maintaining the basic groups (Figure 6.10D). This fact produces an augment of the basic character of these samples.

These results are summarized in Table 6.3, where the amount (μmol/g_{sample}) of CO_2, CO and total O, as a representation of the total amount of oxygenated functional groups, can be observed for all the catalysts synthetized before and after reduction step. The CO/CO_2 ratio is also indicated in the table and serves as an indicator of a more or less acidic and/or basic character of the samples.

Table 6.3 Results of TPD-MS desorption of CO_2 and CO for the catalysts after reduction.

Sample	***CO_2 (μmol/g_{sample})***	***CO (μmol/g_{sample})***	***Total O (μmol/g_{sample})***	***CO/CO_2 (-)***
PdCu/GA-r	*431*	*332*	*1193*	*0.77*
PdCu/GA-a	*255*	*306*	*817*	*1.20*
PdCu/GA-U-r	*245*	*311*	*800*	*1.27*
PdCu/GA-U-a	*146*	*250*	*542*	*1.71*
PdCu/GA-HNO_3-r	*139*	*173*	*451*	*1.24*
PdCu/GA-HNO_3-a	*73*	*265*	*410*	*3.64*

Regarding the atmosphere of synthesis, the catalysts from the reducing atmosphere have more oxygenated groups and a lower CO/CO_2 relation than their counterparts from the reducing atmosphere. On the other hand, the chemical treatments increase the CO/CO_2 ratio, regardless of the synthesis atmosphere used, that is, the basic character of the modified catalysts is greater than that of the base catalysts. The catalyst where this effect is most pronounced is PdCu/GA-HNO_3-a, with a CO/CO_2 ratio of 3.64.

6.3. Catalytic test

6.3.1. Influence of thermal treatment atmosphere

Figure 6.11 shows nitrate conversion along reaction time for all catalysts tested. Focusing on the effect of the atmosphere used during catalyst synthesis, it can be observed that PdCu/GA-r (filled red circles) and the reference PdCu/Al_2O_3 (black circles) had similar activity during the reaction, which can be due to their similar particle size. The catalyst synthetized in oxidizing atmosphere, PdCu/GA-a (empty red circles), exhibited a slower initial conversion of nitrates, although finally achieved total conversion in a similar time. The increase in the particle size that this catalyst presents after reduction, not observed in the catalyst synthesized in reducing atmosphere, may affect its activity, since it shows a lower number of available active centres. Furthermore, nitrate elimination step requires the two active metals of the catalyst, Pd and Cu, to carry out, so dispersion and good interaction between the metals is essential in the performance of this reaction step. The increment in the particle size of the catalyst also worsens the dispersion and interaction of the metals. This increase in the particle size of the catalyst synthesized in oxidizing atmosphere may be due to the rearrangement of the nanoparticle which were in it oxidate state when reduced.

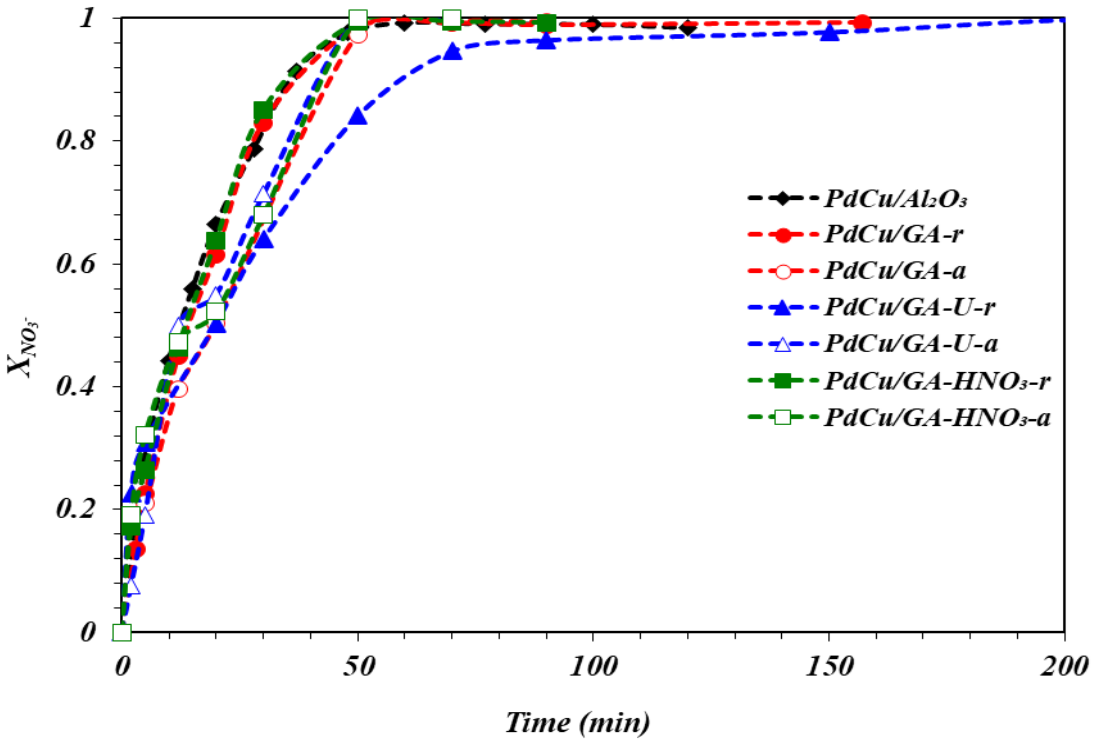

Figure 6.11 *Evolution of nitrate conversion along time for the catalysts supported on GA.*

The influence of the atmosphere used during the catalyst synthesis on the selectivity to nitrites, represented versus nitrate conversion, can be observed in Figure 6.12. All the catalysts reduced the nitrites present in the solution at the end of the reaction. The behavior of PdCu/GA-a is very similar to this showed for $PdCu/Al_2O_3$. However, PdCu/GA-r showed greater selectivity to this intermediate product during the reaction, higher than 5% almost until the end of the reaction. As commented in the characterization results, catalysts thermally treated in reducing atmosphere exhibit smaller pore diameter (Table 6.1), which hinders the diffusion of ions through the internal pores of the catalyst, slowing down the neutralization of the OH- ions formed during the reaction with the CO_2 introduced with the alimentation. This fact is very relevant in this reaction step since the OH- adsorbed on the Pd surface hinder the adsorption of nitrites, consequently observing a slower speed in its transformation, that is, greater selectivity to these products [26,27].

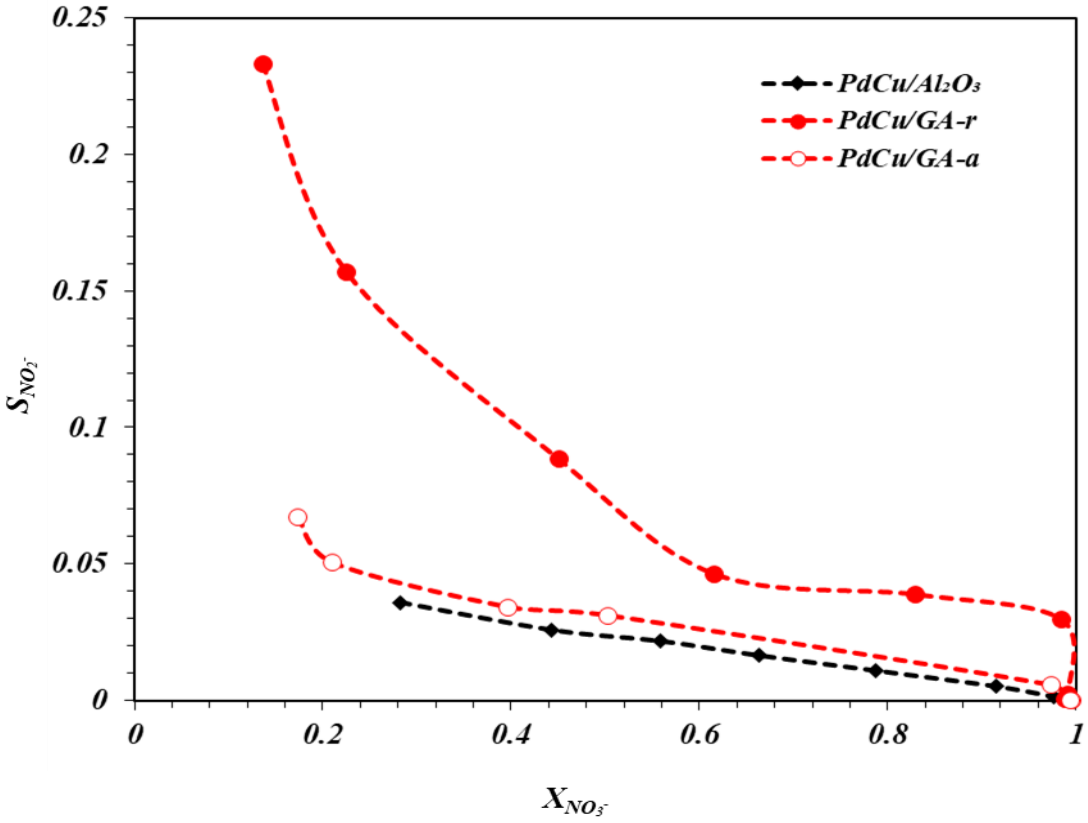

Figure 6.12 *Nitrite selectivity versus nitrate conversion for the catalysts PdCu/GA-r, PdCu/GA-a and PdCu/Al_2O_3.*

Figure 6.13 shows selectivity to ammonium versus nitrate conversion. The catalyst treated in oxidizing atmosphere, PdCu/GA-a, showed low selectivity to ammonium, achieving even lower values than the reference catalyst PdCu/Al_2O_3 at the end of the reaction. The higher pore diameter of this catalyst, as commented previously, enhances the diffusion of ions through the catalyst's internal pores, facilitating the neutralization of OH^- ions formed during the reaction with the CO_2 fed and preventing the formation of high pH spots. The presence of locally elevated pH levels, higher than those measured in solution, can significantly alter the catalysts selectivity to final products since ammonia formation is strongly favoured under basic conditions [26,27]. Besides, the higher amount of NO_2^- adsorbed on the catalyst surface (i.e., lower selectivity to nitrites) leads to a higher density of adsorbed nitrogen species and a low value of H/N ratio on the surface of the catalysts, which improves selectivity to nitrogen [28–34]. Therefore, the improvement of mass transport phenomena allowed improving the selectivity results of the catalysts.

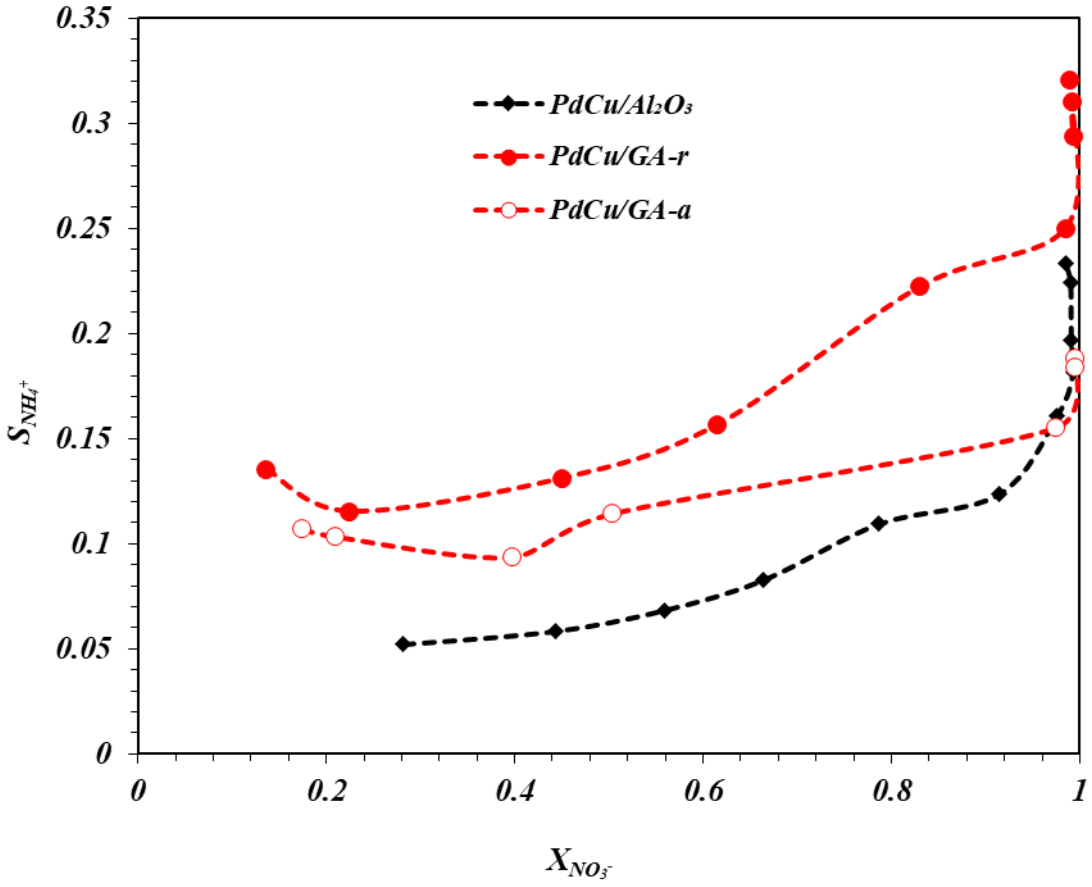

Figure 6.13 *Ammonium selectivity versus nitrate conversion for the catalysts PdCu/GA-r, PdCu/GA-a and PdCu/Al_2O_3.*

These considerations have already been bibliography by other authors. For example, Soares et al. [16] showed that catalysts supported on carbon nanotubes were more selective to nitrogen than catalysts supported on activated carbons, which have an extensive microporosity compared to the textural properties of the carbon nanotubes. That is, high mesoporous surface area and the absence of microporosity, which minimizes mass transfer limitations, prevented the over-reduction of nitrite to ammonia [16].

Finally, it can be observed that all the catalysts showed an increase in ammonium selectivity when nitrate conversion was close to 100% (Figure 6.12). The decrease in the nitrogen-containing species (N-species) at the end of the reaction, and in consequence, the lower density of N species adsorbed on the surface of the catalyst while a constant flow of H_2 is fed, produces the increment of H/N ratio on the surface of the catalysts, which leads to a higher NH_4^+ selectivity, as commented before and in agreement with literature [28–34].

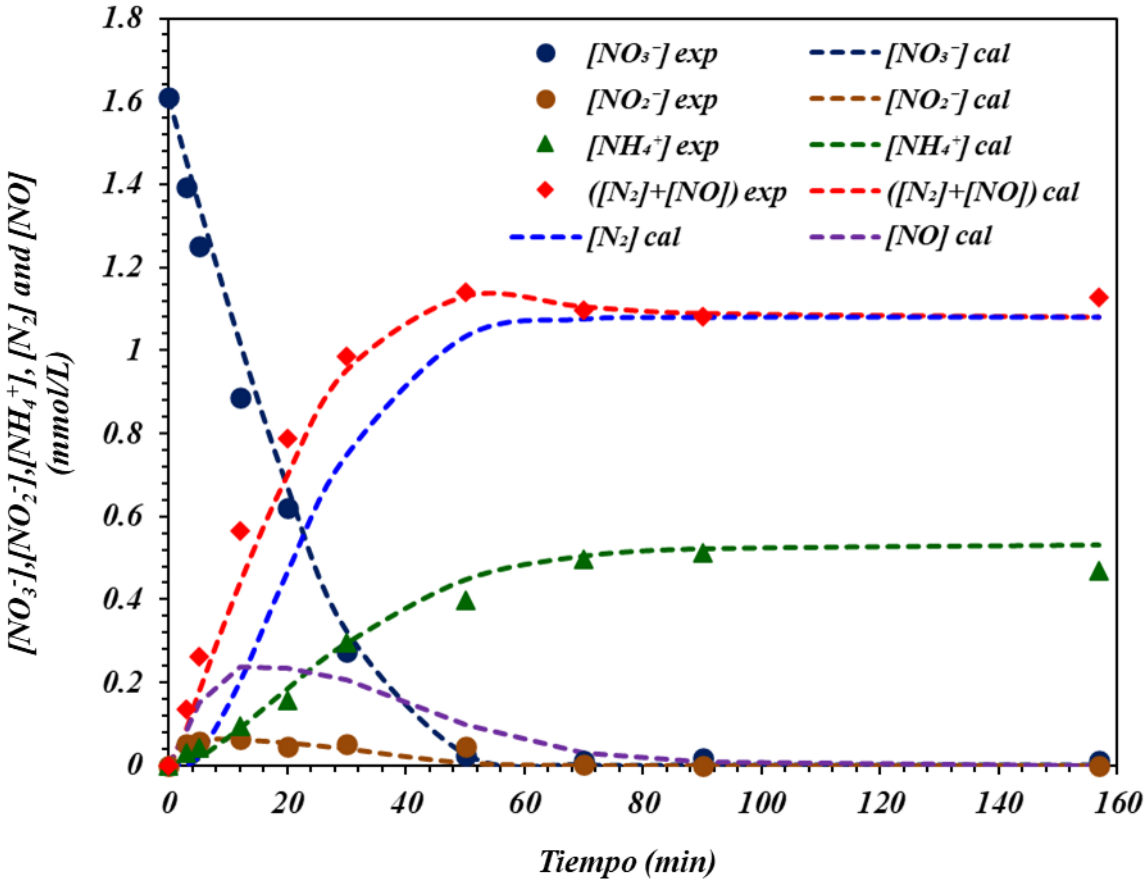

Figure 6.14 *Comparation of the evolution of nitrate (NO_3^-), nitrite (NO_2^-), nitrogen (N_2), nitrogen oxide (NO) and ammonia (NH_4^+) concentrations between experimental and calculated results over time of the catalyst PdCu/GA-r.*

The results were fitted with the kinetic model exposed in Chapter 3, section 3.2.2.1. Figure 6.14 shows, as an example, the evolution of nitrate (NO_3^-), nitrite (NO_2^-) and ammonia (NH_4^+) experimental concentrations along the reaction time obtained using the catalyst PdCu/GA-r, as well as the results calculated by the kinetic model. As can be observed, nitrates decreased during reaction time until complete conversion, and nitrites, intermediate product of the reaction, showed a typical maximum in its concentration. In general, the concentrations of this compound were very low along all the reaction. The product curves ([N_2+NO] (calculated with mass balance) and [NH_4^+]) showed a progressive increase, with a higher concentration of N_2+NO than NH_4^+ in this case. As can be observed, the model perfectly fits the experimental results and besides allows to predict the separate evolution of NO and N_2 concentrations.

The value of the kinetic constants obtained from the fitting of the experimental results can be observed in Table 6.4.

Table 6.4 *Values of the kinetic parameters for the catalyst tested.*

Catalyst	***PdCu/ GA-r***	***PdCu/ GA-U-r***	***PdCu/ GA-HNO$_3$-r***	***PdCu/ GA-a***	***PdCu/ GA-U-a***	***PdCu/ GA-HNO$_3$-a***
k_1 (NO_3^-) ($mol.g.L^{-1}.min^{-1}$)	*0.064 ± 0.006*	*0.035 ± 0.004*	*0.062 ± 0.005*	*0.046 ± 0.005*	*0.051 ± 0.004*	*0.061 ± 0.007*
K_{obs} (NO_3^-) * (mol^{-1})	*2.495 ± 0.684*	*2.569 ± 0.806*	*2.539 ± 0.572*	*4.032 ± 1.938*	*3.576 ± 1.216*	*1.923 ± 0.532*
k_2 (NO_2^-) ($g.L^{-1}.min^{-1}$)	*0.757 ± 0.122*	*0.151 ± 0.015*	*0.735 ± 0.099*	*1.644 ± 1.046*	*3.028 ± 2.178*	*1.604 ± 0.625*
k_3 (N_2) ($g.mol^{-1}.L^{-1}.min^{-1}$)	*0.579 ± 0.203*	*1.641 ± 0.067*	*0.692 ± 0.182*	*1.038 ± 0.134*	*0.583 ± 0.079*	*0.135 ± 0.018*
k_4 (NH_4^+) ($g.L^{-1}.min^{-1}.$)	*0.05 ± 0.009*	*0.108 ± 0.037*	*0.082 ± 0.011*	*0.035 ± 0.002*	*0.02 ± 0.001*	*0.011 ± 0.004*
$k_3 \cdot \overline{NO} / k_4$	*0.759*	*0.306*	*0.732*	*2.935*	*4.741*	*3.641*

In accordance as commented above, comparing catalysts PdCu/GA-r and PdCu/GA-a, it can be observed that k_1, kinetic constant related to nitrate elimination, is higher for PdCu/GA-r. This indicates a higher intrinsic rate of nitrate transformation, which can be due to the smaller size of the particles of this catalyst and the better dispersion and contact between metals, as previously mentioned. However, the value of nitrate adsorption constant, K_{abs}, is lower than in the case of the catalyst synthesized in oxidizing atmosphere, caused, as already mentioned, by diffusion limitations. The combination of both opposite effects results in a similar global behaviour at the end of the reaction with respect to the elimination of nitrates, as seen in Figure 5.10.

On the other hand, k_2, constant related to nitrite conversion, showed higher value for PdCu/GA-a than for PdCu/GA-r, indicating faster conversion of nitrites, in concordance with the lower selectivity to nitrite showed for this catalyst.

Finally, regarding the selectivity to final reaction products, it can be observed that the ratio, $k_3 \cdot \overline{C_{NO}} / k_4$, which allows to relate the intrinsic selectivity to nitrogen versus ammonium, is significatively higher for the catalyst PdCu/GA-a, being almost four

times higher than that of the PdCu/GA-r catalyst, indicating higher N_2 selectivity when thermal treatment is realized in oxidizing atmosphere.

Therefore, the results obtained with the kinetic model corroborate and quantify the behaviors discussed above.

6.3.2. Influence of chemical treatments. Catalysts prepared in reducing atmosphere.

This section shows the influence on the activity and selectivity in the CSNR reaction when two different treatments (pre-oxidation of the support with HNO_3 or addition of urea) were carried out in the catalysts synthesized in reducing atmosphere.

The previous oxidation of the graphitic support realized with HNO_3 to the catalysts thermally treated in reducing atmosphere (PdCu/GA-HNO_3-r) did not affect the rate of nitrate elimination or the final conversion, achieving total conversion at 50 min, as can be seen in Figure 6.11. In contrast, co-impregnation with urea (PdCu/GA-U-r) slowed significantly the reaction, reaching total nitrate conversion at 210 min. As mentioned in the previous section, the nitrate reduction step is strongly influenced by the size of the metal particle formed in each catalyst, which heavily depends on the synthesis procedure used. When the graphitic support was pre-treated with nitric acid, the catalyst particle size obtained did not significantly vary compared to the PdCu/GA-r catalyst, being of 6 nm and not being modified by the reduction and reaction processes. However, when urea was added to the catalyst, the observed particle size after reduction step increased to 21 nm (Figure 6.5), decreasing the activity in nitrate reduction step for this catalyst. As commented before, this variation in the particle size means that the anchoring with the addition of urea was weak and the thermal reduction process produces a sintering effect of these particles.

The selectivity to nitrite versus nitrate conversion can be observed in Figure 6.15 for the catalysts PdCu/GA-U-r and PdCu/GA-HNO_3-r, as well as the catalyst without chemical treatment PdCu/GA-r and PdCu/Al_2O_3 as references. All catalysts completely reduced nitrites during the reaction time considered. However, the catalysts supported on graphite showed higher selectivity to nitrite during the reaction than those supported on alumina, especially PdCu/GA-U-r. This effect, caused for the diffusion limitations of the reactants and products, as commented before, continued for the catalysts PdCu/GA-U-r and PdCu/GA-HNO_3-r because the textural properties of the catalysts varied very

slightly with the chemical treatments. Although the specific surface area increased, the pore size and pore volume values were very similar to the base catalyst PdCu/GA-r (Table 6.2).

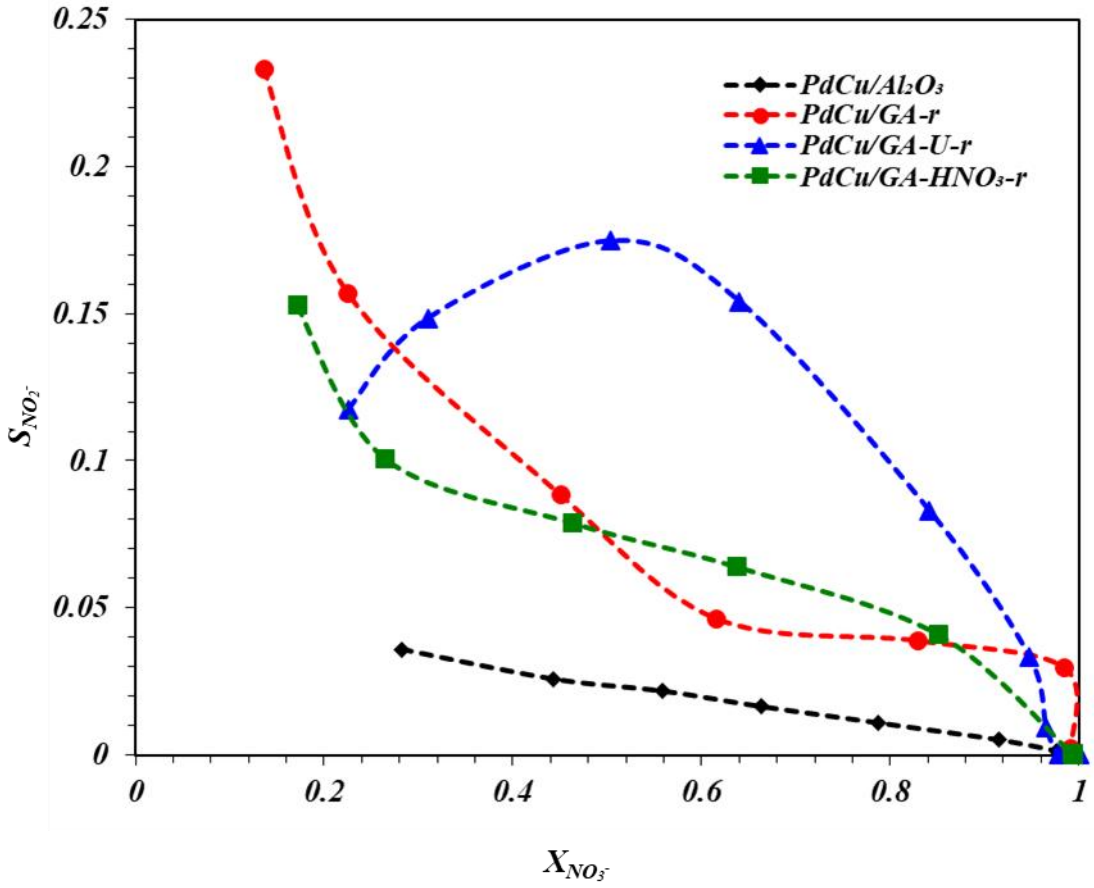

Figure 6.15 *Nitrite selectivity versus nitrate conversion for the catalysts PdCu/GA-r, PdCu/GA-U-r, PdCu/GA-HNO_3-r and PdCu/Al_2O_3.*

Therefore, the diffusion limitations of the reactants and products are still present and significantly influence the phenomena occurring at this stage. Additionally, these diffusional problems were incremented by the chemical treatments realized. The reduction of the quantity of oxygenated functional groups found on the surface of the catalysts compared to the base catalyst PdCu/GA-r, as analysed in the results of the TPD-MS tests (Figure 6.10 and Table 6.3) made the catalysts more hydrophobic. Yong Tae Kim et al. already reported this effect in their study on the oxidation effect of multi-walled carbon nanotubes (MWNT) using H_2SO_4/HNO_3 [35]. In this study, the authors demonstrated a direct relationship between hydrophilicity and the carboxyl groups created by oxidation. Lin Li et al. [36] showed similar results in their study of coconut shell-based carbons chemically treated by ammonia, sodium hydroxide, nitric acid, sulfuric acid, and phosphoric acid to determine the appropriate modification to improve

adsorption capacity of hydrophobic volatile organic compounds (VOCs) on granular activated carbons (GAC). In this study, the carbon samples modified with acid contained more oxygen compared to the untreated ones, resulting in a hydrophilic surface, which was a disadvantage for the absorption of hydrophobic VOCs.

Therefore, the increased hydrophobicity of the catalysts further augmented the diffusional problems, which, combined with the higher particle size and the poorer dispersion of the metal on the catalyst surface in the case of urea addition (PdCu/GA-U-r), caused a slower removal of nitrites, consequently resulting in higher selectivity, mainly in the case of the PdCu/GA-U-r catalyst.

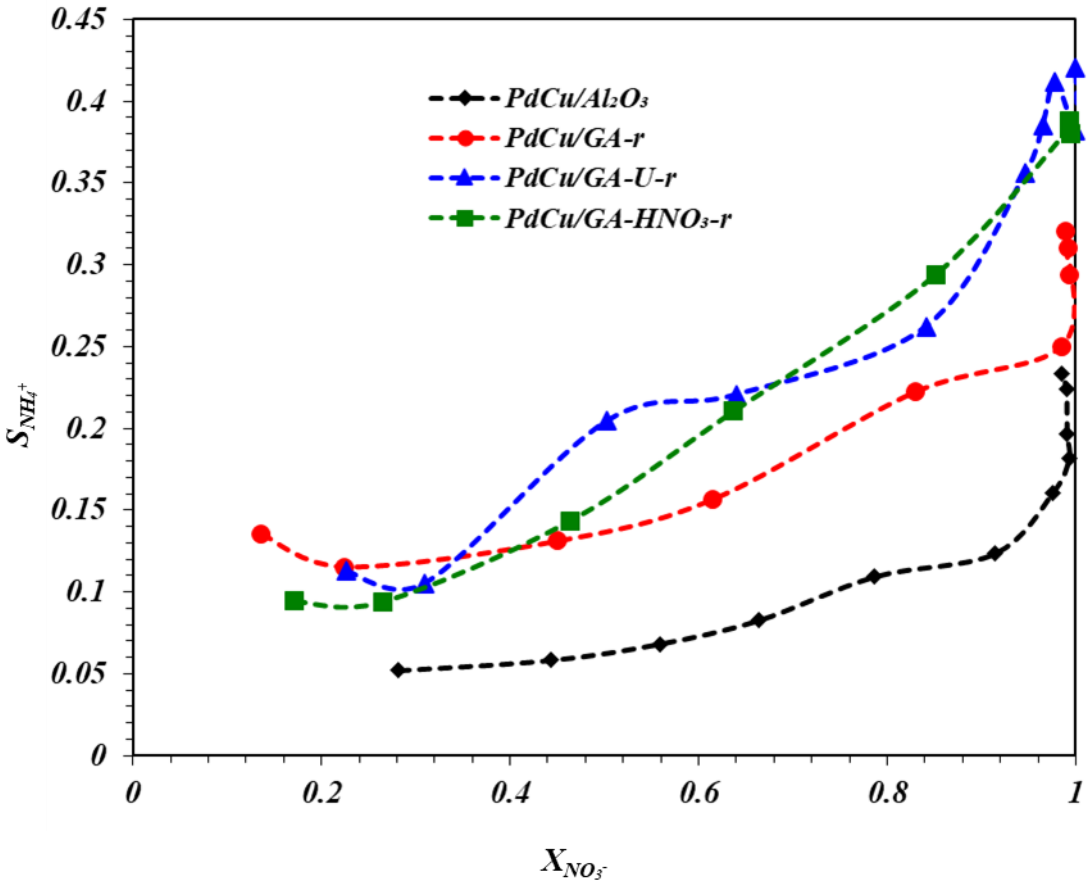

Figure 6.16 *Ammonium selectivity versus nitrate conversion for the catalysts PdCu/GA-r, PdCu/GA-U-r, PdCu/GA-HNO$_3$-r and PdCu/Al$_2$O$_3$.*

Finally, Figure 6.16 shows the selectivity to ammonium versus nitrate conversion for the previously mentioned catalysts. The catalyst PdCu/Al_2O_3 showed the lowest selectivity to ammonium in these tests. The catalysts treated chemically in reducing atmosphere, PdCu/GA-U-r and PdCu/GA-HNO_3-r, exhibited higher ammonium selectivity than PdCu/GA-r. As mentioned in the previous section, high selectivities to nitrite do not favor high densities of nitrogen species adsorbed on the surface of the

catalysts, thus favouring the over-reduction of nitrite to ammonia and not the formation of N_2 [16].

The kinetic parameters obtained from fitting of the experimental data with the model can be observed in Table 6.4. As can be seen, the adsorption nitrate constant remains practically constant, which is consistent with the similar textural properties exhibited by the catalysts. However, k_1 decreases significantly in the case of the PdCu/GA-U-r catalyst due to the poorer dispersion of the metal and, consequently, the worse interaction of the two metals necessary for this stage. This fact leads to lower activity observed in the nitrate reduction stage for the PdCu/GA-U-r catalyst.

On the other hand, as the experimental results showed, the nitrite reduction rate is much lower in the case of this catalyst, consequently exhibiting a much lower k_2 constant. Finally, the ratio $k_3 \cdot \overline{C_{NO}} / k_4$ is also reduced, indicating the higher selectivity to ammonia observed for these catalysts.

6.3.3. Influence of chemical treatments. Catalysts prepared in oxidizing atmosphere.

Finally, in this section the effects of the same chemical treatments proposed in the previous section will be studied on the activity and selectivity of the catalysts synthesized in oxidizing atmosphere.

Studying the effect of these treatments on nitrate conversion (Figure 6.11), it can be observed that the catalysts with chemical treatment and thermal treatment in oxidizing atmosphere (PdCu/GA-HNO_3-a and PdCu/GA-U-a) showed similar behaviour to the base catalyst PdCu/GA-a. It is important to remark that catalysts PdCU/GA-HNO·-a showed similar particle size than the base catalyst PdC_U/GA-r and PdCu/GA-HNO_3-r, which didn't change after reaction proving a good anchoring of these nanoparticles. However, it shows lower activity than the catalysts with similar particle size. This fact may be due to the higher CO/CO_2 relation observed in Table 6.3, this higher relation may influence the hydrophilicity of the catalyst and the contact of the aqueous solution with the surface of the catalyst.

Figure 6.17 represents the nitrite selectivity versus nitrate conversion for the different catalysts thermally treated in oxidizing atmosphere and PdCu/Al_2O_3 catalyst. The entire series of catalysts synthesized in oxidizing atmosphere showed high pore size (Table

6.2), which improves the diffusion of the ions in the inner pores of the catalyst. Therefore, all the catalysts showed low selectivities to nitrites, less than 7% for all nitrate conversions, which are much lower than in the case of the catalysts synthesized in reducing atmosphere, and similar to the $PdCu/Al_2O_3$ reference catalyst. Furthermore, all catalysts completely reduced the nitrites, not being observed residual nitrite at the end of the reaction for none of the catalysts. In this case, the chemical treatments carried out on the catalysts did not significantly change nitrite selectivity, being the values found very low in all cases, and indicating that the absence of difficulty in mass transfer phenomena is essential to achieve this objective. The treatments even slightly improved the nitrite selectivity, especially in the case of the urea-modified catalyst (PdCu/GA-U-a).

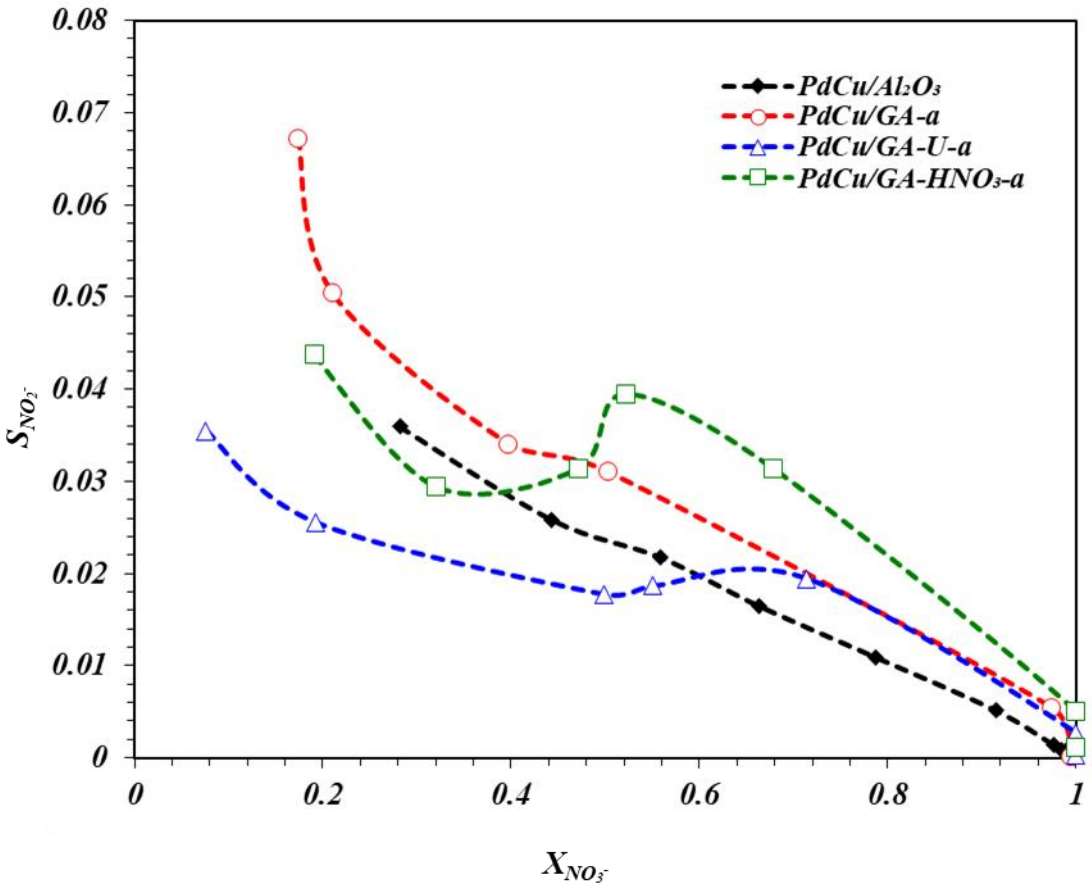

Figure 6.17 *Nitrite selectivity versus nitrate conversion for the catalysts PdCu/GA-a, PdCu/GA-U-a, PdCu/GA-HNO_3-a and PdCu/Al_2O_3.*

The ammonium selectivity versus nitrate conversion is represented in Figure 6.18. It can be observed that all carbon-based catalysts showed lower ammonium selectivity than the $PdCu/Al_2O_3$ at the end of the reaction.

As commented in section 6.3.1, the improvement in the diffusion processes achieved a catalyst that showed good results in activity and selectivity. The improvement of this catalyst by modifying it by different chemical treatments did not have significant changes in the activity but improved the selectivity, decreasing the ammonium concentration formed, especially in the case of the PdCu/GA-HNO_3-a and PdCu/GA-U-a at high nitrate conversions. When diffusion effects are no longer important, other effects produced by the changes made to the catalysts can be observed.

As in the catalysts synthesized in reducing atmosphere, the chemical treatments performed reduced the amount of oxygenated surface groups present in the catalyst (Figure 6.10 and Table 6.3). However, in this case, this fact resulted in a decrease in the observed selectivity to ammonium. The more hydrophobic character of the catalyst does not seem longer relevant here because the diffusion limitations have been eliminated by the thermal treatment performed. However, the type of oxygenated groups formed also changed the acid/base character of the support of the catalysts [37]. The catalysts subjected to chemical treatment exhibited more basic character (higher CO/CO_2 ratio, Table 6.3). This increased basicity appears to favor low ammonium selectivity, as other authors has already reported. Soares et al. [9] demonstrated that carboxylic acid groups formed by the oxidation of CNT with HNO_3 were mainly responsible for the low nitrogen selectivity shown by the catalyst. This effect may result from their role in anchoring the metal precursors, avoiding the close contact between Pd and Cu. Other studies have also highlighted the significant role of the support's surface chemistry in catalyst activity and selectivity, being generally catalysts supported on basic carbon materials more active [9].

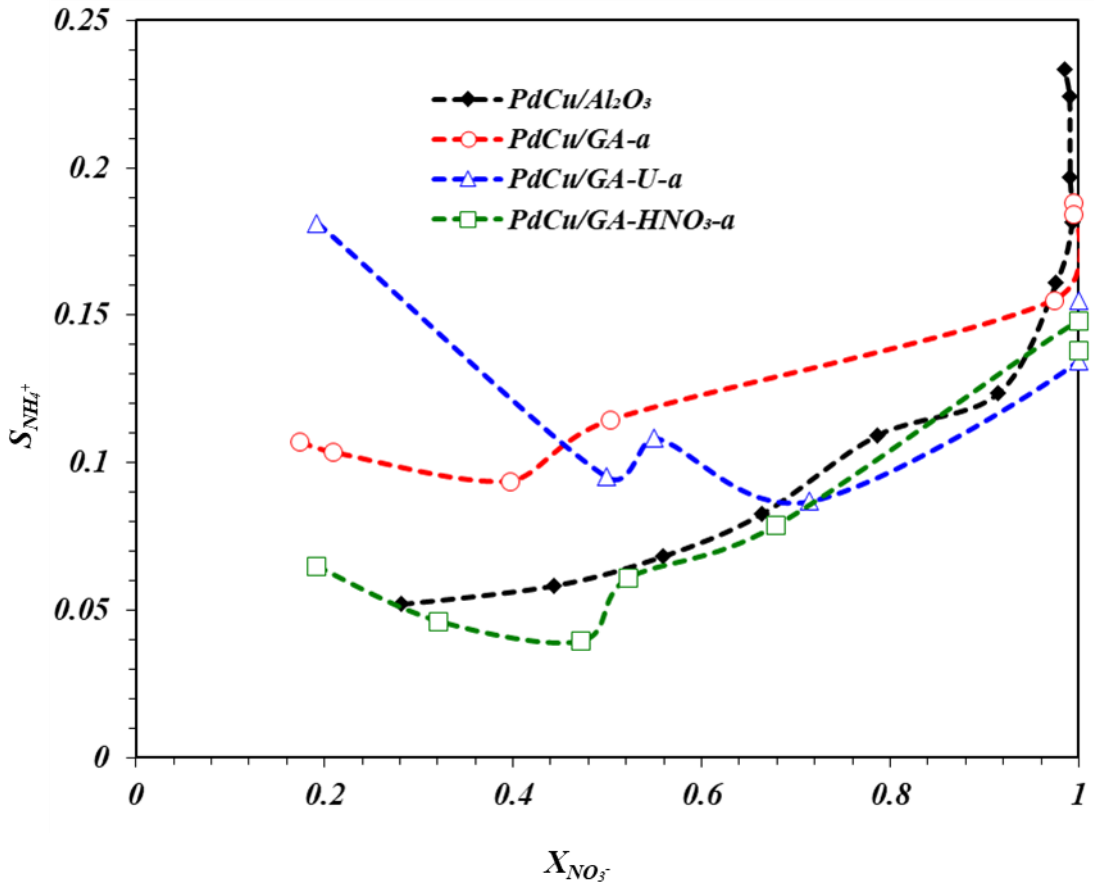

Figure 6.18 *Ammonium selectivity versus nitrate conversion for the catalysts PdCu/GA-a, PdCu/GA-U-a, PdCu/GA-HNO_3-a and PdCu/Al_2O_3.*

Therefore, these catalysts are promising in terms of maximizing N_2-selectivity for catalytic reduction of nitrates because of the enhanced mass transfer achieved and the optimization of the support's surface chemistry.

As in previous cases, the experimental results obtained have been fitted using the developed kinetic model, and the results can be observed in Table 6.4. As can be seen, the combination of chemical treatments with thermal treatment in oxidizing atmosphere (PdCu/GA-HNO_3-a and PdCu/GA-U-a) compared to PdCu/GA-a resulted in an increase of k_1 and a decrease of $K_{NO_3^-}$. These changes reflect the opposite phenomena that are occurring caused by the modification of the quantity and type of oxygenated functional groups on the catalyst surface. On one hand, the decrease in formed functional groups increases the hydrophobicity of the catalysts, thereby affecting the nitrate adsorption constant. However, the improvement in the contact between metals by eliminating functional groups and the augment of the basicity of the support enhanced the intrinsic

rate of the nitrate elimination reaction. In global, the product of the two constants would be the effective rate of this reaction step, balancing the two effects and consequently achieving similar activity values during the reaction time and leading to the complete conversion of nitrates in a very similar reaction time.

The constant k_2, related to nitrite elimination rate, shows very similar values for all catalysts synthesized in oxidizing atmosphere, consistent with the experimental results obtained. Additionally, it is worth noting that these values are much higher than those shown by the catalysts synthesized in a reducing atmosphere, which clearly explains that the diffusion limitations have been eliminated. Consequently, the reduction of nitrites has been favored, reducing the selectivity to this product.

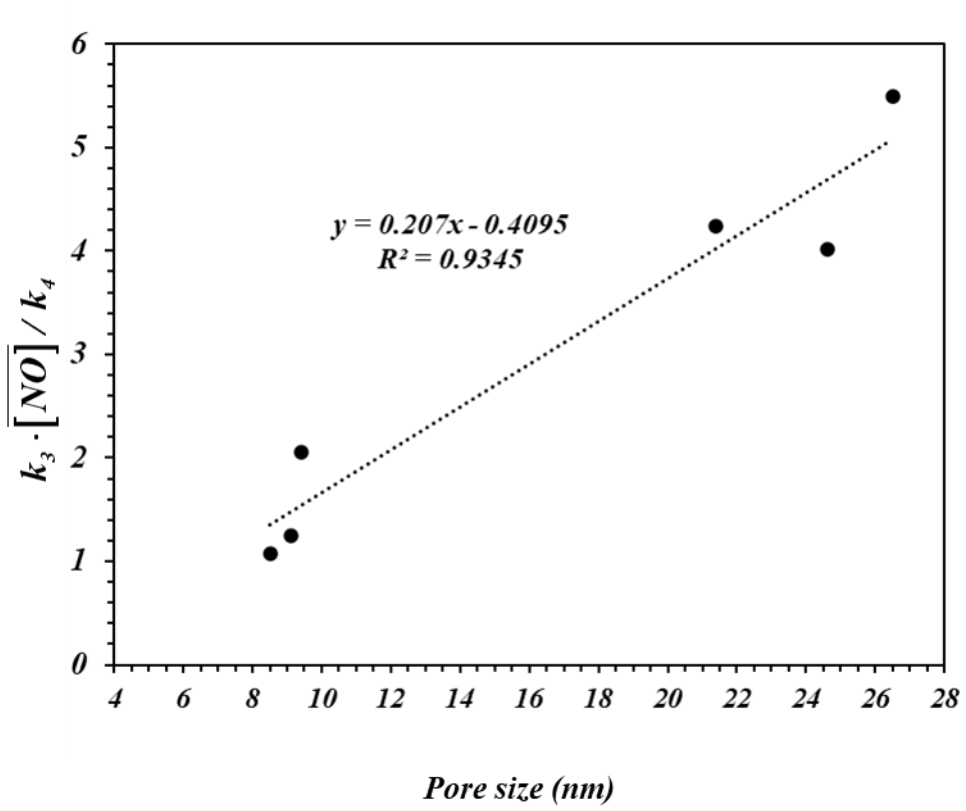

Figure 6.19 *Graphic correlation between N_2/NH_4^+ selectivity calculated by the model (relation $k_3 \cdot \overline{C_{NO}} / k_4$) and the pore size of the catalysts in nanometer (nm).*

Finally, the $k_3 \cdot \overline{C_{NO}} / k_4$ ratio is significantly increased for the catalysts PdCu/GA-HNO_3-a and PdCu/GA-U-a, in accordance with the experimental observations and as a result of the improvements mentioned previously.

Figure 6.19 shows the $k_3 \cdot \overline{C_{NO}} / k_4$ ratio versus the pore size of all the synthetized catalysts. As observed, there is a direct relationship between the selectivity to ammonium and the pore size of the catalysts; a higher pore diameter leads to a higher $k_3 \cdot \overline{C_{NO}} / k_4$ ratio, and therefore, lower ammonium selectivity. In conclusion, the main factor in the variation of ammonium selectivity was the atmosphere used in the catalyst synthesis, well-differentiated two groups of catalysts in the graph. After this, the rest of the effects produced by the different modifications of the catalysts change slightly, increasing or decreasing, this selectivity.

6.4. Conclusions

The catalysts prepared using commercial graphite Asbury® 4124 as support were active on the selective nitrate catalytic reduction reaction. The selectivity to NH_4^+ strongly depends on surface properties of the support, mainly pore diameter and functional groups on the surface of this graphitic support. In fact, the influence of the pore size is a keystone on the control over ammonium selectivity. Thus, the increase of pore size enhances the internal diffusion of the reactants, helping in the neutralization of the hydroxyls with the carbon dioxide, and improving the adsorption of nitrites and therefore the concentration of N-species in the surface of the Pd. On the other hand, the surface chemistry of the catalyst plays a secondary role in the selectivity towards NH_4^+, and it will affect the selectivity in different ways depending on other characteristic of the catalyst. Catalysts supported on graphite Asbury® 4124 thermally treated in the oxidizing atmosphere show higher pore diameter due to the partial decomposition of the inner structure and the elimination of the microporosity. The chemical treatment by co-impregnation with urea and oxidation with HNO_3 creates superficial groups on the support that helps the anchoring of the metal particles and increase the particle size in the case of co-impregnation with urea but maintaining a stable particle size in case of the HNO_3. Catalysts PdCu/GA-U-a and PdCu/GA-HNO_3-a show the lowest ammonium selectivity and maintain good activity finishing the reaction before 60 minutes at the typical operating conditions used in this thesis. From an operational view, to reduce the ammonium production, the reaction should be stopped before the 100% nitrate conversion where the ammonium selectivity is still low, and the nitrate concentration already meets the legal standards.

Finally, the model proposed adjusts the experimental data very satisfactorily, which has allowed to obtain the kinetic parameters involved in the process, a better understanding of the mechanisms that that take place in the reaction, allowing the quantification of the effect of all the variables studied.

6.5. References

[1] U. Prüsse, M. Hähnlein, J. Daum, K.D. Vorlop, Improving the catalytic nitrate reduction, Catal Today 55 (2000) 79–90. https://doi.org/10.1016/S0920-5861(99)00228-X.

[2] F. Papa, I. Balint, C. Negrila, E. Olaru, I. Zgura, C. Bradu, Supported Pd − Cu Nanoparticles for Water Phase Reduction of Nitrates . In fl uence of the Support and of the pH Conditions, (2014). https://doi.org/10.1021/ie503070f.

[3] A.E. Palomares, J.G. Prato, F. Márquez, A. Corma, Denitrification of natural water on supported Pd/Cu catalysts, Appl Catal B 41 (2003) 3–13. https://doi.org/10.1016/S0926-3373(02)00203-5.

[4] A. Pintar, G. Berčič, J. Levec, Catalytic liquid-phase nitrite reduction: kinetics and catalyst deactivation, AIChE Journal 44 (1998) 2280–2292. https://doi.org/10.1002/aic.690441017.

[5] P. Xu, S. Agarwal, L. Lefferts, Mechanism of nitrite hydrogenation over Pd/γ-Al2O3 according a rigorous kinetic study, J Catal 383 (2020) 124–134. https://doi.org/10.1016/j.jcat.2020.01.003.

[6] J.B. Salazar, L.S. Ferreira, F.C. Peixoto, M.P. Maia, F.B. Passos, Kinetics of nitrate hydrogenation in water on alumina and niobia supported palladium-copper catalysts, International Journal of Chemical Reactor Engineering 10 (2012). https://doi.org/10.1515/1542-6580.A46.

[7] U. Prüsse, J. Daum, C. Bock, K.D. Vorlop, Catalytic nitrate reduction: Kinetic investigations, Stud Surf Sci Catal 130 C (2000) 2237–2242. https://doi.org/10.1016/s0167-2991(00)80801-0.

[8] C. Bradu, C. Căpăţ, F. Papa, L. Frunza, E.A. Olaru, G. Crini, N. Morin-Crini, É. Euvrard, I. Balint, I. Zgura, C. Munteanu, Pd-Cu catalysts supported on anion exchange

resin for the simultaneous catalytic reduction of nitrate ions and reductive dehalogenation of organochlorinated pollutants from water, Appl Catal A Gen 570 (2019) 120–129. https://doi.org/10.1016/j.apcata.2018.11.002.

[9] O.S.G.P. Soares, J.J.M. Órfão, M.F.R. Pereira, Nitrate reduction catalyzed by Pd-Cu and Pt-Cu supported on different carbon materials, Catal Letters 139 (2010) 97–104. https://doi.org/10.1007/s10562-010-0424-y.

[10] L. Lemaignen, C. Tong, V. Begon, R. Burch, D. Chadwick, Catalytic denitrification of water with palladium-based catalysts supported on activated carbons, Catal Today 75 (2002) 43–48. https://doi.org/10.1016/S0920-5861(02)00042-1.

[11] O.S.G.P. Soares, X. Fan, J.J.M. Órfão, A.A. Lapkin, M.F.R. Pereira, Kinetic modeling of nitrate reduction catalyzed by Pd-Cu supported on carbon nanotubes, Ind Eng Chem Res 51 (2012) 4854–4860. https://doi.org/10.1021/ie202957v.

[12] Y. Yun, Z. Li, Y.H. Chen, M. Saino, S. Cheng, L. Zheng, Reduction of nitrate in secondary effluent of wastewater treatment plants by Fe0 reductant and Pd-Cu/graphene catalyst, Water Air Soil Pollut 227 (2016) 1–10. https://doi.org/10.1007/s11270-016-2792-4.

[13] O.S.G.P. Soares, J.J.M. Órfão, M.F.R. Pereira, Nitrate reduction in water catalysed by Pd-Cu on different supports, Desalination 279 (2011) 367–374. https://doi.org/10.1016/j.desal.2011.06.037.

[14] E. Crespo, F.J. Luque, J.F. Barrenechea, M. Rodas, Influence of grinding on graphite crystallinity from experimental and natural data: implications for graphite thermometry and sample preparation, Mineral Mag 70 (2006) 697–707. https://doi.org/10.1180/0026461067060358.

[15] D.J. Lim, N.A. Marks, M.R. Rowles, Universal Scherrer equation for graphene fragments, Carbon N Y 162 (2020) 475–480. https://doi.org/10.1016/j.carbon.2020.02.064.

[16] O.S.G.P. Soares, J.J.M. Órfão, J. Ruiz-Martínez, J. Silvestre-Albero, A. Sepúlveda-Escribano, M.F.R. Pereira, Pd-Cu/AC and Pt-Cu/AC catalysts for nitrate reduction with hydrogen: Influence of calcination and reduction temperatures, Chemical Engineering Journal 165 (2010) 78–88. https://doi.org/10.1016/j.cej.2010.08.065.

[17] S. Brunauer, P.H. Emmett, E. Teller, Adsorption of Gases in Multimolecular Layers, 1938. https://pubs.acs.org/sharingguidelines.

[18] O.N. Shornikova, E. V. Kogan, N.E. Sorokina, V. V. Avdeev, The specific surface area and porous structure of graphite materials, Russian Journal of Physical Chemistry A 83 (2009) 1022–1025. https://doi.org/10.1134/S0036024409060260.

[19] K. Morishige, M. Shikimi, Adsorption hysteresis and pore critical temperature in a single cylindrical pore, Journal of Chemical Physics 108 (1998) 7821–7824. https://doi.org/10.1063/1.476218.

[20] S. Reich, C. Thomsen, Raman spectroscopy of graphite, Philosophical Transactions of the Royal Society A: Mathematical, Physical and Engineering Sciences 362 (2004) 2271–2288. https://doi.org/10.1098/rsta.2004.1454.

[21] C. Brolly, J. Parnell, S. Bowden, Raman spectroscopy: Caution when interpreting organic carbon from oxidising environments, Planet Space Sci 121 (2016) 53–59. https://doi.org/10.1016/j.pss.2015.12.008.

[22] C.I. Contescu, S. Azad, D. Miller, M.J. Lance, F.S. Baker, T.D. Burchell, Practical aspects for characterizing air oxidation of graphite, Journal of Nuclear Materials 381 (2008) 15–24. https://doi.org/10.1016/j.jnucmat.2008.07.020.

[23] P. Brender, R. Gadiou, J.C. Rietsch, P. Fioux, J. Dentzer, A. Ponche, C. Vix-Guterl, Characterization of carbon surface chemistry by combined temperature programmed desorption with in situ X-ray photoelectron spectrometry and temperature programmed desorption with mass spectrometry analysis, Anal Chem 84 (2012) 2147–2153. https://doi.org/10.1021/ac102244b.

[24] H.F. Gorgulho, J.P. Mesquita, F. Gonçalves, M.F.R. Pereira, J.L. Figueiredo, Characterization of the surface chemistry of carbon materials by potentiometric titrations and temperature-programmed desorption, Carbon N Y 46 (2008) 1544–1555. https://doi.org/10.1016/j.carbon.2008.06.045.

[25] M. Thommes, C. Morlay, R. Ahmad, J.P. Joly, Assessing surface chemistry and pore structure of active carbons by a combination of physisorption (H2O, Ar, N2, CO 2), XPS and TPD-MS, Adsorption 17 (2011) 653–661. https://doi.org/10.1007/s10450-011-9360-4.

[26] N. Krawczyk, S. Karski, I. Witońska, The effect of support porosity on the selectivity of Pd-In/support catalysts in nitrate reduction, Reaction Kinetics, Mechanisms and Catalysis 103 (2011) 311–323. https://doi.org/10.1007/s11144-011-0321-4.

[27] M. D'Arino, F. Pinna, G. Strukul, Nitrate and nitrite hydrogenation with Pd and Pt/SnO2 catalysts: The effect of the support porosity and the role of carbon dioxide in the control of selectivity, Appl Catal B 53 (2004) 161–168. https://doi.org/10.1016/j.apcatb.2004.05.015.

[28] J. Sá, J. Montero, E. Duncan, J.A. Anderson, Bi modified Pd/SnO2 catalysts for water denitration, Appl Catal B 73 (2007) 98–105. https://doi.org/10.1016/j.apcatb.2006.06.012.

[29] J.K. Chinthaginjala, L. Lefferts, Support effect on selectivity of nitrite reduction in water, Appl Catal B 101 (2010) 144–149. https://doi.org/10.1016/j.apcatb.2010.09.023.

[30] S. Hörold, K.D. Vorlop, T. Tacke, M. Sell, Development of catalysts for a selective nitrate and nitrite removal from drinking water, Catal Today 17 (1993) 21–30. https://doi.org/10.1016/0920-5861(93)80004-K.

[31] A. Pintar, J. Batista, J. Levec, Potential of mono- and bimetallic catalysts for liquid-phase hydrogenation of aqueous nitrite solutions, Water Science and Technology 37 (1998) 177–185. https://doi.org/10.1016/S0273-1223(98)00248-0.

[32] Y. Matatov-Meytal, V. Barelko, I. Yuranov, M. Sheintuch, Cloth catalysts in water denitrification. I. Pd on glass fibers, Appl Catal B 27 (2000) 127–135. https://doi.org/10.1016/S0926-3373(00)00141-7.

[33] Y. Yoshinaga, T. Akita, I. Mikami, T. Okuhara, Hydrogenation of nitrate in water to nitrogen over Pd-Cu supported on active carbon, J Catal 207 (2002) 37–45. https://doi.org/10.1006/jcat.2002.3529.

[34] C. Franch, R.G.H. Lammertink, L. Lefferts, Partially hydrophobized catalyst particles for aqueous nitrite hydrogenation, Appl Catal B 156–157 (2014) 166–172. https://doi.org/10.1016/j.apcatb.2014.03.020.

[35] Y.T. Kim, T. Mitani, Competitive effect of carbon nanotubes oxidation on aqueous EDLC performance: Balancing hydrophilicity and conductivity, J Power Sources 158 (2006) 1517–1522. https://doi.org/10.1016/j.jpowsour.2005.10.069.

[36] L. Li, S. Liu, J. Liu, Surface modification of coconut shell based activated carbon for the improvement of hydrophobic VOC removal, J Hazard Mater 192 (2011) 683–690. https://doi.org/10.1016/j.jhazmat.2011.05.069.

[37] O.S.G.P. Soares, X. Fan, J.J.M. Órfão, A.A. Lapkin, M.F.R. Pereira, Kinetic modeling of nitrate reduction catalyzed by Pd-Cu supported on carbon nanotubes, Ind Eng Chem Res 51 (2012) 4854–4860. https://doi.org/10.1021/ie202957v.

7. SUMMARY AND CONCLUSIONS

7.1. Summary

The present Doctoral Thesis has been developed under the "*Programa de Doctorado Ingeniería Química y del Medio Ambiente*" of the Department of Chemical Engineering and Environmental Technologiesof the University of Zaragoza, in the labs of the Institute of Nanoscience and Materials of Aragon-INMA (CSIC-UNIZAR), placed in the "Escuela Politécnica Superior" of Huesca.

Population growth and the need to supply a high demand for food has led to inefficient production and use of fertilisers leading to nitrate pollution in water, with the danger, among others, of causing cancer or blue baby syndrome in humans. Despite extensive legislation on nitrate, nitrite and ammonium pollution, nitrate, nitrite and ammonium contamination is widespread worldwide.

However, an optimal industrial-scale method to solve this problem with the lowest possible drawback has not yet been found. Among the existing methods, selective catalytic nitrate reduction shows great potential to decompose nitrates into nitrogen gas, an inert and harmless gas, in a short period of time, in a reduced space and without producing other products that require further treatment, as brines or sludge. The main goal of this Doctoral Thesis has been to extend the knowledge on the influence of the operating variables of reaction, and of the composition and properties of the catalysts on their activity, stability and selectivity.

To fulfil this purpose, different PdCu and PdSn catalysts supported on γ-alumina, and PdCu catalysts supported on a commercial graphite (Asbury-4124®) modified with thermal and chemical treatments have been synthesized. After the synthesis of these catalysts, physico-chemical characterization of the catalysts was carried out to know the influence of synthesis variables studied on the catalyst properties and subsequently on its catalytic performance. The techniques used were: X-ray diffraction (XRD), Scanning electron microscopy (SEM), Transmission electron microscopy (TEM), Nitrogen adsorption analysis, Temperature programmed reduction (TPR), Atomic absorption spectroscopy (AAS), Temperature programmed desorption coupled to a mass spectrometer (TPD-MS), Raman spectroscopy (Raman) and X-ray photoelectron spectroscopy (XPS).

A series of $PdCu/Al_2O_3$ catalysts were synthesized fixing the Cu content at 0.4% w.t. and varying the Pd content between 0.25, 0.5, 0.75 and 1% w.t. Using these catalysts, the influence of the amount of noble metal in the catalyst was studied. Furthermore, using the $1Pd0.4Cu/Al_2O_3$ catalyst, the influence of the stirring speed was studied by varying it from 520 rpm to 1500 rpm. After that, the influence of the catalyst loading on the reaction was studied by introducing catalyst concentrations from 0.25g/L to 2g/L. The influence of the ratio of H_2 and CO_2 in the feed was also studied, in this case the ratio of H_2 and CO_2 in the feed was varied while the total flow remained constant at 900 Nml/min. To study the influence of the ions in the dissolution, a catalytic study was carried out using 3 different types of water: distilled water, mineral water and tap water.

Finally, using the $1Pd0.4Cu/Al_2O_3$ catalyst, a study of the combination of the catalytic selective reduction of nitrates in conjunction with Amberlite® H^+ cation exchange resins was carried out, varying the load of cation exchange resin introduced from 0g to 6g of resin.

Using the same Al_2O_3 support, a series of catalysts was synthesized using Sn as promoter metal. In this case, first two catalysts were prepared with 1%Pd w.t. and 0.4%Sn w.t. varying the order of impregnation of the metals. After this first test, it was decided to continue the synthesis with a first Sn impregnation followed by Pd impregnation. After that, the studies continued with the amount of promoter metal in the catalyst varying the amount of Sn between 0.2 and 2.5% w.t. and fixing 1% of Pd. Subsequently, the amount of Sn was fixed at 1.2% w.t. and the influence of the amount of Pd was studied, varying this percentage between 0.6 and 4% w.t. The results obtained were similar to those obtained in the case of the $PdCu/Al_2O_3$ study.

After these tests, it was decided to use the $1Pd1.2Sn/Al_2O_3$ catalyst to study the influence of the ratio of H_2 and CO_2 in the feed by varying the ratio between these two gases in the feed, however in this case the H_2 flow rate was kept constant at 100NmL/min and the CO_2 flow rate was varied from 0 to 400 NmL/min. In the same way as for $PdCu/Al_2O_3$, the influence of ions in water was studied using distilled water and tap water in the reaction. Finally, the influence of the reduction temperature of the catalyst prior to the reaction was studied by varying the reduction temperature from 250ºC to 550ºC.

The last studies were carried out using the catalysts synthesized with commercial graphite (Asbury® 4124). In this case six catalysts were synthesized: three were synthesized in reducing atmosphere using a flow rate of 300NmL/min and a H_2/N_2 ratio of 1, while the other 3 were synthesized in an oxidizing atmosphere using an air flask. In addition, four of these catalysts were modified by chemical treatments, two of the catalysts (one in a reducing atmosphere and one in an oxidizing atmosphere) were co-impregnated with urea during the synthesis, while the other two (one in a reducing atmosphere and one in an oxidizing atmosphere) were subjected to oxidation with HNO_3 prior to impregnation with the metals. All these catalysts were then tested in the selective catalytic reduction of nitrates.

Using all these results, a kinetic model has been developed and adjusted to take into account the evolution of the main reactants and products, nitrates, nitrites, ammonium and nitrogen gas. In addition, this model takes into account the possible deactivation of the catalyst, the evolution of the intermediate compound NO or the reconversion of NO to NO_2^-. This model has even been modified to take into account the presence of cation exchange resins, all of which has allowed us to quantify the influence of the different variables and deepen our knowledge of the reaction. This model allows the simultaneous calculation of the evolution of all relevant species: NO_3^-, NO_2^-, NO, N_2 and NH_4^+. The calculation of the kinetic parameters has been made by a multi-response non-linear regression procedure, solving numerically the set of differential-algebraic equations proposed.

7.2. Resumen

La presente Tesis Doctoral se ha desarrollado al amparo del «Programa de Doctorado Ingeniería Química y del Medio Ambiente» del Departamento de Ingeniería Química y Tecnologías del Medio Ambiente de la Universidad de Zaragoza, en los laboratorios del Instituto de Nanociencia y Materiales de Aragón-INMA (CSIC-UNIZAR), ubicado en la Escuela Politécnica Superior de Huesca.

El crecimiento de la población y la necesidad de abastecer una gran demanda de alimentos ha llevado a una producción y uso ineficientes de fertilizantes que provocan la contaminación del agua por nitratos, con el peligro, entre otros, de causar cáncer o el síndrome del bebé azul en humanos. A pesar de la amplia legislación sobre

contaminación por nitratos, nitritos y amonio, la contaminación por nitratos, nitritos y amonio está muy extendida en todo el mundo.

Sin embargo, aún no se ha encontrado un método óptimo a escala industrial para resolver este problema. Entre los métodos existentes, la reducción catalítica selectiva de nitratos muestra un gran potencial para descomponer los nitratos en nitrógeno gas, un gas inerte e inocuo, en un corto periodo de tiempo, en un espacio reducido y sin producir otros productos que requieran tratamiento posterior, como salmueras o lodos. El objetivo principal de esta Tesis Doctoral ha sido ampliar el conocimiento sobre la influencia de las variables operativas de reacción, y de la composición y propiedades de los catalizadores en su actividad, estabilidad y selectividad.

Para ello se han sintetizado diferentes catalizadores de PdCu y PdSn soportados sobre γ-alúmina, y catalizadores de PdCu soportados sobre un grafito comercial (Asbury-4124®) modificado con tratamientos térmicos y químicos. Tras la síntesis de estos catalizadores, se llevó a cabo la caracterización físico-química de los mismos para conocer la influencia de las variables de síntesis estudiadas sobre las propiedades del catalizador y posteriormente sobre su rendimiento catalítico. Las técnicas utilizadas fueron: Difracción de rayos X (XRD), Microscopía electrónica de barrido (SEM), Microscopía electrónica de transmisión (TEM), Análisis de adsorción de nitrógeno, Reducción programada por temperatura (TPR), Espectroscopía de absorción atómica (AAS), Desorción programada por temperatura acoplada a un espectrómetro de masas (TPD-MS), Espectroscopía Raman (Raman) y Espectroscopía de fotoelectrones de rayos X (XPS).

Se sintetizaron una serie de catalizadores $PdCu/Al_2O_3$ fijando el contenido de Cu al 0.4% en peso y variando el contenido de Pd entre 0.25, 0.5, 0.75 y 1% en peso. Utilizando estos catalizadores, se estudió la influencia de la cantidad de metal noble en el catalizador. Además, utilizando el catalizador $1Pd0.4Cu/Al_2O_3$, se estudió la influencia de la velocidad de agitación variándola de 520 rpm a 1500 rpm. A continuación, se estudió la influencia de la carga de catalizador en la reacción introduciendo concentraciones de catalizador de 0.25g/L a 2g/L. También se estudió la influencia de la proporción de H_2 y CO_2 en la alimentación, en este caso se varió la proporción de H_2 y CO_2 en la alimentación mientras que el caudal total se mantuvo constante a 900 Nml/min. Para estudiar la influencia de los iones en la disolución, se

realizó un estudio catalítico utilizando 3 tipos diferentes de agua: agua destilada, agua mineral y agua del grifo.

Por último, utilizando el catalizador 1Pd0.4Cu/Al_2O_3, se realizó un estudio de la combinación de la reducción selectiva catalítica de nitratos junto con resinas de intercambio catiónico Amberlite® H^+, variando la carga de resina de intercambio catiónico introducida desde 0g hasta 6g de resina.

Utilizando el mismo soporte de Al_2O_3, se sintetizó una serie de catalizadores empleando Sn como metal promotor. En este caso, los dos primeros catalizadores se prepararon con 1%Pd en peso y 0.4%Sn en peso variando el orden de impregnación de los metales. Tras esta primera prueba, se decidió continuar la síntesis con una primera impregnación de Sn seguida de la impregnación de Pd. Después, los estudios continuaron con la cantidad de metal promotor en el catalizador variando la cantidad de Sn entre 0.2 y 2.5% en peso y fijando un 1% de Pd. Posteriormente, se fijó la cantidad de Sn en 1.2% en peso y se estudió la influencia de la cantidad de Pd, variando este porcentaje entre 0.6 y 4%. Los resultados obtenidos fueron similares a los obtenidos en el caso del estudio de PdCu/Al2O3.

Tras estas pruebas, se decidió utilizar el catalizador 1Pd1.2Sn/Al_2O_3 para estudiar la influencia de la relación de H_2 y CO_2 en la alimentación variando la relación entre estos dos gases en la alimentación, sin embargo, en este caso el caudal de H_2 se mantuvo constante en 100NmL/min y el caudal de CO_2 se varió de 0 a 400 NmL/min. De la misma manera que para PdCu/Al_2O_3, se estudió la influencia de los iones en el agua utilizando agua destilada y agua del grifo en la reacción. Por último, se estudió la influencia de la temperatura de reducción del catalizador antes de la reacción variando la temperatura de reducción de 250ºC a 550ºC.

Los últimos estudios se realizaron utilizando los catalizadores sintetizados con grafito comercial (Asbury® 4124). En este caso se sintetizaron seis catalizadores: tres se sintetizaron en atmósfera reductora utilizando un caudal de 300NmL/min y una relación H_2/N_2 de 1, mientras que los otros 3 se sintetizaron en atmósfera oxidante utilizando un matraz de aire. Además, cuatro de estos catalizadores se modificaron mediante tratamientos químicos, dos de los catalizadores (uno en atmósfera reductora y otro en atmósfera oxidante) se coimpregnaron con urea durante la síntesis, mientras que los otros dos (uno en atmósfera reductora y otro en atmósfera oxidante) se sometieron a

oxidación con HNO_3 antes de la impregnación con los metales. A continuación, todos estos catalizadores se ensayaron en la reducción catalítica selectiva de nitratos.

A partir de todos estos resultados, se ha desarrollado y ajustado un modelo cinético que tiene en cuenta la evolución de los principales reactivos y productos, nitratos, nitritos, amonio y nitrógeno gas. Además, este modelo tiene en cuenta la posible desactivación del catalizador, la evolución del compuesto intermedio NO o la reconversión de NO en NO_2^-. Este modelo ha sido incluso modificado para tener en cuenta la presencia de resinas de intercambio catiónico, todo lo cual ha permitido cuantificar la influencia de las distintas variables y profundizar en el conocimiento de la reacción. Este modelo permite calcular simultáneamente la evolución de todas las especies relevantes: NO_3^-, NO_2-, NO, N_2 y NH_4^+. El cálculo de los parámetros cinéticos se ha realizado mediante un procedimiento de regresión no lineal multirrespuesta, resolviendo numéricamente el conjunto de ecuaciones diferenciales-algebraicas propuestas.

7.3. Conclusions

The main objective of this work is the study and development of active, selective, and stable Pd-based catalysts in the reaction of selective nitrate reduction in aqueous phase. From the catalytic and characterization results obtained it can be concluded that:

Bimetallic PdCu and PdSn catalysts supported on a commercial graphite (Asbury-4124®); and/or γ-Al_2O_3 are active and selective to N_2 in the catalytic selective nitrate reduction reaction.

When successive impregnation is used in the synthesis of the catalyst, the impregnation of the metallic promoter (Cu or Sn) first facilitates the dispersion of the Pd nanoparticles attaining smaller average sizes, increasing the activity of the catalyst. Moreover, in the case of PdSn samples, it has been found that the increase of the promoter content does not significantly change the size of the nanoparticles and the promotor is homogeneously distributed over the surface of the support. This fact leads to an increase in the nitrate conversion rate and a reduction in NH_4^+ selectivity, reaching an optimum with the 1Pd2Sn/Al_2O_3 catalyst, due to the fact that a larger quantity of Sn produces a decrease in the accessible surface area of the Pd. On the other hand, the increase of Pd loading in the catalyst implies an increase of the nanoparticle size and a higher nitrate conversion without significantly modifying the NH_4^+ selectivity.

Obviously, the price of this noble metal must be taken into account in the selection of the proper catalysts.

The temperature of activation/reduction is a critical factor for achieving effective reduction of active metals, preventing sintering, and optimizing the formation of metal alloys. While higher temperatures (T>300 ºC) can facilitate the reduction of Sn species, they can also lead to nanoparticle sintering, which reduces catalytic activity. Another important consideration is the formation of the Pd-Sn alloy. In the Pd-Sn catalysts examined in this study, alloy formation appears to be favourable; however, an excess of Pd-Sn alloy can increase the amount of isolated Pd, which is associated with the formation of undesirable NH_4^+. The optimal reduction temperature identified for the 1Pd1.2Sn/Al_2O3 catalyst was 300ºC.

One of the keys to control the selectivity of the reaction is the density of N-species adsorbed on the noble metal, as well as the H/N ratio on the surface of the Pd-Me nanoparticles. Thus, a higher H_2 concentration facilitates the reduction of nitrates but increases the H/N ratio, increasing the selectivity to NH_4^+. This ratio can be controlled by operating variables in different ways, such as varying the H_2/CO_2 feed ratio or increasing the agitation of the mixture to increase H_2 diffusion.

Thus, the optimal value found for the stirring rate is 750 rpm. Higher values of agitation diminish the external transfer limitation increasing the H/N ratio at the surface of Pd nanoparticles enhancing the ammonia formation. At low stirring rates, the reaction rate is very low, due to the very low value of the external transfer factor, and the conversion decreases below the limit marked by the legal restrictions.

The presence of another type ions in the solution increases the difficulty to convert the nitrates, maintaining a low selectivity to the formation of ammonium. This fact can be explained by considering that the additional anions have a competitive adsorption with the N-target species, increasing the H/N ratio, and therefore favouring ammonium formation. Of special interest are the presence of OH^- anions, which are also produced during the reaction, because they are strongly adsorbed on the surface of Pd nanoparticles poisoning the catalyst. For this reason, it is essential to have a flow of CO_2 to neutralize these OH^- formed during the reactions involved in the global process. It has also been shown that reducing the H_2/CO_2 ratio in the feed, despite losing some

nitrate conversion rate, considerably reduces the selectivity to NH_4^+, since, as mentioned above, the H/N ratio of species adsorbed on the Pd surface is also reduced.

The catalytic hydrogenation treatment in combination with the simultaneous adsorption on a cationic resin Amberlite® H^+ is able to control the process decreasing notoriously the presence of NH_4^+ in the aqueous phase. Moreover, the results obtained with the developed kinetic model showed that the improvement in NH_4^+ selectivity is not only due to the ammonium adsorbed by the resins, but also to the decrease of the intrinsic NH_4^+ formation constant, probably due to a better control of the pH in the reaction, improving again the H/N ratio of the species adsorbed on the Pd surface.

Catalysts supported on commercial graphite Asbury4124® have shown that their selectivity to NH_4^+ is strongly dependent on the textural and surface properties of the support. Clearly the more important factor is the pore diameter. The increase of their value enhances the internal diffusion of the reagents facilitating the neutralization of hydroxyls and the adsorption of nitrites and nitrates increasing the concentration of N-species on the Pd surface. Thermal treatment in oxidizing atmosphere during the activation stage increases the pore diameter due to the controlled gasification of the graphitic support. Meanwhile, surface chemistry plays a subordinate role, and affects to the NH_4^+ selectivity. The chemical treatment by co-impregnation with urea or oxidation with HNO_3 creates superficial groups on the support, modifying the dispersion of the metallic particles. Thus, it has been observed an increase of the average particle size in the case of co-impregnation with urea, but in case of the treatment with HNO_3 the particle size is maintained stable. In summary, the best performances of PdCu graphite-supported catalysts are PdCu/GA-HNO_3-a and PdCu/GA-U-a.

Finally, the kinetic model proposed is based on all relevant reactions of the global process, including the reduction of nitrates to nitrites and to intermediate nitrogen oxides, and finally the formation of nitrogen and/or ammonia. As a relevant aspect of the developed model, the deactivation of the catalyst is taken into account, which is assumed to be caused by the partial poisoning of the Pd nanoparticles with competitive anions present in the aqueous solution.

Moreover, this model has been modified to consider the effect of the presence of cationic resins during the catalytic reaction, in order to decrease, by selective adsorption, the concentration of ammonia ions in the aqueous phase.

The kinetic model fits satisfactorily all the experiments carried out, allowing the quantification of the effect of all the variables studied, including preparation/activation of the catalyst, and reaction conditions, in each stage of the global reaction. In summary, this model can be used as a valuable tool to optimize the catalyst composition and the operating conditions during the activation and the reaction.

7.4. Conclusiones

El objetivo principal de este trabajo es el estudio y desarrollo de catalizadores basados en Pd activos, selectivos y estables en la reacción de reducción selectiva de nitratos en fase acuosa. De los resultados catalíticos y de caracterización obtenidos se puede concluir que:

Los catalizadores bimetálicos de PdCu y PdSn soportados sobre un grafito comercial (Asbury-4124®); y/o γ-Al_2O_3 son activos y selectivos al N_2 en la reacción catalítica de reducción selectiva de nitratos.

Cuando se utiliza la impregnación sucesiva en la síntesis del catalizador, la impregnación del promotor metálico (Cu o Sn) facilita primero la dispersión de las nanopartículas de Pd alcanzando tamaños medios más pequeños, aumentando la actividad del catalizador. Además, en el caso de las muestras de PdSn, se ha comprobado que el aumento del contenido de promotor no modifica significativamente el tamaño de las nanopartículas y el promotor se distribuye homogéneamente por la superficie del soporte. Este hecho conduce a un aumento de la tasa de conversión del nitrato y a una reducción de la selectividad del NH_4^+, alcanzándose un óptimo con el catalizador 1Pd2Sn/Al_2O_3, debido a que una mayor cantidad de Sn produce una disminución del área superficial accesible del Pd. Por otro lado, el aumento de la carga de Pd en el catalizador implica un aumento del tamaño de nanopartícula y una mayor conversión de nitrato sin modificar significativamente la selectividad de NH_4^+.

Obviamente, el precio de este metal noble debe tenerse en cuenta a la hora de seleccionar los catalizadores adecuados.

La temperatura de activación/reducción es un factor crítico para lograr una reducción eficaz de los metales activos, evitar la sinterización y optimizar la formación de aleaciones metálicas. Aunque las temperaturas más altas (T>300 ºC) pueden facilitar la reducción de las especies de Sn, también pueden provocar la sinterización de las

nanopartículas, lo que reduce la actividad catalítica. Otra consideración importante es la formación de la aleación Pd-Sn. En los catalizadores Pd-Sn examinados en este estudio, la formación de la aleación parece ser favorable; sin embargo, un exceso de aleación Pd-Sn puede aumentar la cantidad de Pd aislado, lo que se asocia a la formación de NH_4^+ indeseable. La temperatura óptima de reducción identificada para el catalizador $1Pd1.2Sn/Al_2O_3$ fue de 300ºC.

Una de las claves para controlar la selectividad de la reacción es la densidad de las especies N adsorbidas en el metal noble, así como la relación H/N en la superficie de las nanopartículas de Pd-Me. Así, una mayor concentración de H_2 facilita la reducción de nitratos, pero aumenta la relación H/N, incrementando la selectividad a NH_4^+. Esta relación puede controlarse mediante variables de operación de diferentes maneras, como variando la relación de alimentación H_2/CO_2 o aumentando la agitación de la mezcla para incrementar la difusión de H_2.

Así, el valor óptimo encontrado para la velocidad de agitación es de 750 rpm. Valores más altos de agitación disminuyen la limitación de transferencia externa aumentando la relación H/N en la superficie de las nanopartículas de Pd potenciando la formación de amoníaco. A bajas velocidades de agitación, la velocidad de reacción es muy baja, debido al valor muy bajo del factor de transferencia externa, y la conversión disminuye por debajo del límite marcado por las restricciones legales.

La presencia de otro tipo de iones en la solución aumenta la dificultad para convertir los nitratos, manteniendo una baja selectividad para la formación de amonio. Este hecho puede explicarse considerando que los aniones adicionales tienen una adsorción competitiva con la especie N-objetivo, aumentando la relación H/N, y por tanto favoreciendo la formación de amonio. De especial interés es la presencia de aniones OH^-, que también se producen durante la reacción, ya que se adsorben fuertemente en la superficie de las nanopartículas de Pd envenenando el catalizador. Por esta razón, es esencial disponer de un flujo de CO_2 para neutralizar estos OH- formados durante las reacciones implicadas en el proceso global. También se ha demostrado que la reducción de la relación H_2/CO_2 en la alimentación, a pesar de perder algo de tasa de conversión de nitratos, reduce considerablemente la selectividad a NH_4^+, ya que, como se ha mencionado anteriormente, también se reduce la relación H/N de las especies adsorbidas en la superficie de Pd.

El tratamiento de hidrogenación catalítica en combinación con la adsorción simultánea sobre una resina catiónica Amberlite® H^+ es capaz de controlar el proceso disminuyendo notoriamente la presencia de NH_4^+ en la fase acuosa. Además, los resultados obtenidos con el modelo cinético desarrollado mostraron que la mejora en la selectividad del NH_4^+ no se debe únicamente al amonio adsorbido por las resinas, sino también a la disminución de la constante intrínseca de formación de NH_4^+, probablemente debido a un mejor control del pH en la reacción, mejorando de nuevo la relación H/N de las especies adsorbidas en la superficie de Pd.

Los catalizadores soportados sobre grafito comercial Asbury4124® han demostrado que su selectividad al NH_4^+ depende en gran medida de las propiedades texturales y superficiales del soporte. Claramente, el factor más importante es el diámetro de los poros. El aumento de su valor potencia la difusión interna de los reactivos facilitando la neutralización de los hidroxilos y la adsorción de nitritos y nitratos aumentando la concentración de N-especies en la superficie de Pd. El tratamiento térmico en atmósfera oxidante durante la etapa de activación aumenta el diámetro de los poros debido a la gasificación controlada del soporte grafítico. Mientras tanto, la química de la superficie juega un papel subordinado, y afecta a la selectividad del NH_4^+. El tratamiento químico mediante coimpregnación con urea u oxidación con HNO_3 crea grupos superficiales sobre el soporte, modificando la dispersión de las partículas metálicas. Así, se ha observado un aumento del tamaño medio de partícula en el caso de la coimpregnación con urea, pero en el caso del tratamiento con HNO_3 el tamaño de partícula se mantiene estable. En resumen, los mejores rendimientos de los catalizadores soportados por grafito de PdCu son PdCu/GA-HNO_3-a y PdCu/GA-U-a.

Finalmente, el modelo cinético propuesto se basa en todas las reacciones relevantes del proceso global, incluyendo la reducción de nitratos a nitritos y a óxidos de nitrógeno intermedios, y finalmente la formación de nitrógeno y/o amoníaco. Como aspecto relevante del modelo desarrollado, se tiene en cuenta la desactivación del catalizador, que se supone causada por el envenenamiento parcial de las nanopartículas de Pd con aniones competitivos presentes en la solución acuosa.

Finalmente, el modelo cinético propuesto se basa en todas las reacciones relevantes del proceso global, incluyendo la reducción de nitratos a nitritos y a óxidos de nitrógeno intermedios, y finalmente la formación de nitrógeno y/o amoníaco. Como aspecto relevante del modelo desarrollado, se tiene en cuenta la desactivación del catalizador,

que se supone causada por el envenenamiento parcial de las nanopartículas de Pd con aniones competitivos presentes en la solución acuosa.

Además, este modelo se ha modificado para considerar el efecto de la presencia de resinas catiónicas durante la reacción catalítica, con el fin de disminuir, por adsorción selectiva, la concentración de iones amonio en la fase acuosa.

El modelo cinético se ajusta satisfactoriamente a todos los experimentos realizados, permitiendo cuantificar el efecto de todas las variables estudiadas, incluyendo preparación/activación del catalizador, y condiciones de reacción, en cada etapa de la reacción global. En resumen, este modelo puede utilizarse como una valiosa herramienta para optimizar la composición del catalizador y las condiciones de operación durante la activación y la reacción.